Seismic Vulnerability of Typical Maltese Chapels

Ylenia Camilleri

Dissertation submitted to the Faculty for the Built Environment, University of Malta in part fulfilment of the requirements for the attainment of the degree of Master of Engineering (Structural Engineering)

June 2024

This dissertation is dedicated to my loving family.

Thank you for your constant support and encouragement.

L-Università ta' Malta

FACULTY/INSTITUTE/CENTRE/SCHOOL Faculty for the Built Environment

DECLARATIONS BY POSTGRADUATE STUDENTS

(a) Authenticity of Dissertation

I hereby declare that I am the legitimate author of this Dissertation and that it is my original work.

No portion of this work has been submitted in support of an application for another degree or qualification of this or any other university or institution of higher education.

I hold the University of Malta harmless against any third party claims with regard to copyright violation, breach of confidentiality, defamation and any other third party right infringement.

(b) Research Code of Practice and Ethics Review Procedures

I declare that I have abided by the University's Research Ethics Review Procedures. Research Ethics & Data Protection form code Ben - 2024 - 00010.

As a Master's student, as per Regulation 77 of the General Regulations for University Postgraduate Awards 2021, I accept that should my dissertation be awarded a Grade A, it will be made publicly available on the University of Malta Institutional Repository.

Acknowledgements

First and foremost, I want to thank my supervisor, Chev. Prof. Marc Bonello B.E.&A. (Hons)(Melit.), M.Sc. (Lond.), Ph.D. (Lond.), D.I.C., M.A.S.C.E., M.S.E.I., Eur.Ing. (FEANI), Perit, for his consistent guidance and invaluable advice throughout this dissertation. I also express my gratitude to Gruppo Sismica for granting an educational license for the 3D Macro software and for their assistance during the development of the numerical models.

I thankfully appreciate Prof. Sebastiano D'Amico from the Geosciences Department at the University of Malta help for his assistance with the Ambient Noise Readings of St. Philip & St. James Chapel in San Gwann.

Lastly, but certainly not the least, I am deeply thankful to my family for their continuous love, unwavering care, and support during my research and the writing of this dissertation.

Abstract

The vulnerability of Maltese chapels to seismic activity is a significant concern due to Malta's location in a seismic zone. These chapels, constructed with unreinforced masonry (URM), have historical significance but may not be adequately resistant to earthquakes. Despite surviving significant historical earthquakes in 1693, 1743, and 1856 with varying degrees of damage and subsequent repairs, their structural integrity remains uncertain for future seismic events. Key chapels like St. Philip & St. James in San Gwann, St. Marija Maddalena in Dingli, and St. Matthew’s in Qrendi exemplify this architectural vulnerability, requiring assessment and potential reinforcement to ensure conservation and safety against seismic risks.

The study examines the seismic vulnerability of chapels by comparing two pairs: San Gwann Chapel and Dingli Chapel, and San Gwann Chapel with Qrendi Chapel. It focuses on how the differences in foundation geology and structural regularity affect vulnerability to earthquakes. San Gwann Chapel, situated on Lower Globigerina Limestone, shows structural regularity, while Dingli Chapel, on Upper Coraline Limestone over Blue Clay, faces different challenges. Similarly, despite both being on Lower Globigerina Limestone, San Gwann Chapel contrasts with Qrendi Chapel due to Qrendi's structural irregularities. These insights underscore the role of geological and structural factors in assessing and mitigating seismic risks for the buildings.

This research was conducted under a non-linear pushover seismic analysis using "3DMacro" software to model the three selected chapels. The study focused on their seismic performance under moderate earthquake conditions (approximately 0.1g). All chapels, characterized as single-story buildings with alpha values exceeding 1, demonstrated sufficient safety margins against seismic forces at this intensity level. However, under higher earthquake intensities, the analysis predicted a sequence of failure starting with Dingli Chapel, followed by Qrendi Chapel, and finally San Gwann Chapel.

The study examines the seismic safety of several chapels in Malta, focusing on Dingli Chapel and San Gwann Chapel. San Gwann Chapel, built on Globigerina Limestone, shows better safety performance and less displacement compared to Dingli Chapel, which rests on Upper Coralline Limestone over Blue Clay. Qrendi Chapel, also on Globigerina Limestone but with asymmetrical additions, exhibits reduced safety compared to San Gwann Chapel. Despite regular architectural layouts, Dingli Chapel's safety factor is lower than Qrendi Chapel's due to subsoil conditions, emphasizing the critical role of subsoil type in structural integrity over design irregularities. All the three studied chapels, demonstrate resilience against seismic events, with alpha values above 1, indicating no need for retrofitting for an earthquake of 0.1g. This study contributes to understanding the seismic vulnerability of Maltese chapels, essential for preserving these culturally significant buildings.

Keywords: **Seismic Vulnerability, Masonry Heritage Buildings, 3D Macro Analysis, Maltese Chapel.**

Table of Contents

List of Tables

List of Figures

List of Equations

Symbols

A_b	Area of Block
A_m	Area of Mortar
C_b	Base Shear Coefficient
E_b	Young's Modulus of Elasticity of Block
E_m	Young's Modulus of Elasticity of Mortar
E_v	Young's Modulus of Elasticity of Vault
E_x	Normal Modulus of Elasticity of Vault in x-direction
E_y	Normal Modulus of Elasticity of Vault in y-direction
F	Vault Rise
F_b	Base Shear Force
G_b	Shear Modulus of Elasticity of Block
G_M	Shear Modulus of Elasticity of Mortar
G	Shear Modulus of Elasticity of Vault
L	Vault Width
L_{max}	Perimeter of Vault
T	Fundamental Period of Vibration
T_R	Return Period
W	Weight per unit surface of slab
e	Eccentricity
f	frequency
f_k	Characteristic Compressive Strength of the Masonry
f_m	Characteristic Compressive Strength of Mortar
s_{eq}	Equivalent orthotropic plate thickness
t_0	Thickness of Barrel Vault at base.
w	Vault Depth
α	Factor of Safety
Γ	Participation Factor
ϕ	Mode Shape
ν	Poisson's Ratio

Glossary

3D	Three-Dimensional
ACC	Acceleration
CM	Centre of Mass
CS	Centre of Stiffness
DL	Damage Limitation
DOF	Degrees of Freedom
DSHA	Deterministic Seismic Hazard Analysis
EC8	Eurocode 8
EMS	European Macroseismic Scale
H/H	Horizontal to Horizontal
H/V	Horizontal to Vertical
HVSR	Horizontal to Vertical Spectral Ratio
ISCARSAH	International Scientific Committee on the Analysis and restoration of Structure of Architectural Heritage
LS	Limit State
MDOF	Multi-Degree of Freedom
NC	Near Collapse
PA	Pushover Analysis
PGA	Peak Ground Acceleration
PGV	Peak Ground Velocity
PSHA	Probabilistic Seismic Hazard Analysis
SCRZ	Sicily Channel Rift Zone
SD	Significant Damage
SDOF	Single Degree of Freedom
SLC	Stato Limite di Collasso
SLD	Stato Limite di Danno
SLV	Stato Limite di Vita
URM	Unreinforced Masonry

Chapter 1: Introduction

For centuries, the predominant building material across the Maltese Islands has been unreinforced masonry (URM). This construction method, deeply rooted in tradition, is evident in the multitude of historical buildings that adorn the islands. The use of URM has persisted into the 21st century, relying largely on the contractor's experience and customary practices rather than formal seismic design codes. While this has resulted in many durable and aesthetically pleasing structures, it has also introduced significant vulnerabilities particularly in the context of seismic activity.

The Maltese Islands are in a region of low to moderate seismic risk. Lack of seismic design considerations elevates the local seismic risk, especially for historical URM buildings, which have deteriorated over time. Consequently, significant uncertainty exists regarding the performance of these historical structures under seismic action.

The conservation of Maltese cultural heritage necessitates the protection of these historical buildings, particularly chapels from seismic disasters. Despite the relatively low frequency of strong seismic events in the region, the potential impact on historic masonry structures must not be overlooked. The conservation of these buildings is crucial, given their cultural and historical significance.

The Maltese Islands are dotted with chapels that play a vital role in the local heritage. These chapels vary in size and shape but share common construction characteristics. This research focuses on several selected chapels, providing details regarding their ground geology, height, width, and length. Some of these chapels are standalone structures, while others are connected to adjacent buildings.

The chapels chosen for this study include the Chapel of St. Philip & St. James in San Gwann, located on the Lower Globigerina, and the Chapel of St. Matthew in Qrendi, which also sits on the Lower Globigerina and has an adjacent structure. Additionally, the isolated Chapel of St. Mary Magdalene in Dingli, situated on the Upper Coralline, will be examined. These chapels exemplify typical local designs, and their seismic vulnerability is a significant issue.

By examining the seismic vulnerability of these representative chapels, this dissertation aims at the contribution to the understanding and mitigation of seismic risks to Malta's historical

URM buildings. The findings will inform strategies for the preservation and protection of these invaluable cultural assets, ensuring their endurance for future generations.

1.1 Goals and Objective

The main objective of this research is to explore the seismic susceptibility of chapels in Malta using numerical structural modelling. This investigation will focus on various case studies, particularly examining Maltese chapels that are either isolated or adjacent to other buildings. Additionally, the study will consider chapels situated on different ground types, further expanding the scope of analysis. Ultimately, these case studies will be subjected to a comprehensive seismic vulnerability evaluation.

The objective about this dissertation aims to assess the seismic vulnerability of Maltese chapels that are either isolated or adjacent to other buildings. Secondly, it seeks to evaluate the vulnerability of these chapels when located on varying ground types. Finally, the study will examine the chapels under seismic conditions in accordance with the relevant Limit States as outlined in Eurocode 8. By linking these objectives, the research will provide a thorough understanding of the factors influencing the seismic resilience of Maltese chapels and offer insights for improving their structural integrity.

1.2 Research Questions

- What is the seismic performance of the chapels for the damage limit state?
- What is the seismic performance of the chapels for the ultimate limit state?
- What is the effect of having chapels on different geology and different geometry?

1.3 Methodology and Source of Information

The initial phase of this research study employs a qualitative approach, focusing on the collection of data regarding seismic activity and the damage sustained by historic structures. Investigating the impact of previous earthquakes on the chapels in the Maltese Islands is crucial. This research aims to chart the development of selected Maltese chapels, noting any structural additions, renovations, or repairs carried out over time. To verify whether these buildings have ever been damaged by an earthquake, archival research will be conducted, examining documents dating back to the 1693 earthquake.

The seismic analysis program, 3D Macro, will be employed to create 3D numerical models of the selected Maltese chapels. These models will help determine the seismic vulnerability of the chapels. Through these numerical models, the buildings' responses to seismic loading will be analysed.

The seismic assessments will focus on three main areas: modal analysis, determination of the critical earthquake direction affecting the building, and limit state analyses according to Eurocode 8: Part 3. By performing these analyses, several observations, and assessments regarding the seismic vulnerability of these structures will be mentioned and discussed.

1.4 Dissertation Structure

This document is composed of six chapters:

Chapter 1 – Introduction

This chapter presents a summary of the study's goals and describes the research methodology employed.

Chapter 2 – Literature Review

This chapter explores essential concepts related to seismic activity, divided into eight sections, the main aspects researched are:

- The effect of seismicity on society, causes of earthquake and on the Maltese Islands
- Seismic design principles for structural seismic analysis in accordance with Eurocode 8.
- Failure mechanisms and seismic load distribution in Unreinforced Masonry (URM) buildings
- Seismic vulnerability of local historical masonry buildings
- Overview of the retrofitting techniques

Chapter 3 – Selected Case Studies

This chapter examines in detail three specific case studies: St. Philip & St. James Chapel in San Gwann, St. Mary Magdalene Chapel in Dingli, and St. Matthew’s Chapel in Qrendi. It studies the characteristics of these chapels, including materials, geometry, and structural properties, using photographic data from site visits and literature sources. The chapter also discusses the historical background of these chapels.

Chapter 4 – Research Methodology

This chapter describes the methodology employed for the study, including the use of a numerical analysis program for conducting non-linear pushover seismic analyses. It offers a concise summary of the software's theory and limitations, as well as the assumptions made during the modelling process of these three chapels.

Chapter 5 – Seismic Analysis and Discussion of Results

This chapter presents the findings from non-linear pushover seismic analyses, discussing them comprehensively. It includes observations and interpretations regarding the seismic vulnerability of the three chapels, modal analysis, use of capacity curves, and limit state analysis. Additionally, the chapter compares the behaviour of these chapels, highlighting distinctions due to varying geological and geometrical characteristics.

Chapter 6 - Conclusion and Recommendations for Future Research Work

The final chapter concludes the study by summarizing its findings and suggesting possible directions for future research in this study.

Chapter 2: Literature Review

In the Maltese Islands, unreinforced masonry (URM) has been utilised in various constructions along the years and still being used nowadays. Since being able to sustain compressive loads adequately, it is frequently employed. On the other hand, it does not function as effectively under tensile pressures brought on by the overturning moments caused on by seismic activity. This chapter investigates the seismic vulnerability of unreinforced masonry buildings and retrofitting techniques.

2.1 Effect of Seismicity on Society

Seismic risk refers to the likelihood of experiencing losses from earthquakes over time, encompassing harm to human lives, societal disruptions, economic losses, and property damage (one mcm world, 2022). Influenced by hazard, vulnerability, exposure, and predictive models, it is crucial to note that a high hazard doesn't always translate to high risk, and vice versa. Without vulnerability, even a high hazard may not pose a risk (Wang, 2006; Wang, 2011).

Therefore, seismic risk can be represented through the following qualitative expression:

$$\text{Seismic Risk} = \text{Seismic Hazard} * \text{Vulnerability} * \text{Exposure}$$

Equation 1 - Seismic Risk.

Seismic hazards, which include natural phenomena such as ground shaking, fault rupture, or soil liquefaction caused by earthquakes, are a scientific concern with substantial societal impacts. Two prevalent methods for evaluating seismic hazards are probabilistic seismic hazard analysis (PSHA) and deterministic seismic hazard analysis (DSHA; Wang, 2011).

PSHA involves creating a seismic hazard curve that shows the relationship between a specific ground motion parameter and its return period. The "return period" signifies the probability of ground motion events happening within a given timeframe (Wang, 2006).

Seismic vulnerability, critical for both historical and modern structures, correlates earthquake magnitude with expected damage, emphasizing structural deficiencies and potential human and economic losses. While achieving maximum earthquake resistance is ideal, practical constraints such as cost, and the infrequency of extreme seismic events make this goal impractical. Nevertheless, safeguarding historical structures remains culturally significant despite the rarity of strong local earthquakes.

Seismic design aims to balance investment in resistance with potential damage. Quantitative evaluation of ground shaking levels is essential in the initial stages, incorporating structural vulnerability, cultural significance, and economic considerations to develop effective seismic risk mitigation strategies (Elghazouli & Peppin, 2011).

Exposure encompasses individuals, structures, infrastructure, commercial, and industrial establishments in regions prone to potential earthquake effects. Typically, planners and investors determine the extent of exposure, and decisions regarding new infrastructure may be influenced by the need to avoid significant geological hazards (Elghazouli & Peppin, 2011). In earthquake events, the majority of economic and human losses result from the collapse of buildings and infrastructure, either directly or indirectly. The trend of rapid urbanization, marked by poorly constructed housing, unregulated land use, overburdened public services, and high population densities, has increased vulnerability to earthquake effects, elevating the potential for disasters. This highlights the importance of strategic planning and risk mitigation measures to address the growing challenges associated with urban development and earthquake vulnerabilities (one mcm world, 2022).

2.2 Causes of Earthquakes

Earthquakes result from the abrupt discharge of energy within specific rock regions on Earth. The elastic energy is unleashed, producing vibrations that propagate in all directions across the Earth. These propagating vibrations are commonly known as seismic waves (Nelson, 2015). This energy discharge can stem from multiple sources, including elastic strain, gravity, chemical reactions, or the movement of large objects. Among these factors, the release of elastic strain is the most significant cause since it is the only type of energy that can accumulate in quantities substantial enough to trigger major disruptions. Earthquakes linked to this release of elastic strain are referred to as tectonic earthquakes. The elastic rebound theory offers an explanation for these tectonic earthquakes (Bolt, 2023).

The Hypocentre or Focus, often known as the earthquake's origin, determines the seismic wave's intensity. The focal depth, or the distance from the origin to the epicentre, is a measure of how much the seismic waves' energy is lost. The magnitude of an earthquake and its intensity may both be measured using accelerometers (Bányai, 1992).

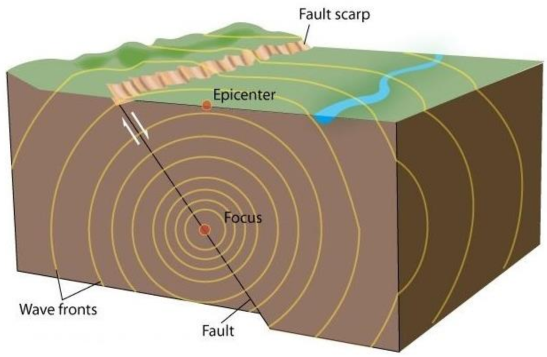

Figure 1 - The structure of an earthquake (University of Waikato Te Whare Wānanga o Waikato, 2007).

2.3 Seismicity of the Maltese islands

Malta is situated in an area characterized by low-to-moderate seismic hazards. However, the region has encountered a number of earthquakes in the past and there is a lack of seismic awareness within Maltese society. Many people tend to believe that the islands are largely immune to significant earthquakes. Nevertheless, history has demonstrated that disregarding the potential seismic threat would be an irresponsible course of action (D'Amico & Galea, 2013).

The islands of Malta are situated centrally within the Mediterranean and form a pivotal part of a complex fault system stretching from Tunisia to Sicily. Although some of the faults traversing Malta and Gozo have become inactive, others remain active. These seismic faults belong to the Pantelleria Rift, also known as the Sicily Channel Rift Zone (SCRZ) and are crucial in influencing the tectonic and geomorphic development of the Maltese Islands (Galea, 2007).

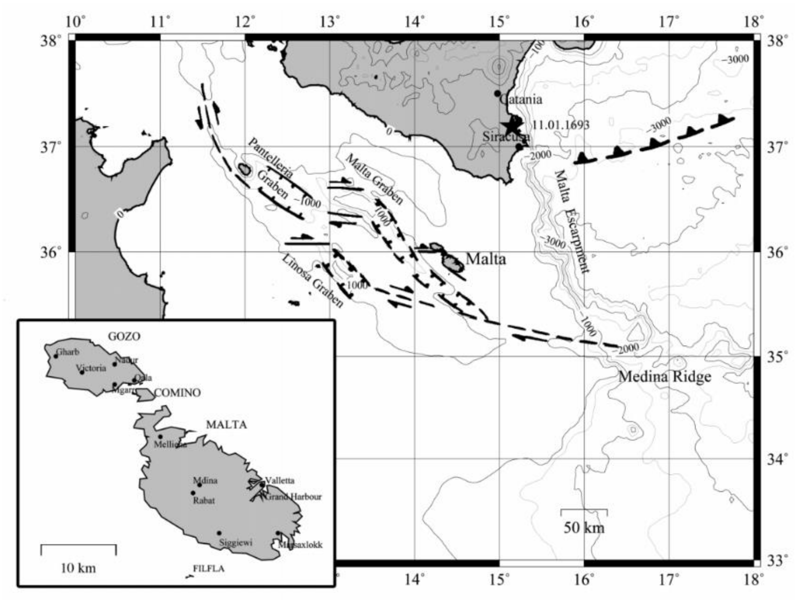

Figure 2 - The bathymetry of the Sicily Channel and the principal tectonic characteristics of the Sicily Channel Rift Zone, including normal faults and strike-slip lineaments, are depicted, adapted from Reuther and Eisbacher (1985) and Reuther (1990). Additionally featured are the subduction zone of the Calabrian Arc and the epicenter of the earthquake on November 1, 1693, as per Boschi et al. (2000). An inset displays the Maltese Island. (Galea,2007).

2.3.1 Past Earthquakes

The historical records of the Maltese islands are mainly documented from the Knights of the Order of St. John in 1530. Limited surviving documentation exists prior to this period, primarily related to Spanish dominion over the islands in the 14th century. Despite engaging with local historians, there appears to be little mention of significant earthquake consequences in these historical documents (Galea, 2007).

Addressing the issue of seismic hazard assessment begins with creating a historical earthquake record, a challenging task for a small island during the pre-instrumental era. While some felt seismic events can be linked to significant earthquakes in neighbouring regions such as Sicily or Southern Greece, others may result from offshore earthquakes in the Sicily Channel. The absence of detailed historical documentation may pose difficulties in accurately evaluating the seismic history of the Maltese islands during this period (Galea, 2007).

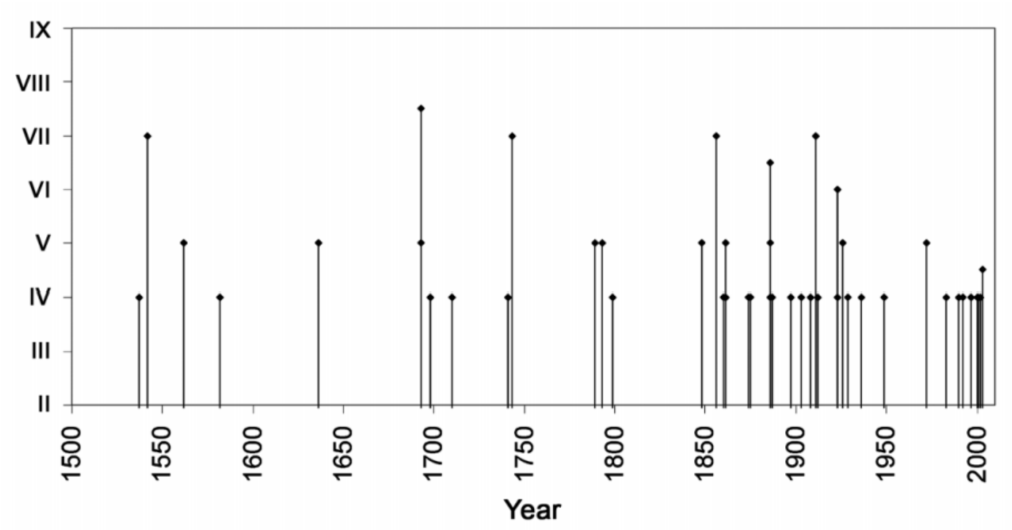

Figure 3 - Site seismic history for the Maltese islands since 1500, showing EMS-98 I≥IV (Galea, 2007).

The seismic record of the Maltese Islands begins with a mild tremor on September 1, 1537, marking the onset of a series of earthquakes and tremors documented over time. A stronger quake on March 8, 1562, caused minor injuries to workers in Vittoriosa. Subsequent tremors in 1582, 1636, 1650, 1653, 1654, 1657-1658, and November-December 1658 raised concerns but didn't cause significant damage. The most devastating earthquake hit on January 11, 1693, triggered by Mount Etna's eruption. Significant damage to buildings occurred in Valletta, Gozo, and the Three Cities as a result. This event emphasized the need to protect chapels and cultural heritage from such disasters. A detailed representation of intensities and magnitudes of recorded seismic events in the Maltese Islands since 1530 is provided in Figure 4, highlighting the importance of conservation efforts to safeguard local cultural heritage from earthquakes (Abela, 1969).

Year	Month	Day	Hour	Lat	Long	Region	I_{max} on Maltese islands	I_o	M	Parameter reference
1542	12	10	15:15	37.20	14.90	E. Sicily	VII	XI	M_w 6.6	Gruppo di Lavoro CPTI (2004)
1562	3	8	Morning			Sicily Channel?	V?			
1636	9	1				Sicily Channel(?)	V?			
1693	1	11	13:30	37.18	15.02	E. Sicily	VII-VIII	XI	M_w 7.4	Boschi *et al.* (2000)
1743	2	20	16:30	39.87	18.78	Ionian Sea	VII	IX	M_w 6.9	Gruppo di Lavoro CPTI (2004)
1789	1	19	Morning			Sicily Channel(?)	V?			
1793	2	26	Morning			Sicily Channel?	V?			
1848	1	11	12:00	37.20	15.20	E. Sicily	V	VIII-IX	M_w 5.5	Gruppo di Lavoro CPTI (2004)
1856	10	12	00:45	35.60	26.00	Crete	VII		M_w 7.7	Papazachos *et al.* (2000)
1861	2	8	23:45			Sicily Channel(?)	V?			
1886	8	15	02:45			Sicily Channel(?)	V			
1886	8	27	22:00	37.00	27.20	Aegean Sea	VI-VII	XI	M_w 7.3	Papazachos *et al.* (2000)
1911	9	30	09:25	36.4?	13.5?	Sicily Channel	VII			
1923	9	18	07:30	35.5?	14.5?	Sicily Channel	VI			ISC (2001)
1926	6	26	19:46	36.50	27.50	Aegean Sea	V		M_w 7.6	Papazachos *et al.* (2000)
1972	3	21	23:06	35.80	15.00	Sicily Channel	V		M_b 4.5	ISC (2001)

Figure 4 - A subset of the earthquake catalogue highlights events on the Maltese Islands that have registered EMS-98 intensities of V and higher (Galea, 2007).

Given the seismic history of the Maltese Islands and the deterministic impact of significant seismic sources, an estimated intensity level of VII-VIII with a return period of 475 years can be reasonably inferred. Although specific accelerometric data is not accessible, it is conceivable to propose that peak ground accelerations (PGA) expected for this return period, would probably range between 0.04 and 0.1 g (gravity). Such ground motion characteristics would classify as falling within the category that necessitates seismic design procedures as detailed in the European standard EC8 (Galea, 2007).

2.3.2 Present Situation

The urban landscape of the Maltese Islands has evolved significantly over time. Before the Knights of the Order of St. John arrived in 1530, Mdina, Birgu, and Rabat in Gozo were the main cities, with scattered villages in the countryside. The Knights fortified cities and expanded villages, influencing the region. During British rule in the 19th and 20th centuries, population and economic growth spurred urban expansion and new settlements. Post-World War II, there was substantial construction and urbanization. By 2001, the built-up area had increased from 4.5% in the mid-1960s, driven by limited land availability and taller buildings. Malta became the most densely populated EU member state. Population growth has surged, with a 60% increase since 1923 and four times the size of the population in 1693, the year of a recorded earthquake. The built-up footprint has expanded significantly, heightening exposure, and emphasizing the need to consider social and economic consequences (Borg et al., 2008).

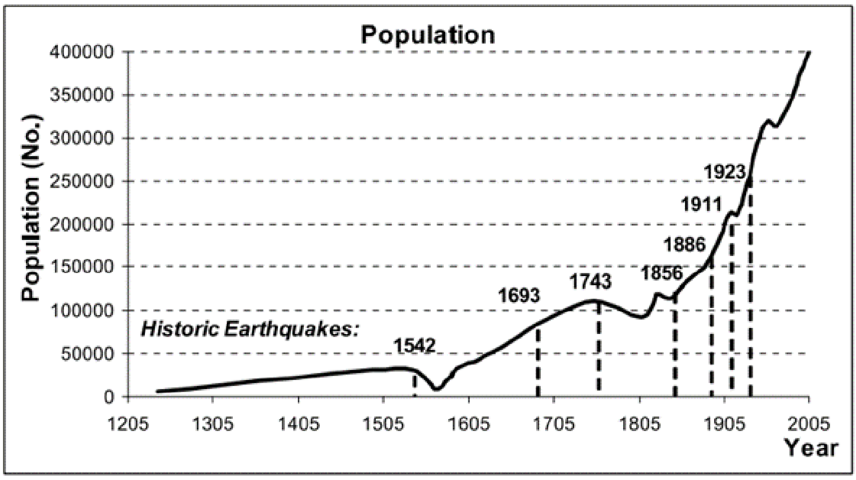

Figure 5 - Population census and historic development (NSO,2006; Abela ,1969; Galea 2007; Borg et al.,2008).

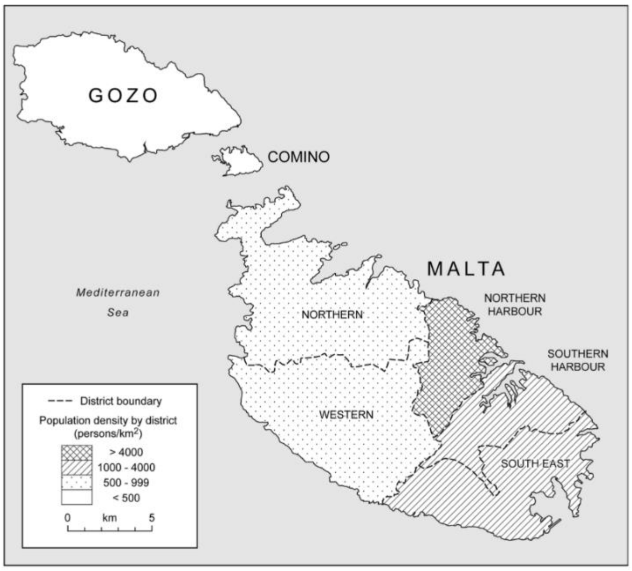

Figure 6 - Population Density Distribution by District (Main et al.,2018).

2.4 Eurocode 8

Eurocode 8 (EC8) focuses on standards and guidelines for seismic design, with primary objectives being the safeguarding of human life and minimizing structural damage. Part 3 of EC8 addresses the seismic evaluation and analysis of existing buildings, offering specific provisions applicable to all building categories. The study considers Eurocode 8's recommended seismic zones and limit states to determine seismic action.

2.4.1 Limit States

"Structures in general should be able to resist minor earthquakes without damage, resist moderate earthquakes without structural damage, but with some non-structural damage, resist major earthquakes of severity without collapse, but with some structural as well as non-structural damage" (Key, 1988).

It should be noted that there are three Limit States are specified in EC8 Part 3 with progressively higher allowable damage levels after different earthquake events.

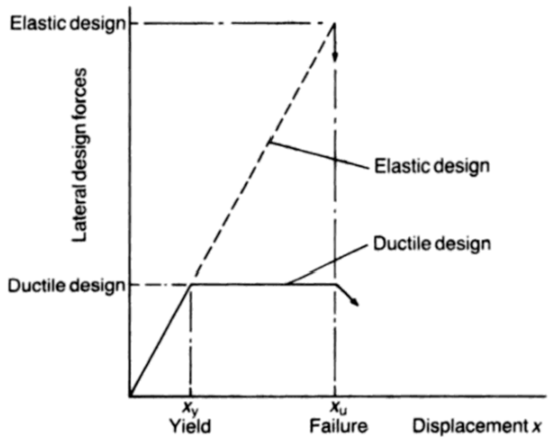

Figure 7 - Lateral design forces and ductility (Key,1988).

- Eurocode 8 emphasizes "damage limitation" during earthquakes, aiming to protect lives and assets by ensuring structures withstand minor to moderate seismic events. Provisions focus on ductility and energy dissipation to prevent failure in less severe earthquakes.

- In severe earthquakes, Eurocode 8-designed structures can sustain "significant damage," enabling extensive repairs while preserving structural integrity, surpassing the primary objective of damage limitation, highlighting greater earthquake resistance.
- Eurocode 8 addresses near-collapse scenarios, prioritizing safety, and functionality during earthquakes. It emphasizes averting imminent structural failure, aligning with its goal of safeguarding lives and preserving building integrity during seismic events. (En.1998.1.2004)

2.4.2 Seismic Actions

Malta's seismicity, according to the Italian seismic hazard map, is rated at 0.05g, placing it within EC8's Low Hazard area. The European Seismic Hazard Map slightly elevates the rating to around 0.06g. It is crucial to acknowledge the potential underestimation of seismic risk due to reliance on an incomplete seismic catalogue in southeast Sicily limits. Seismic hazard calculations commonly use Peak Ground Acceleration (PGA) associated with a return period of 475-years, roughly aligning with a 10% probability of exceeding this level within a 50-year timeframe (Borg et al., 2008; Galea, 2007).

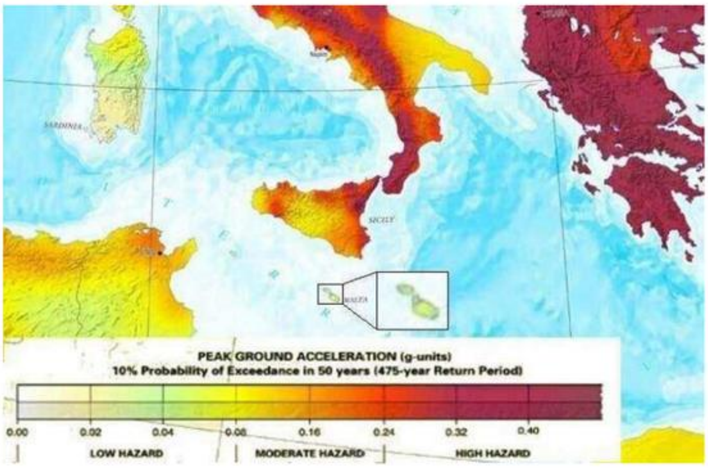

Figure 8 - The European Seismic Hazard Map (Borg et al., 2008).

The hazard model generates local PGA values, drawing from the European Hazard Map. This model illustrates the reference probability of exceedance (Pe) for different limit states on the y-axis, expressed as a percentage, plotted against the PGA on the x-axis. A distinctive curve, specific to each European country, highlights the correlation between these two axes.

2.4.3 Principles for a Good Seismic Design

2.4.3.1 Redundancy

Redundancy is widely acknowledged in structural engineering for its crucial role in enhancing safety. It allows a structural system to reallocate loads among its components or connections in case certain parts sustain damage. To ensure redundancy, having alternative load paths or load-transfer mechanisms is essential.

In contrast, structures without redundancy may immediately fail under local damage, lacking the ability to carry warning signs before complete failure. The effectiveness of structural redundancy is influenced by factors such as the design form, dimensions of the members, properties of the materials, and characteristics of the loads (Fang & Fan, 2011).

2.4.3.2 Ductility

Achieving economic design in seismic conditions often involves accepting some degree of damage instead of striving for elastic resilience, which can be economically unfeasible due to high force demands. Utilizing the inherent ductility of structures becomes essential in this approach, as it allows them to withstand substantial deformations beyond the yield point without fracturing. Ductility, defined as the capacity to endure extensive deformations over numerous cycles, plays a pivotal role in reducing force demands to acceptable levels without leading to complete collapse (Elghazouli & Williams, 2016).

2.4.3.3 Structural Shapes and Configuration

Simple and regular configurations in buildings, with a direct load transfer path, generally result in better performance in earthquakes. However, structures with plan irregularities, especially those exhibiting coupling of motions in both x and y directions, face challenges in seismic analysis. Coupling of motions is caused by stiffness forces acting at the centre of stiffness (CS) and inertia forces at the centre of mass (CM), generating torsional moments and twisting motions in the building (Dhapekar, Apr 27, 2022; Alexander, 2010).

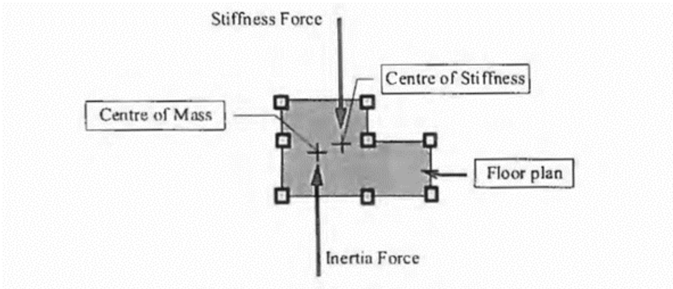

Figure 9 - Irregularity in Plan (Alexander, 2010).

The distance between the CS and CM is referred to as eccentricity, and even in symmetric plans, unsymmetrical live load distribution or accidental eccentricity due to CM movement can occur. The yielding of structural members further complicates the situation as the location of the centre of stiffness changes (Alexander, 2010).

Contemporary seismic design codes, including EC8, introduce the concept of building regularity, distinguishing between plan regularity and elevation regularity. Elevation irregularities, such as setbacks or abrupt size changes, can lead to shifts in the positions of CM and CS, causing torsional motion. This irregularity increases response spectra in the analysis, introducing greater uncertainty in assessing such structures (Alexander, 2010).

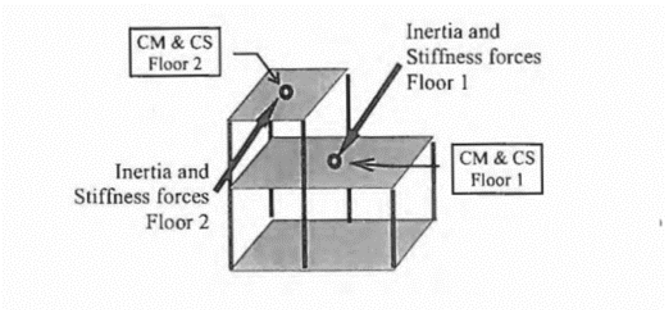

Figure 10 - Irregularity in Elevation (Alexander, 2010).

2.5 Failure Mechanism on URM buildings and Seismic Load Transfer

Unreinforced masonry structures lack seismic resistance as they were originally designed for gravity loads, neglecting earthquake forces. Masonry, made of materials like bricks, blocks, and mortar, typically contains substances such as clay, bitumen, chalk, lime-/cement-based mortar, and adhesives. Despite variations, various stonework types share common traits: specific mass, shear strength, low tensile strength, and low ductility, often showing brittle behaviour. Historically, these buildings were designed to withstand vertical static loads, ignoring seismic impacts (Lourenço et al., 2011a).

During earthquakes, buildings undergo ground displacements, inducing inertial forces. Structural response depends on natural frequencies, damping, mass, and stiffness. In unreinforced masonry (URM) buildings, seismic energy travels through the foundation, reaching sturdy in-plane structural walls. The response of these walls, influenced by height, stiffness, and stress, excites the floor diaphragm via wall-to-floor connections. This motion, filtered by the shear wall, affects out-of-plane walls through the same connection. Dynamic characteristics directly affect out-of-plane wall severity, emphasizing differences in input excitation at bottom and top of face-loaded walls (Doherty et al., 2002).

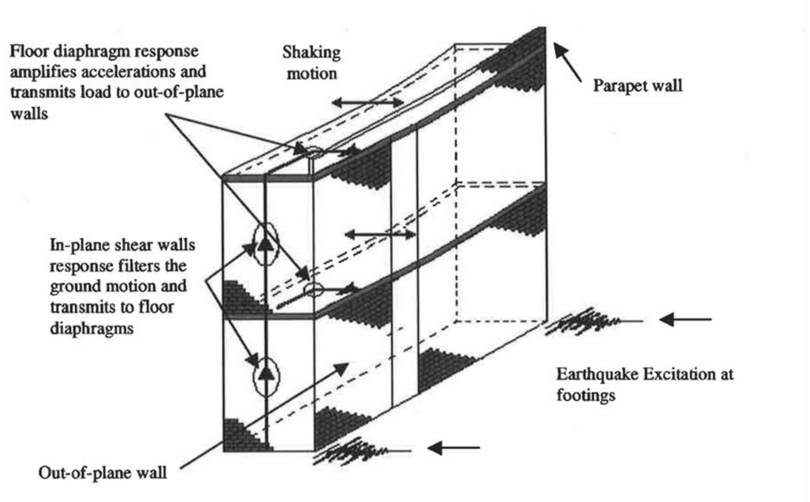

Figure 11 - Seismic Load Path for Unreinforced Masonry Building (Doherty et al.,2002).

2.5.1 Walls

Enhancing the seismic performance of structures involves promoting simplicity and regularity in both the horizontal plane and elevation. This includes aspects such as geometric uniformity, mass distribution, and stiffness distribution. These characteristics serve to mitigate local damage and reduce torsional effects. Usually, masonry buildings have load-bearing walls with in-plane dimensions significantly greater than their depth. Consequently, the seismic performance of these load-bearing walls is greatly influenced by the direction in which horizontal loads are applied (Lourenço et al., 2011b).

Unreinforced masonry shear walls play a crucial role in supporting lateral loads in buildings, such as those from wind and seismic forces. Understanding the fracture and failure of these walls involves navigating the complex interplay between mortar joint shear failure and compressive failure, typically occurring at the base or toe of the wall, due to the combination of lateral and vertical loads inducing tension, shear, and compression forces within the masonry wall (Chaimoon & Attard, 2007).

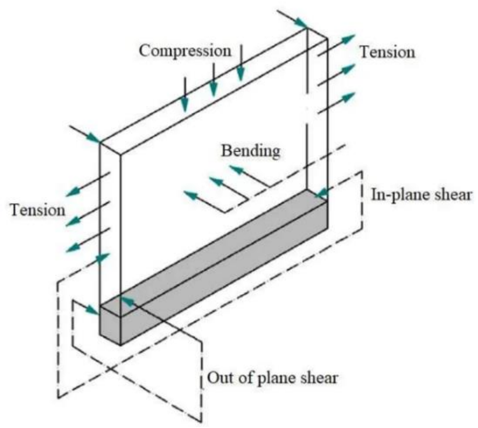

Figure 12 - Static and Seismic Loads Operate on Masonry Wall (Marku, 2022).

2.5.1.1 In -Plane Loading

Masonry walls predominantly experience in-plane forces, such as the combined effects of vertical and lateral loads (wind and/or seismic forces). Moreover, owing to its complex nature and vulnerable orientations, unreinforced masonry exhibits significant anisotropic behaviour. This underscores the critical need for accurately determining the strength parameters of masonry (Mojsilovic, 2011).

In-plane loading induces compressive stresses across the section of the wall. The compressive strength of unreinforced f_k masonry, constructed with standard mortar, is determined by the following equation:

$$f_k = K\, f_b^{\,0.7}\, f_m^{\,0.3}$$

Equation 2 - Characteristic Compressive Strength of Masonry (Equation 3.1 of Eurocode 6, Part 1-1).

Where:

f_k	Characteristic compressive strength of the masonry, in N/mm^2
K	Constant
α, β	Constants recommended 0.7, 0.3 respectively
f_b	Normalized mean compressive strength of the units, in N/mm^2
f_m	Compressive Strength of the Mortar, in N/mm^2

In-plane failure occurs when there is an excessive in-plane load. Figure 13 presents the three possible modes of local failure, which depend on the condition of biaxial stress.

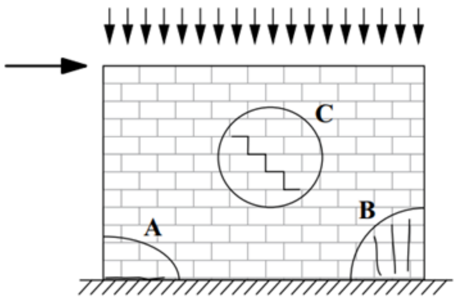

Figure 13 - Different types of failure that can occur in masonry wall (Lang, 2002).

Tensile failure at the heel (region A) occurs when horizontal forces dominate over low vertical loads, leading to horizontal sliding along bed joints. Flexural failure at the toe (region B) results from tensile cracks developing at the base. Final failure involves either wall overturning or the compression corner crushing, commonly observed in walls with a significant height-to-length ratio. Shear failure (region C) is characterised by diagonal cracks, typically seen in walls with a small aspect ratio. In cases of small vertical loads, cracks appear in mortar joints, allowing sliding and causing notable deformations. With larger vertical loads and weaker bricks, diagonal cracks may extend through the bricks, prompting sliding along a more regular diagonal crack (Lang, 2002).

2.5.1.2 Out of Plane Loading

In the presence of an evenly distributed vertical load applied concentrically, each segment of the structure is presumed to bear an equivalent compressive force. However, when the wall experiences lateral loads and undergoes bending or flexure, stress distribution at any cross-section may transition from compression on one side to tension on the opposite side, unless the wall has previously cracked. Figure 14, the resultant tensile stress, stemming from the wall's flexural deformation, is referred to as the flexural tensile stress. If these tensile stresses exceed the wall's resistance to tension, the section will ultimately experience cracking (Curtin et al., 2006).

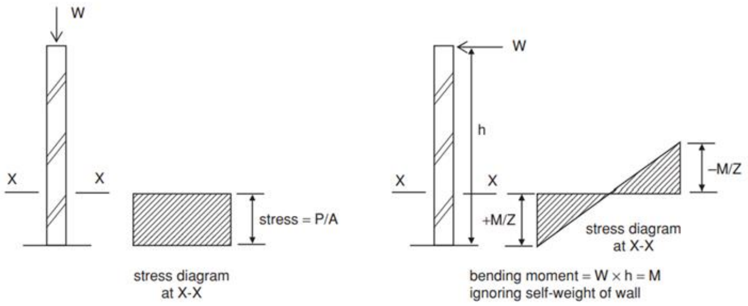

Figure 14 - Behaviour of Blocks Under Vertical and Horizontal Stress (Curtin et al.,2006).

Masonry exhibits anisotropic characteristics, meaning it lacks uniform properties in both vertical and horizontal directions. Consequently, it does not offer equal resistance to bending in these orientations. The choice of span orientation, whether vertical or horizontal, is contingent upon the supporting condition, aligning with distinct failure planes (Curtin et al., 2006).

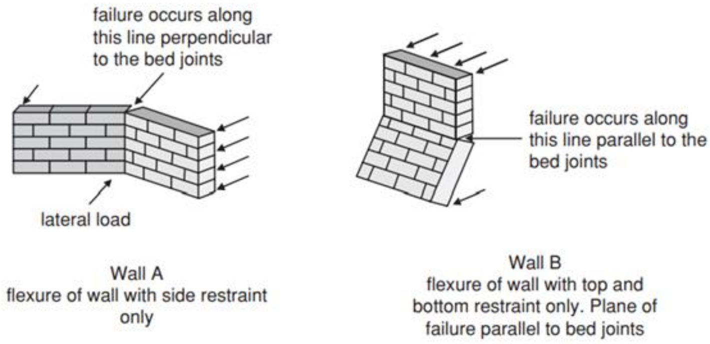

Figure 15 - Critical failure planes of laterally loaded masonry wall panels (Curtin et al., 2006).

With increasing wall height, the compressive force induced by the dead load of the masonry also increases. This augmented stress, combined with flexural tensile stresses, suggests that, particularly under significant vertical loading, the wall becomes more capable of resisting lateral loads when spanning between its upper and lower supports (Curtin et al., 2006).

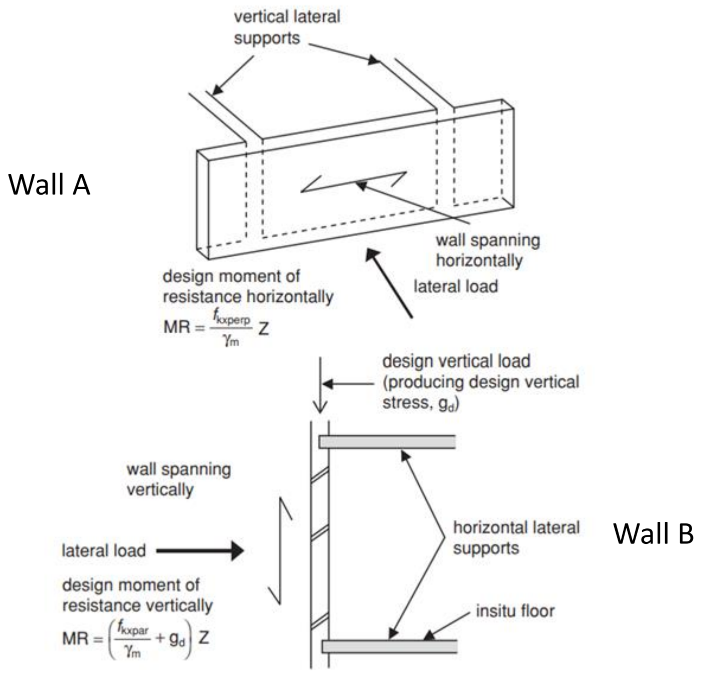

Figure 16 - Effective resistance moment for masonry wall panels under lateral loads (Curtin et al., 2006).

Wall-floor connections significantly affect masonry wall stability. Strong connections reduce out-of-plane risks, making in-plane issues more critical. Weak links between walls and floors can cause out-of-plane failures first. Without these connections, walls function as fragile cantilevers, prone to bending failures, changing building vulnerability (Curtin et al., 2006).

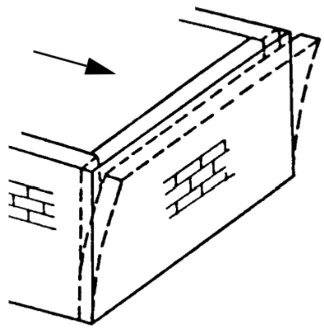

Figure 17 - Out of Plane Behaviour (Lang, 2002).

Moreover, in practical terms, earthquake forces often do not align with the principal directions of the building. As a result, the walls undergo both lateral and perpendicular movement (Lang, 2002).

2.5.1.3 Wall Openings

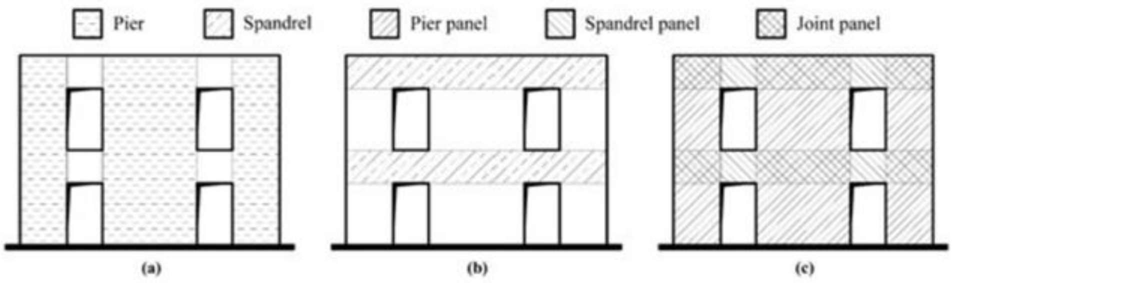

Figure 18 - Identification of (a) piers, (b) spandrels, and (c) macro elements in a standard masonry wall with openings (Parisi & Augenti ,2013).

Unreinforced masonry walls often incorporate openings like windows and doors, which can compromise their structural integrity, particularly in seismic events. Masonry walls with irregularly positioned or sized openings experience nonuniform gravity load distribution among piers, leading to potential localized damage and a heightened risk of premature collapse during earthquakes (Parisi & Augenti, 2013).

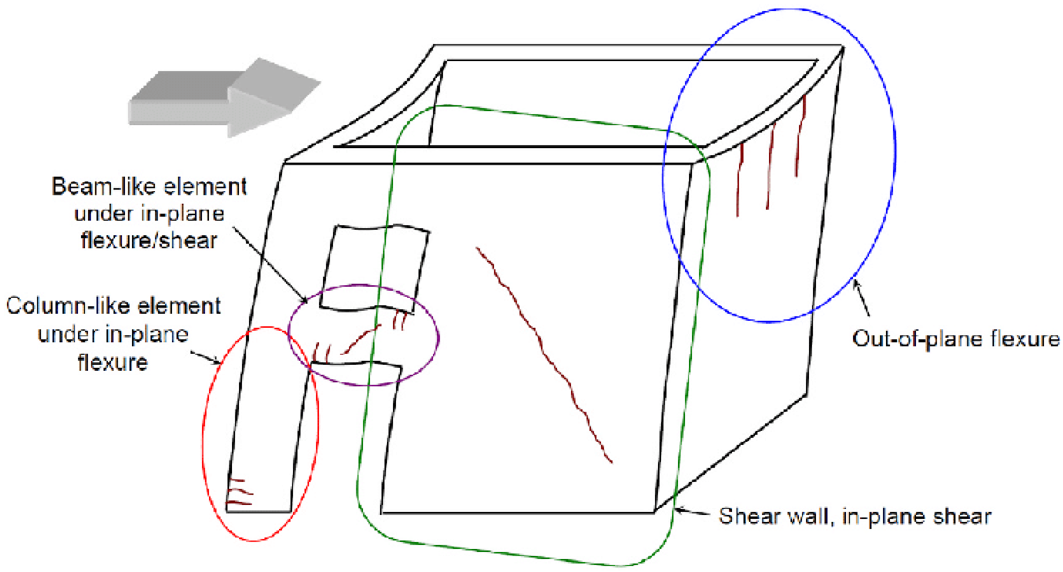

Figure 19 - Effects of Seismic Actions on Unreinforced Masonry (Gkournelos et al.,2022).

The presence of concentrated stresses around these openings may result in cracks or complete failure, jeopardizing the stability of the entire wall or adjacent sections. The presence of large openings in shear walls reduces their ability to withstand lateral forces, leading to diagonal cracking in the masonry around and near the openings. To mitigate these risks, it is advisable to keep openings small and away from corners, as cracks induced by in-plane shear forces and out-of-plane flexure may pose uncertainty concerns, especially if there is significant relative displacement across the cracks (Jamal, 2017).

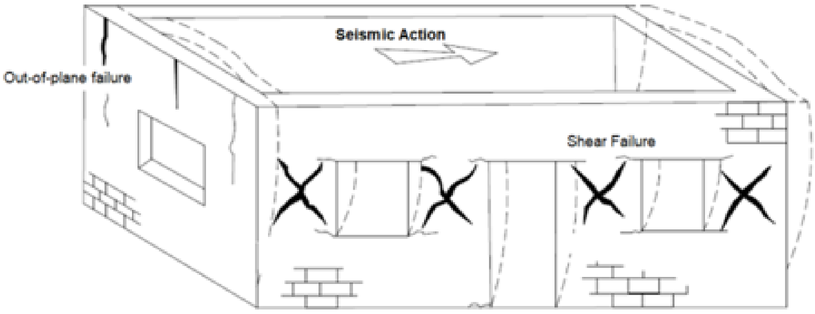

Figure 20 - Collapse Mechanisms in Masonry Walls (Megalooikonomou et al., 2018).

2.5.2 Diaphragm

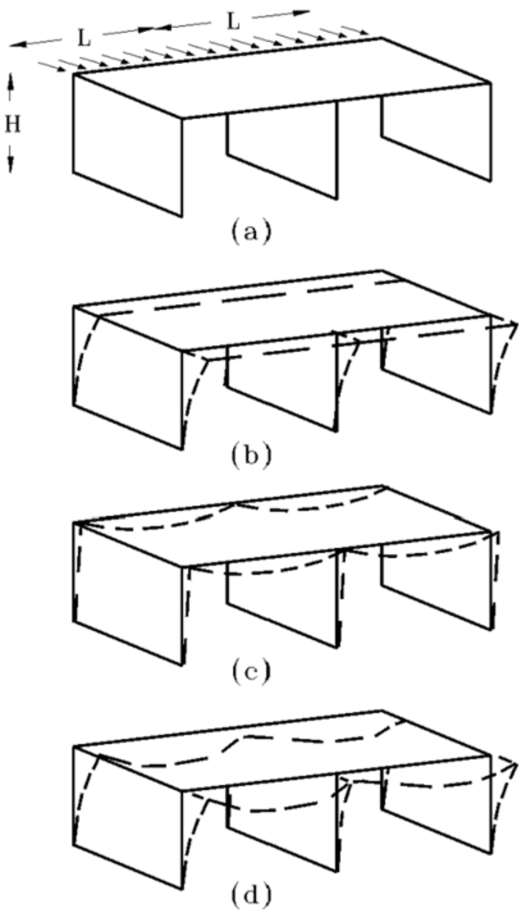

Figure 21 - Diaphragm behaviour (a) Loading and building proportions (b) Rigid diaphragm behaviour (c) Flexible diaphragm behaviour (d) Semi rigid diaphragm behaviour (Naeim & Boppana, 1989).

The stability of a building relies on its horizontal elements, like floors and roofs, serving as diaphragms to resist lateral forces. In earthquakes, unreinforced masonry structures may face diaphragm failures, including cracking, detachment, or collapse, jeopardizing overall stability, and potentially causing progressive collapse. Insufficient anchoring results in a diaphragm pushing against the wall, while inadequate shear transfer between diaphragms and reaction walls can lead to corner damage a rare occurrence during seismic events. The separation of walls and diaphragms can lead to building collapse (Jamal, 2017).

Diaphragms play a critical role in transferring lateral forces from the floor system to the vertical elements of the seismic resistance system. Beyond gravity load resistance, building floors and roofs are designed as diaphragms to distribute seismic forces to horizontal resistance elements and unify the structure during earthquakes. The effectiveness of a structure's robustness and redundancy is heavily reliant on diaphragm performance (RangaRajan, 2011).

Primary diaphragms include flexible, rigid, and semirigid types. Flexibility determines lateral force resistance. Rigid diaphragms transfer load to frames or shear walls, while semirigid ones mimic actual stiffness. Diaphragm type affects lateral force distribution to vertical elements. Rigid diaphragms resist membrane deformation, unlike semirigid ones (Adams, 2022).

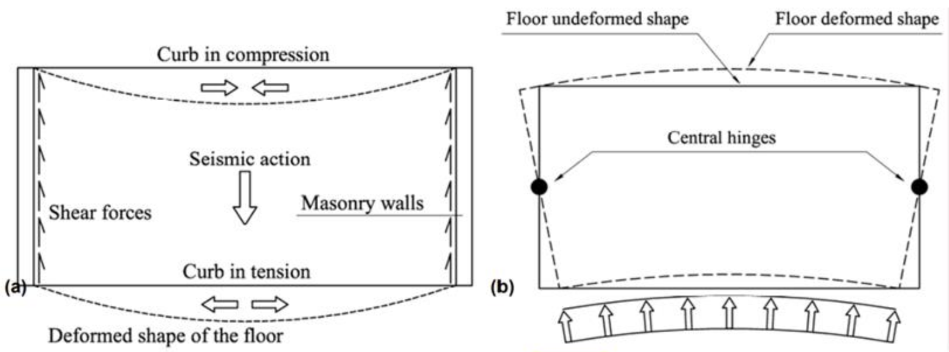

Figure 22 - (a) actual behaviour of the horizontal diaphragm, considering actual boundary conditions and the function of lateral connections.; (b) The experimental setup configured for laboratory tests (Piazza et al., 2008).

2.5.3 Pounding

Damage during seismic events often results from structural interactions between neighbouring buildings, known as earthquake-induced pounding. This occurs when adjacent buildings in proximity or with minimal separation collide due to out-of-phase vibrations. Insufficient gaps exacerbate the issue. Pounding has been identified as a major contributor to damage or collapse in certain earthquakes. Amplification of pounding occurs when neighbouring structures have different natural periods, leading to out-of-phase vibrations a common scenario due to varying dynamic properties, as depicted in Figure 23 (Miari et al., 2019).

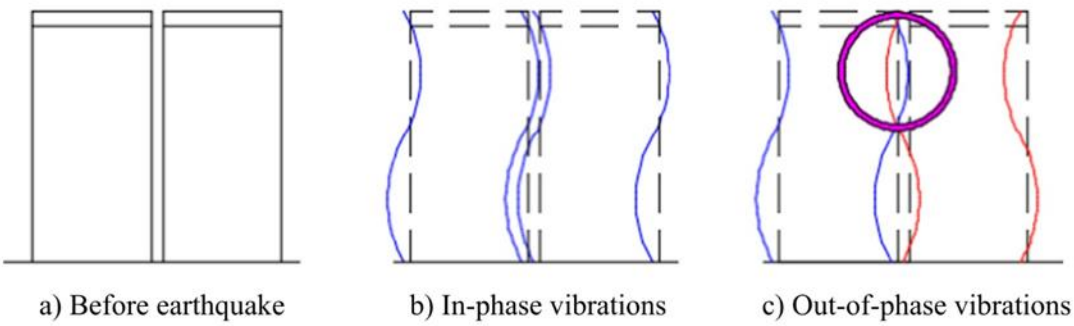

Figure 23 - Seismic Behaviour of Adjacent Buildings (Miari et al., 2019).

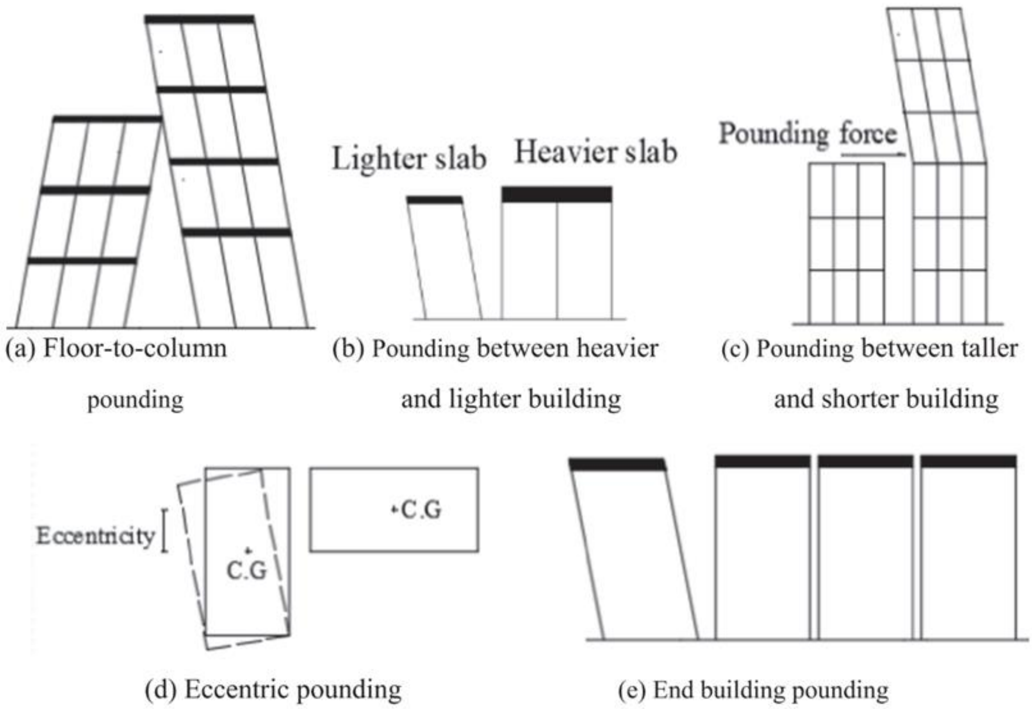

Figure 24 - Pounding Configurations (Miari et al., 2019).

2.5.4 Arches, Vaults, and Cupolas

Masonry arches, vaults, and domes are crucial factors contributing to the seismic risk of historical buildings. Pushover analysis is used to assess their seismic capacity, revealing their susceptibility to earthquake-induced damage and collapses, particularly in historic structures (Rodrigues et al., 2017).

In the past, curved masonry structures, particularly vaults, served as a primary solution for spanning wide openings (De Fabrizio & Mallardo, 2023). Arches structurally bear horizontal loads through internal compression, and their classification is based on geometrical shape, influencing their structural behaviour. Arches, being fundamental geometric forms, serve as the foundational elements for the evolution of domes and vaults (Mahdi, 2016). Vaults, functioning as one-way roofing systems, transfer loads through arch action along a single curved plane to constant supports, with stresses being compressive. Traditional construction featured vaults of various shapes and forms (Mahdi, 2016).

Arches, being among the oldest and aesthetically appealing structural forms, are well-suited for masonry construction due to their inherent ability to resist compressive forces. Over time, there have been captivating advancements in masonry construction, evolving from arches to vaults and domes (Curtin et al., 2006).

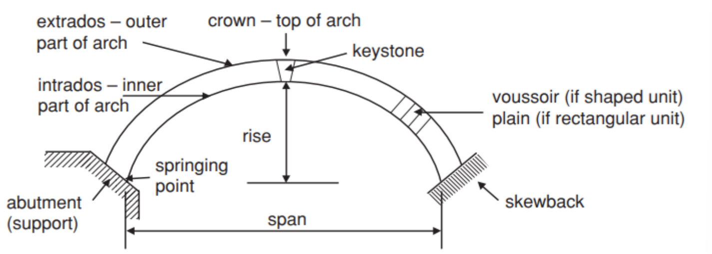

Figure 25 - Typical Arch (Curtin et al., 2006).

Fixed masonry arches, lacking hinges, endure downward loads that generate lateral and compression thrusts within the length. These thrusts create compression among the masonry units, with the arch applying pressure against the abutments. When the thrust line is centred, the arch ring experiences uniform compressive stress (Curtin et al., 2006).

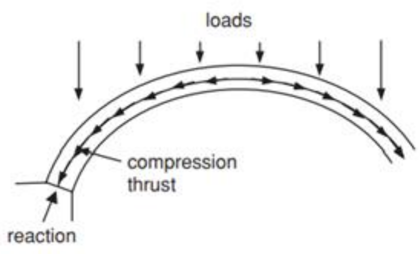

Figure 26 - Loading and Thrust in an arch (Curtin et al.,2006).

To keep masonry structures safe, the thrust line must stay inside the arch. If forces go beyond the middle third, it causes tension, leading to deformation. Interaction between the thrust line and the arch's curves can create hinges, causing cracks from voussoirs rotating. Many hinges can lead to collapse (De Matteis & Cacace, 2019).

2.6 Seismic Vulnerability

The vulnerability of a structure to seismic activity is determined by its vulnerability to damage caused by seismic shaking at a defined intensity level. In the analysis of vulnerability, the anticipated damage for a structure or a group of structures is expressed as a function of ground motion, shown in Figure 27. Two critical components of vulnerability analysis include the structural capacity of the building and the seismic forces it encounters. This analysis estimates seismic damage by comparing the building's ability to resist constraints (capacity) with the constraints imposed by earthquake ground motion (Lang, 2002). Structural vulnerability, as outlined by (Mohan & Suresh, 2017), pertains to the susceptibility of the essential supporting components of a building when exposed to high earthquakes or additional hazards.

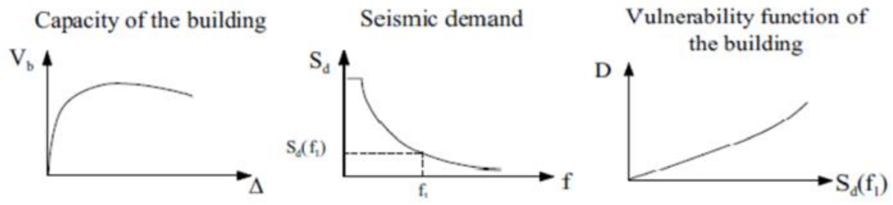

Figure 27 - Relationship of a Seismic Vulnerability Function (Lang,2002; Mohan & Suresh,2017).

Vulnerability assessment methods are typically categorized into four groups based on the origin of damage information: judgment-based, empirical/statistical, analytical, and hybrid approaches (Eleftheriadou & Karabinis, 2012).

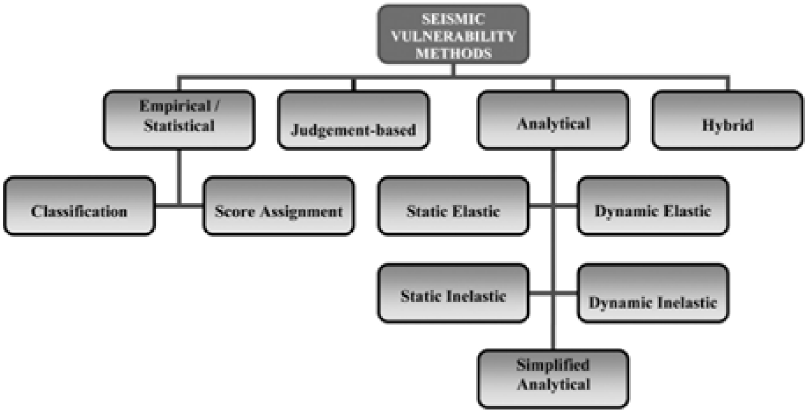

Figure 28 - Seismic Vulnerability Methods (Rossetto and Elnashai ,2003).

Fragility and vulnerability functions are developed using empirical and analytical methods. Empirical approaches rely on lab tests or damage reports but may lack objectivity and accuracy in ground motion assessment. Analytical methods involve modelling structures and subjecting them to loads or accelerograms for improved precision, overcoming empirical limitations (Díaz Guzmán et al., 2023).

2.6.1 Judgement-Base Methods

Seismic vulnerability assessment through judgment-based methods entails experts utilizing their expertise to qualitatively assess the potential impact of earthquakes on structures, particularly when quantitative data is scarce. The level of uncertainty in this approach is heavily influenced by this. However, a significant drawback is the subjectivity of the results and the challenge in checking them. An additional problem is that the degree of uncertainty in the seismic analysis may be underestimated (Porter, 2021; Calvi et al., 2006).

2.6.2 Empirical Methods

Empirical seismic assessment predicts building vulnerability using historical data. It observes damage in similar buildings during earthquakes but has limited scope. Fragility functions are derived from observational data, offering insights but face challenges in data scarcity and repair cost estimation. Empirical methods categorize buildings and derive vulnerability functions through regression but lack information on damage causes and specific structural behaviour effects (Porter, 2021; Ayala & Speranza, 2003; Calvi et al., 2006).

2.6.3 Analytical Methods

Analytical methods for estimating vulnerability functions in engineering involve four key stages: defining the asset at risk, conducting a hazard analysis to assess environmental excitation probabilities, performing structural analysis to estimate facility responses, and analysing probabilistic damage and losses. This iterative process considers uncertainties and connects environmental factors to overall risk. It emphasizes integrating the vulnerability function and hazard curve for comprehensive risk assessment and management (Porter, 2021).

2.6.3.1 Hazard Analysis

Seismic hazard assessment uses methods like hazard curves on x-y charts. Shaking intensity is on the x-axis, and y-axis shows exceedance probability. Instrument constraints limit capturing true 3-dimensional ground motion. Seismic design often employs equivalent static force based on max acceleration response, shown in acceleration response spectra. Elastic response spectra, like EC8's Figure 29, categorize seismicity and soil types for detailed hazard understanding in design and risk reduction (Elghazouli & Williams, 2016b; Porter, 2021).

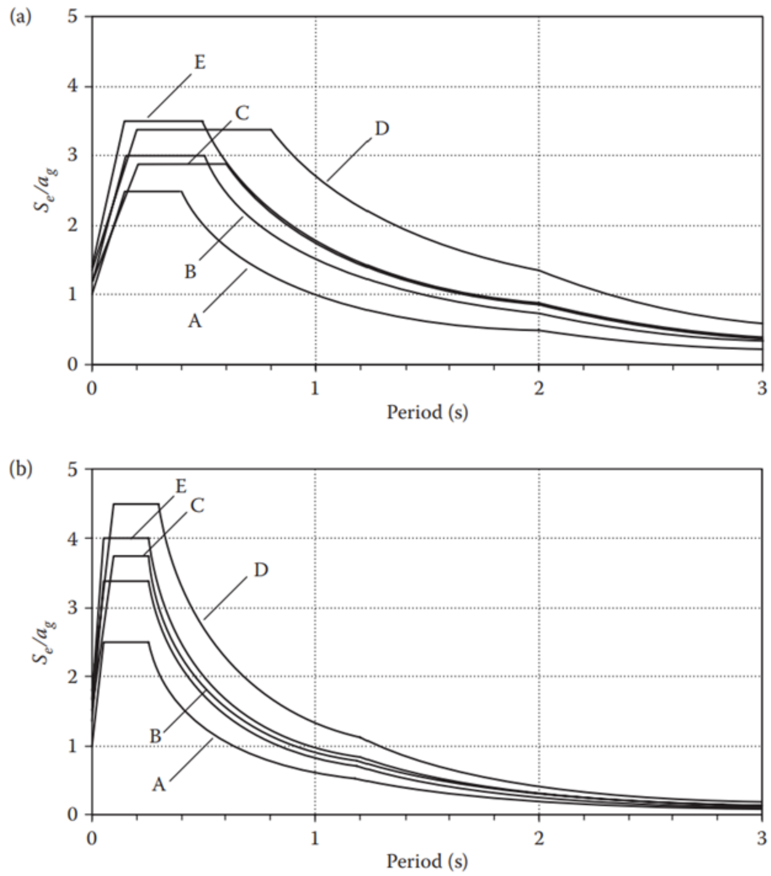

Figure 29 - EC8 5% Damped, Elastic Spectra (Elghazouli & Wiliams,2016).

2.6.3.2 Structural Analysis

In structural analysis, engineers build a model of a building to predict its response to seismic loading. This response is quantified using engineering demand parameters, influenced by seismic excitation and design factors. Structural analysis usually includes a series of nonlinear time-history analyses (Porter, 2003).

Engineers often use computer models to represent structures, mainly for linear analysis. However, this approach falls short in capturing masonry structures' behaviour accurately. Linear analysis is only suitable for initial assessments. For more realistic results, non-linear material models are necessary. These models are vital to simulate non-linear anisotropic behaviour and post-peak load capacity, this could potentially clarify the historical durability of masonry buildings under seismic stress (Mistler et al., 2006).

The procedures for analysis can be categorized into linear methods, encompassing both static and dynamic linear analyses, and nonlinear methods, including both static and dynamic non-linear analyses (Lang, 2002).

- Linear Static Analysis

  The building is represented in a linear static procedure as an equivalent single-degree-of-freedom (SDOF) system, characterised by linear elastic. The model incorporates stiffness and an equivalent viscous damping factor. In this approach, seismic excitation is simulated using an equivalent lateral force to generate stresses and strains equivalent to those caused by the represented earthquake (Lang, 2002).

- Linear Dynamic Analysis

  The earthquake motion is simulated using either modal response spectrum analysis or historical time analysis in a dynamic linear approach. Additionally, the structure is represented as a multi-degree-of-freedom (MDOF) system with a linear elastic stiffness matrix and an equivalent viscous damping matrix (Lang, 2002).

- Non-Linear Static Analysis (Push Over Analysis)

  Non-linear static analysis, also known as pushover analysis, subjects a structure to gravity loading through a monotonic lateral load pattern. The applied lateral load represents the earthquake-induced base shear range, producing a static pushover curve that charts a strength-related parameter in relation to deflection (Rana & Rana, 2015). This method is valuable for identifying structural weaknesses and provides insights into ductile capacity, revealing details about failure mechanisms, load levels, and deflection points (Mistler et al., 2006; Napier & Ondrej, 2014).

- Non-Linear Dynamic Analysis

  In non-linear dynamic procedures, the structure model incorporates inelastic material response through finite elements, like non-linear static procedures. The key difference lies in seismic input modelling, which utilizes time-history analysis, involving a step-by-step evaluation of the building response over time.

Developed using a 3D numerical model, the capacity curve is created to depict the building's primary mode response, assuming the structure primarily reacts to seismic input through its fundamental vibration mode. In this study, a non-linear static procedure is employed to create the numerical model using 3D Macro (Lang, 2002).

Masonry's properties vary due to mortar joints, especially bed and head joints acting as weak planes. Failure depends on joint orientation, unit dimensions, and properties. Failure can arise either exclusively within joints or affect both joints and units. Brick masonry models, commonly used, are grouped into three categories based on refinement, showing various levels of sophistication (Asteris et al., 2014):

- Macro-Modelling (Masonry as One-Phase Material)
  - Treats masonry as a unified entity without classifying individual units and joints.
  - Suitable for analysing large structures but lacks detailed stress analysis for smaller panels.
  - Challenges in capturing all potential failure mechanisms, especially the impact of mortar joints as planes of weakness (Asteris et al., 2014).

- Simplified Micro-Modelling (Masonry as a Two-phases Material)
  - Models expanded units using continuum elements, while mortar joints and unit-mortar interfaces are simulated with discontinuous finite elements.
  - Views masonry as a dual-phase material, with elastic blocks interconnected by potential fracture or slip lines at joints.
  - Aims to balance computational intensity and versatility for a wide range of structural systems (Roca et al., 2010; Asteris et al., 2014).

- Detailed Micro-Modelling (Masonry as a Three-phases Material)
  - Includes detailed descriptions of the units, mortar, and the interface between units and mortar.
  - Uses continuum finite elements for units and mortar at joints, while the unit-mortar interface is represented by discontinuum elements accommodating potential crack or slip planes.

- Highly accurate in simulating actual masonry behaviour, especially in capturing local material responses.
- However, greater precision results in higher computational demands, restricting its use to smaller laboratory specimens and structural intricacies (Asteris et al., 2014).

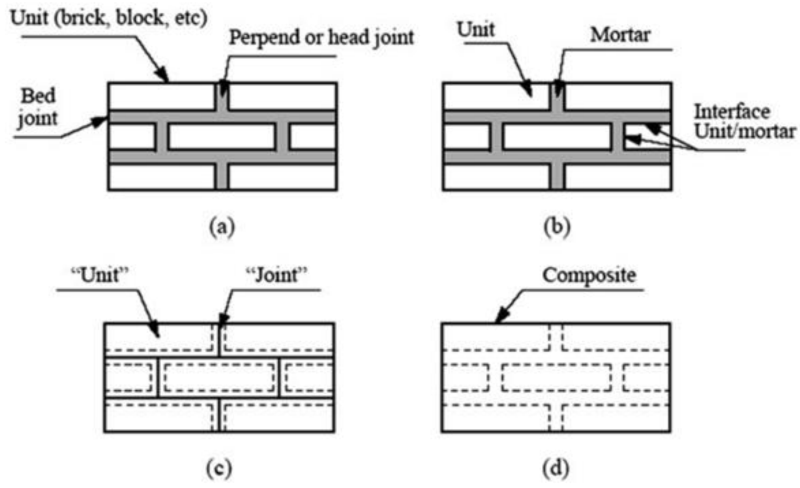

Figure 30 - Modelling Strategies for Masonry Structures Masonry Sample: (a) Detailed (b) Simplified (c) Micro-Modelling (d) Macro-Modelling (Roca et al., 2010).

Choosing a modelling approach for masonry structures balances accuracy and simplicity. Micro-modelling provides detailed insights into local behaviour, while macro-modelling is ideal for structures with large solid walls, prioritizes practicality, efficiency, and user-friendly mesh generation. This makes macro-modelling suitable for real-world applications with relatively uniform stresses along a macro-length (Lourenço & Oliveira, 2007).

2.6.3.3 Damage Analysis

Damage analysis uses insights from various sources to quantify structural and non-structural damage based on engineering demand parameters. The results, typically presented in fragility curves, offer a valuable framework for assessing the conditional probability of different damage states in relation to these parameters. These curves aid in quantifying building damage measures through engineering demand parameters derived from response analysis (Yang et al., 2009).

2.6.3.4 Loss Analysis

Loss analysis is essential for informed risk management decisions, converting damage quantities into actionable variables. This includes evaluating materials for repair, labour expenses, repair durations, and impacts on individuals affected by specific damage conditions. Results can be quantified using metrics such as the average rate of exceeding repair cost thresholds, impact on human life, cumulative expected monetary loss from recurring hazards, and total financial impact on a facility under specific hazard scenarios (Yang et al., 2009; Dyanati et al., 2017).

2.7 Seismic Vulnerability of Local Historical Masonry Buildings

The prevalence of Unreinforced Masonry (URM) structures in developing nations poses a significant earthquake risk due to their rigid and low-ductile characteristics. Past seismic events have resulted in extensive damage, causing economic and human losses (Mazumder et al., 2021).

Heritage buildings, particularly old structures with historical or artistic significance, face heightened uncertainties. Challenges include the rarity of original design documents, difficulties in defining structural diagrams, and assessing material properties in both original and current states. Differentiating between 'historical' and 'monumental' heritage buildings, seismic vulnerability varies based on multiple parameters (Augusti & Ciampoli, 2000a; Mohan & Suresh, 2009).

Guidelines from ISCARSAH in 2003, based on the ICOMOS Charter, stress structural engineering's role in preserving architectural heritage. A multidisciplinary approach is vital, with engineers considering cultural values, historical states, construction methods, changes over time, and present conditions (ICOMOS, 2003).

Structures of architectural heritage present unique challenges due to their historical context, requiring analysis and repair methods aligned with cultural considerations. Challenges in dealing with uncertainties, such as limited availability of original documents and difficulties in defining structural diagrams (Augusti & Ciampoli, 2000b). The guidelines stress the importance of transparently declaring assumptions and exercising cautious interpretation to ensure reliable results in representing material characteristics and structural behaviour (ICOMOS, 2003).

Some uncertainties include:

- Building History (anything conducted previously on the structure)
- Soil and Foundation
- Lack of experimental data
- Material Deterioration
- Structural Geometry and Methodologies

Seismic vulnerability assessment in heritage buildings is complex due to uncertainties in structural characteristics and material properties. Effectively managing this uncertainty is crucial, emphasizing the need for calculating non-linear dynamic responses and estimating damage under different earthquake intensities. Results should be presented probabilistically, considering material strength distributions and relevant parameters. However, vulnerability assessments often express deterministically, lacking clarity in conveying true structural vulnerability (Pelà, 2014; Augusti & Ciampoli, 2000b).

2.8 Retrofitting

This research focuses on retrofitting Unreinforced Masonry (URM) chapels to preserve historical architectural heritage facing seismic risks. Limited available information necessitates emphasis on URM building retrofitting. Stone masonry structures, vulnerable during seismic events, need retrofitting for resilience. Given economic and cultural constraints, extensive removal is impractical. Retrofitting approach depends on socio-economic and technical factors, including construction materials, building condition, and anticipated ground shaking. Interventions include preservation, rehabilitation, and reconstruction. Tailoring strategies for each project is challenging, considering retrofit degree, risk assessment, technical constraints, historical value, and economic limitations. Prioritizing strategies aims to maintain historical integrity while minimizing material removal (Bothara et al., 2004 ; Zucca et al., 2022 ; Guh et al., 2006).

2.8.1 Retrofitting Techniques

2.8.1.1 Tie Rods

Ties play a critical role in seismic retrofitting of historical structures, linking opposite walls. Although timber tie beams are considered, steel rods (16 to 20 mm in diameter) are more frequently used, anchored into masonry walls with steel anchor plates. Accurate dimensions of these plates are essential to prevent shear failure. This retrofitting improves the structural integrity, minimizing the risk of out-of-plane instability and collapse. Figure 31 illustrates the typical placement of steel tie rods beneath floors to avoid disruption of occupied spaces (Bernardini & Ferreira, 2022). Experimental studies on brick masonry buildings confirmed ties' crucial role in preventing wall separation and disintegration (Zucca et al., 2022); (Tomazevie, 1999).

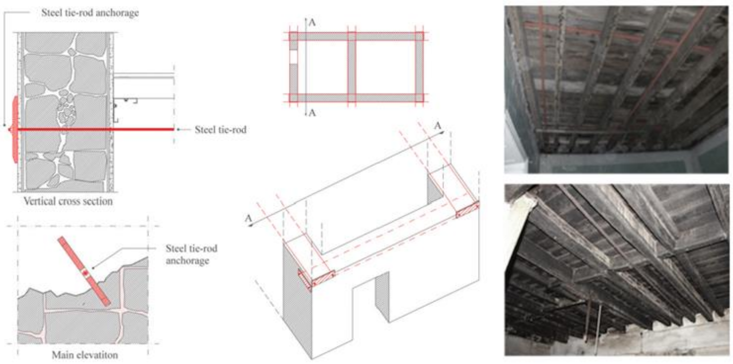

Figure 31 - Enhancement of inter-wall connections using steel tie rods (Bernardini & Ferreira, 2022).

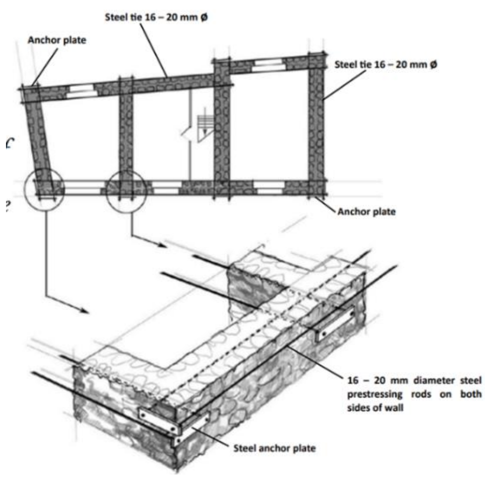

Figure 32 - Plan view of a building displaying the layout of steel ties and anchor plates (Tomazevic,1999).

2.8.1.2 Seismic Bands

Seismic bands, crucial for earthquake resistance in stone masonry buildings, are typically installed at lintel, floor, and/or roof levels, forming a ring or belt. Made from reinforced concrete (RC) or timber, they play a vital role in holding walls together and ensuring integral box action. Proper placement, continuity, and quality materials are essential for effectiveness.

Lintel bands, specifically, reduce effective wall height, diminishing bending stresses during earthquakes and reducing the risk of wall detachment. During earthquake tremors, the band undergoes both bending and tensile forces, as illustrated in Figure 33 (Bothara et al., 2004).

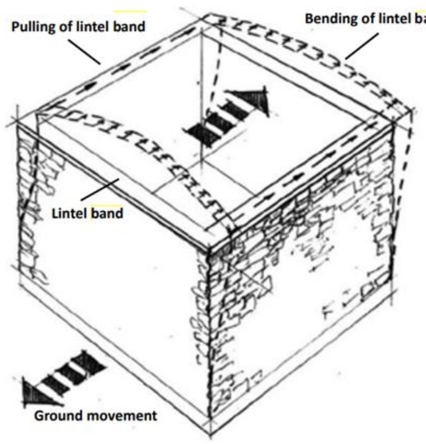

Figure 33 - Pulling and bending of a lintel band in a stone masonry building (Borthara et al.,2004).

2.8.1.3 Ring Beams

The suggested enhancement involves a reinforced concrete strapping beam with longitudinal steel bars and stirrups positioned at the upper part of stone masonry walls surrounding the building. This modification fortifies the link between the roof and load-bearing stone masonry, dispersing lateral forces and bolstering resilience against overturning forces, as depicted in Figure 34. The reinforcement specifics of the roof-to-gable masonry wall connection are also emphasized in the corresponding figure.

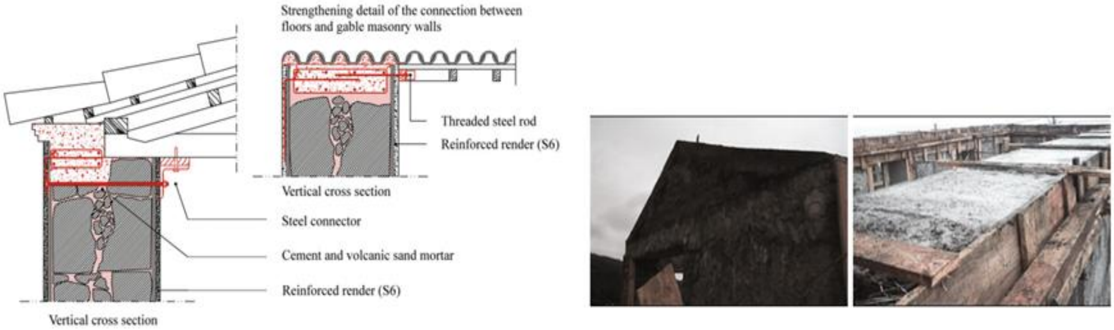

Figure 34 - Detail of Retrofitting Solution (Ferreira et al., 2017).

Two main variations, reinforced concrete, and steel ring beams are commonly used for this purpose. Steel ring beams are often preferred due to their adaptability to wall irregularities and the minimal impact on the existing structure and its seismic implementation, attributed to their low self-weight (Babilio et al., 2018).

2.8.1.4 Base Isolation

Base isolators reduce seismic impact by isolating the building's reaction from ground movement. In major earthquakes, they minimize structural and architectural damage by altering the structure's natural period. Two main types are elastomeric bearings, made of natural rubber or neoprene, and sliders, using Teflon and stainless steel. Implementing base isolation should be considered early in the seismic design phase, as retrofitting existing buildings can be challenging due to complex installation issues (Guh et al., 2006).

2.8.1.5 Post Tensioning

Post-tensioning is an effective retrofit solution for reinforced concrete or masonry structures, boosting strength and ductility while minimizing disruption. Masonry's low tensile strength under lateral loads necessitates extra reinforcement, often with steel members. Post-tensioning elevates compressive stresses, preventing brittle tensile failures. The process involves drilling a core hole, inserting a high-strength steel rod, and applying tensile force with a jack. This technique enhances structural resilience against various loads (Guh et al., 2006).

2.8.1.6 Jacketing

Jacketing is a seismic retrofitting method where a thin layer of reinforced mortar or shotcrete is applied to wall surfaces with through wall anchors. This technique enhances wall integrity against seismic effects, increasing mass and stiffness. Common materials include cement plaster or shotcrete reinforced with welded wire mesh, applied on both exterior and interior surfaces. Continuous steel mesh and anchoring to floors and foundations are essential for secure installation, potentially requiring foundation reinforcement (Bothara et al., 2004).

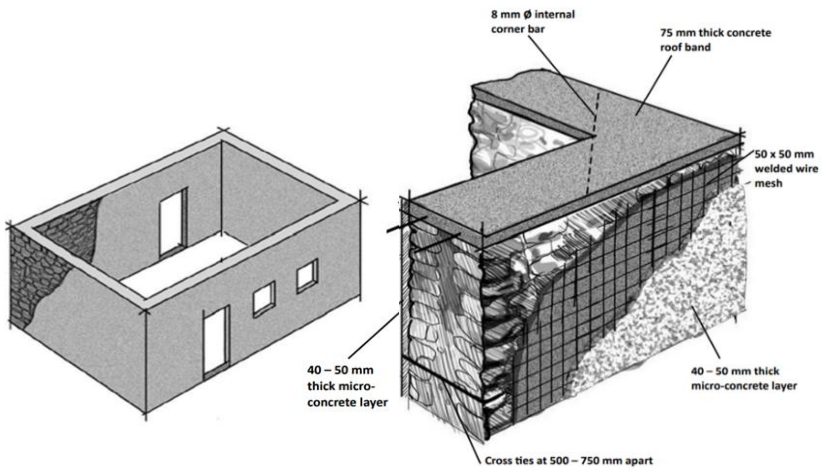

Figure 35 - Jacketing Stone Masonry Walls (Bothara et al., 2004).

2.8.1.7 Grout Epoxy Injections

Grouting, using cement or polymer-based materials, is a common method for retrofitting structures, including historical ones. Caution is advised with polymer-based grouts due to potential incompatibility with old materials, making cement-based grouts preferred for architectural heritage. Grout injection, a widely applied technique since the 1976 Friuli earthquake, involves injecting cementitious grout into masonry walls' air voids to strengthen against out-of-plane forces. This method, detailed in Tomazevic (1999) and Lutman and Tomazevic (2002), preserves historical integrity through low-pressure injection into stone joints (Bothara et al., 2004).

2.8.1.8 Steel Frames and Trusses

Research findings from international case studies indicate that employing steel frames and trusses serves as an effective seismic retrofitting method. An example is the work by Abeling et al. (2018), where vertical steel trusses were utilized to strengthen the building against in-plane loading. The use of a steel frame also contributes to enhancing the structural rigidity of the building. However, it is crucial to note that retrofitting approach is most appropriate for tall and slender structures. As such, it will not be further considered in the objective of this research study.

Chapter 3: Selected Case Studies

The Maltese Island is encompassed by chapels that significantly contribute to Maltese heritage. These chapels exhibit diversity in both size and shape, yet they share common characteristics. Several Maltese chapels mentioned hereunder, outline details regarding their ground geology, height, width, and length. Some of these chapels stand alone, while others are connected to adjacent structures.

	Chapels	Locality	Geology	Height	Extra Height	Length	Width
1	Chapel of Saint Mary Magdalene	Ħad Dingli	Upper Coraline	6m	1m	11.98m	9.2m
2	Chapel of Our Lady of Itria	Bingemma	Upper Coraline	6m	2m	12.5m	9m
	Adjacent to right			5m		6.5m	4m
3	Chapel of Immaculate Conception	L-Aħrax tal-Mellieha	Upper Coraline	5m	1m	10.8 m	5.2m
	Adjacent on both sides			4m		5m	3m
4	Chapel of San Dimitri	Gharb	Upper Globigerina	7m	2m	10.8m	7.9m
5	Chapel of San Xmun l-Imħeġġeġ (Wied Qanotta Chapel)	Wardija	Upper Globigerina	8m	1m	8.54m	7.1m
6	Chapel of Santa Katerina Wied il-Għasel	Naxxar	Middle Globigerina	8m	2m	10.5m	7.8m
7	Chapel of the Annunciation	Ħal Millieri	Middle Globigerina	4m	1m	9.5m	6.8m
8	Chapel of San Blas	Siġġiewi	Middle Globigerina	8m	1m	10.15m	8m
	Adjacent to back			6m		6.5m	7.3m
9	Chapel of tal-Prepostu	San Gwann	Lower Globigerina	6m	1m	9.5m	7.3m
10	Chapel of Santa Margerita tal-Ħereb	San Gwann	Lower Globigerina	5m	1m	9m	6.65m
11	Chapel of Santa Katerina tat-Torba	Qrendi	Lower Globigerina	6m	2m	13m	8m
12	Chapel of tal-Assunta tal-Magħtab	Naxxar	Lower Globigerina	7m	1m	10m	7.69m
	Adjacent to left			4m		6.76m	4m
13	Chapel of Saint Matthew	Qrendi	Lower Globigerina	10m	2m	18.9m	12.3m

	Adjacent to back/side			5m		5.5m	15m
14	Chapel of L-Assunzjoni taż-Żellieqa	Għargħur	Lower Globigerina	9m	2m	15.5m	9.6m
	Adjacent to left			6m		7.6m	3.6m
15	Chapel of the Addumption of Our Lady (Ta' Qrejqca)	Ħal Qormi	Lower Globigerina	4m	2m	8.85m	6.2m
16	Chapel of the Assumption of Mary (Santa Marija tal-Blat)	Ħal Qormi	Lower Globigerina	6m	1m	8.4m	6m
	Adjacent to right			8m		7.6m	3.8m
17	Chapel of St. Nicholas	Siġġiewi	Lower Globigerina	7m		8.6m	6.8m
18	St. Clement's Chapel	Żejtun	Lower Globigerina	7m	1m	10.1m	8.3m
19	Chapel of St. Agatha	Bubaqra/ Żurrieq	Lower Globigerina	6m	1m	8m	5.4m
	Adjacent to Left			5m		6.5m	4.24m
20	Santa Marija Ta' Bernarda Chapel	Għargħur	Lower Globigerina	6m	1m	5.7m	12.9m
21	St. Nicholas' Chapel	Għargħur	Lower Globigerina	6m	2m	11.67m	7m
22	Chapel of Santa Marija tax-Xagħra	Naxxar	Lower Coraline	8m	2m	12.7m	8.2m
	Adjacent to right			4m		9.8m	3.2m
23	Chapel of St. Anthony's	Marsascala	Lower Coraline	7m	2m	13.3m	7.6m
	Adjacent to right			3m		4.4m	2.2m

Figure 36 - Chapel of San Dimitri in Gharb (VisitGozo,2020).

Figure 37 - Chapel of the Addumption of Our Lady (Ta' Qrejqca) (Author,2024).

The selected chapels for this research are situated on specific geological formations. One of them is a solitary chapel located on the Lower Globigerina, Chapel of St. Philip & St. James in San Gwann, and another is located on the same geology is the Chapel of St. Matthew in Qrendi, having an adjacent structure. Additionally, an isolated Chapel of St. Mary Magdalene in Dingli, situated on the Upper Coralline, is also included in this study.

Figure 38 - Chapel of St Mary Magdalene in Dingli (Author, 2024).

Figure 39 - Chapel of tal-Prepostu in San Gwann (Author, 2024).

Figure 40 - Chapel of St Matthew in Qrendi (Author, 2024).

3.1 Chapel of St. Philip & St. James in San Gwann

3.1.1 Overview

The St. Philip and St. James Chapel in the tal-Balal area of San Gwann, situated on Triq tal-Prepostu, was constructed in 1733 on the Lower Globigerina Limestone formation according to the Maltese geological map.

In a notarized document dated October 18, 1732, Fr. Gaspare Giuseppe Vassallo, the provost of the Birkirkara Chapter, declared the erection of a chapel on a plot known as Ta' Wied Ghomor. The chapel was entitled to an annual rent of nine scudi, payable from a property adjacent to the St. Roque church in Birkirkara. The chapel was to be presided over by the Preposito pro tempore, distinct from the parish priest, until the separation of the prepositure and arcipretura, which occurred towards the end of the 20th century, placing the chapel outside the parish limits of Birkirkara (Mallia & Chetcuti, 2023).

Constructed to serve the spiritual needs of residents in Tax-Xwieki and tal-Ghorfa tal-Balal, then part of the Birkirkara parish, the chapel featured an altar adorned with a titular painting depicting the two saints, attributed to the 18th-century Maltese painter Gannikol Buhagiar. In 1965, with the establishment of the Kuncizzjoni parish in Tal-Ibragg, the chapel was transferred to the San Gwann parish (Xuereb, 2012).

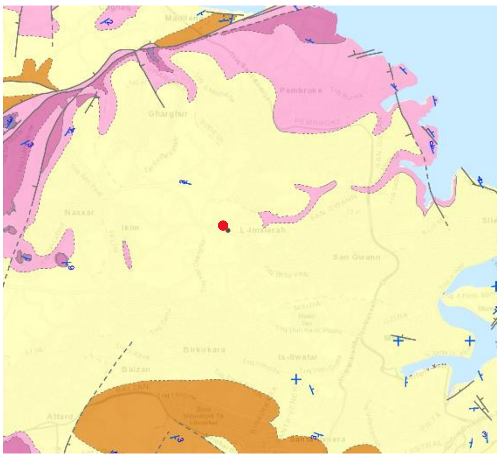

Figure 41 - Geological Map of Chapel of St. Philip & St. James in San Gwann (Geological Map of the Maltese islands,2016).

Figure 42 - Google Earth: Chapel of St. Philip & St. James in San Gwann (Google Earth, 2023).

3.1.2 General Layout and Composition Elements

Located just off the main road known as Tal-Balal within the San Gwann limits, the chapel features a rectangular plan with all four elevations visible (Xuereb, 2012).

The main facade exhibits a simple design, adorned with a cornice above the main door and another beneath the chapel's curved frontispiece. Above the main door, a small window provides natural light to the interior, while the masonry below the window suggests preparation for a sculpted coat-of-arms. Flanking the pediment, two sturdy pillars with finials stand on either side. At the centre of the curved frontispiece, there is an arched bell-cot topped by a plain limestone cross. The side and back elevations maintain a plain, undecorated masonry design.

The chapel's side includes water ducting (mżieweb). Internally, the chapel has a rectangular form with a single altar, featuring a barrel vault ceiling and limestone slab flooring. The altar is positioned within an arch, stepped inside the wall thickness, housing a titular painting. The entire chapel is adorned with embossed coving (Mallia & Chetcuti, 2023).

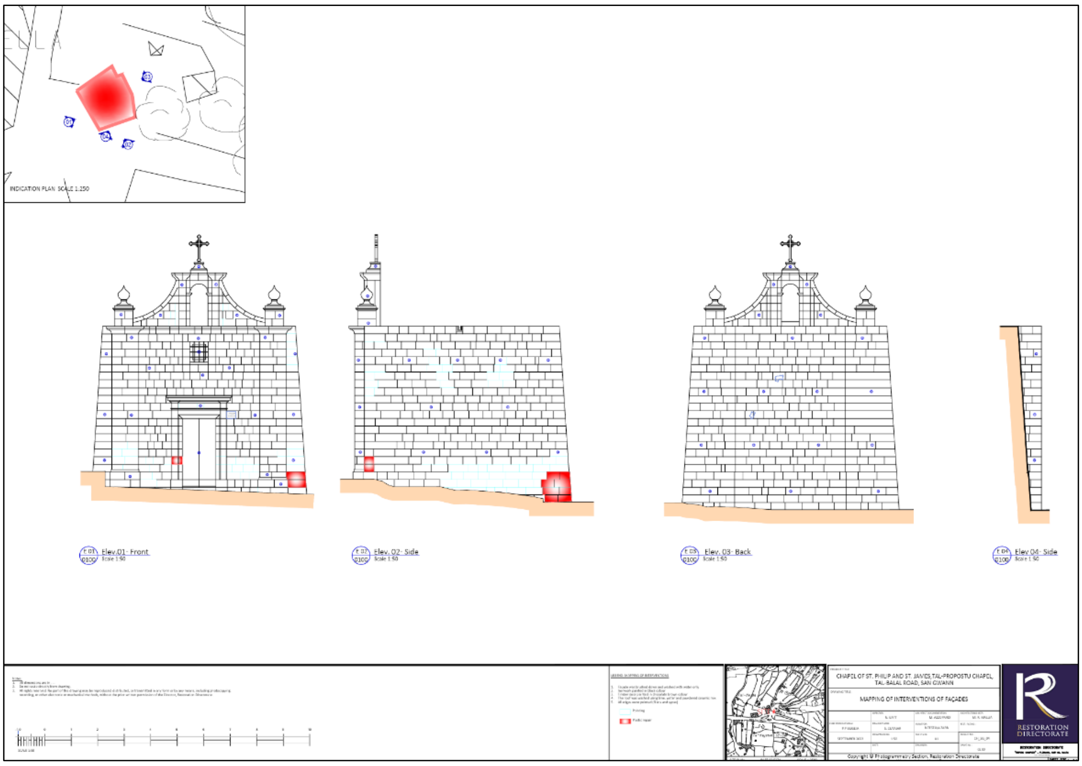

Figure 43 - Elevations of Chapel of St Philip and St James, tal-Propostu (Restoration and Preservation Department,2022).

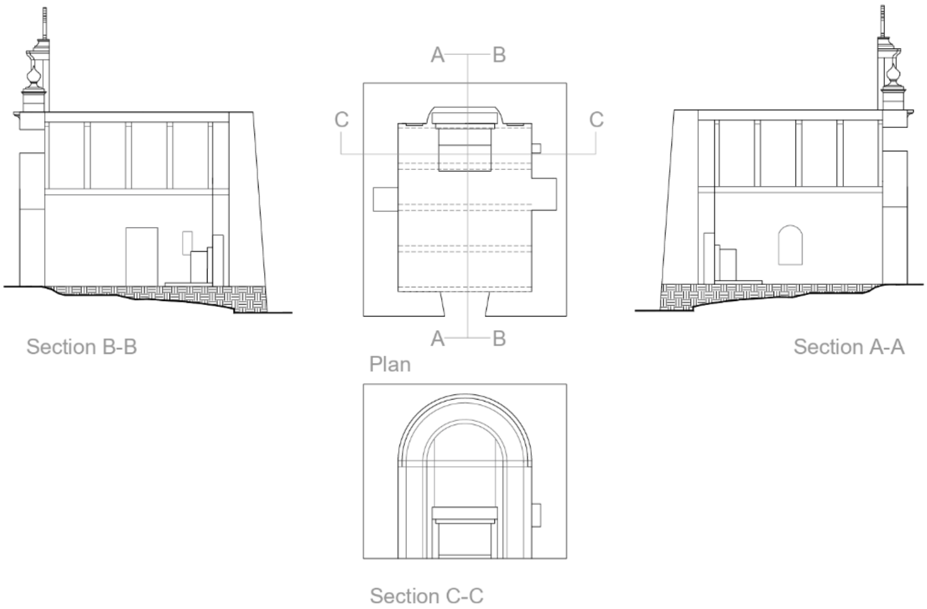

Figure 44 - Plan and Sections of Chapel of St Philip and St James, tal-Propostu. (Author,2024)

Figure 45 - Façade of St Philip and St James, tal-Propostu Chapel (Author, 2024).

Figure 46 - Interior of St Philip and St James, tal-Propostu Chapel (Author, 2024).

Figure 47 - Barrel Vault Ceiling of St Philip and St James, tal-Propostu Chapel (Author, 2024).

Figure 48 - Interior of St Philip and St James, tal-Propostu Chapel (Author, 2024).

3.1.3 Interventions

In 2022, the restoration department unit meticulously restored this chapel in accordance with the ICOMOS Venice Charter, aiming to preserve it for future generations. The restoration involved removing harmful accretions and addressing current damages to slow down the deterioration process.

Various interventions were undertaken, such as manually removing metals, dead cables, and accretions from the masonry facade. To prevent rust, wider holes were drilled, blocked with stone dowels or plastic repairs. Loose pointing, cement rich pointing, and other issues in joints were carefully addressed (TVMNews, 2023).

Dry brushing with stiff bristle brushes removed flaked stone, dirt, soot, and superficial deposits. Delicate manual methods and tools like microscalpels were used for cleaning, with approved poultices for stubborn deposits. Stone replacement was minimized to retain the original structure.

Chiselling away deteriorated sections utilized small handheld and power tools to avoid damaging the structure. When stone replacement was necessary, high-quality stones matching the original in characteristics were used and securely tied to the remaining structure. Voids around new stones were filled with pre-approved lime mixes.

Fluid lime mortar was injected into interstices and delaminated stonework, avoiding excess pressure. Carbon fibre rods bridged weak layers, grouted with lime mortar. Plastic repair techniques filled missing areas and alveoli, matching the adjacent masonry fabric in colour and strength. Transparent finishing coats (velatura) were applied selectively, and all repairs were approved by the overseeing Architect and Civil Engineer (Mallia & Chetcuti, 2023).

3.2 Chapel of St. Mary Magdalene in Dingli

3.2.1 Overview

Saint Mary Magdalene Chapel, dedicated to Mary Magdalene, is a Roman Catholic chapel situated on the outskirts of Dingli, Malta. Accessible from Panoramic Road and positioned atop the Dingli Cliffs, it is frequently referred to as the Chapel of the Cliffs. This chapel served as a crucial point of reference for fishermen navigating the southwestern waters of the Maltese Islands (Vassallo, 2022).

On the Maltese geological map, the chapel is constructed on the Upper Coralline Limestone formation. Although the exact date of its construction remains unknown, the earliest reference to the chapel dates to 1446. Isolated from the town and utilized by nearby farmers, the chapel fell into disrepair by 1575 and eventually collapsed. However, it underwent reconstruction in the 17th century, reopening its doors on 15 April 1646.

Throughout its history, the chapel faced challenges such as a lightning strike on 4 February 1936, resulting in damage to the round window on the front, subsequently restored. A more significant incident occurred during a storm on the night of 9th and 10th December 2014, when the chapel was struck by lightning again. The incident resulted in significant damage to the window and the upper section of the facade, with debris affecting the altar and the altarpiece. The restoration team promptly restored the damage, and the chapel reopened in April 2015. Due to its cultural importance, the chapel is included in the National Inventory of Cultural Property of the Maltese Islands (Micallef & Brincat, 2012).

Figure 49 - Chapel of St Mary Magdalene Incident Struck by Lightning 2014 (Vassallo,2014).

Figure 50 - Chapel of St Mary Magdalene Incident Struck by Lightning 2014 (Vassallo,2014).

Figure 51 - Google Earth: Chapel of St Mary Magdalene in Dingli (Google Earth, 2023).

Figure 52 - Geological Map of Chapel of St Mary Magdalene in Dingli (Geological Map of the Maltese islands,2016).

3.2.2 General Layout and composition elements

St. Mary Magdalene Chapel exhibits a modest layout characteristic of Maltese wayside chapels. Accessible by a staircase, this small chapel features a rectangular structure with a slanting roof, presenting a simple façade housing a lone doorway. Above the entrance, there is a round window, and a small Cross adorns the apex.

An inscription in Latin is positioned just above the door, while an originally adorned coat of arms is found overhead the window. Outside the chapel, there is a petite parvis (referred to as "zuntier" in Maltese), and a protective railing is situated nearby to safeguard visitors from the cliffs' edge. The church interior boasts an altar crafted from Maltese limestone (Micallef & Brincat, 2012).

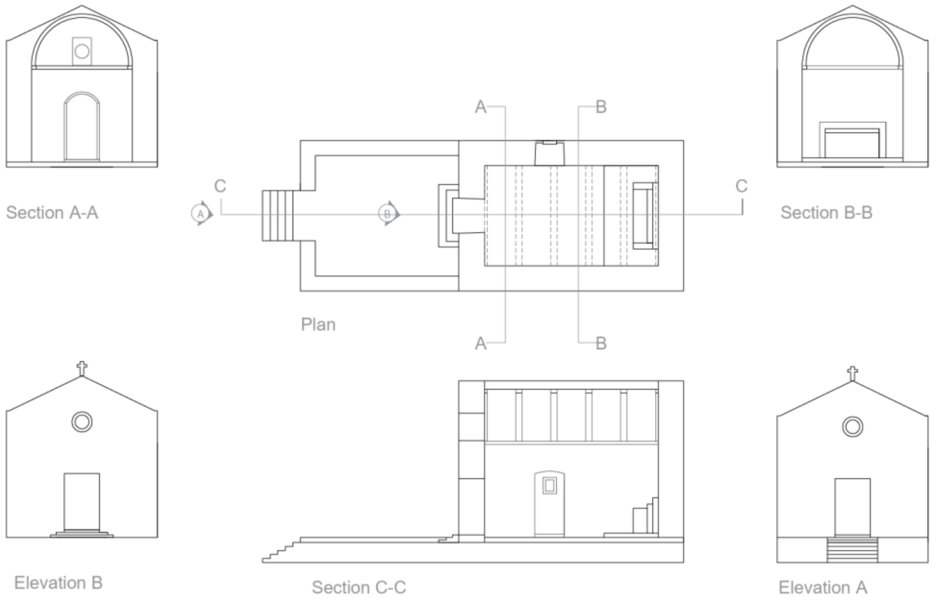

Figure 53 - Plan, Sections and Elevations of St Mary Magdalene Chapel (Author, 2024).

Figure 54 - Façade of St Mary Magdalene Chapel (Author, 2024).

Figure 55 - Side Façade of St Mary Magdalene Chapel (Author, 2024).

Figure 56 - Interior of St Mary Magdalene Chapel (Author, 2024).

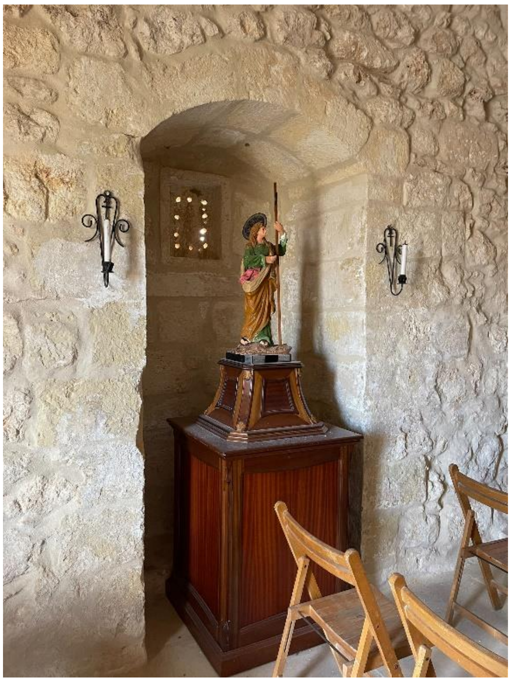

Figure 57 - Interior of St Mary Magdalene Chapel (Author, 2024).

Figure 58 - Interior of St Mary Magdalene Chapel (Author, 2024).

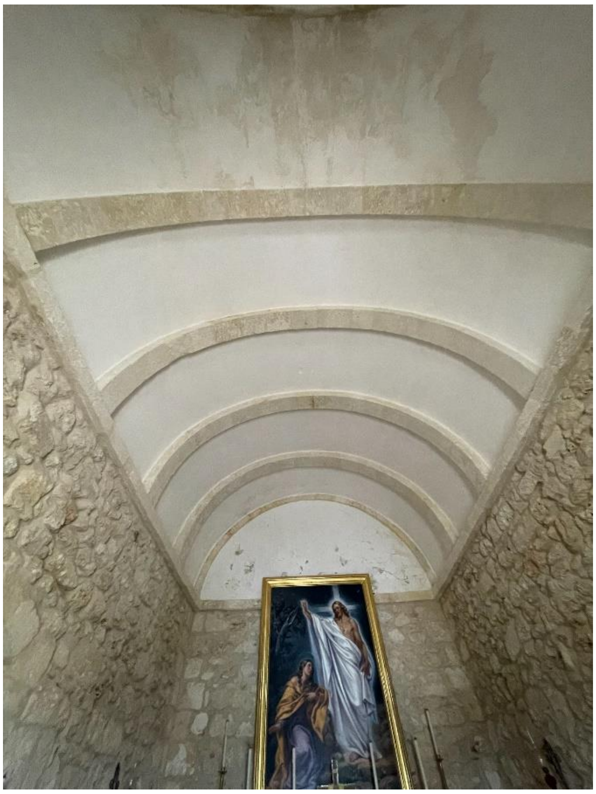

Figure 59 - Barrel Vault Ceiling of St Mary Magdalene Chapel (Author, 2024).

3.2.3 Interventions

Over time, St. Mary Magdalene Chapel underwent substantial restoration endeavours. Starting in May 2005, the Restoration Unit of the Ministry of Resources and Infrastructure, overseen by architect David Vassallo, commenced the restoration initiative. The extensive restoration project included strengthening the roof, replacing outdated cement with hydraulic lime, and installing new flooring for both the chapel and its surrounding area. A replica of the stolen "non gode l'immunita ecclesias" plaque was also installed. Additionally, the Dingli parish commissioned a new altar, and an altarpiece was generously donated by Dun Ġwann Abela and his family. The fully renovated chapel was officially initiated on May 20, 2007 (Times of Malta, 2007).

The restoration efforts entailed eliminating detrimental cement from the outer walls and introducing a new stone cross and plaque on the façade. Original flagstones were uncovered during tile removal and were placed around the altar, alongside other original slabs preserved by an individual during previous tiling. The parvis was also re-paved, utilizing an imported material provided by a benefactor.

While the exterior, situated on the cliff's edge, was in good condition, proper maintenance was still imperative. Extensive interior work was required due to past use of cement to cover the walls, adversely affecting the stone. Removal of the cement exposed primitive architecture, highlighting rubble construction throughout the chapel. A lime based mixture was employed to cover the walls, underscoring the restoration's dedication to preserving the historical authenticity of the chapel (Times of Malta, 2005).

3.3 St. Matthew’s Chapel in Qrendi

3.3.1 Overview

St. Matthew’s Chapel, located near Tempesta Road, is easily accessible and stands before a square like opening. It is constructed on the Lower Globigerina Limestone formation, according to the Maltese geological map (Busuttil et al., 2012).

Adjacent to the chapel lies a deep pit, formed by an earthquake and storm in 1343, resulting in a visible round sinkhole depicted in the site plan below. This natural depression, known as a doline in geological terms, led to the area being named ‘Tal-Maqluba’.

The chapel consists of two parts. The older chapel (iz-Zghir), situated on the sinkhole's edge, is one of Malta's oldest, believed to have been built in the fifteenth century. The main chapel (il-Kbir) was constructed between 1674 and 1682. In 1688, a painting by Mattia Preti, commissioned by Knight Nicolo Communet, adorned the chapel but was stolen and later recovered (Qrendi Local Council, 2013).

During World War II on April 12, 1942, the church suffered significant damage from Nazi bombs due to its proximity to a nearby military airfield. Architect S. Privitera repaired the church, adding a new facade and replacing the central belfry with two smaller belfries (De Giovanni, 2013).

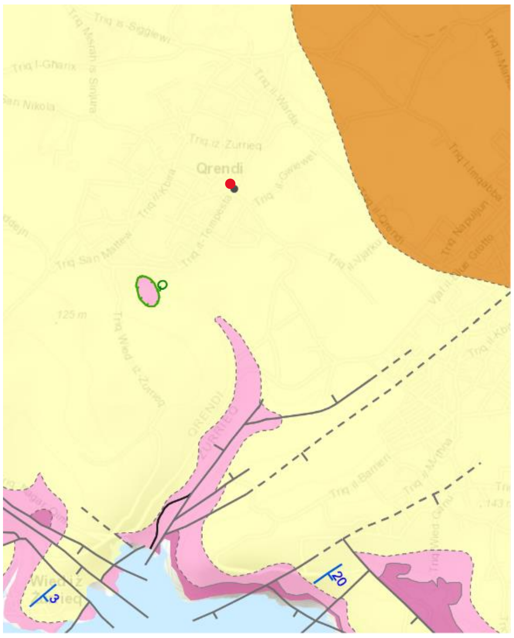

Figure 60 - Geological Map of Chapel of St Matthew’s in Qrendi (Geological Map of the Maltese islands,2016).

Figure 61 - Google Earth: Chapel of St Matthew’s in Qrendi (Google Earth, 2023).

Figure 62 - Old Façade of St Matthew's Chapel 1942 (Qrendi Local Council,2013).

3.3.2 General Layout and composition elements

The main chapel (il-Kbira) is a later construction, measuring an average size of 17m by 12m with a height of 36 courses externally. This chapel features a rectangular design with a barrel vault ceiling supported by 9 arches extending from the side walls. Behind the main door, there is a balcony for the organ, constructed in 1834 and resting on 6 Doric-style columns. The main altar, crafted from limestone, highlights sculptural elements, and includes a framed painting of the patron saint. Adjacent doors lead to the sacristy and the old chapel (iz-Zghira), accessible via a staircase (De Giovanni, 2013).

The facade of the main chapel is characterised by two long Tuscan-style pillars, and the top coving flattens at each end. Bell towers were added to the chapel after World War II during the restoration efforts. The main chapel door, rounded with embossed coving and flanked by two Tuscan-style pillars, has a square design. Above the door, a cross-shaped window, enlarged during the post-war restoration, is visible. Additionally, two small windows adorn each side of the door (Busuttil et al., 2012).

The old chapel (iz-Zghir) is situated to the left of the main chapel (il-Kbir), with the two structures adjacent and separated by a slanting wall that enhances the overall structure. Externally, the small chapel features a straightforward facade with a simple rectangular door. While facing the valley, it has one window, while two additional windows overlook the field at the back. Internally, the small chapel accommodates approximately ten people, with a square roof supported by limestone slabs on pointed arches. The limestone altar, adorned with paint and sculpture, is positioned beneath a sculpted sea clam in the ceiling. Notably, the altar displays a terracotta statue of Saint Matthew, surrounded by a sculpted date of 1897, indicating a renovation. Despite its limited capacity, a flight of stairs has been constructed within the small chapel to provide access to the main chapel (il-Kbira) and sacristy (Qrendi Local Council, 2013).

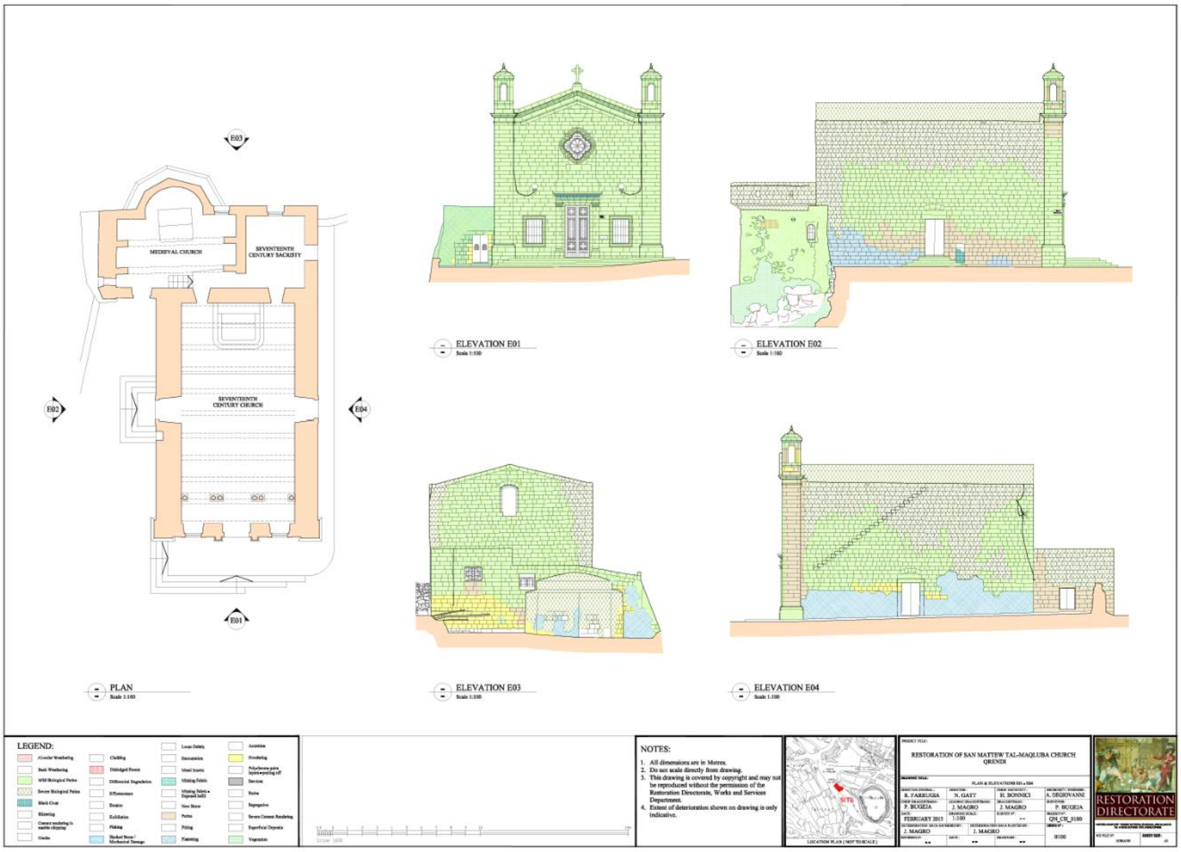

Figure 63 - Plan and Elevations of Chapel of St Philip and St James, tal-Propostu (Restoration and Preservation Department,2013).

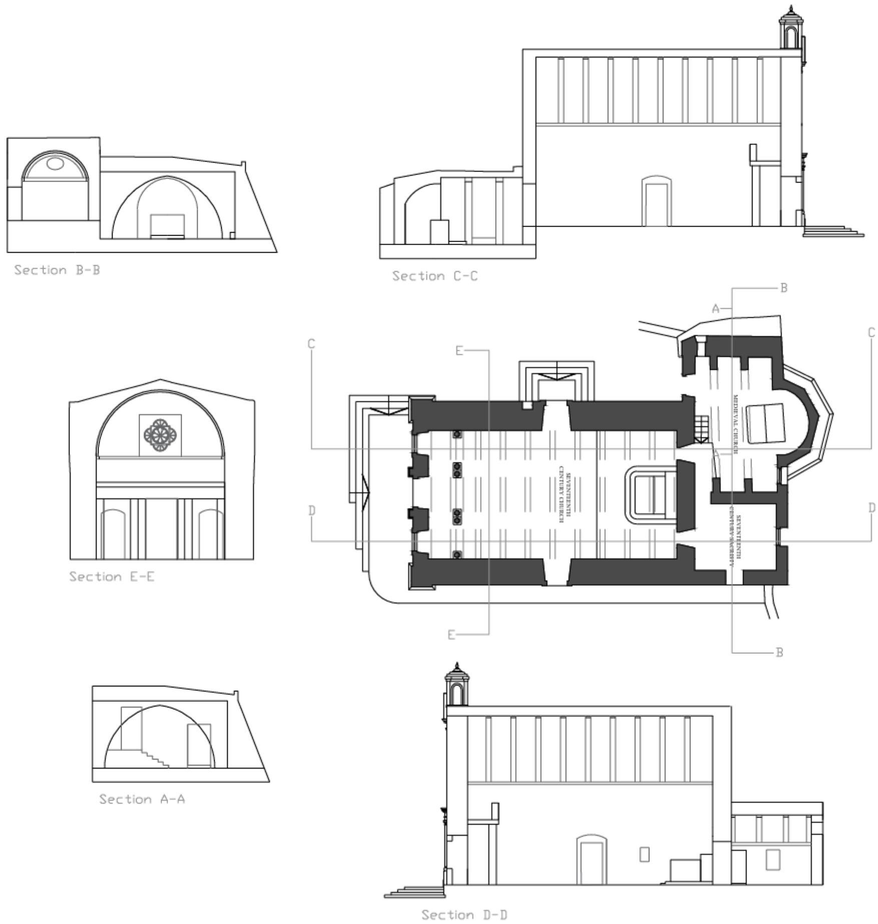

Figure 64 - Plan and Sections of St. Matthew's Chapel (Author, 2024).

Figure 65 - Exterior Façade of the Old St Matthew's Chapel (iz-Zghira) (Author,2024).

Figure 66 - Side View of St Matthew's Chapel (Author,2024).

Figure 67 - Back/Side View of St Matthew's Chapel in Qrendi (Author, 2024).

Figure 68 - Interior of the Main St Matthew's Chapel (il-Kbira) (Author, 2024).

Figure 69 - Interior of the Main St Matthew's Chapel (il-Kbira) (Author, 2024).

Figure 70 - Interior of St Matthew's Chapel Sacristy (Author, 2024).

Figure 71 - Interior Doorway from sacristy to the Old Chapel (iz-Zghira) (Author, 2024).

Figure 72 - Interior of St Matthew's Old Chapel (iz-Zghira) (Author, 2024).

Figure 74 - Interior Stairs leading from Old Chapel (iz-Zghira) to the Main Chapel (il-Kbira) (Author, 2024).

Figure 73 - Interior of St Matthew's Old Chapel (iz-Zghira) showing the carved scallop fresco (Author, 2024).

3.3.3 Interventions

The church underwent significant damage during World War II, prompting restoration efforts led by architect S. Privitera. To address potential hazards, alterations were made to enhance safety (Busuttil et al., 2012).

Key modifications included the removal of the original cross atop the facade, replaced by a smaller version. Bell towers were erected at the ends of the facade, replacing the stone acorns present before the war. The facade window underwent enlargement and lowering to improve interior lighting. The sculpture on the main door was replaced, and arches were added to strengthen the rectangular openings of the side chapel entrances.

A flight of stairs on the west side, embedded into the wall, was removed for safety reasons. Near the east door, there were indications of planning around 1934 for a crypt door, although this appears incomplete. At the back of the main chapel (il-Kbira), an empty niche is visible.

In recent years, the Restoration Directorate of the Ministry for Resources and Rural Affairs undertook the restoration of St. Matthew's Chapel. An extensive visual and photographic inspection assessed the facade's condition and guided the formulation of a conservation strategy.

While the overall building fabric was in good condition, with minimal deterioration on external areas, a significant concern emerged about the advanced disrepair of the old chapel's roof. This required immediate attention, despite the chapel's overall structural stability.

Specific issues identified during the inspection included vegetation, powdering and flaking, open mortar joints, visible plasters needing testing, a layer of biological dirt, and hairline cracks inside the old chapel. To address these concerns, restoration tasks such as cleaning the facade, removing cement plasters, eliminating biological growth, plastic repairs, and repointing joints were carried out. These activities, executed with scaffolding and mitigation measures, aimed to preserve the chapel while preventing further deterioration (De Giovanni, 2013).

3.4 Validation of Selected Case Studies

The selection of the mentioned chapels has been deliberately chosen, based on specific considerations. Two out of the three chapels are located on Lower Globigerina, distinguished by one being standalone and the other being attached to an adjacent building. The third chapel is also standalone, this is built on Upper Coraline limestone, representing a unique case.

These variations prompted the examination of three distinct yet commonly encountered historical unreinforced masonry (URM) buildings. This analysis was conducted under similar seismic conditions. The chosen approach allows for a comprehensive and direct comparison of their seismic behaviour. The subsequent findings from this comparative study yield valuable insights.

Chapter 4: Research Methodology

This chapter outlines and explains the research methodology used to evaluate the seismic vulnerability of existing structure configurations. The suitability of different methodologies depends on factors like the necessary level of detail, building typology, and technology accessibility. It also defines the building typology, floor plan, and material characteristics. The main goal of this dissertation is to model the case studies mentioned in chapter 3 and analyse how they behave under seismic conditions in relation to each other. Therefore, the chosen approach must strike a balance between computational efficiency and sufficient accuracy.

4.1 Selection of the Methodology

In discussing research methodologies, three primary approaches emerge: experimental, numerical, and analytical. The experimental method typically involves laboratory settings, allowing for controlled conditions and direct observation. Meanwhile, numerical methodology relies on software to simulate complex systems, offering versatility and scalability. On the other hand, analytical investigation employs mathematical equations to derive solutions, particularly suitable for simpler structures and straightforward loading scenarios. Given the constraints of time and the need for expeditious research, the numerical methodology has been opted for. This decision creates greater efficiency and flexibility, enabling comprehensive analysis within the given timeframe.

The numerical methodology for structural analysis is divided into three main approaches: macro element method, simplified micro element method, and detailed micro element method. The micro element method discretizes a building into various elements, including 1-dimensional elements, such as beam-column elements capable of modelling axial compression, shear forces, and bending moments, 2-dimensional elements like plates or shells, and 3-dimensional brick elements. This approach allows for detailed modelling of structures but comes with the drawback of high computational costs and significant storage requirements, making it impractical for large buildings. In contrast, the macro element method treats units, mortar, and interfaces as a continuous material, which is advantageous for analysing large structures but lacks the capability to manage the complexities of small panels, particularly their potential failure modes due to weak mortar joints. Each method offers its own set of advantages and limitations, catering to different needs in structural analysis. Further details on the discussed methodologies can be found in Chapter 2, Section 2.6.3.2 on Structural Analysis.

The numerical methodology will utilize numerical analysis through a macro element software's, with an educational license of Histra Arches and Vaults and 3D Macro, developed by the software developer Gruppo Sismica from Italy.

4.2 Method of Seismic Analysis

The methodology for analysing the three chapels below is based on guidelines set forth by ICOMOS, which draws on principles outlined by ISCARSAH. This study follows these established principles and recommendations, alongside similar works, to develop a restoration approach for historical masonry structures. The methodology, outlined here as a contribution to addressing this intricate issue, consists of six specific steps (Asteris et al., 2014).

<u>Step 1: Historical Documentation</u>

To comprehend the development of the building materials, an extensive research study was conducted. This involved archival research to gather information on all three chapels, along with site visits to measure and collect observational data. Chapter 3 contains copies of the plans and documents obtained during this process.

<u>Step 2: Material Characteristics</u>

The essential data needed for structural analysis encompass the material properties of the structure's components, like compressive/tensile strength, modulus of elasticity, and Poisson's ratio. Considering the parameters and goals of this research, no on-site tests were performed due to their historical structure. Instead, the material properties were drawn from the research findings, ensuring consistency by utilizing values obtained from previous studies.

<u>Step 3: Ambient Noise Measurements</u>

Ambient noise measurements were conducted at the Chapel of St. Philip and St. James on Triq tal-Balal in San Gwann. These measurements aimed to calibrate the numerical model accurately. The fundamental period values of the building derived from on-site readings were compared to those obtained from the numerical model through modal analysis. This comparison ensured the highest level of accuracy for the numerical model. The data was gathered from site by the Geophysics Department at the University of Malta.

Step 4: Structural Model

The chapels were 3D-modeled using 3D Macro and Histra, Arches and Vaults macro element software, with adjustments made to material and geometric properties to accommodate the software's limitations while preserving the accuracy of the structural layout. Analyses were conducted based on Eurocode 8: Part 3 (EN1998-3) standards for seismic design, considering Near Collapse (NC), Significant Damage (SD), and Damage Limitation (DL) scenarios.

Step 5: Actions

Various loading scenarios must be considered, particularly seismic forces for structures located in seismic zones. Combinations of dead loads, live loads, and earthquake forces need to be accounted for.

Step 6: Analysis

Various pushover analyses were conducted, and capacity curves were generated for each analysis. These analyses took into consideration different potential load orientations:

Main Axis	**Main Axis & Eccentricities**		**Reduced Eccentricities**
Pushover +X Acc	Pushover +X Acc - e	Pushover +X Acc + e	Pushover Ex + 0.3Ey Acc
Pushover -X Acc	Pushover -X Acc - e	Pushover -X Acc + e	Pushover 0.3Ex +Ey Acc
Pushover +Y Acc	Pushover +Y Acc - e	Pushover +Y Acc + e	Pushover -0.3Ex + Ey Acc
Pushover -Y Acc	Pushover -Y Acc - e	Pushover -Y Acc + e	Pushover -Ex + 0.3Ey Acc

Table 1 - Load orientation types of the pushover analysis considered.

The pushover analysis results are directly influenced by the selection of control points, which represent the entire deformed model. Given the chapel's small plan footprint, the software considers a single control point for each. These seismic analyses results are then utilized to evaluate the building's seismic vulnerability and determine the relevant factors of safety.

4.3 Macro Element Method (Histra Arches and Vaults and 3D Macro)

Two types of macro element software were used to model the chapels as accurately as possible and to avoid limitations of each of the programs. The barrel vaults of the chapels were built using Histra Arches and Vaults, while the rest of the chapels, including the parameters of the barrel vaults from Histra Arches and Vaults, were modelled in 3D Macro. Both programs are designed with the same approach but having distinctive features.

Histra Arches and Vaults is a specialized software designed for the 3D structural modelling and non-linear analysis of masonry structures featuring curved geometry. Its modelling approach enables the simulation of the structure's inelastic response by utilizing a method known as discrete macro-elements. These elements are three-dimensional and curved, specifically developed to replicate the non-linear behaviour observed in vaulted masonry structures.

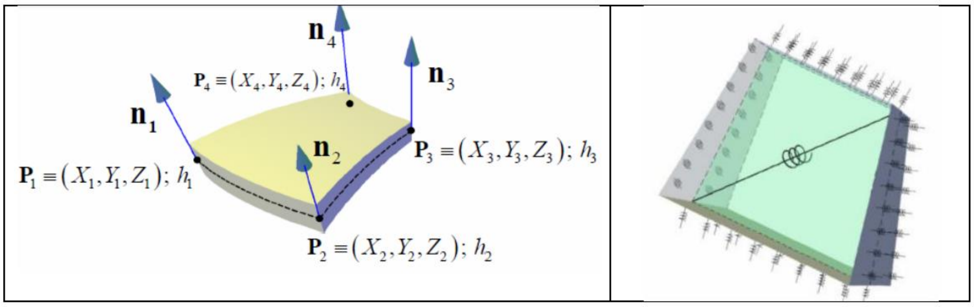

Figure 75 - 4 node macro-element (Gruppo Sismica,2011).

The idea behind 3D Macro is the discretization of macro-components, which makes it possible to construct a structure with discrete elements. Depending on how these components fit into the larger model, their levels of complexity differ.

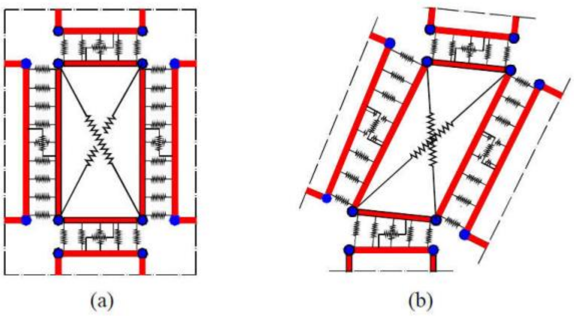

Figure 76 - The plane discrete-element a) undeformed configuration; b) deformed configuration (Calio et al., 2008).

The Quad is a 4-node macro-element, an irregular quadrilateral with rigid sides. Its deformation is controlled by non-linear springs along one diagonal, while interaction with other elements occurs through inclined spatial interfaces hosting springs. This model comprises two primary components: the quadrilateral element and the interface element. The quadrilateral includes shear deformability simulated by a diagonal spring and is defined by vertex coordinates, surface normal, and thicknesses. Interface properties derive from surface normal and thicknesses, concentrating deformability and sliding control.

A quad element has 7 degrees of freedom, including 3 translations, 3 rotations of the centre of mass in space comparative to the global reference system, and 1 angular slip from shear deformability within the macro-element's plane. The method employed achieves response accuracy comparable to other advanced FEM modelling approaches, with low computational overhead. This is because the model's degrees of freedom are resolved by the number of macro-elements used for discretization, rather than the number of nodes (Gruppo Sismica, 2011).

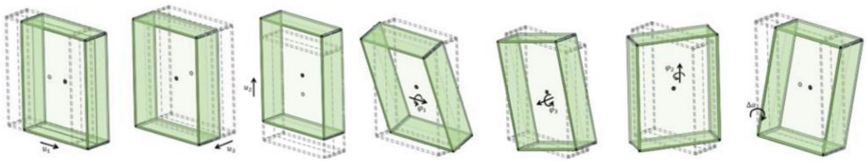

Figure 77 - Degrees of Freedom (Gruppo Sismica,2011).

In case of the modelling of barrel vaults the discretization involves using a grid of curved lines to divide the structure into macro-squares as shown in Figure 78. It is important to ensure that each square is represented by a flat element coinciding with its average plane for more accurate results. The proposed macro-modelling method mainly targets structural elements with curved geometries, such as roofing elements. For cylindrical surfaces, the surface subdivision grid is typically constructed along the generating line and parallel to the guiding curve.

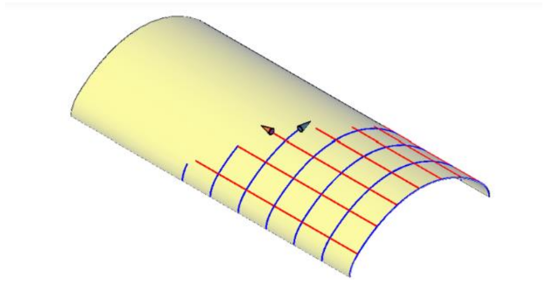

Figure 78 - Generators and directors of a cylindrical vault (Gruppo Sismica,2011).

The membrane behaviour between two wall portions, each represented by macro-elements, is governed by non-linear springs arranged in sequence and substituted with a single equivalent spring. The simulation of gradual material failure uses non-linear springs in the interface plane. Additionally, the simulation of diagonal cracking shear failure in the wall panel utilizes a nonlinear diagonal spring.

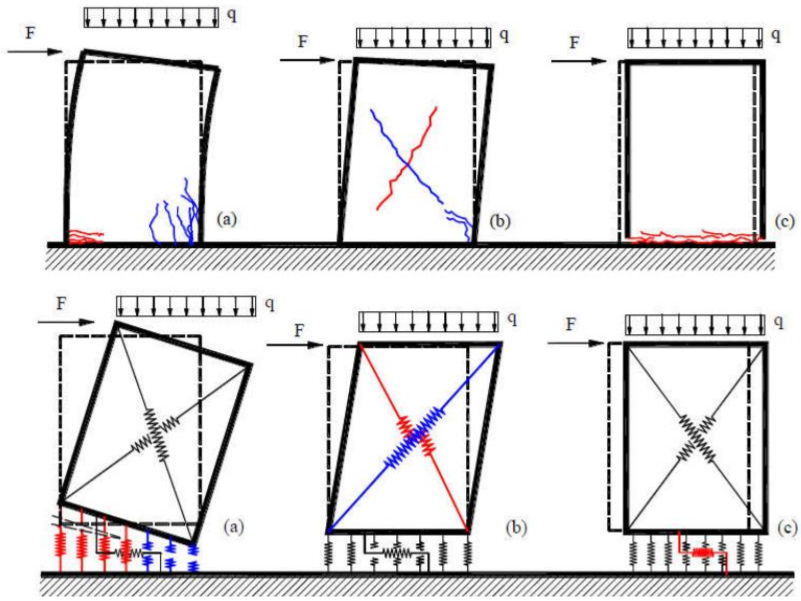

Figure 79 - (top) In-plane failure mechanisms; (bottom) simulation of in-plane failure mechanisms. a) crushing failure/tension cracks; b) shear-diagonal failure; c) shear-sliding failure (Calio et al., 2008).

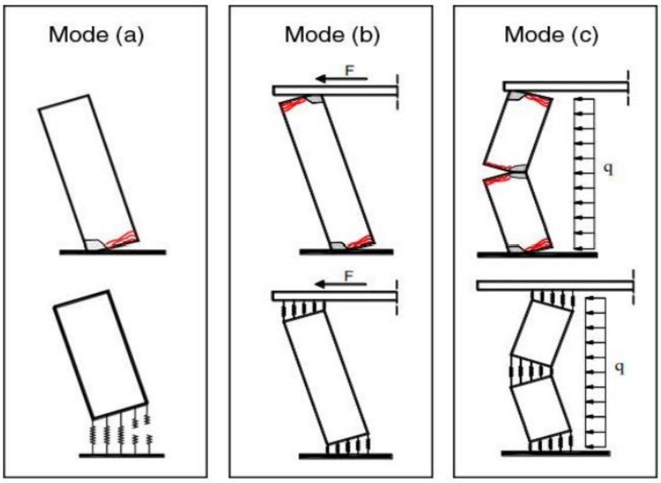

Figure 80 - Out -of-plane failures. Top image: actual failure mode, Bottom image: Macro simulation. Mode a: cantilever overturning, Mode b: overturning, Mode c: horizontal hinge formation (Caliò et al.,2005).

The macro-element approach presents a basic numerical model of a wall, as shown in Figure 81. The calibration methods for each non-linear spring are founded in the analysis of the mechanical properties of masonry and the geometric attributes of the elements. Additional details regarding the mathematical modelling and calibration procedures can be obtained in the publications by (Occhipinti et al., 2015; Caliò, I. et al., 2010 and Caliò, Ivo et al., 2005).

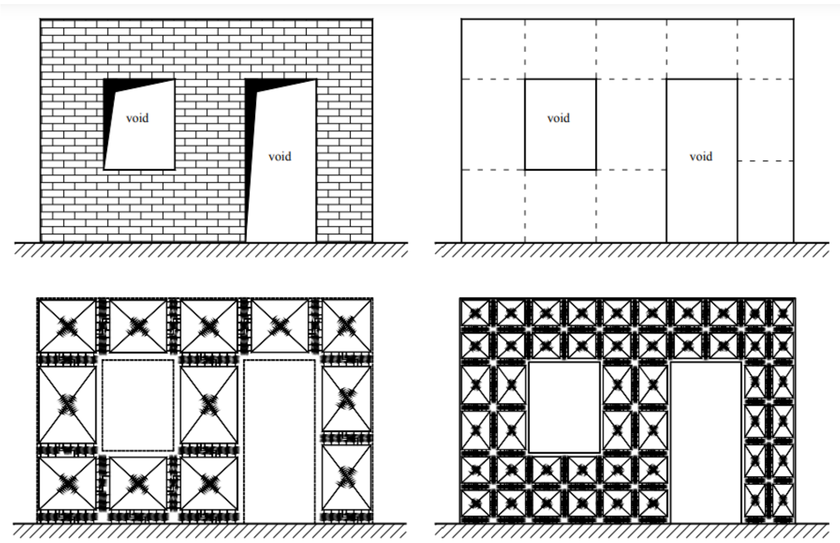

Figure 81 - Masonry Wall and corresponding discrete equivalent schemes (Caliò et al.,2005).

4.4 Modelling the Three Chapels

The following segment outlines the material and geometric properties employed in the numerical modelling of these three chapels: the Chapel of St. Philip & St. James in San Gwann, the Chapel of St. Mary Magdalene in Dingli, and St. Matthew's Chapel in Qrendi. It also includes any assumptions and adjustments deemed necessary for modelling these chapels. Appendix B contains detailed screenshots that depict the specific materials, elements, ground motion parameters, and configuration settings necessary for inputting data into both Histra Arches and Vault, as well as 3D Macro software.

4.4.1 Material Properties

The program adopts a macro-modelling strategy, considering the masonry walls as a single element composed of homogeneous material. The mechanical characteristics outlined in Table 2 were uniformly applied across all three chapels. This approach facilitated the derivation of smeared properties for the masonry elements.

Mechanical Properties of Masonry Blocks and Mortar		
Description	**Value (N/mm^2)**	**Reference**
Young's Modulus of Elasticity of limestone block, E_b	21,000	Brincat, 2020
Young's Modulus of Elasticity of mortar, E_m	8,000	Brincat, 2020
Shear Modulus of Elasticity of block, $G_b = 0.4 * E_b$	8,400	Brincat, 2020
Shear Modulus of Elasticity of mortar, $G_m = E_m / (2*(1+v))$	3,076.9	Brincat, 2020
Compressive Strength of block	17.5	Xuereb ,1991
Compressive Strength of mortar	2[134]	Brincat, 2020
Tensile strength of block	3	Cachia,1985
Tensile strength of mortar	0	Brincat, 2020
Characteristic Strength of masonry	4.108	Buhagiar, 2020

Table 2 - Mechanical properties of masonry blocks and mortar.

The calculation using equation 3 of smeared physical properties for building materials involves considering the relative areas occupied by masonry blocks and mortar with respect to the total area of the masonry wall. The program employs these refined characteristics, which are detailed in Table 3 (Buhagiar, 2020).

$$X_t = \frac{[X_b * A_b] + [X_m * A_m]}{[A_m + A_b]}$$

Equation 3 - Smear Material.

Where:

X_t	Smeared material used in macro software
X_b	Material property of masonry blocks
A_b	Total wall area, in elevation, in m^2
X_m	Material property of mortar
A_m	Total area of mortar in elevation, in m^2

Smeared properties of Masonry		
Description	**Value (N/mm^2)**	**Reference**
Young's Modulus	20337.12	Brincat, 2020
Shear Modulus	8128.52	Brincat, 2020
Compressive Strength	20.03	Brincat, 2020
Tensile Strength	2.85	Brincat, 2020
Shear Strength	0.603	Brincat, 2020

Table 3 - Smear properties used in the software (Author,2024).

4.4.2 Geometric Properties

4.4.2.1 Site Topography and Foundations

The Chapel of St. Philip & St. James in San Gwann and St. Matthew's Chapel in Qrendi, are located on Lower Globigerina Limestone which based on EN 1998-1 (2004) Cl.3.2.2.2. The ground is classified as Type A according to Table 4. While the Chapel of St. Mary Magdalene in Dingli is located on Upper Coralline, ideally a ground investigation is done to identify the proper materials but due to limited amount of time the ground type is assumed to be taken as B. The parameters from Figure 82 and Table 6 were taken according to the ground types considered.

These chapels hold significant importance as places of congregation, which are categorized as class 2 in Table 5 due to their nature as chapels. This designation entails special additional protection against earthquake damage. All three chapels are to be modelled for the most severe conditions, necessitating an increase in peak ground acceleration by 40%. This precaution is crucial as the loss of these heritage structures would be irreplaceable.

Ground type	Description of stratigraphic profile	Parameters		
		$v_{s,30}$ (m/s)	N_{SPT} (blows/30cm)	c_u (kPa)
A	Rock or other rock-like geological formation, including at most 5 m of weaker material at the surface.	> 800	_	_
B	Deposits of very dense sand, gravel, or very stiff clay, at least several tens of metres in thickness, characterised by a gradual increase of mechanical properties with depth.	360 – 800	> 50	> 250
C	Deep deposits of dense or medium-dense sand, gravel or stiff clay with thickness from several tens to many hundreds of metres.	180 – 360	15 - 50	70 - 250
D	Deposits of loose-to-medium cohesionless soil (with or without some soft cohesive layers), or of predominantly soft-to-firm cohesive soil.	< 180	< 15	< 70
E	A soil profile consisting of a surface alluvium layer with v_s values of type C or D and thickness varying between about 5 m and 20 m, underlain by stiffer material with v_s > 800 m/s.			
S_1	Deposits consisting, or containing a layer at least 10 m thick, of soft clays/silts with a high plasticity index (PI > 40) and high water content	< 100 (indicative)	_	10 - 20
S_2	Deposits of liquefiable soils, of sensitive clays, or any other soil profile not included in types A – E or S_1			

Table 4 - Ground Types (EN 1998-1 :2004).

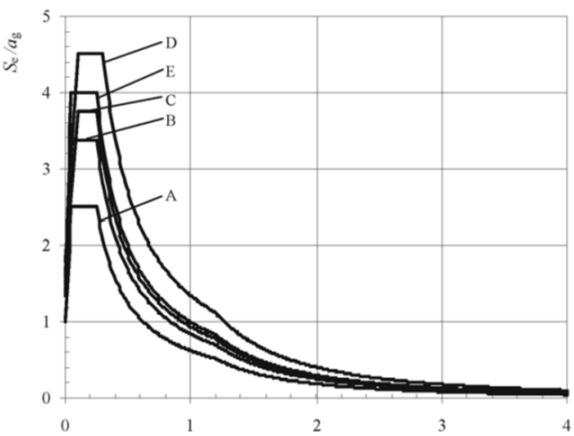

Figure 82 - Recommended Type 2 Elastic Response Spectra for Ground Types A to E (5% Structural Damping) (EN 1998-1 :2004).

Importance class	Buildings
I	Buildings of minor importance for public safety, e.g. agricultural buildings, etc.
II	Ordinary buildings, not belonging in the other categories.
III	Buildings whose seismic resistance is of importance in view of the consequences associated with a collapse, e.g. schools, assembly halls, cultural institutions etc.
IV	Buildings whose integrity during earthquakes is of vital importance for civil protection, e.g. hospitals, fire stations, power plants, etc.

Table 5 - Importance Classes for buildings (EN 1998-1 :2004).

Ground type	S	T_B (s)	T_C (s)	T_D (s)
A	1,0	0,05	0,25	1,2
B	1,35	0,05	0,25	1,2
C	1,5	0,10	0,25	1,2
D	1,8	0,10	0,30	1,2
E	1,6	0,05	0,25	1,2

Table 6 - Values of the parameters describing the recommended Type 2 elastic response spectrum (EN 1998-1 :2004).

4.4.2.2 Structural Walls

Due to software constraints explained in Section 4.4.3, all walls were simulated as single wall, with an overall thickness determined based on the survey measurements of the chapel. This approach was taken because no destructive testing was conducted to determine the actual size of the masonry or the infill between.

The plan configuration had to be adjusted due to software constraints, ensuring that most angles were perpendicular. Additionally, in areas where three or more walls converged closely, they were treated as if they were converging to a single point.

4.4.2.3 Barrel Vault

The software enables the input of barrel vaults with rectangular plan shapes, offering options for equal or varying rise and ray, as well as elliptic or parabolic profiles. Moreover, users can specify a linearly variable thickness from the base to the key stone of the vault. It also supports the modelling of base piers with adjustable height, width, and thickness, including the incorporation of openings within the piers.

Both programs were utilized to model the chapels due to the limitations of each. The barrel vaults of all three chapels were initially modelled using Histra Arches and Vaults to obtain the necessary parameters. These parameters were then inputted into an equivalent orthotropic slab in 3D Macro. For further details, Section 4.4.4.2 provides additional information regarding this process.

4.4.3 Limitations

Creating numerical models for these chapels required making specific assumptions, driven by both the intricate nature of the structure and the constraints of the software utilized. This section outlines the encountered limitations during the model construction process. Subsequently, Section 4.4.4 delves into the explanation of the assumptions made and adjustments implemented.

- The software is prone to issues with plan configurations that feature significant irregularity, particularly in cases where walls deviate from perpendicular alignment with each other.
- The software lacks the capability to effectively represent the individual inner and outer structural layers of a double-leaf wall made of masonry.
- Utilizing Eurocode standards led to the inability to easily customize masonry materials, as the software confines users to a predefined limestone material. This constraint arises from the current software's restriction to masonry editing solely with Italian codes.
- The macro modelling approach treats masonry as a uniform material.
- Unable to model typical limestone arches.
- Walls that were not properly aligned needed to be adjusted so that they were centred.

4.4.4 Assumptions

This part outlines the necessary changes and adjustments required to model the chapels due to limitations in the software. As the study pertains to an existing building, design assumptions must be made regarding the sizing and materials of structural elements.

4.4.4.1 Seismic Levels

At ground level, all chapels are assumed to be situated on a uniform plane, meaning variations such as slopes, or stepped ground profiles are not considered. Instead, it is assumed that they are all at a single level.

In case of St. Matthew's Chapel, the adjacent rooms are located at different levels from the main chapel. Thus, the numerical modelling of the chapel rationalized the 1-meter difference in floor levels by considering the respective areas, as detailed in Equation 4. Further calculations are provided in Appendix A.4.

$$Average\ Level = \frac{\sum_1^j (Level_i * Area_i)}{\sum_1^j Area}$$

Equation 4 - Calculation for Seismic Levels.

4.4.4.2 Barrel Vault Equivalent to an Orthotropic Slab

An alternative approach was necessary for analysing all three chapels, as the 3D Macro software cannot model vaulted roofs. To address this, a different software solution called Histra Arches and Vaults, licensed from Gruppo Sismica, was utilized specifically for modelling vaults and domes. In order to completely model and analyse the chapel as one whole building the Ex, Ey , G , v , s_{eq} and w mechanical parameters were derived from Histra Arches and Vaults of the barrel vault to be equivalent to an orthotropic slab in 3D Macro.

When calculating the parameters, the procedure can be defined using the following Equations. The full calculation can be found in Appendix A.

$$E_x = \frac{F(L+t_0)}{u \cdot s_{eq} \cdot w}$$

Equation 5 - The value of the equivalent stiffness in the X direction.

$$E_y = \frac{F \cdot w}{u \cdot s_{eq} \cdot (L + t_0)}$$

Equation 6 - The value of the equivalent stiffness in the Y direction.

$$\tau_{med} = \frac{F_x}{s_{eq} \cdot (L + t_0)} = \frac{F_y}{s_{eq} \cdot w}$$

Equation 7 - The voltage inside the orthotropic plate.

$$\gamma_{med} = \frac{u_x}{w} + \frac{u_y}{L + t}$$

Equation 8 – The average slip inside the orthotropic plate.

$$G = \frac{\tau_{med}}{}$$

Equation 9 - The estimated value of the tangential modulus.

Where:

Ex	Normal modulus of elasticity in the x-direction
Ey	Normal modulus of elasticity in the y-direction
F	Force
L	Width of Barrel Vault
w	Depth of Barrel Vault
t_0	Thickness of Barrel Vault at Base
G	Shear modulus of elasticity
v	Poisson's ratio
s_{eq}	Equivalent orthotropic plate thickness
W	Weight per unit surface area of slab

Chapels	E_x (N/mm²)	E_y (N/mm²)	G (N/mm²)	s_{eq} (cm)	W (kN/m²)
St. Philip & St. James in San Gwann	317.3886	26251.54	4.551	48.8	9.272
St. Matthew's in Qrendi	196.61	29879.9	0.0621	89.9	17.081
St. Mary Magdalene in Dingli	298.37	29096.25	4.233	45.1	8.569

Table 7 – Equivalent Orthotropic Slab (Author, 2024).

The resulting values, shown in Table 7 are the parametric values used in the 3D Macro software as an equivalent orthotropic slab. Although the program is interesting and useful, it is still a work in progress, with certain options not yet addressed. As shown in Figure 83, the program identifies a warning when it fails to meet the following condition: (Ex > Ey * ni^2). To resolve this issue, Gruppo Sismica suggested exchanging the values of the elasticity modules (Ex → Ey) and (Ey → Ex) to ensure the condition is satisfied. Additionally, any material located on top of the barrel vault and the roof of the chapel was taken as load on top equivalent orthotropic slab as outlined in Table 8.

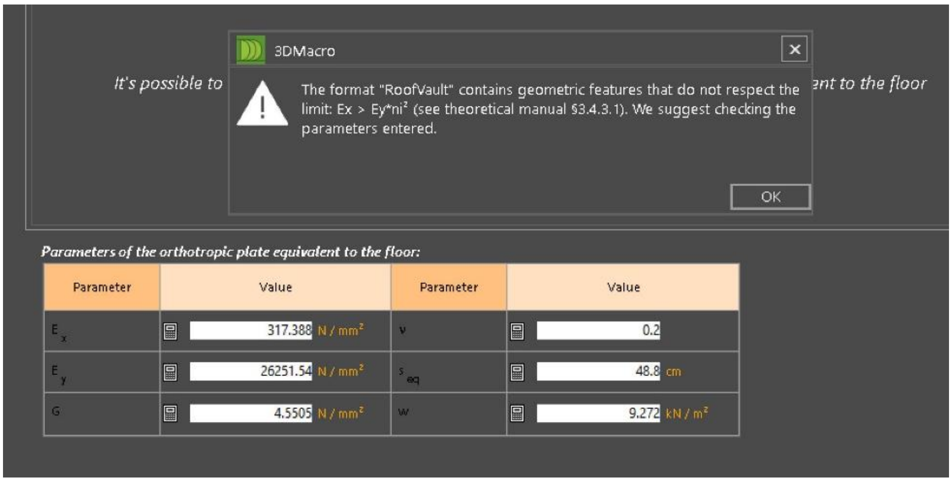

Figure 83 - 3D Macro warning message meaning violating a mechanical condition of the orthotropic constitutive law adopted in plate elements.

Chapels	Area (m^2)	Length (m)	Height Average = A/L (m)	Material "Torba" (kN/m^3)	Load (kN/m^2)
St. Philip & St. James in San Gwann	4.3755	5.10	0.8579	16	13.73
St. Matthew's in Qrendi	6.1142	8.87	0.6893	16	11.03
St. Mary Magdalene in Dingli	0.9904	4.60	0.2153	16	3.444

Table 8 - Load on roof of chapels (Author,2024).

4.4.4.3 Roof Diaphragm

In the case of St. Matthew's Chapel in Qrendi, the additional rooms adjacent to the main chapel are constructed with authentic stone arches. These arches transfer the load from the roof to the arches and subsequently from the arches to the walls, resulting in point loads on the supports of the stone arches.

However, the 3D Macro program does not accurately model the roof of the additional rooms as they are actually constructed. Therefore, the actual stone arches were replaced with linear members (timber beams) in the model. These timber beams provide a diaphragm that is somewhat equivalent to the actual masonry roof. These timber beams are slabbed over with a custom masonry slab. Table 9 provide all the properties used for the timber material and Table 10 for the properties of the custom masonry slab. Additionally, a load of 1.8 kN/m^2 is applied on top of the masonry slab having a 0.1 m thickness of material with a specific weight of 18 kN/m^3.

Materials for Frame: Timber	Value	Units	Reference
Young's Modulus, E_T	13000	N/mm^2	(Otani et al., 2022)
Poisson's Ratio, v_T	0.43	/	(Otani et al., 2022)
Specific Weight	15	kN/m^3	(Otani et al., 2022)

Table 9 - Properties used for 3D Macro for Timber Beams (Author,2024).

	E_x (N/mm^2)	E_y (N/mm^2)	G(N/mm^2)	s_{eq} (cm)	W (kN/m^2)
Masonry Slab	20337.12	20337.12	10168.56	20	3.8

Table 10 - Properties used for 3D Macro for Masonry Slab (Author,2024).

4.4.5 Numerical Analysis

4.4.5.1 Modal Analysis

To ensure the numerical model's accuracy, regular modal analyses were conducted and evaluated with spectral acceleration measurements obtained from ambient noise surveys conducted at one of the chapels. This comparison identified minor discrepancies between the numerical model and the actual building (Buhagiar, 2020).

One of the findings depicted in the figure illustrates the H/H value of the East-West Component. The peak observed in the graph signifies the building's inherent frequency at that specific location. This peak provides a basis for determining the structure's fundamental period using the following relationship:

$$T = \frac{1}{f}$$

Equation 10 - Relationship between Natural Frequency and Fundamental period of the building.

Where:

T	The fundamental period of the structure
f	The natural frequency of the building at the specific point, usually obtained from modal analysis.

The peak at roughly 10Hz indicates a fundamental period of approximately 0.1 seconds for the structure. However, the modal analysis of the numerical model reveals a fundamental period of 0.036 seconds. This discrepancy arises from several factors related to the ambient noise measurement process. Firstly, the measurement was not accurately conducted due to the absence of a stabilizing weight on the instrument. Without this weight, vibrations caused by passing vehicles could affect the instrument, leading to inaccurate readings as it was not securely anchored to the ground. Additionally, accessing the centre of the chapel's roof was not feasible for safety reasons, preventing us from stepping on the roof. The tower ladder provided by the civil protection department could only reach the chapel's edge due to various obstacles. Consequently, the ambient noise measurement was taken from the top of the chapel's external wall rather than the centre of the barrel vault. These factors contribute to the observed discrepancy in the fundamental period values.

Appendix D contains more information on the ambient noise measurements.

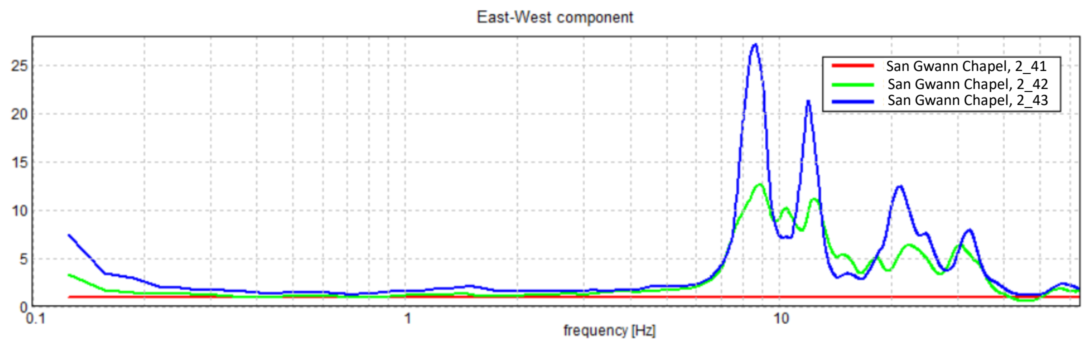

Figure 84 - H/H reading of the East-West component.

4.4.5.2 Pushover Analysis

The 3D Macro seismic analysis employs a non-linear pushover approach, featuring two loading phases: force-controlled and displacement-controlled. During the force-controlled phase, a load vector of consistent triangular shape is applied, adjusting based on the masses and heights of the floor slabs above ground level. This stage theoretically extends until the structure's maximum peak resistance. During the displacement-controlled phase, forces are applied by specifying displacements to all "control points," which represent nodes of the deformed model. The resulting capacity curve combines base shear and building displacement at chosen control points.

The pushover analysis progresses through steps with monotonically increasing loads, rendering seismic analysis results sensitive to specified load steps and sub-steps. Initial analyses yielded incomplete capacity curves due to reaching the maximum specified steps. Experimentation with different settings ensued, aiming to halt the pushover analysis upon reaching maximum building displacement. Figure 85 underneath details the settings to the typical seismic analysis, and it was decided to increase the maximum number of iterations to beyond 1,000 only in those seismic analysis where encountered convergence problems to conclude the seismic analysis.

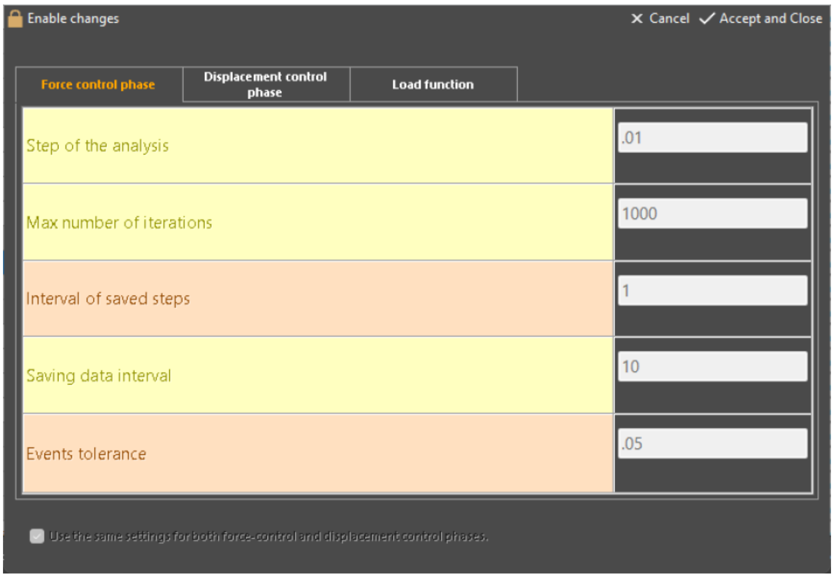

Figure 85 - Analysis Settings.

4.4.5.3 Limit State Seismic

The numerical seismic analyses were specifically focused on assessing conditions defined in EN1998-1-3 (2005) , which these correspond to the Near Collapse (NC), Significant Damage (SD), and Damage Limitation (DL) states used in seismic design for existing structures. Many existing buildings were not originally designed to withstand seismic forces, making it crucial to evaluate their capacity beyond significant damage. The primary objective is to prevent collapse during earthquakes with a low return period. However, the impact intensifies with earthquakes of higher return periods, occurring typically over several years.

During a low-grade earthquake, damage may be minimal, such as broken glass and manageable disruptions. Contrastingly, a strong earthquake with a return period of 475 years can cause extensive damage that severely impairs the building without collapsing it entirely this scenario characterizes significant damage. The transition towards near collapse involves incrementally increasing the earthquake load on the building. As the load escalates from significant damage, the structure moves closer to complete collapse. For limestone buildings, the seismic load that results in substantial damage is only marginally less than the load that could lead to near-collapse. This indicates that there is a minimal safety margin between causing significant damage and reaching a state of near-collapse.

Nevertheless, incorporating steel reinforcement offers the potential to extend this margin by approximately 10%, allowing the structure to enter the strain hardening region and withstand greater seismic forces effectively.

Displacement data from graphical analyses are utilized to calculate α-values for various limit states. An α-value below 1.00 denotes structural failure, whereas values of 1.00 or higher indicate structural integrity. These α-values, also known as safety factors, represent the ratio of actual horizontal displacement to the structure's horizontal displacement capacity.

Opting for seismic analyses according to NTC 2018 instead of EN1998-1 (2004) was driven by the limitations of the “3D Macro” modelling software, which does not produce capacity curves under EN1998-1 (2004) conditions. Furthermore, EN1998-1 (2004) does not allow for custom material properties input, hindering an accurate representation of Globigerina Limestone's unique mechanical characteristics in the numerical model. Therefore, the analyses adhered to NTC 2018.

Moreover, a correspondence exists between the limit states defined in NTC 2018 and those in EN1998-1-1 (2004) and EN1998-1-3 (2005) , as shown in Table 11. Specifically, the "Stati Limite di Salvaguardia della Vita" (SLV) or "Limit State for the Safeguard of Human Life," as specified according to the Italian Technical Standards for Construction, as established by the Ministerial Decree dated January 17, 2018, this corresponds to the Significant Damage Limit State specified in EN1998-1-3 (2005) for existing buildings, and to the No Collapse Requirement outlined in EN1998-1-1 (2004) for new constructions.

The SLV addresses structural stiffness loss due to non-structural component failure and collapse, along with significant damage to structural elements following an earthquake. It requires that structures maintain substantial stiffness and resistance to vertical loads, along with a significant safety margin against collapse under additional horizontal loads (Santucci De Magistris, 2011).

<table>
<tr><th>NTC 2018</th><th>EN1998-1-3 (2005)</th></tr>
<tr><td>SLD</td><td>DL</td></tr>
<tr><td>Stato Limite di Danno</td><td>Damage Limitation</td></tr>
<tr><td>PGA – 0.044</td><td>PGA – 0.07</td></tr>
<tr><td>Return Period, T_R - 50 Years</td><td>Return Period, T_R - 95 Years</td></tr>
<tr><td colspan="2">This guarantees that, in the event of an earthquake, the building's structural elements will maintain their ability to transfer horizontal and vertical loads, even if there is damage to the structural and non-structural components or equipment. Thus, the building will continue to operate effectively despite minor damage to its components.</td></tr>
<tr><td>SLV</td><td>SD</td></tr>
<tr><td>Stato Limite di Vita</td><td>Significant Damage</td></tr>
<tr><td>PGA – 0.1</td><td>PGA – 0.1</td></tr>
<tr><td>Return Period, T_R - 474 Years</td><td>Return Period, T_R - 475 Years</td></tr>
<tr><td colspan="2">After an earthquake, buildings may experience failures in non-structural elements and substantial damage to structural components, resulting in a notable reduction in horizontal stiffness. Nevertheless, the building retains a portion of its structural robustness and rigidity to resist vertical forces, ensuring a safety margin against collapse due to horizontal seismic forces.</td></tr>
<tr><td>SLC</td><td>NC</td></tr>
<tr><td>Stato Limite di Collasso</td><td>Near Collapse</td></tr>
<tr><td>PGA – 0.124</td><td>PGA – 0.35</td></tr>
<tr><td>Return Period, T_R - 974 Years</td><td>Return Period, T_R - 2475 Years</td></tr>
<tr><td colspan="2">After an earthquake, buildings experience significant damage to structural components, resulting in the failure of non-structural elements. Nevertheless, the building maintains a minimal safety margin for both vertical and lateral seismic actions, preventing complete structural failure.</td></tr>
</table>

Table 11 - Comparison of Limit States in NTC 2018 and EN 1998-1 (2004) (Santucci De Magistris, 2011; EN 1998-1 :2004).

Chapter 5: Seismic Analysis and Discussion of Results

This chapter details the results from seismic analyses performed on three chapels, presenting the findings through various charts and pushover curves. Additionally, safety factors for the chapels are compared using graphs. For a comprehensive comparative analysis of the structural responses, the pushover curves for each type of analysis were combined into a unified graph for all three chapels. The capacity curves and analysis results were derived from the non-linear static analyses conducted with 3D Macro software. The seismic vulnerability assessment compares San Gwann Chapel and Dingli Chapel, both nearly regular but on different sub-surface geologies ground type A for San Gwann and ground type B for Dingli. It also compares San Gwann Chapel with Qrendi Chapel, both on ground type A, but with Qrendi being irregular in plan and elevation. These comparisons highlight how ground type and structural regularity influence seismic vulnerability.

5.1 Seismic Vulnerability Assessment

The following analysis examines the seismic performance of three chapels in Malta, an area characterized by moderate earthquake intensity, approximately 0.1g. These structures are single-story buildings with alpha values exceeding 1, suggesting a satisfactory safety margin against seismic forces. Despite all alpha values being greater than 1, the chapel with the lowest alpha is the most vulnerable when comparing among them. Table 12 indicates the lowest alpha of each of the three chapels and a full set of these results can be found in Appendix C.

Chapel	Analysis	Limit state	Total Lateral Deflection		Safety Factor α	Check
			Demand (cm)	Capacity (cm)		
St. Philip & St. James in San Gwann	Pushover-X Acc	SLD	0.0038	0.0479	12.6403	Pass
	Pushover-X Acc	SLV	0.0069	0.4460	64.2259	Pass
	Pushover-X Acc	SLC	0.0085	0.7168	84.6837	Pass
	Pushover+X Acc - e	SLD	0.0033	0.0481	14.5717	Pass
	Pushover+X Acc - e	SLV	0.0061	0.1476	24.2358	Pass
	Pushover+X Acc - e	SLC	0.0074	0.2075	27.9333	Pass
St. Mary Magdalene in Dingli	Pushover-X Acc	SLD	0.0042	0.0626	14.8630	Pass
	Pushover-X Acc	SLV	0.0084	0.0801	9.5869	Pass
	Pushover-X Acc	SLC	0.0102	0.1772	17.2905	Pass
	Pushover+X Acc - e	SLD	0.0047	0.0790	16.9300	Pass
	Pushover+X Acc - e	SLV	0.0092	0.0790	8.5747	Pass
	Pushover+X Acc - e	SLC	0.0113	0.1909	16.8972	Pass
St. Matthew's in Qrendi	Pushover-X Acc	SLD	0.0408	0.5291	12.9851	Pass
	Pushover-X Acc	SLV	0.0805	1.7129	21.2893	Pass
	Pushover-X Acc	SLC	0.0971	2.3048	23.7373	Pass
	Pushover+X Acc - e	SLD	0.0326	0.3034	9.3032	Pass
	Pushover+X Acc - e	SLV	0.0607	0.6992	11.5101	Pass
	Pushover+X Acc - e	SLC	0.0734	0.9961	13.5710	Pass

Table 12 - Pushover Results of all three chapels highlighting minimum alpha.

When the earthquake intensity is increased from 0.1g to higher levels such as 0.2g or 0.3g, the first chapel to fail is Dingli Chapel, due to its lowest alpha value. This would be followed by the failure of the Qrendi Chapel, and ultimately, the San Gwann Chapel would fail last. The comparative safety factors for these chapels are as follows: Dingli has the lowest safety factor at 8.58, followed by Qrendi at 9.30, and San Gwann at 12.64. All data and results comparisons of all three chapels are gathered in Table 13.

Chapel	St. Philip & St. James Chapel in San Gwann	St. Mary Magdalene Chapel in Dingli	St. Matthew's Chapel in Qrendi
Subsurface Geology	Middle Globigerina Limestone	Upper Coraline Limestone on Deep Clay	Middle Globigerina Limestone
Ground Type (EC8 - Part 1)	A	B	A
Regular in Plan	Yes	Yes	No
Regular in Elevation	Yes	Yes	No
Masonry Block Type	Globigerina Limestone	Globigerina Limestone	Globigerina Limestone
Assumed Mortar Strength	M2	M2	M2
Earthquake Direction for Minimum Alpha	- X Acc	+ X Acc - e	+ X Acc - e
Minimum Alpha	12.64	8.57	9.30
Critical Limit State for Minimum Alpha	Damage Limitation (SLD)	Significant Damage (SLV)	Damage Limitation (SLD)
Alpha for Earthquake Direction -X Acc	12.64	9.58	12.98
Limit State for Earthquake Direction -X Acc	Damage Limitation (SLD)	Significant Damage (SLV)	Damage Limitation (SLD)

Table 13 - Comparative Table with data of all three chapels.

5.1.1 Comparism between St. Philip & St. James Chapel in San Gwann and St. Mary Magdalene Chapel in Dingli.

In understanding the effect of subsoil, a comparison between Dingli and San Gwann Chapel is made. Both chapels are nearly symmetrical and regular in plan and elevation having no additional rooms, yet the subsoil type creates a marked difference in their alphas. San Gwann, situated on Globigerina Limestone (ground type A), has a higher safety factor of

12.64 meaning having less amplification of displacement compared to Dingli on Upper Coralline Limestone over Blue Clay (ground type B), with an alpha of 8.58.

5.1.2 Comparism between St. Philip & St. James Chapel in San Gwann and St. Matthew's Chapel in Qrendi

The presence of additional rooms, in case of Qrendi, reduces the safety factor because it introduces asymmetry both the building's layout and vertical profile. This asymmetry results in plan and vertical irregularities, which negatively impact the building's seismic performance. The height variation of these additional rooms compared to the main chapel further exacerbates these irregularities. Comparing Qrendi with San Gwann, both situated on Globigerina subsoil, the safety factor drops from 12.64 to 9.3 due to these irregularities.

5.1.3 Comparism between St. Mary Magdalene Chapel in Dingli and St. Matthew's Chapel in Qrendi.

These alpha values confirm expectations, while the ongoing analysis enables quantification of the actual differences between them. Further comparisons reveal that despite Dingli's chapel regular plan and elevation, its safety factor is lower than Qrendi's Chapel because of the subsoil conditions. The Qrendi Chapel, with plan and vertical irregularities but situated on ground type A, has a higher safety factor of 9.3 than Dingli of 8.58, illustrating that subsoil type has a more profound impact on structural safety than plan irregularities.

5.2 Pushover Curves

- The following pushover curves are essential for understanding the displacement capacity and demand of the chapels. The safety factor, alpha, is identified as the displacement capacity divided by the displacement demand. Displacement capacity refers to the displacement that will cause the structure to reach a limit state, whether SLD (Significant Limit Damage), SLV (Severe Limit Vulnerability), or SLC (Structural Limit Collapse). Displacement demand is the displacement at the roof of the chapel under an earthquake intensity of 0.1g. These pushover curves were for the most critical earthquake direction for all three chapels separately. In case of St. Philip & St. James Chapel in San Gwann the most critical seismic analysis was the Pushover – X Acc, while, in case of St. Mary Magdalene Chapel in Dingli and St. Matthew's Chapel in Qrendi was Pushover + X Acc – e.

5.2.1 Pushover Curve of St. Philip & St. James Chapel in San Gwann for – X Acc.

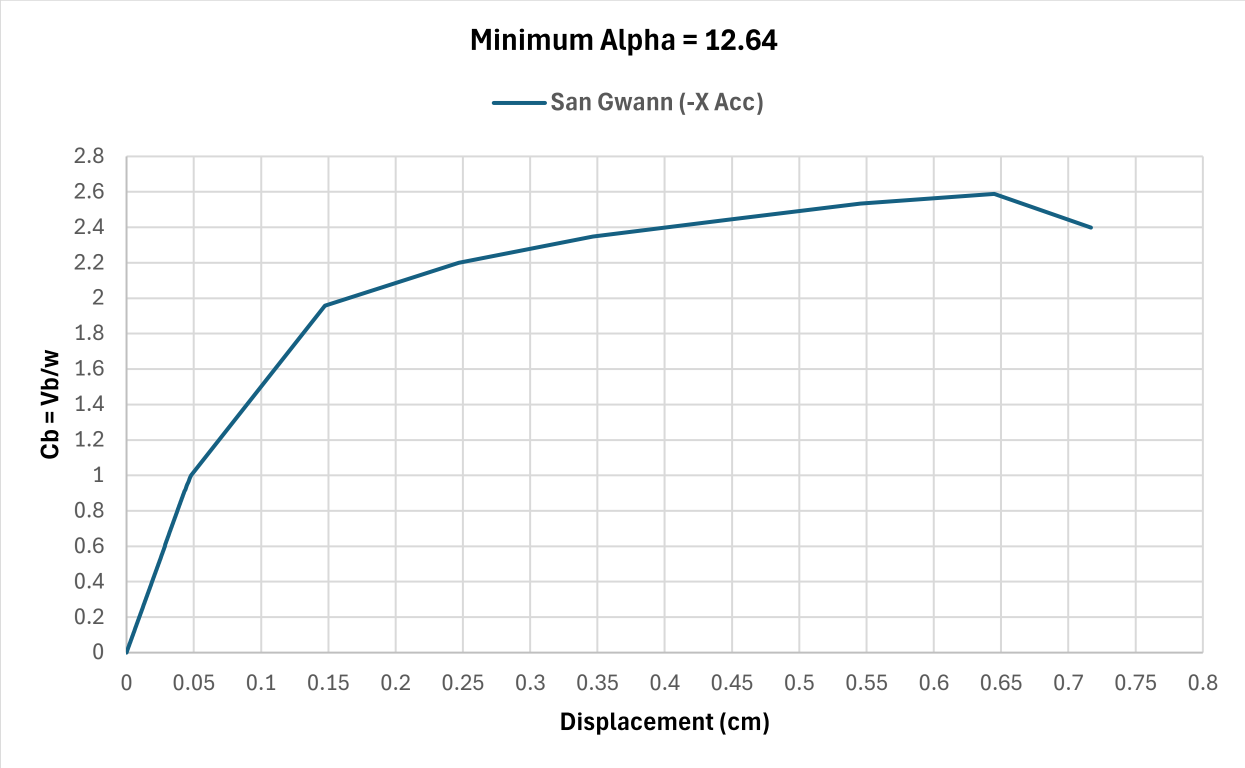

Figure 86 - Pushover Curve of St. Philip & St. James Chapel in San Gwann for – X Acc minimum.

5.2.2 Pushover Curve of St. Philip & St. James Chapel in San Gwann for + X Acc – e.

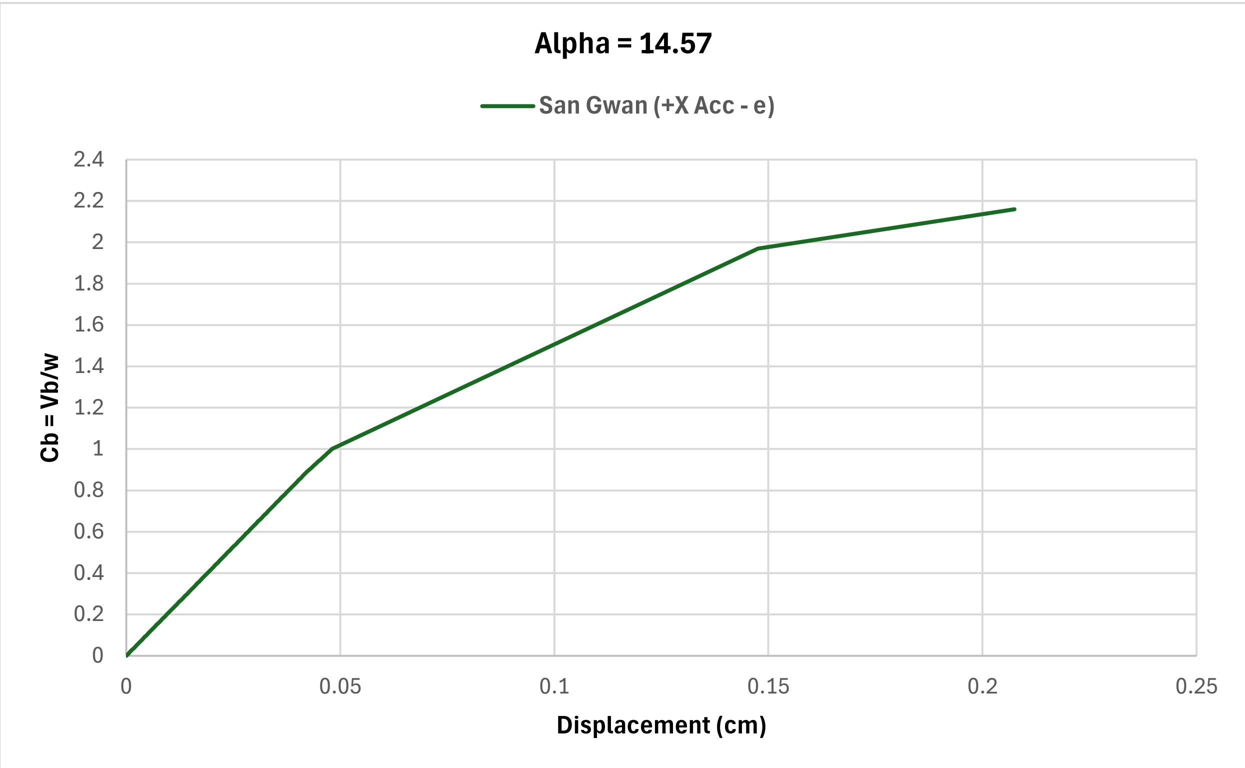

Figure 87 - Pushover Curve of St. Philip & St. James Chapel in San Gwann for + X Acc – e.

5.2.3 Pushover Curve of St. Mary Magdalene Chapel in Dingli for + X Acc – e.

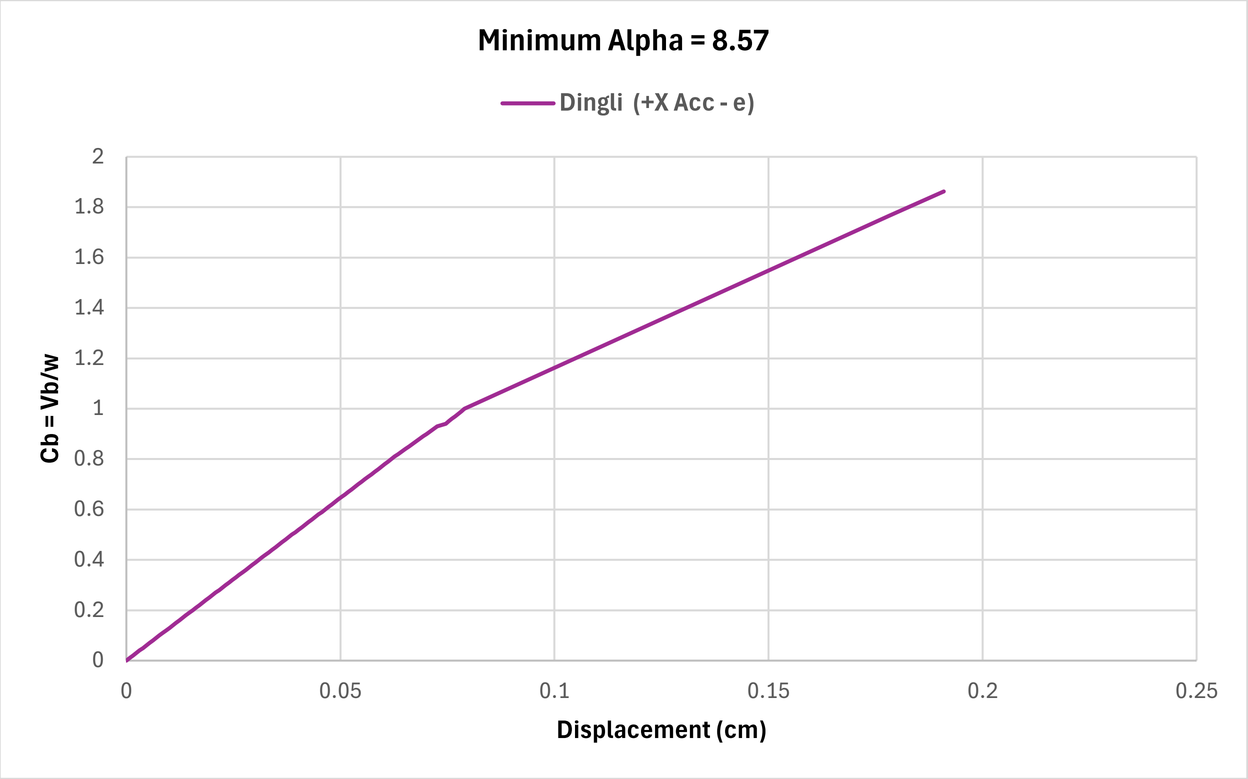

Figure 88 - Pushover Curve of St Mary Magdalene Chapel in Dingli for + X Acc – e minimum alpha.

5.2.4 Pushover Curve of St. Matthew's Chapel in Qrendi for + X Acc – e.

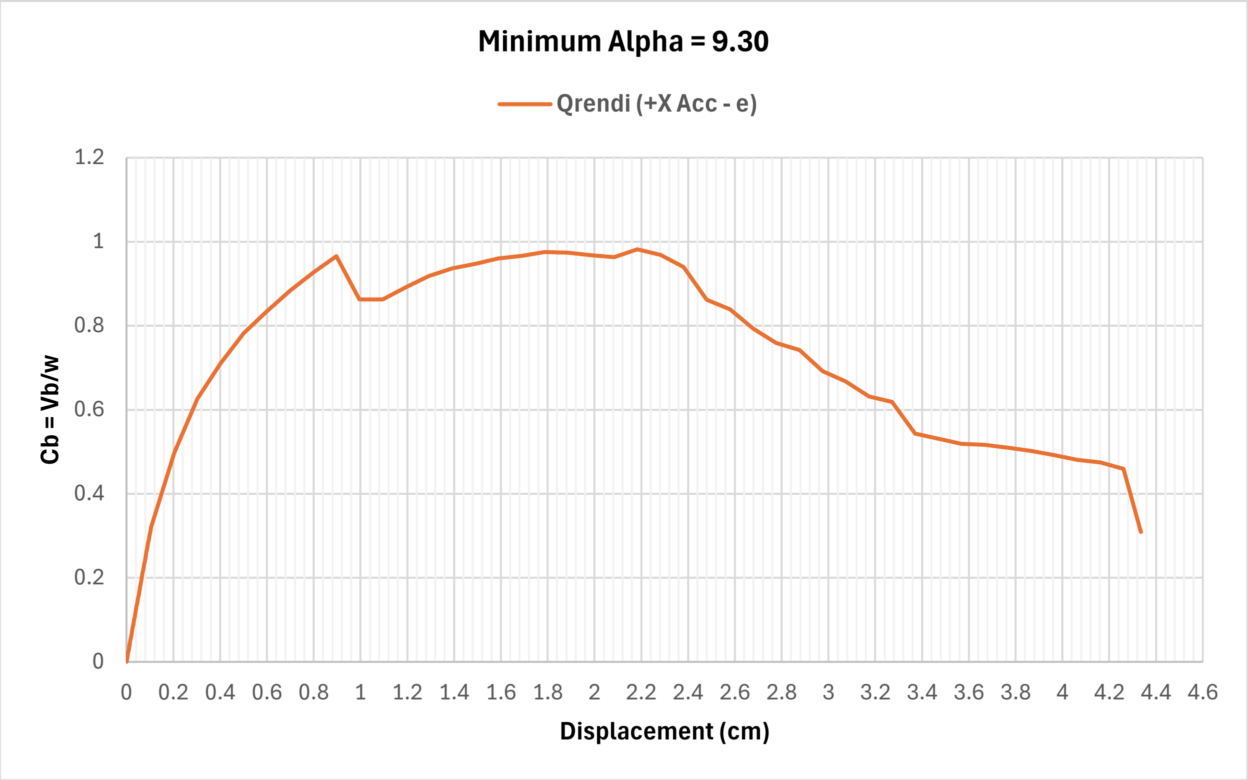

Figure 89 - Pushover Curve of St Matthew's Chapel in Qrendi for + X Acc – e minimum alpha.

5.2.5 Pushover Curve of All Three Chapels for + X Acc – e

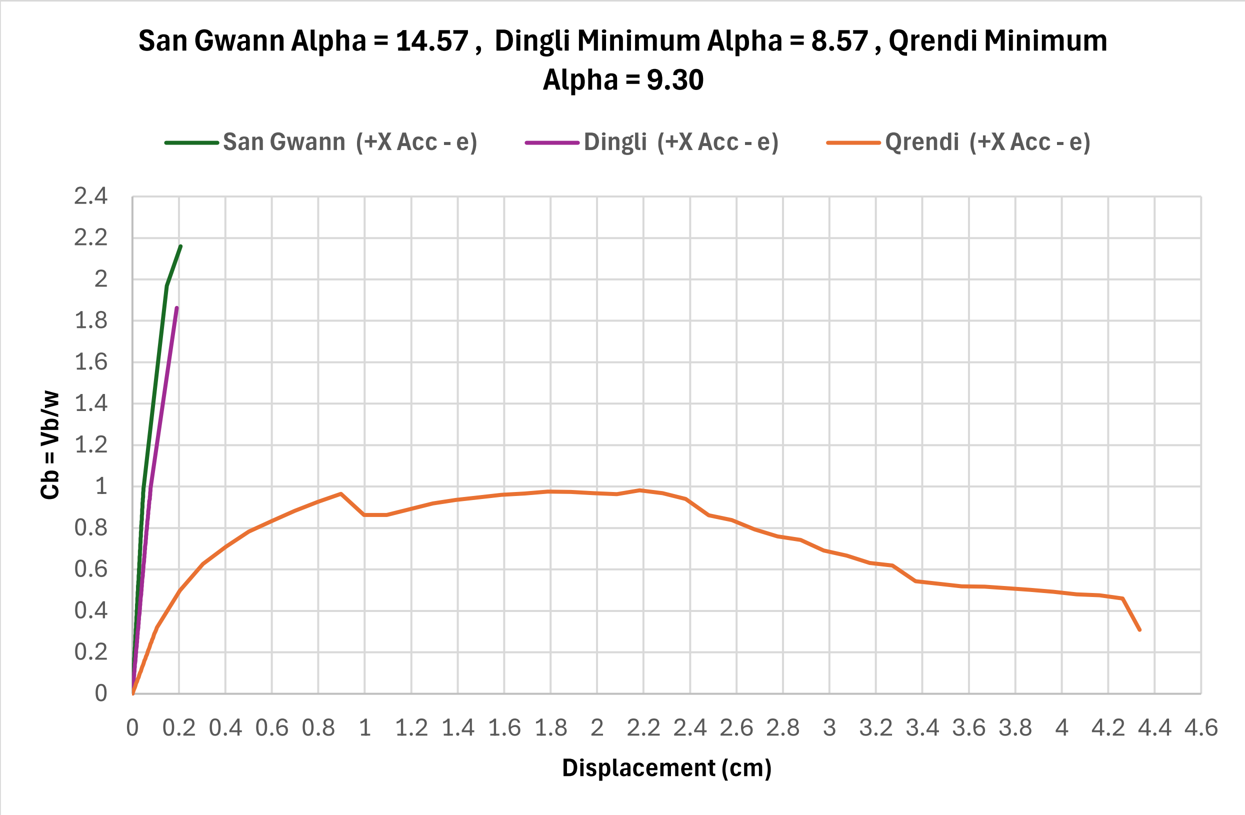

Figure 90 - Pushover Curve of All Three Chapels for + X Acc – e.

5.2.6 Pushover Curve of All Three Chapels for Minimum Alpha

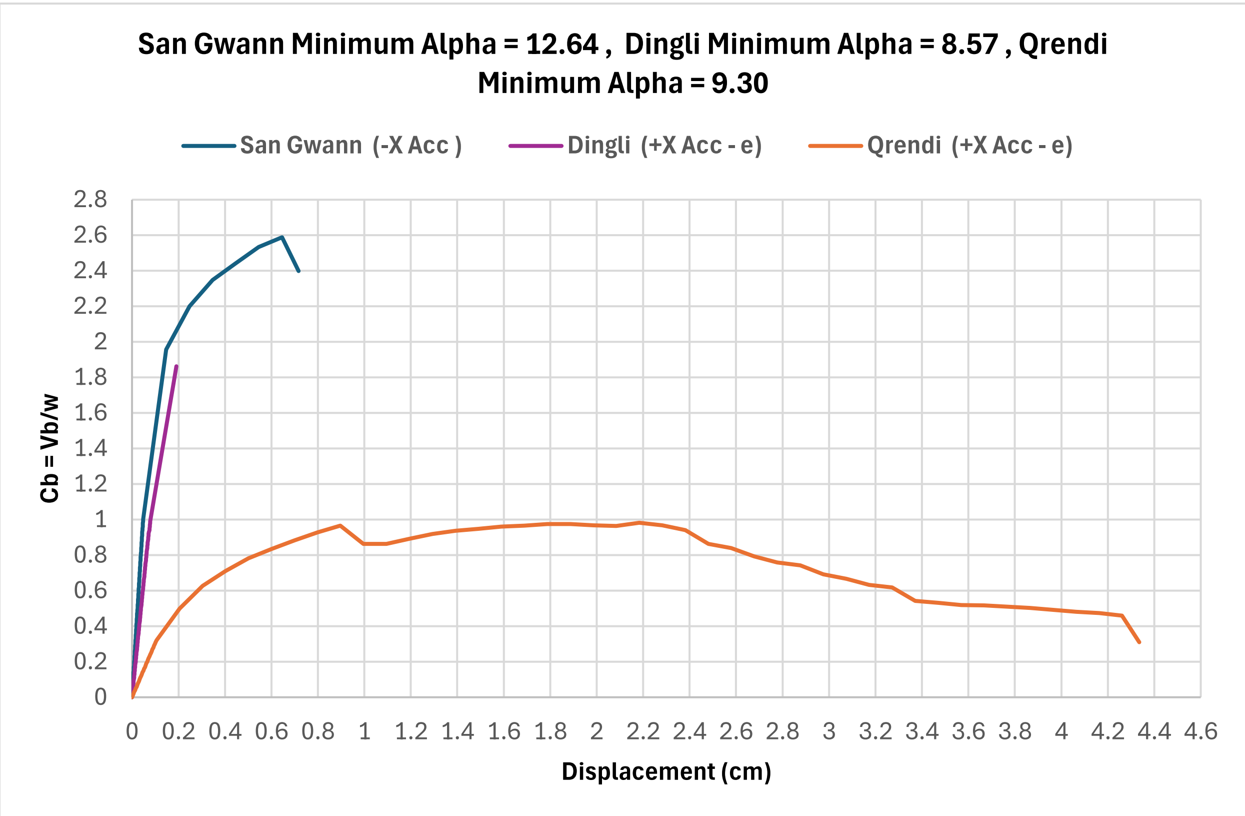

Figure 91 - Pushover Curve of All Three Chapels for Minimum Alpha.

5.3 Limit States

In the following section, the corresponding capacity curves for the most critical pushover seismic analysis are overlaid with bilinear response curves. Each set of curves is paired with a graphical depiction of the structural damage at different performance limit states. Figure 92 and Figure 93 illustrates the legends for the limit state markers and damage patterns. The additional isometric view of the chapels, illustrating damage at the remaining limit states, can be found in Appendix C.

Under the design earthquake intensity of 0.1g, none of the chapels are expected to fail in any limit state, including the Serviceability Limit State (SLD), Significant Damage Limit State (SLV), or Ultimate Limit State (SLC). However, in regions with higher seismic intensities, the sequence of failure begins with the Dingli Chapel, followed by the Qrendi Chapel, and finally the San Gwann Chapel. The Dingli Chapel is projected to reach the SLV first, indicating significant structural damage. Further increases in seismic intensity, lead to the Qrendi Chapel reaching the SLD, followed by the San Gwann Chapel also reaching the SLD. The Dingli Chapel's quicker failure is primarily due to the amplification effects of the blue clay subsoil (ground type B), which causes amplified displacements. Conversely, the strong subsoil (ground type A) at the San Gwann and Qrendi Chapels leads to their failure at the SLD. This highlights the significant influence of subsoil conditions on the seismic response and failure mechanisms of the chapels.

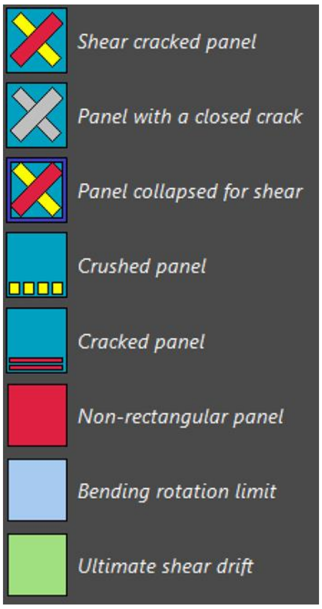

Figure 92 - Legend for damage patterns.

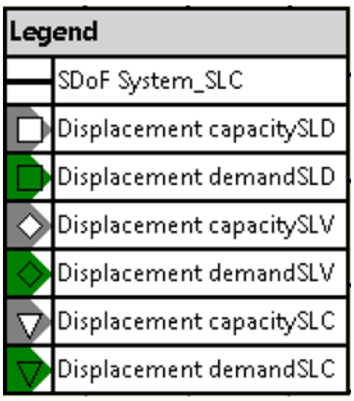

Figure 93 - Legend for when α > 1.

5.3.1 Bilinear curve for - X Acc direction of St. Philip & St. James Chapel in San Gwann.

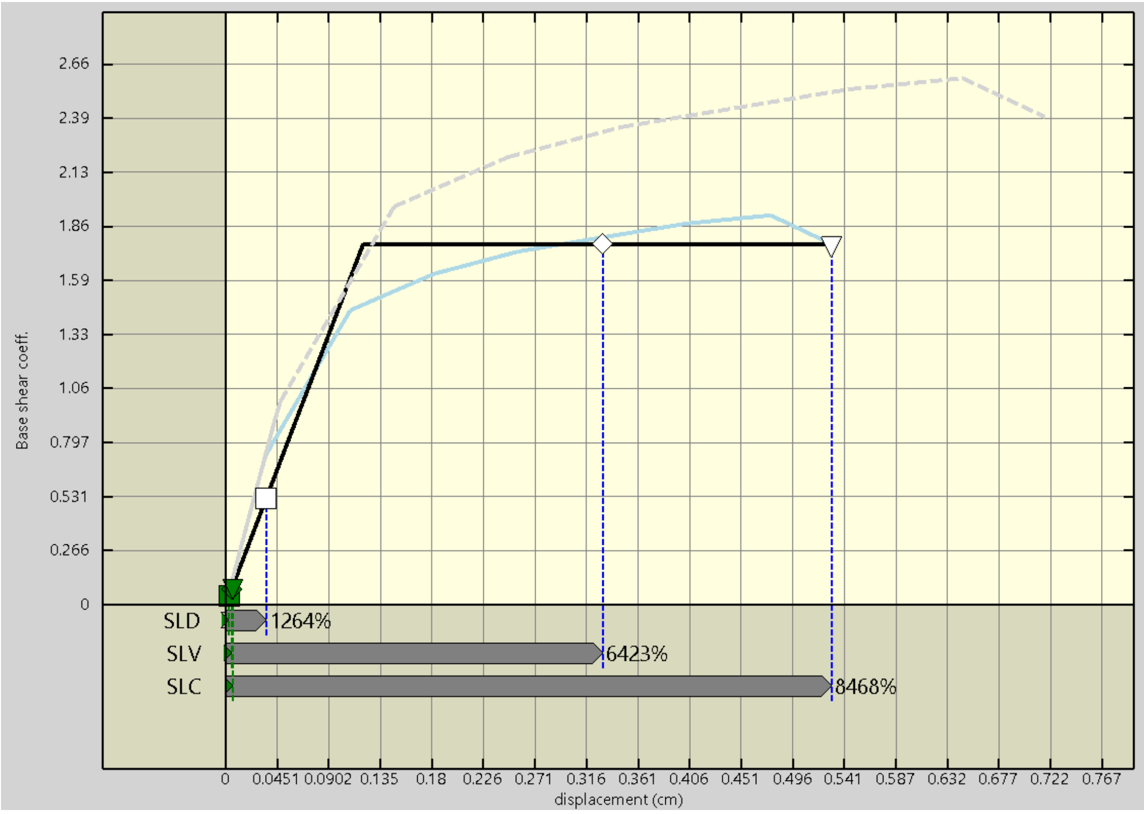

Figure 94 - Bilinear curve for - X Acc direction of St. Philip & St. James Chapel in San Gwann. (Blue Curve: pushover curve from Figure 86).

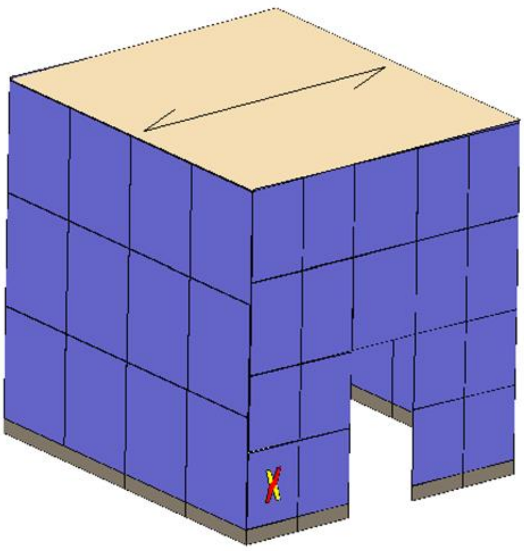

Figure 95 - Front Isometric View of San Gwann Chapel showing damage at Damage Limitation Limit State (SLD) for Earthquake Direction - X Acc.

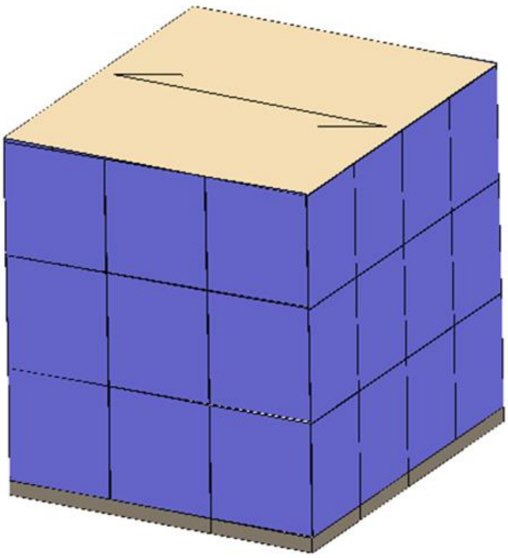

Figure 96 - Back Isometric View of San Gwann Chapel showing damage at Damage Limitation Limit State (SLD) for Earthquake Direction - X Acc.

5.3.2 Bilinear curve for + X Acc - e direction of St. Philip & St. James Chapel in San Gwann.

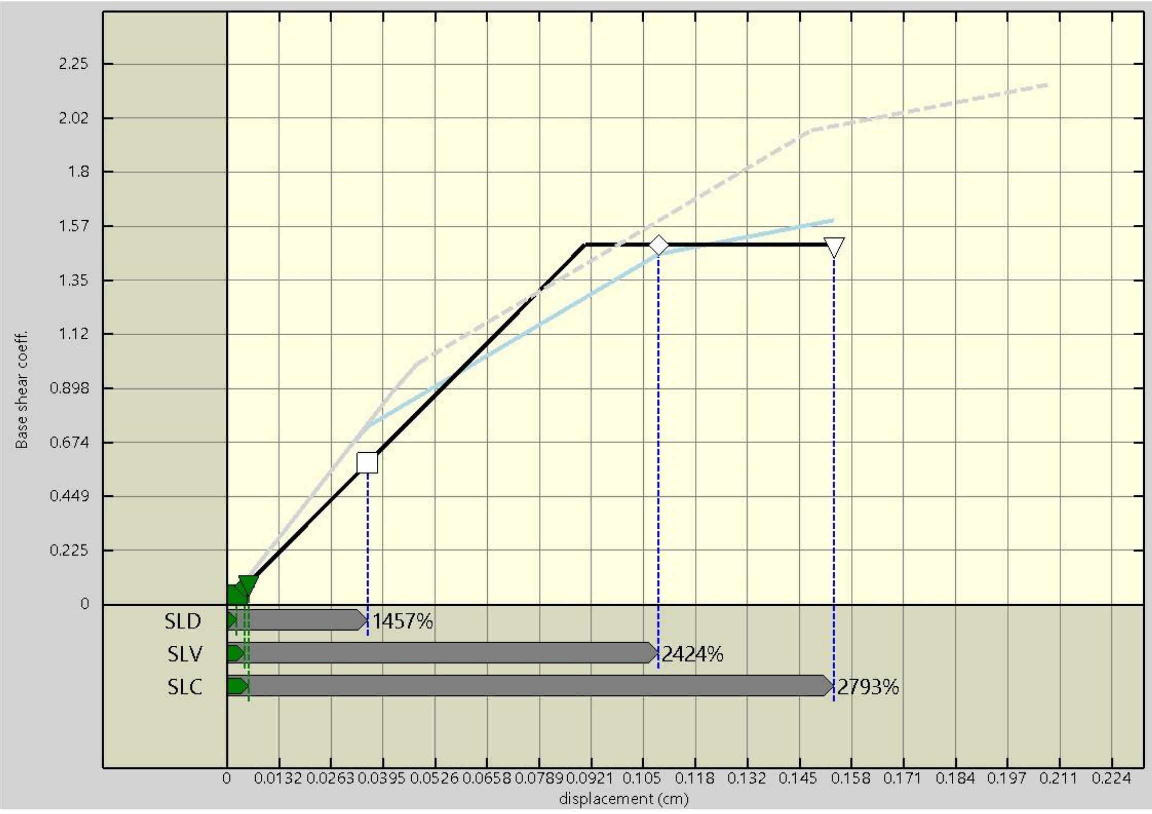

Figure 97 - Bilinear curve for + X Acc - e direction of St. Philip & St. James Chapel in San Gwann. (Blue Curve: pushover curve from Figure 87).

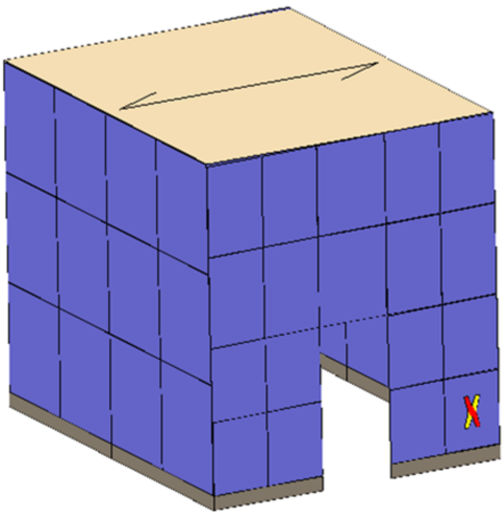

Figure 98 - Front Isometric View of San Gwann Chapel showing damage at Damage Limitation Limit State (SLD) for Earthquake Direction + X Acc – e.

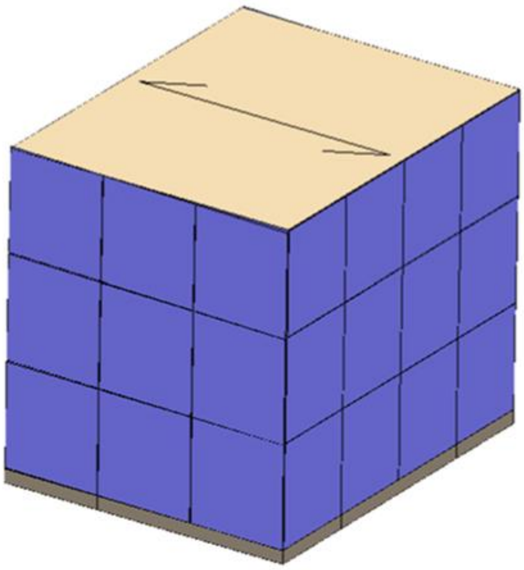

Figure 99 - Back Isometric View of San Gwann Chapel showing damage at Damage Limitation Limit State (SLD) for Earthquake Direction + X Acc – e.

5.3.3 Bilinear curve for + X Acc - e direction of St. Mary Magdalene Chapel in Dingli.

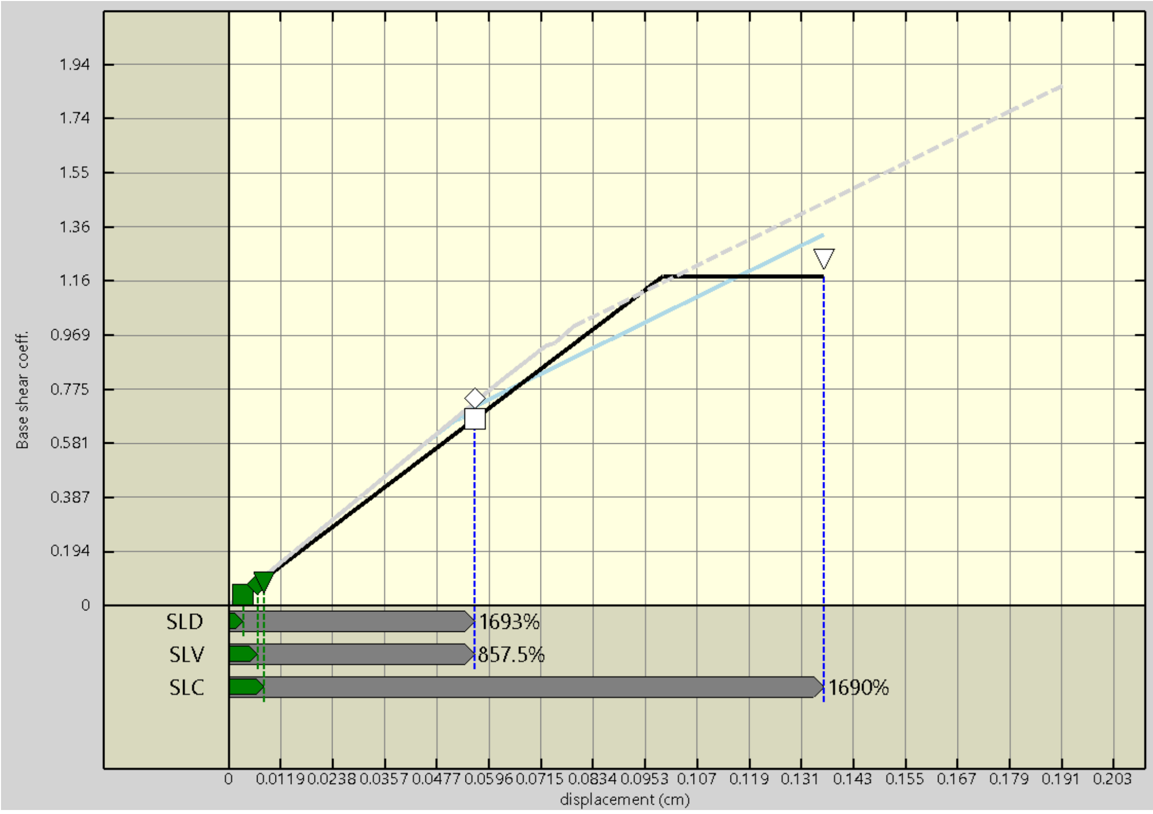

Figure 100 - Bilinear curve for + X Acc - e direction of St Mary Magdalene Chapel in Dingli. (Blue Curve: pushover curve from Figure 88).

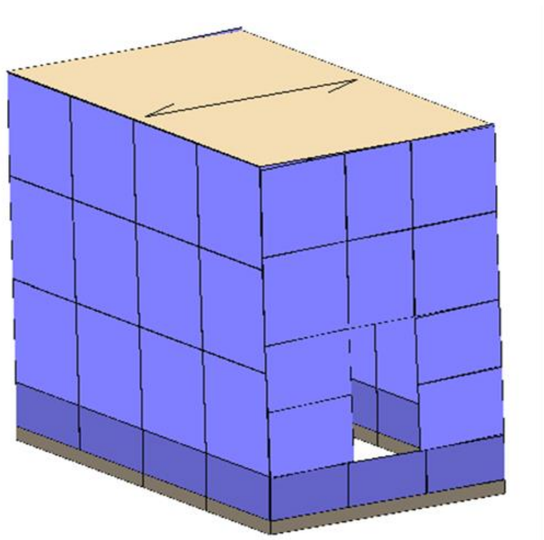

Figure 101 - Front Isometric View of Dingli Chapel showing damage at Significant Damage Limit State (SLV) for Earthquake Direction + X Acc – e.

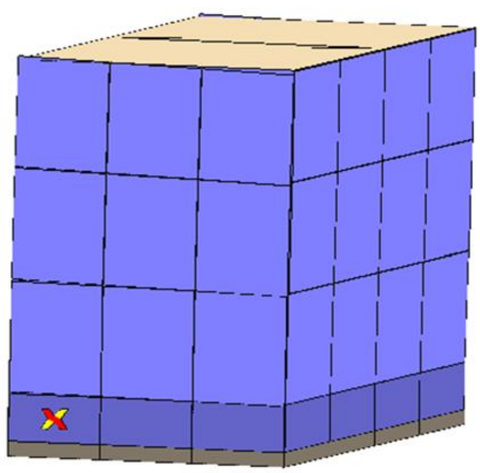

Figure 102 - Back Isometric View of Dingli Chapel showing damage at Significant Damage Limit State (SLV) for Earthquake Direction + X Acc – e.

5.3.4 Bilinear curve for + X Acc - e direction of St. Matthew's Chapel in Qrendi.

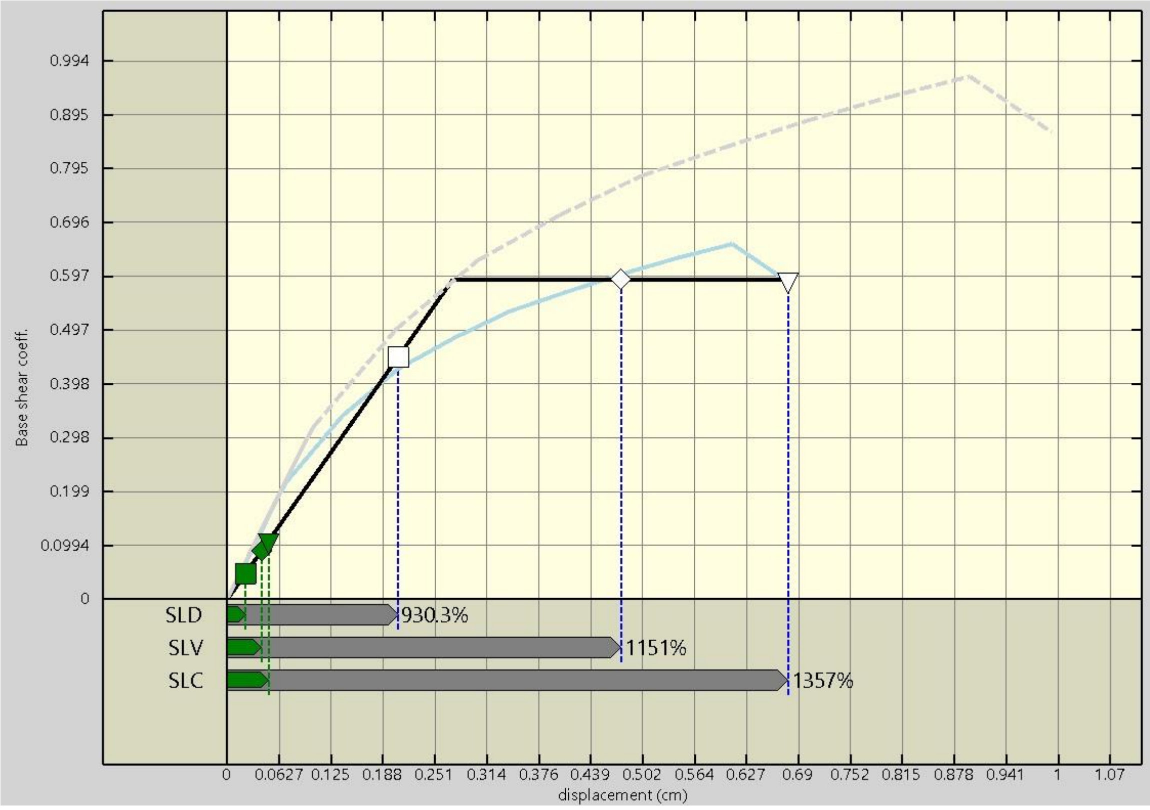

Figure 103 - Bilinear curve for + X Acc - e direction of St Matthew's Chapel in Qrendi. (Blue Curve: pushover curve from Figure 89).

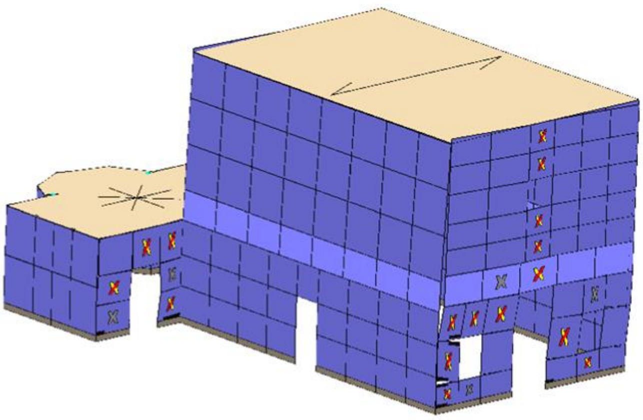

Figure 104 - Front Isometric View of Qrendi Chapel showing damage at Damage Limitation Limit State (SLD) for Earthquake Direction + X Acc – e.

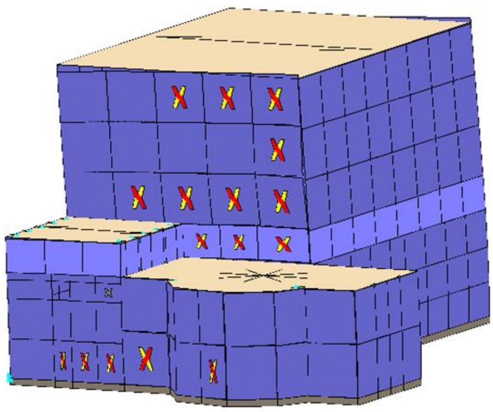

Figure 105 - Back Isometric View of Qrendi Chapel showing damage at Damage Limitation Limit State (SLD) for Earthquake Direction + X Acc – e.

5.4 General Observation from the Results

The obtained results highlight significant differences in the structural performance and seismic resilience of three historical chapels, the St. Philip & St. James Chapel in San Gwann, St. Mary Magdalene Chapel in Dingli, and St. Matthew's Chapel in Qrendi.

The sway stiffnesses of the San Gwann Chapel and the Dingli Chapel are significantly greater than that of the Qrendi Chapel. This can be attributed to the plan and elevation irregularities associated with the Qrendi Chapel, which substantially reduce the chapel sway stiffness compared to the larger sway stiffnesses of the San Gwann Chapel and the Dingli Chapel, both of which are (almost) regular in elevation and plan.

Furthermore, the sway stiffness of the San Gwann Chapel is slightly greater than that of the Dingli Chapel. This difference is primarily due to the San Gwann Chapel being founded on Upper Globigerina Limestone, while the Dingli Chapel is founded on Upper Coralline Limestone above a deep clay layer. The geological differences in the foundations contribute to the variations in sway stiffness between these two chapels.

Additionally, the maximum base shear coefficient for the San Gwann Chapel is approximately 2.60 times that for the Qrendi Chapel. This indicates that the San Gwann Chapel is capable of withstanding a seismic horizontal load much higher than the Qrendi Chapel. Although the maximum base shear coefficient for the Dingli Chapel was not traced by 3D Macro. However, given that the sway stiffness of the Dingli Chapel was observed to be slightly less than that for the San Gwann Chapel, it is expected that likewise the maximum base shear coefficient for the Dingli Chapel would be slightly less than that of the San Gwann Chapel, also due to the fact that the Dingli Chapel is founded on weaker subsoil than that on which the San Gwann Chapel is founded on. In fact, the weaker subsoil beneath the Dingli Chapel would lead to larger amplifications of horizontal displacements during a seismic event when compared to those of the San Gwann Chapel.

In contrast, the post-ultimate curve for the Qrendi Chapel exhibits a long plateau, indicating a structurally ductile (safe) form of unloading. This form of unloading retains significant residual strength over a long post-ultimate displacement range. Since 3D Macro did not trace the post-ultimate curves for both the San Gwann Chapel and the Dingli Chapel, no observations may be made at this stage about the structural ductility, or otherwise, of their corresponding post-ultimate curves.

The maximum base shear coefficients for all three chapels range between approximately 1.00 (Qrendi Chapel) and 2.60 (San Gwann Chapel), indicating that the maximum horizontal seismic shear force at the chapel foundations varies between approximately 1.00 times and 2.60 times the seismic weight of the corresponding chapels. Considering that the typical maximum base shear coefficients in modern multi-storey buildings vary between 0.10 to 0.20, the maximum base shear coefficients exhibited by the three chapels are significantly higher. This observation may be attributed to the rather small plan size of the chapels, which are all one-storey buildings. Additionally, it would take a maximum base shear force several times the seismic weight of a typical Maltese Chapel to cause it to reach failure. On the other hand, given the comparatively much larger seismic weight of modern multi-storey buildings, it only requires a small portion (approximately 10% to 20%) of the corresponding seismic weight to cause the building to reach failure.

In conclusion, the comparative analysis reveals distinct seismic characteristics among the St. Philip & St. James Chapel in San Gwann, St. Mary Magdalene Chapel in Dingli, and St. Matthew’s Chapel in Qrendi, highlighting varying levels of structural behaviours that influence their resilience to seismic events. Given that the minimum alpha is 8.58, none of the chapels are expected to sustain any damage or failure of any sort even with a design earthquake of 0.1g, indicating no need for retrofitting.

Chapter 6: Conclusion and Recommendations for Future Research Work

6.1 Conclusion

The objective of this dissertation was to determine the seismic vulnerability of several historical chapels in Malta, an area characterized by low-to-moderate seismic risk. The Maltese islands are encompassed by chapels that significantly contribute to Maltese heritage. These chapels exhibit diversity in both size and shape, yet they share common characteristics. Three typical Maltese chapels were chosen, each outlined with details regarding their ground geology, height, width, and length. Some of these chapels stand alone, while others are connected to adjacent structures.

The seismic vulnerability assessment involved a detailed comparison and assessment of these three chapels St. Philip & St. James Chapel in San Gwann, St. Mary Magdalene Chapel in Dingli, and St. Matthew's Chapel in Qrendi. San Gwann and Dingli Chapels, both of which are nearly regular in plan and elevation, were evaluated based on their different sub-surface geologies ground type A for San Gwann Chapel and ground type B for Dingli Chapel. Additionally, the comparison included San Gwann and the Qrendi Chapels, both founded on ground type A. In this case, the San Gwann Chapel is regular in both plan and elevation, while the Qrendi Chapel is irregular in elevation and plan. These comparisons allow for a comprehensive understanding of how different factors, such as ground type and structural regularity, influence seismic vulnerability.

To model the chapels as accurately as possible and avoid limitations of each program, two types of macro element software were used. The barrel vaults of the chapels were built using Histra Arches and Vaults, while the rest of the chapels, including the parameters of the barrel vaults from Histra Arches and Vaults, were modelled in 3D Macro.

Furthermore, the analysis examined the seismic performance of the chapels in an area with moderate earthquake intensity, approximately 0.1g. The structures, being single-story buildings with alpha values exceeding 1, indicated a satisfactory safety margin against seismic forces. However, under increased earthquake intensities, the sequence of failure would begin with the Dingli Chapel, followed by the Qrendi Chapel, and finally, the San Gwann Chapel.

The safety factors were 8.58 for Dingli, 9.30 for Qrendi, and 12.64 for San Gwann, indicating varying levels of vulnerability.

Comparing the effect of subsoil, the Dingli Chapel and San Gwann Chapel are nearly symmetrical and regular in plan and elevation, yet the subsoil type creates a marked difference in their safety margin. San Gwann, situated on globigerina (ground type A), has a higher safety factor of 12.64 meaning having less amplification of displacement compared to Dingli on Upper Coralline Limestone over Blue Clay (ground type B), with an alpha of 8.58. In Qrendi's case, the inclusion of extra rooms decreases the safety margin due to asymmetry introduced in both the building's layout and elevation. This asymmetry results in plan and vertical irregularities, which negatively impact the building's seismic performance. Comparing Qrendi Chapel with San Gwann Chapel, both situated on Globigerina subsoil, the safety factor drops from 12.64 to 9.3 due to these irregularities. Further comparisons reveal that despite Dingli's Chapel regular plan and elevation, its safety factor is lower than Qrendi's Chapel due to the effect of subsoil conditions. The Qrendi Chapel, with plan and vertical irregularities but situated on ground type A, has a higher safety factor of 9.3 than Dingli of 8.58, illustrating that subsoil type has a more profound impact on structural safety than plan irregularities.

The pushover curves are essential for understanding the displacement capacity and demand of the chapels. In the case of St. Philip & St. James Chapel in San Gwann, the most critical seismic analysis was the Pushover – X Acc, while in the case of St. Mary Magdalene Chapel in Dingli and St. Matthew’s Chapel in Qrendi, it was Pushover + X Acc – e.

In terms of limit states, the Dingli Chapel is projected to reach the SLV first, indicating significant structural damage. Further increases in seismic intensity led to the Qrendi Chapel reaching the SLD, followed by the San Gwann Chapel also reaching the SLD. The Dingli Chapel's quicker failure is primarily due to the amplification effects of the Blue Clay subsoil (ground type B), which causes amplified displacements. Conversely, the strong subsoil (ground type A) at the San Gwann and Qrendi Chapels leads to their failure at the SLD. This highlights how subsoil conditions strongly affect the seismic response and failure mechanisms of the chapels.

The results obtained highlight significant differences in the structural performance and seismic resilience of three historical chapels. The sway stiffnesses of the San Gwann Chapel and the Dingli Chapel are significantly greater than that of the Qrendi Chapel. This difference is due to the plan and elevation irregularities associated with the Qrendi Chapel, which reduce its sway stiffness. Additionally, the geological differences in the foundations contribute to variations in sway stiffness, with the San Gwann Chapel, founded on Upper Globigerina Limestone, having slightly greater stiffness than the Dingli Chapel, founded on Upper Coralline Limestone above a deep clay layer.

Additionally, the maximum base shear coefficient for the San Gwann Chapel is approximately 2.60 times that for the Qrendi Chapel, indicating a higher capacity to withstand seismic loads. In contrast, the post-ultimate curve for the Qrendi Chapel exhibits a long plateau, indicating significant residual strength and structural ductility, a characteristic not observed in the other chapels due to limitations in the tracing by 3D Macro.

In conclusion, this dissertation reveals distinct seismic characteristics among the St. Philip & St. James Chapel in San Gwann, St. Mary Magdalene Chapel in Dingli, and St. Matthew's Chapel in Qrendi. The minimum alpha value of 8.58 suggests that none of the chapels are expected to sustain damage or failure with the design earthquake of 0.1g, indicating no need for retrofitting. This comparative analysis enhances the understanding of factors influencing the seismic vulnerability of Maltese chapels, contributing to the preservation and resilience of these historical structures.

6.2 Recommendations for Future Research Work

This analysis has identified areas where further investigation could significantly expand upon the findings. The following suggestions outline potential research initiatives that could complement the results obtained and explore related fields or aspects that require additional research input.

- Future research should explore the precise levels of peak ground acceleration (PGA) at which structural collapses occur for chapels exhibiting high alpha values. Given the minimum alpha value of 8.58 at 0.1g PGA, it is crucial to identify the specific PGA levels that precipitate structural failure.

- Investigate sensitive and effective retrofitting methodologies for historical chapels in scenarios of potential structural failure. This research should focus on minimally invasive techniques that maintain the architectural and historical integrity of the structures while significantly enhancing their seismic resilience.

- Extend studies to include chapels with varying height to width and length to width ratios. Analysing structures that are elongated and narrow or significantly tall and narrow will provide a comprehensive understanding of how different geometries impact seismic performance.

- Conduct research on chapels constructed directly on Blue Clay, contrasting these with structures on layered soil types such as Upper Coralline Limestone over Blue Clay. This is particularly relevant for chapels in regions like Mgarr, where the sub-soil ground type C can substantially influence seismic behaviour.

- Future studies should aim to draw out the complete post-ultimate behaviour curves for the San Gwann and Dingli chapels. This can be achieved by either using different non-linear convergence criteria in 3D Macro or else by resorting to a different non-linear seismic analysis software to enhance the precision and reliability of the results.

- Finally , in order to improve accuracy, it would also be useful to carry out seismic analyses of typical Maltese Chapels using numerical models of the whole building, including the double skin masonry walls and the overlying masonry barrel vault. For this purpose, more sophisticated numerical analysis software would be required, such as software based upon the Applied Element Method.

Bibliography

Abela, M. (. (1969). *Earthquakes in Malta*. University of Malta; Faculty of Arts. Department of History.

Adams, A. (2022, Aug 19,). *Diaphragms.* Structural Engineer. https://www.thestructuralengineer.info/education/structural-analysis/structural-stability/diaphragms

Alexander, N. (2010). *Seismic analysis (2nd edition).*

Asteris, P. G., Chronopoulos, M. P., Chrysostomou, C. Z., Varum, H., Plevris, V., Kyriakides, N., & Silva, V. (2014). Seismic vulnerability assessment of historical masonry structural systems. *Engineering Structures, 62-63*, 118-134. 10.1016/j.engstruct.2014.01.031

Augusti, G., & Ciampoli, M. (2000a). *Heritage buildings and seismic reliability*. Wiley. 10.1002/1528-2716(200004/06)2:2<225::aid-pse28>3.0.co;2-5

Augusti, G., & Ciampoli, M. (2000b). *Heritage buildings and seismic reliability*. Wiley. 10.1002/1528-2716(200004/06)2:2< 225:aid-pse28>3.0.co;2-5

Babilio, E., Landolfo, R., Formisano, A., & di Lorenzo, G. (2018). Capacity design criteria of 3D steel lattice beams for applications into cultural heritage constructions and archaeological sites. *Key Engineering Materials, 763*, 320-328. 10.4028/www.scientific.net/KEM.763.320

Bányai, L. (1992). The role of the elastic rebound theory in design and evaluation of deformation surveys. *Tectonophysics, 202*(2), 107-110. 10.1016/0040-1951(92)90087-M

Bernardini, G., & Ferreira, T. M. (2022). Combining structural and non-structural risk-reduction measures to improve evacuation safety in historical built environments. *International Journal of Architectural Heritage, 16*(6), 820-838. 10.1080/15583058.2021.2001117

Borg, R. P., Borg, R. C., Borg Axisa, G., & COST, A. C. (2008). *The seismic risk of buildings in Malta*. University of Malta. Department of Building & Civil Engineering.

Bothara, J. K., PANDEY, B., & GURAGAIN, R. (2004). Seismic retrofitting of low strength unreinforced masonry non-engineered school buildings. *Bulletin of the New Zealand Society for Earthquake Engineering, 37*(1), 13-22. 10.5459/bnzsee.37.1.13-22

Buhagiar, L. (2020). *Seismic vulnerability assessment of the inquisitor's palace at vittoriosa in Malta* https://www.um.edu.mt/library/oar/handle/123456789/76339

Busuttil, R., Brincat, A. M., & Ciantar, N. (2012). *San mattew tal-maqluba il-kbir.*

Caliò, I., Cannizzaro, F., Marletta, M., & Pantò, B. (2010). *A discrete-element approach for the simulation of the seismic behaviour of historical buildings.*

Caliò, I., Marletta, M., & Pantò, B. (2005). *A simplified model for the evaluation of the seismic behaviour of masonry buildings*. Civil-Comp Press. 10.4203/ccp.81.195

Calvi, G. M., Pinho, R., & Magenes, G. (2006). *Traditional and innovative methods for seismic vulnerability assessment at large geographical scales*. Springer Netherlands. 10.1007/978-1-4020-8609-0_12

Chaimoon, K., & Attard, M. M. (2007). Modeling of unreinforced masonry walls under shear and compression. *Engineering Structures, 29*(9), 2056-2068. 10.1016/j.engstruct.2006.10.019

Curtin, W. G., Shaw, G., Beck, J. K., & Bray, W. A. (2006). *Structural masonry designers' manual*. Wiley. 10.1002/9780470774403

D'amico, S., & Galea, P. (2013). *Earthquake ground-motion simulations for the maltese archipelago*. Malta Chamber of Scientists. 10.7423/XJENZA.2013.1.01

De Fabrizio, M., & Mallardo, V. (2023). Structural analysis of masonry square vaults in the italian region of apulia. *Buildings (Basel), 13*(8), 1997. 10.3390/buildings13081997

De Giovanni, A. (2013). *Condition report and method statement -st. mathew chapel -'tal-maqluba' qrendi.*

De Matteis, G., & Cacace, D. (2019). *Masonry vaults: Architectural evolution, structural behaviour, and collapse mechanisms.*

Doherty, K., Griffith, M. C., Lam, N., & Wilson, J. (2002). Displacement-based seismic analysis for out-of-plane bending of unreinforced masonry walls. *Earthquake Engineering & Structural Dynamics, 31*(4), 833-850. 10.1002/eqe.126

Dyanati, M., Huang, Q., & Roke, D. (2017). Sensitivity analysis of seismic performance assessment and consequent impacts on loss analysis. *Bulletin of Earthquake Engineering, 15*(11), 4751-4790. 10.1007/s10518-017-0150-6

Eleftheriadou, A., & Karabinis, A. (2012). Seismic vulnerability assessment of buildings based on damage data after a near field earthquake (7 September 1999 athens - greece). *Earthquakes and Structures, 3*(2), 117-140. 10.12989/eas.2012.3.2.117

Elghazouli, A. Y., & Peppin, R. J. (2011). Seismic design of buildings to Eurocode 8. *Noise Control Engineering Journal, 59*(2), 212. 10.3397/1.3532782

Elghazouli, A. Y., & Williams, M. S. (2016). *Chapter 3 structural analysis*. Crc Press. 10.1201/9781315368221-4

En.1998.1.2004 *Eurocode 8: Design of structures for earthquake resistance-part 1: General rules, seismic actions and rules for buildings. Brussels: European Committee for Standardization,*

Fang, Z. X., & Fan, H. T. (2011). Redundancy of structural systems in the context of structural safety. *Procedia Engineering, 14*, 2172-2178. 10.1016/j.proeng.2011.07.273

Galea, P. (2007). *OA - seismic history of the Maltese islands and considerations on seismic risk.*

Gruppo Sismica. (2011). *Histra arches and vaults USER MANUAL.*

Guh, Y. Y., Wee, H. M., & Po, R. W. (2006). *Establishing a multiple structures AHP evaluation by extending hierarchies consistency analysis*. Atlantis Press. 10.2991/jcis.2006.290

ICOMOS. (2003). *Icomos International Scientific Committee F O R Analysis And Restoration O F Structures Of Architectural Heritage Recommendations For The Analysis, Conservation And Structural Restoration Of Architectural Heritage Contents.*

Jamal, H. (2017, Dec 17,). *Effects of earthquake on unreinforced masonry buildings.* Civil Engineering Lectures, Civil Engg. Notes, Books, Software's site. https://www.aboutcivil.org/earthquake-effects-masonry-buildings

Key, D. (1988). *Earthquake design practice for buildings*. T.Telford.

Lang, K. (2002). *Seismic vulnerability of existing buildings.* (). vdf, Hochschulverlag an der ETH Zürich. 10.3929/ethz-a-004333389 http://hdl.handle.net/20.500.11850/146255

Lourenço, P. B., Mendes, N., Ramos, L. F., & Oliveira, D. V. (2011a). Analysis of masonry structures without box behaviour. *International Journal of Architectural Heritage, 5*(4-5), 369-382. 10.1080/15583058.2010.528824

Lourenço, P. B., Mendes, N., Ramos, L. F., & Oliveira, D. V. (2011b). Analysis of masonry structures without box behaviour. *International Journal of Architectural Heritage, 5*(4-5), 369-382. 10.1080/15583058.2010.528824

Mahdi, T. (2016). *Seismic vulnerability of arches, vaults, and domes in historical buildings*. IGI Global. 10.4018/978-1-4666-9619-8.ch004

Mallia, R., & Chetcuti, F. (2023). *Kappella tal-prepostu method statement report.*

Mazumder, R. K., Rana, S., & Salman, A. M. (2021). First level seismic risk assessment of old unreinforced masonry (URM) using fuzzy synthetic evaluation. *Journal of Building Engineering, 44*, 103162. 10.1016/j.jobe.2021.103162

Miari, M., Choong, K. K., & Jankowski, R. (2019). Seismic pounding between adjacent buildings: Identification of parameters, soil interaction issues and mitigation measures. *Soil Dynamics and Earthquake Engineering, 121*, 135-150. 10.1016/j.soildyn.2019.02.024

Micallef, M., & Brincat, J. (2012). *Il-kappella ta' santa marija maddalena -ħad-dingli.*

Mistler, M., Butenweg, C., & Meskouris, K. (2006). Modelling methods of historic masonry buildings under seismic excitation. *Journal of Seismology, 10*(4), 497-510. 10.1007/s10950-006-9033-z

Mohan, V. M., & Suresh, E. S. M. (2009). *Seismic vulnerability assessment of existing buildings in india using gis techniques.*

Mohan, V. M., & Suresh, E. S. M. (2017). *Seismic vulnerability assessment of existing buildings in india using gis techniques.*

Mojsilovic, N. (2011). Strength of masonry subjected to in-plane loading: A contribution. *International Journal of Solids and Structures, 48*(6), 865-873. 10.1016/j.ijsolstr.2010.11.019

Occhipinti, G., Caddemi, S., Caliò, I., & Cannizzaro, F. (2015). *A parsimonious discrete model for the seismic assessment of monumental structures.*

one mcm world. (2022, March,). *Seismic risk assessment.* https://www.mcmdev.com/stories/risk.

Otani, L., Pereira, A. H. A., Segundinho, P. G. A., & Morales, E. A. M. (2022). *Determination of wood and byproducts elastic moduli using the impulse excitation technique.*

Parisi, F., & Augenti, N. (2013). Seismic capacity of irregular unreinforced masonry walls with openings. *Earthquake Engineering & Structural Dynamics, 42*(1), 101-121. 10.1002/eqe.2195

Pelà, L. (2014). *Seismic assessment of historical masonry construction including uncertainty savvas saloustros école polytechnique fédérale de Lausanne.*

Porter, K. (2003). An overview of PEER's performance-based earthquake engineering methodology.https://www.researchgate.net/publication/237390996_An_Overview_of_PEER's_Performance-Based_Earthquake_Engineering_Methodology

Porter, K. (2021). Beginner's guide to fragility, vulnerability, and risk. *Encyclopedia of earthquake engineering* (pp. 235-260). Springer Berlin Heidelberg. 10.1007/978-3-642-35344-4_256

Qrendi Local Council. (2013,*The "San matthew tal-maqluba" chapel and crypt.* http://www.qrendilocalcouncil.org.mt/poi/chapels/en/sanmatthew

RangaRajan, T. (2011). *Floor diaphragms*

Roca, P., Cervera, M., Gariup, G., & Pela', L. (2010). Structural analysis of masonry historical constructions. classical and advanced approaches. *Archives of Computational Methods in Engineering, 17*(3), 299-325. 10.1007/s11831-010-9046-1.

Rodrigues, H., Elnashai, A., & Calvi, G. M. (2017). Seismic performance of masonry arches and vaults. *Facing the challenges in structural engineering* (pp. 23-41). Springer International Publishing AG. 10.1007/978-3-319-61914-9_3

Santucci De Magistris, F. (2011). *Beyond EC8: The new italian seismic code.*

Times of Malta. (2005, August 10,). *Restoration of dingli chapel.* https://timesofmalta.com/articles/view/restoration-of-dingli-chapel.81532

Times of Malta. (2007, May 22,). *400-year-old dingli chapel restored.* https://timesofmalta.com/articles/view/400-year-old-dingli-chapel-restored.17066

Tomazevie, M. (1999). *Earthquake-resistant design of masonry buildings.*

TVMNews. (2023, Aug 09,). *St. philip and St. james chapel in san ġwann restored.* https://tvmnews.mt/en/news/st-philip-and-st-james-chapel-in-san-gwann-restored/

Vassallo, D. (2022). *Il-kappella ta' santa marija maddalena f'Ħad-dingli.*

Wang, Z. (2006). Motion of adria and ongoing inversion of the pannonian basin : Seismicity GPS velocities and stress transfer in (continental intraplate earthquakes : Hazard and policy issues geological society of america special paper. *Continental Intraplate Earthquakes: Science, Hazard, and Policy Issues,* 10.1130/2007.2425

Wang, Z. (2011). Seismic hazard assessment: Issues and alternatives. *Pure and Applied Geophysics, 168*(1-2), 11-25. 10.1007/s00024-010-0148-3

Xuereb, P. (2012). *San_Gwann tal-prepostu.*

Yang, T. Y., Moehle, ;. J., Stojadinovic, ;. B., ;, & Der Kiureghian, A. (2009). *Seismic performance evaluation of facilities: Methodology and implementation*10.1061/ASCE0733-94452009135:101146

Zucca, M., Reccia, E., Longarini, N., & Cazzani, A. (2022). Seismic assessment and retrofitting of an historical masonry building damaged during the 2016 centro italia seismic event. *Applied Sciences, 12*(22), 11789. 10.3390/app122211789

Appendices

Appendix A - Calculations

A.1 – Vault to Orthotropic Slab: St. Philip & St. James Chapel in San Gwann

A.2 – Vault to Orthotropic Slab: Santa Marija Maddalena Chapel in Dingli

A.3 – Vault to Orthotropic Slab: St. Matthew’s Chapel in Qrendi

A.4 – Areas for Different Levels: St. Matthew’s Chapel in Qrendi

Appendix B- Parameters defined in Macro Element Software.

B.1 – Parameters defined in Histra Arches and Vaults

B.2 – Parameters defined in 3D Macro

B.3 - 3D Visuals of Chapels

Appendix C – Results

C.1 – 3D Macro Analysis: St. Philip & St. James Chapel in San Gwann

C.2 - 3D Macro Analysis: Santa Marija Maddalena Chapel in Dingli

C.3 - 3D Macro Analysis: St. Matthew’s Chapel in Qrendi

Appendix D – Ambient Noise Measurement

Appendix List of Figures

Appendix A – Calculations

Appendix A.1 – Vault to Orthotropic Slab

St. Philip & St. James Chapel in San Gwann

Histra Arches and Vaults

Barrel Vault of St. Philip & St. James Chapel in San Gwann :

L_1	=	4.4	m
L_2	=	6.2	m
f	=	2	m
t_0	=	0.5	m
t_1	=	0.334	m
Shape	=	Elipse	
L_{max}	=	0.6	m
Area Histra	=	Area 3D Macro	
Seq	=	0.488	m
Density of Masonry	=	19	kN/m^3
W	=	9.272	kN/m^2

Equivalent normal stiffness in direction-x.

Pushover curve response in the x-direction :

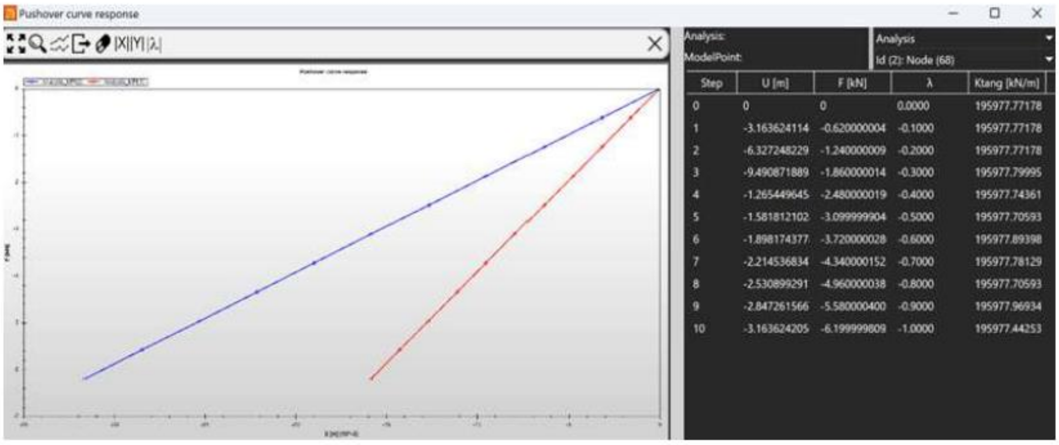

Step	U [m]	F [kN]	λ	Ktang [kN/m]
0	0	0	0.0000	195977.77178
1	-3.163624114	-0.620000004	-0.1000	195977.77178
2	-6.327248229	-1.240000009	-0.2000	195977.77178
3	-9.490871889	-1.860000014	-0.3000	195977.79995
4	-1.265449645	-2.480000019	-0.4000	195977.74361
5	-1.581812102	-3.099999904	-0.5000	195977.70593
6	-1.898174377	-3.720000028	-0.6000	195977.89398
7	-2.214536834	-4.340000152	-0.7000	195977.78129
8	-2.530899291	-4.960000038	-0.8000	195977.70593
9	-2.847261566	-5.580000400	-0.9000	195977.96934
10	-3.163624205	-6.199999809	-1.0000	195977.44253

X-direction :

Displacment,	**U**	=	3.163662	$x10^{-5}$	m
Force,	**F**	=	6.2		kN

$$E_x = \frac{F\left(L+t_0\right)}{u \cdot s_{eq} \cdot w}$$

E_x	=	317384.8	kN/m^2
E_x	=	317.3848	N/mm^2

Equivalent normal stiffness in direction-y.

Pushover curve response in the y-direction :

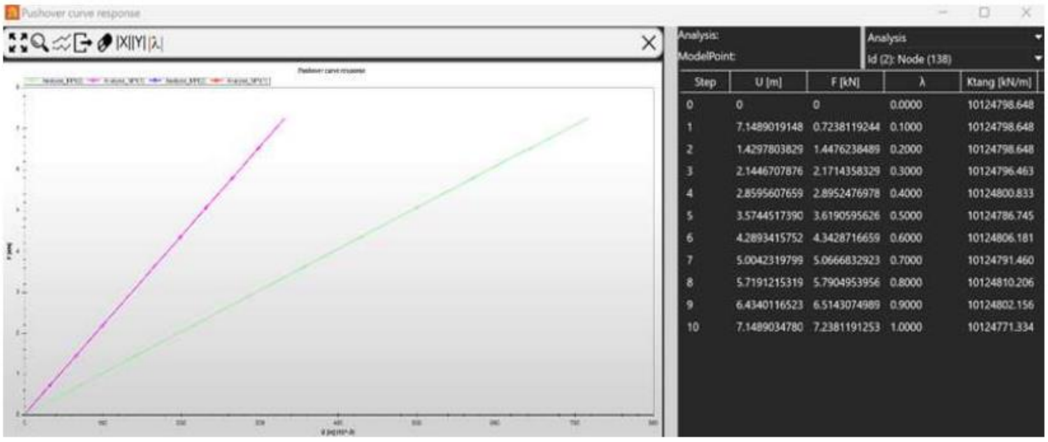

Step	U [m]	F [kN]	λ	Ktang [kN/m]
0	0	0	0.0000	10124798.648
1	7.1489019148	0.7238119244	0.1000	10124798.648
2	1.4297803829	1.4476238489	0.2000	10124798.648
3	2.1446707876	2.1714358329	0.3000	10124796.463
4	2.8595607659	2.8952476978	0.4000	10124800.833
5	3.5744517390	3.6190595626	0.5000	10124786.745
6	4.2893415752	4.3428716659	0.6000	10124806.181
7	5.0042319799	5.0666832923	0.7000	10124791.460
8	5.7191215319	5.7904953956	0.8000	10124810.206
9	6.4340116523	6.5143074989	0.9000	10124802.156
10	7.1489034780	7.2381191253	1.0000	10124771.334

Y-direction :

Displacment,	**U**	=	7.148904	$\times 10^{-7}$	m
Force,	**F**	=	7.238		kN

$$E_y = \frac{F \cdot w}{u \cdot s_{eq} \cdot (L + t_0)}$$	E_y	=	26251549	kN/m^2
	$\mathbf{E_y}$	=	26251.55	N/mm^2

Tangential stiffness

	n_y	=	10	
	n_x	=	12	
	w	=	6.2	m
	L_a	=	7.24	m
$F_y = w(n_y - 2)/n_y$	$\mathbf{F_y}$	$= \pm$	4.960	
$q_y = \dfrac{F_y}{w(n_y - 2)/n_y}$	$\mathbf{q_y}$	$= \pm$	1	
$F_x = F_y \dfrac{L + t_0}{w}$	$\mathbf{F_x}$	$= \pm$	3.92	
$q_x = \dfrac{F_x}{L_a(n_x - 2)/n_x}$	$\mathbf{q_x}$	$= \pm$	0.650	

Results from report of Histra :

Analysis	Node	Ux	Uy	Uz
Unitless	Unitless	m	m	m
Analysis (1) Step (10)	1	1.146E-06	-8.59491E-07	1.03982E-07

U_x	=	1.146	$\times 10^{-6}$	m
U_y	=	8.59491	$\times 10^{-7}$	m

$$\tau_{med} = \frac{F_x}{s_{eq} \cdot (L + t_0)} = \frac{F_y}{s_{eq} \cdot w}$$

= 1.63934426

$$\gamma_{med} = \frac{u_x}{w} + \frac{u_y}{L + t_0}$$

= 3.6025E-07

$$G = \frac{\tau_{med}}{\gamma_{med}}$$

=	4550636.64	N/m^2
=	4.55063664	N/mm^2

Summary of St. Philip & St. James Chapel in San Gwann :

Ex	=	317.384801	N/mm^2
Ey	=	26251.5488	N/mm^2
G	=	4.55063664	N/mm^2

Appendix A – Calculations

Appendix A.2 – Vault to Orthotropic Slab

Santa Marija Maddalena Chapel in Dingli

Histra Arches and Vaults

Barrel Vault of Saint Marija Maddalena Chapel in Dingli :

L_1	=	4	m
L_2	=	6.9	m
f	=	2	m
t_0	=	0.5	m
t_1	=	0.3	m
Shape	=	Elipse	
L_{max}	=	0.6	m
Area Histra	=	Area 3D Macro	
Seq	=	0.451	m
Density of Masonry	=	19	kN/m^3
W	=	8.569	kN/m^2

Equivalent normal stiffness in direction-x.

Pushover curve response in the x-direction :

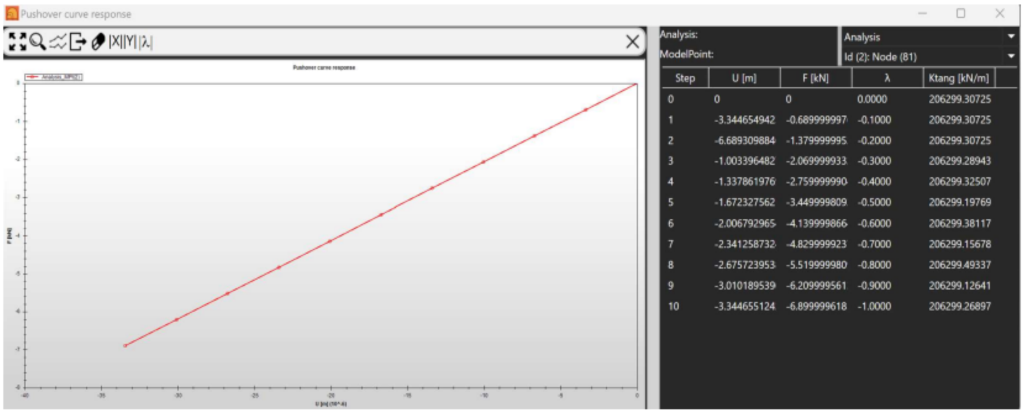

X-direction :

Displacment,	**U**	=	3.34466	$x10^{-5}$	m
Force,	**F**	=	6.9		kN

$$E_x = \frac{F(L+t_0)}{u \cdot s_{eq} \cdot w}$$

E_x	=	298322	kN/m^2
E_x	=	298.322	N/mm^2

Equivalent normal stiffness in direction-y.

Pushover curve response in the y-direction :

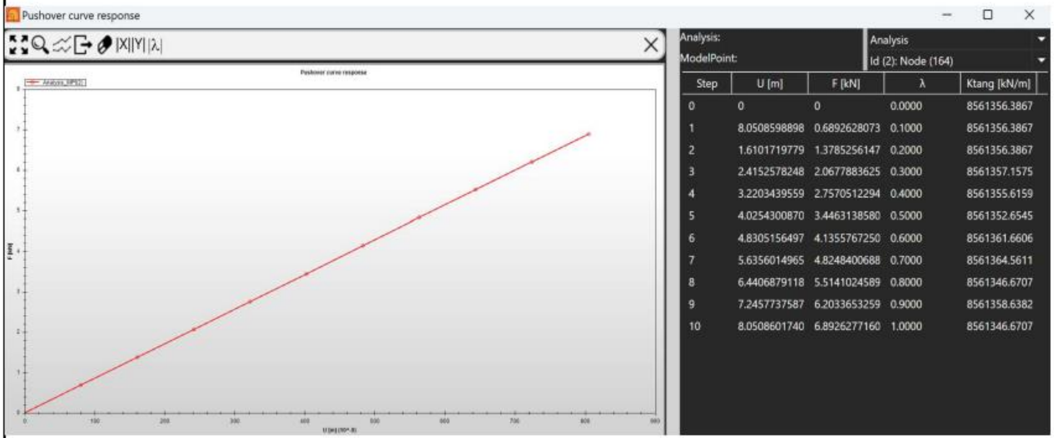

Step	U [m]	F [kN]	λ	Ktang [kN/m]
0	0	0	0.0000	8561356.3867
1	8.0508598898	0.6892628073	0.1000	8561356.3867
2	1.6101719779	1.3785256147	0.2000	8561356.3867
3	2.4152578248	2.0677883625	0.3000	8561357.1575
4	3.2203439559	2.7570512294	0.4000	8561355.6159
5	4.0254300870	3.4463138580	0.5000	8561352.6545
6	4.8305156497	4.1355767250	0.6000	8561361.6606
7	5.6356014965	4.8248400688	0.7000	8561364.5611
8	6.4406879118	5.5141024589	0.8000	8561346.6707
9	7.2457737587	6.2033653259	0.9000	8561358.6382
10	8.0508601740	6.8926277160	1.0000	8561346.6707

Y-direction :

Displacment,	**U**	=	8.05086	$x10^{-7}$	m
Force,	**F**	=	6.89		kN

$$E_y = \frac{F \cdot w}{u \cdot s_{eq} \cdot (L + t_0)}$$

E_y	=	2.9E+07	kN/m^2
$\mathbf{E_y}$	=	29096.2	N/mm^2

Tangential stiffness

n_y	=	12	
n_x	=	12	
w	=	6.9	m
L_a	=	6.89	m

$$F_y = w(n_y - 2)/n_y$$

$$q_y = \frac{F_y}{w(n_y - 2)/n_y}$$

$$F_x = F_y \frac{L + t_0}{w}$$

$$q_x = \frac{F_x}{L_a(n_x - 2)/n_x}$$

$\mathbf{F_y}$	$= \pm$	5.750
$\mathbf{q_y}$	$= \pm$	1
$\mathbf{F_x}$	$= \pm$	3.75
$\mathbf{q_x}$	$= \pm$	0.653

Results from report of Histra :

Analysis	Node	Ux	Uy	Uz
Unitless	Unitless	m	m	m
Analysis (1) Step (10)	1	1.42438E-06	-1.03549E-06	1.05143E-07

U_x	=	1.42438	$x10^{-6}$	m
U_y	=	1.03549	$x10^{-6}$	m

$$\tau_{med} = \frac{F_x}{s_{eq} \cdot (L+t_0)} = \frac{F_y}{s_{eq} \cdot w}$$

=	1.84774575	

$$\gamma_{med} = \frac{u_x}{w} + \frac{u_y}{L+t_0}$$

=	4.3654E-07	

$$G = \frac{\tau_{med}}{\gamma_{med}}$$

=	4232699.13	N/m^2
=	4.23269913	N/mm^2

Summary of Saint Marija Maddalena Chapel in Dingli :

Ex	=	298.321551	N/mm^2
Ey	=	29096.2469	N/mm^2
G	=	4.23269913	N/mm^2

Appendix A – Calculations

Appendix A.3 – Vault to Orthotropic Slab

St. Matthew's Chapel in Qrendi

Histra Arches and Vaults

Barrel Vault of St Matthew's Chapel in Qrendi :

L_1	=	7.6	m
L_2	=	14.9	m
f	=	4.1	m
t_0	=	0.8	m
t_1	=	0.63	m
Shape	=	Elipse	
L_{max}	=	0.8	m
Area Histra	=	Area 3D Macro	
Seq	=	0.899	m
Density of Masonry	=	19	kN/m^3
W	=	17.081	kN/m^2

Equivalent normal stiffness in direction-x.

Pushover curve response in the x-direction :

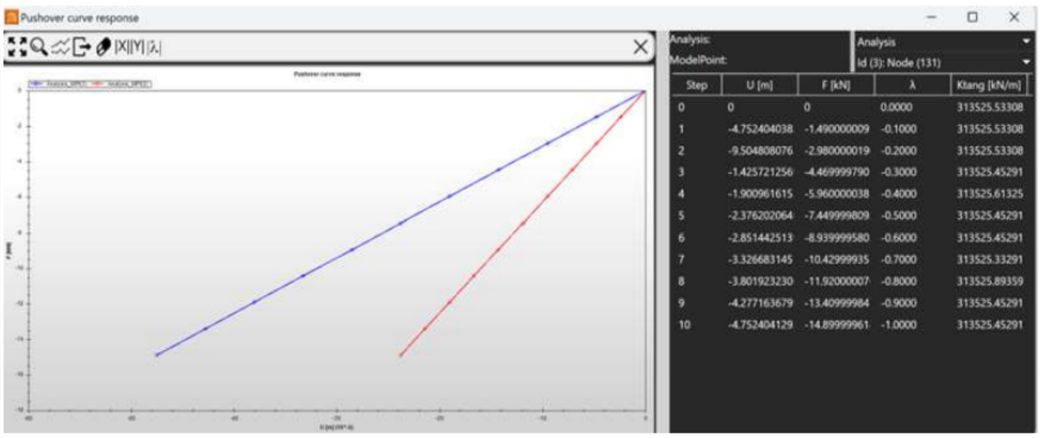

X-direction :

Displacment,	**U**	=	4.7524041	$x10^{-5}$	m
Force,	**F**	=	14.9		kN

$$E_x = \frac{F(L+t_0)}{u \cdot s_{eq} \cdot w}$$

E_x	=	196610.28	kN/m^2
E_x	=	196.61028	N/mm^2

Equivalent normal stiffness in direction-y.

Pushover curve response in the y-direction :

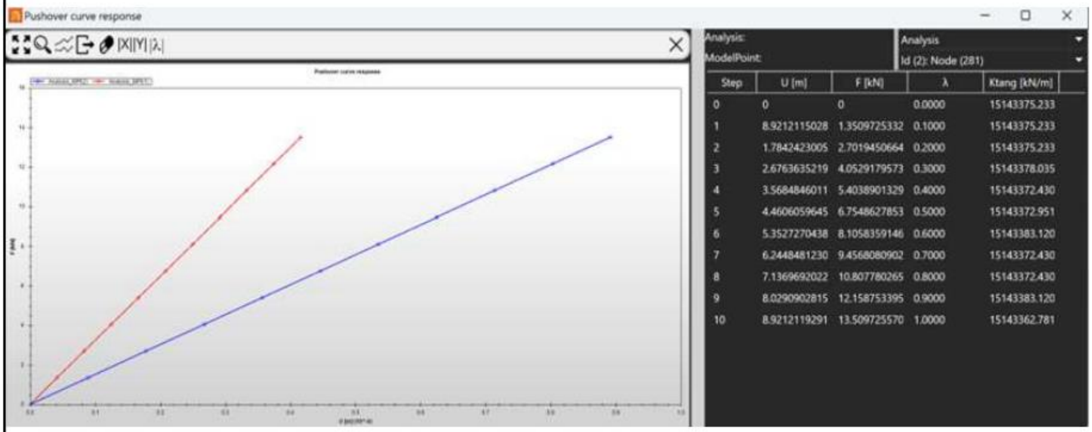

Y-direction :

Displacment,	**U**	=	8.9212119	$x10^{-7}$	m
Force,	**F**	=	13.5097		kN

$$E_y = \frac{F \cdot w}{u \cdot s_{eq} \cdot (L + t_0)}$$	E_y	=	29879212	kN/m^2
	$\mathbf{E_y}$	=	29879.212	N/mm^2

Tangential stiffness

	n_y	=	15	
	n_x	=	17	
	w	=	14.9	m
	L_a	=	13.51	m

$F_y = w(n_y - 2)/n_y$	$\mathbf{F_y}$	$= \pm$	12.913
$q_y = \dfrac{F_y}{w(n_y - 2)/n_y}$	$\mathbf{q_y}$	$= \pm$	1
$F_x = F_y \dfrac{L + t_0}{w}$	$\mathbf{F_x}$	$= \pm$	7.28
$q_x = \dfrac{F_x}{L_a(n_x - 2)/n_x}$	$\mathbf{q_x}$	$= \pm$	0.611

Results from report of Histra :

Analysis	Node	Ux	Uy	Uz
Unitless	Unitless	m	m	m
Analysis (1) Step (10)	1	0.00023113	-6.82093E-05	1.07834E-07

U_x	=	2.311	$x10^{-4}$	m
U_y	=	1.07834	$x10^{-7}$	m

$$\tau_{med} = \frac{F_x}{s_{eq} \cdot (L + t_0)} = \frac{F_y}{s_{eq} \cdot w}$$

=	0.96403411	

$$\gamma_{med} = \frac{u_x}{w} + \frac{u_y}{L + t_0}$$

=	1.5523E-05	

$$G = \frac{\tau_{med}}{\gamma_{med}}$$

=	62103.9775	N/m^2
=	0.06210398	N/mm^2

Summary of St Matthew's Chapel in Qrendi :

Ex	=	196.610284	N/mm^2
Ey	=	29879.212	N/mm^2
G	=	0.06210398	N/mm^2

Appendix A – Calculations

Appendix A.4 – Areas for Different Levels

St. Matthew’s Chapel in Qrendi

Rationalisation of Seismic Floor Levels :

Due to the different floor level in the adjacent rooms of St Matthew's Chapel in Qrendi :

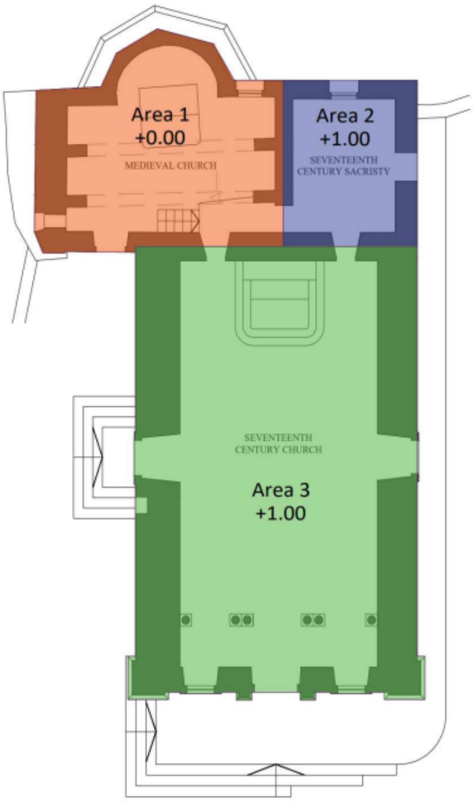

Area 1	=	73.84	m^2
Area 2	=	31.3	m^2
Area 3	=	178.4	m^2

$$Average\ Level = \frac{\sum_1^j (Level_i * Area_i)}{\sum_1^j Area}$$

$$Average\ Level = \frac{(Area\ 1 * 0.00) + (Area\ 2\ * 1.00) + (Area\ 3\ * 1.00)}{(Area\ 1 + Area\ 2 + Area\ 3)}$$

Average Level = 0.7396 m

Therefore :		Original Height		Estimated Height	
Room 1	=	4.6	m	3.96	m
Room 2	=	4.94	m	5.2	m
Room 3	=	10.57	m	10.83	m

Appendix B – Parameters defined in Macro Element Software.

Appendix B.1 – Parameters defined in Histra Arches and Vaults

In this section, snapshots of the settings used in Histra Arches and Vaults to conduct the parameters of the barrel vault equivalent to orthotropic slab.

These shots describe the preliminary geometric input operations of the barrel vault.

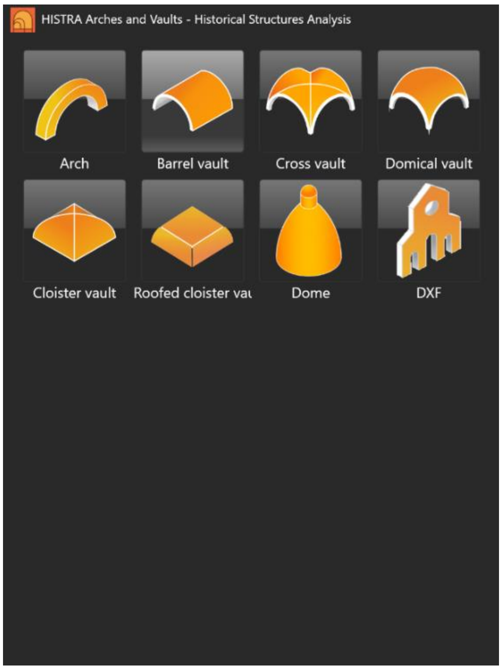

Figure 1 - Histra Wizard beginning of program to choose model.

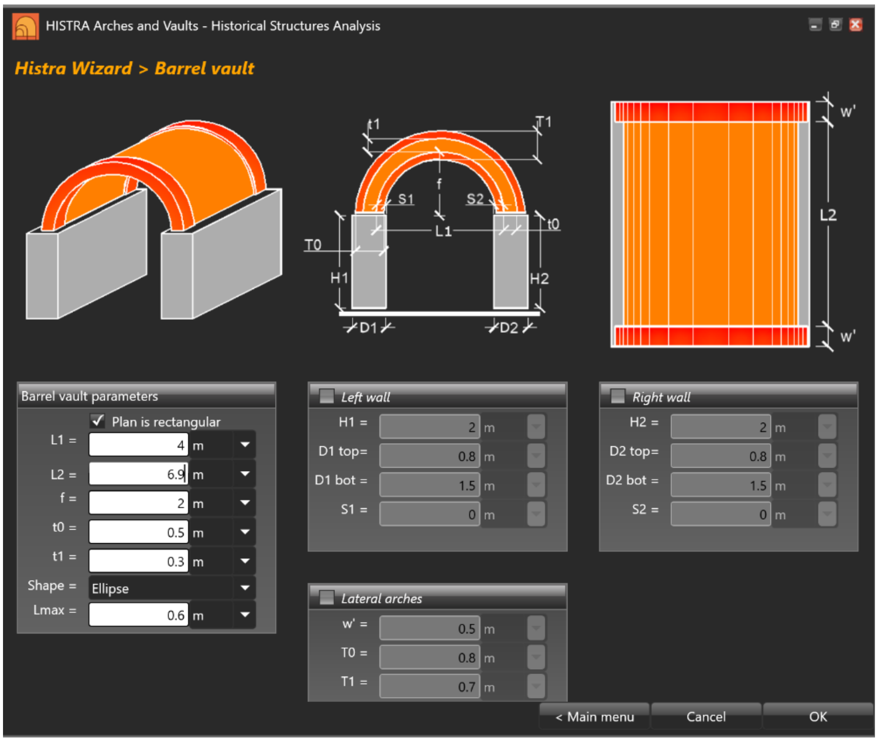

Figure 2 - Inputting dimensions of the barrel vault.

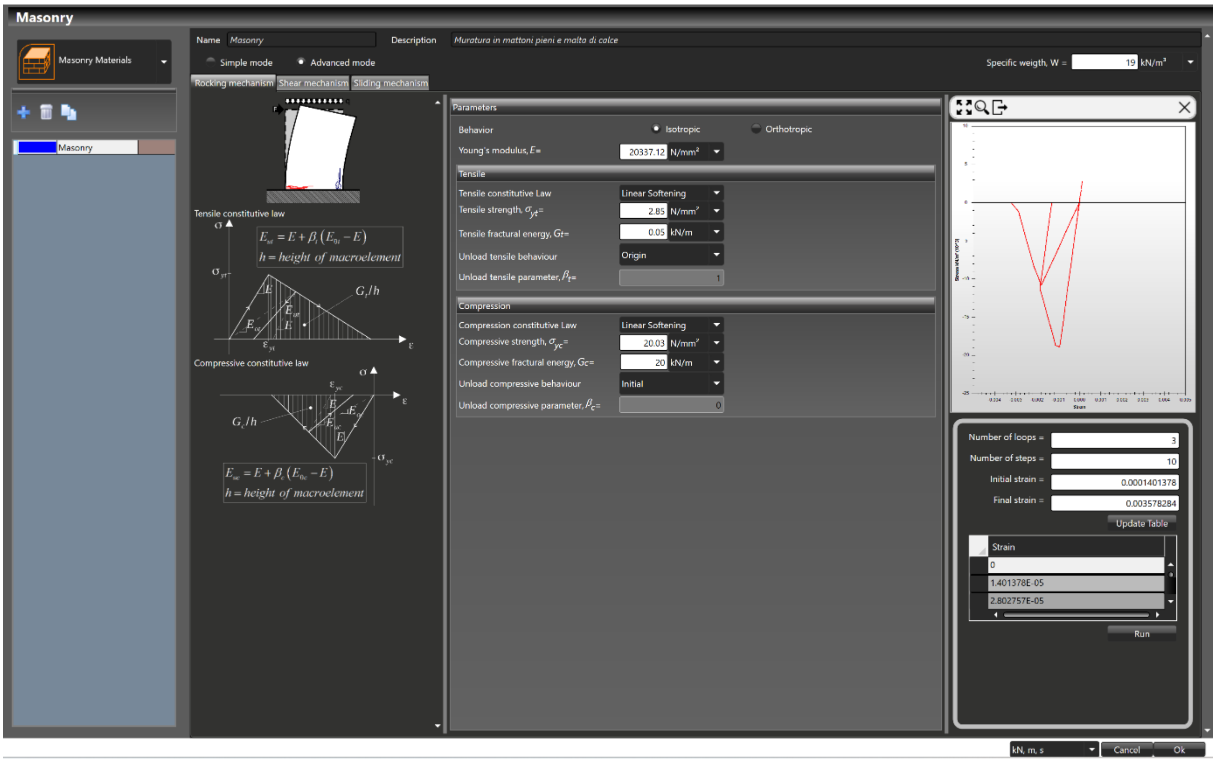

Figure 3 - Advanced masonry properties definition; Rocking Mechanism.

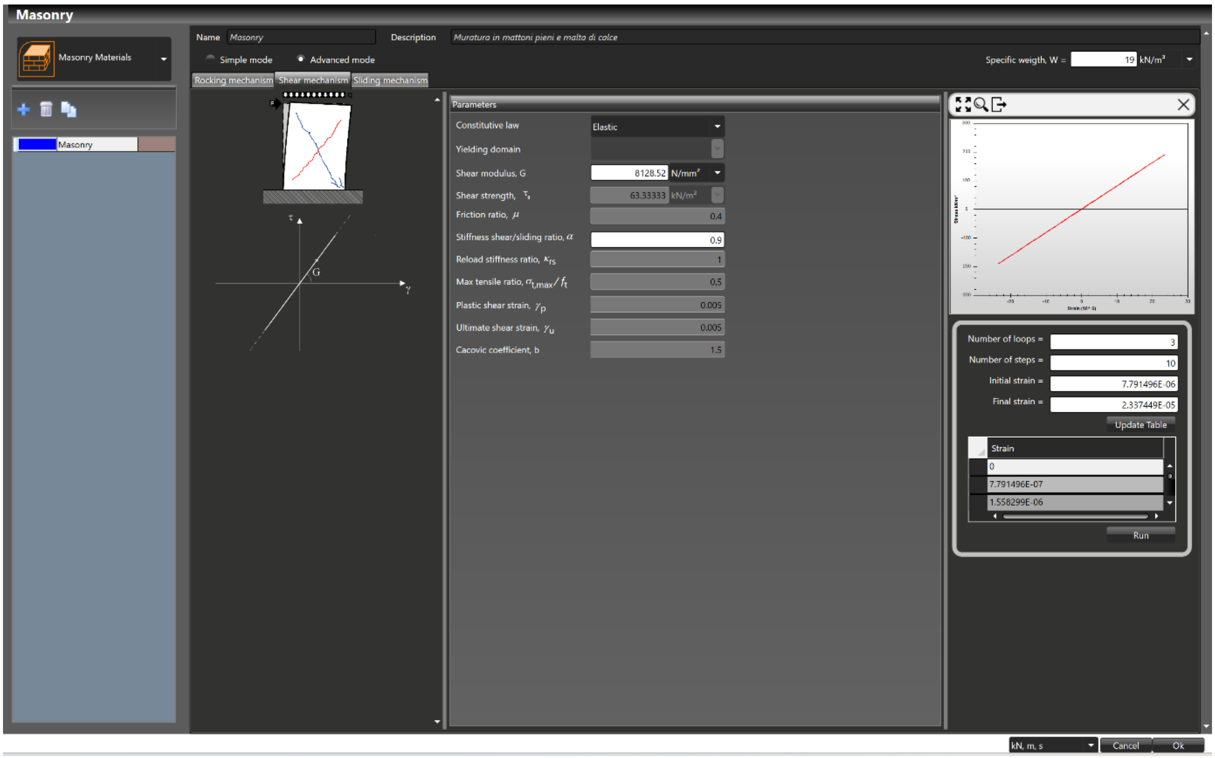

Figure 4 - Advanced masonry properties definition; Shear Mechanism.

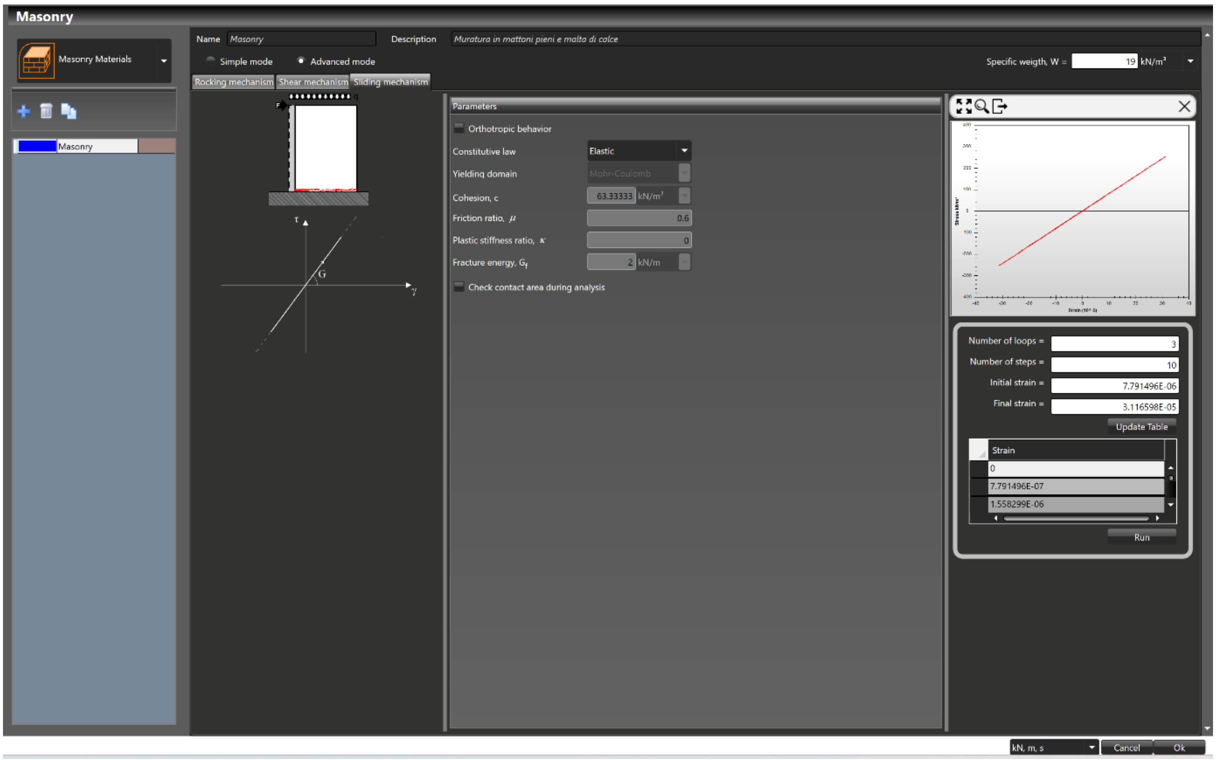

Figure 5 - Advanced masonry properties definition; Sliding Mechanism.

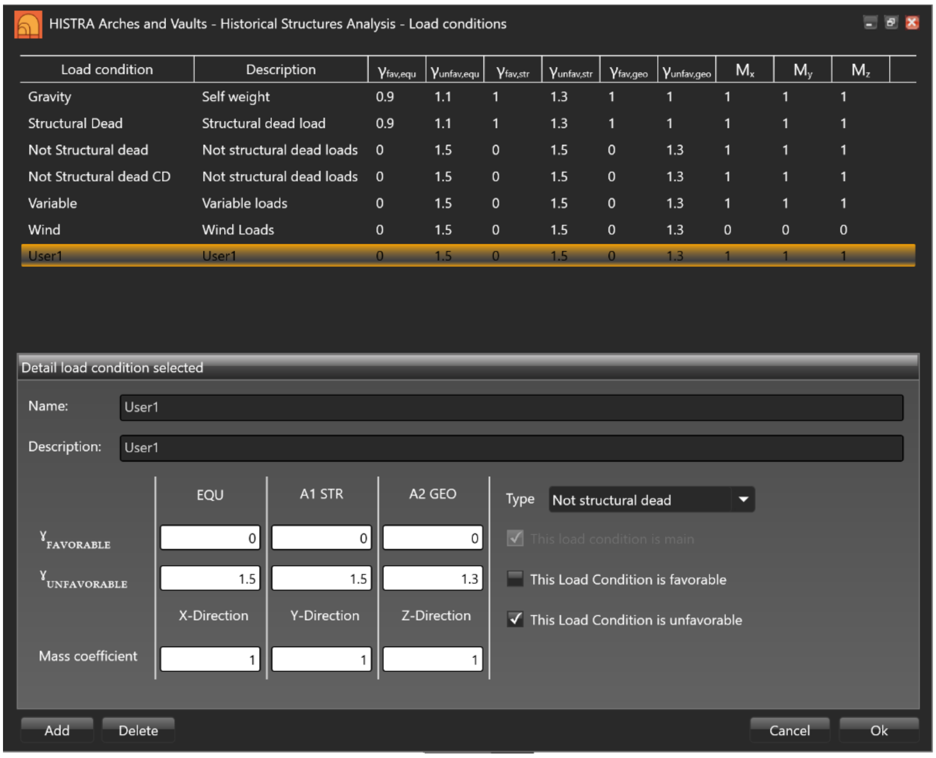

Figure 6 - Defining Load Condition.

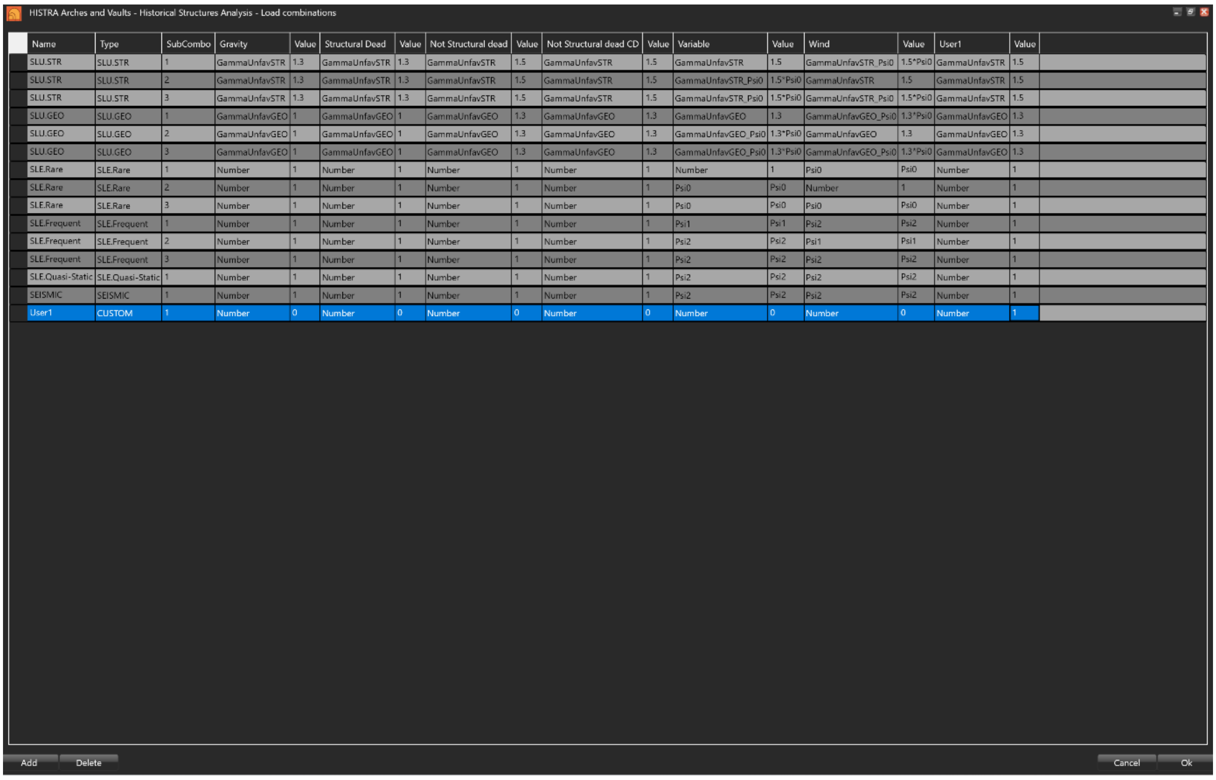

Name	Type	SubCombo	Gravity	Value	Structural Dead	Value	Not Structural dead	Value	Not Structural dead CD	Value	Variable	Value	Wind	Value	User1	Value
SLU.STR	SLU.STR	1	GammaUnfavSTR	1.3	GammaUnfavSTR	1.3	GammaUnfavSTR	1.5	GammaUnfavSTR	1.5	GammaUnfavSTR	1.5	GammaUnfavSTR_Psi0	1.5*Psi0	GammaUnfavSTR	1.5
SLU.STR	SLU.STR	2	GammaUnfavSTR	1.3	GammaUnfavSTR	1.3	GammaUnfavSTR	1.5	GammaUnfavSTR	1.5	GammaUnfavSTR_Psi0	1.5*Psi0	GammaUnfavSTR	1.5	GammaUnfavSTR	1.5
SLU.STR	SLU.STR	3	GammaUnfavSTR	1.3	GammaUnfavSTR	1.3	GammaUnfavSTR	1.5	GammaUnfavSTR	1.5	GammaUnfavSTR_Psi0	1.5*Psi0	GammaUnfavSTR_Psi0	1.5*Psi0	GammaUnfavSTR	1.5
SLU.GEO	SLU.GEO	1	GammaUnfavGEO	1	GammaUnfavGEO	1	GammaUnfavGEO	1.3	GammaUnfavGEO	1.3	GammaUnfavGEO	1.3	GammaUnfavGEO_Psi0	1.3*Psi0	GammaUnfavGEO	1.3
SLU.GEO	SLU.GEO	2	GammaUnfavGEO	1	GammaUnfavGEO	1	GammaUnfavGEO	1.3	GammaUnfavGEO	1.3	GammaUnfavGEO_Psi0	1.3*Psi0	GammaUnfavGEO	1.3	GammaUnfavGEO	1.3
SLU.GEO	SLU.GEO	3	GammaUnfavGEO	1	GammaUnfavGEO	1	GammaUnfavGEO	1.3	GammaUnfavGEO	1.3	GammaUnfavGEO_Psi0	1.3*Psi0	GammaUnfavGEO_Psi0	1.3*Psi0	GammaUnfavGEO	1.3
SLE.Rare	SLE.Rare	1	Number	1	Number	1	Number	1	Number	1	Number	1	Psi0	Psi0	Number	1
SLE.Rare	SLE.Rare	2	Number	1	Number	1	Number	1	Number	1	Psi0	Psi0	Number	1	Number	1
SLE.Rare	SLE.Rare	3	Number	1	Number	1	Number	1	Number	1	Psi0	Psi0	Psi0	Psi0	Number	1
SLE.Frequent	SLE.Frequent	1	Number	1	Number	1	Number	1	Number	1	Psi1	Psi1	Psi2	Psi2	Number	1
SLE.Frequent	SLE.Frequent	2	Number	1	Number	1	Number	1	Number	1	Psi2	Psi2	Psi1	Psi1	Number	1
SLE.Frequent	SLE.Frequent	3	Number	1	Number	1	Number	1	Number	1	Psi2	Psi2	Psi2	Psi2	Number	1
SLE.Quasi-Static	SLE.Quasi-Static	1	Number	1	Number	1	Number	1	Number	1	Psi2	Psi2	Psi2	Psi2	Number	1
SEISMIC	SEISMIC	1	Number	1	Number	1	Number	1	Number	1	Psi2	Psi2	Psi2	Psi2	Number	1
User1	CUSTOM	1	Number	0	Number	0	Number	0	Number	0	Number	0	Number	0	Number	1

Figure 7 – Defining Load Combination.

The following snapshots describes the operations to be conducted to calculate the equivalent normal stiffness in direction-x.

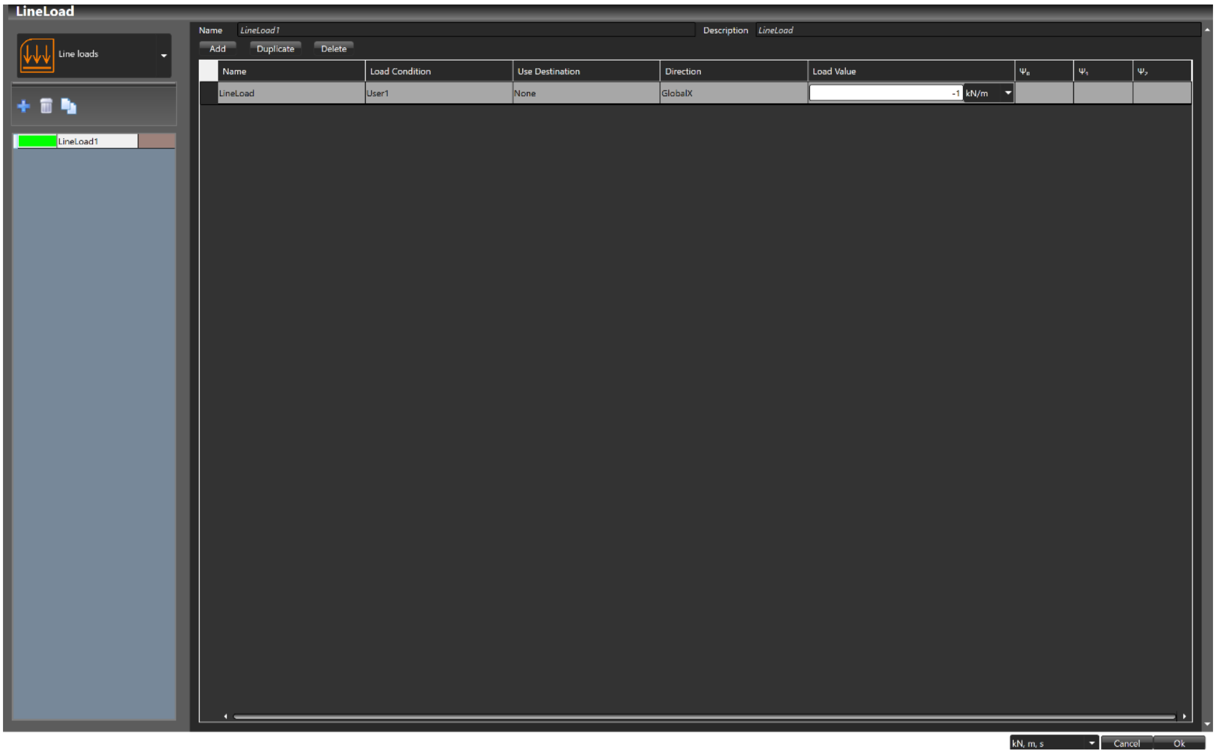

Figure 8 - Defining Line Load in Global X direction

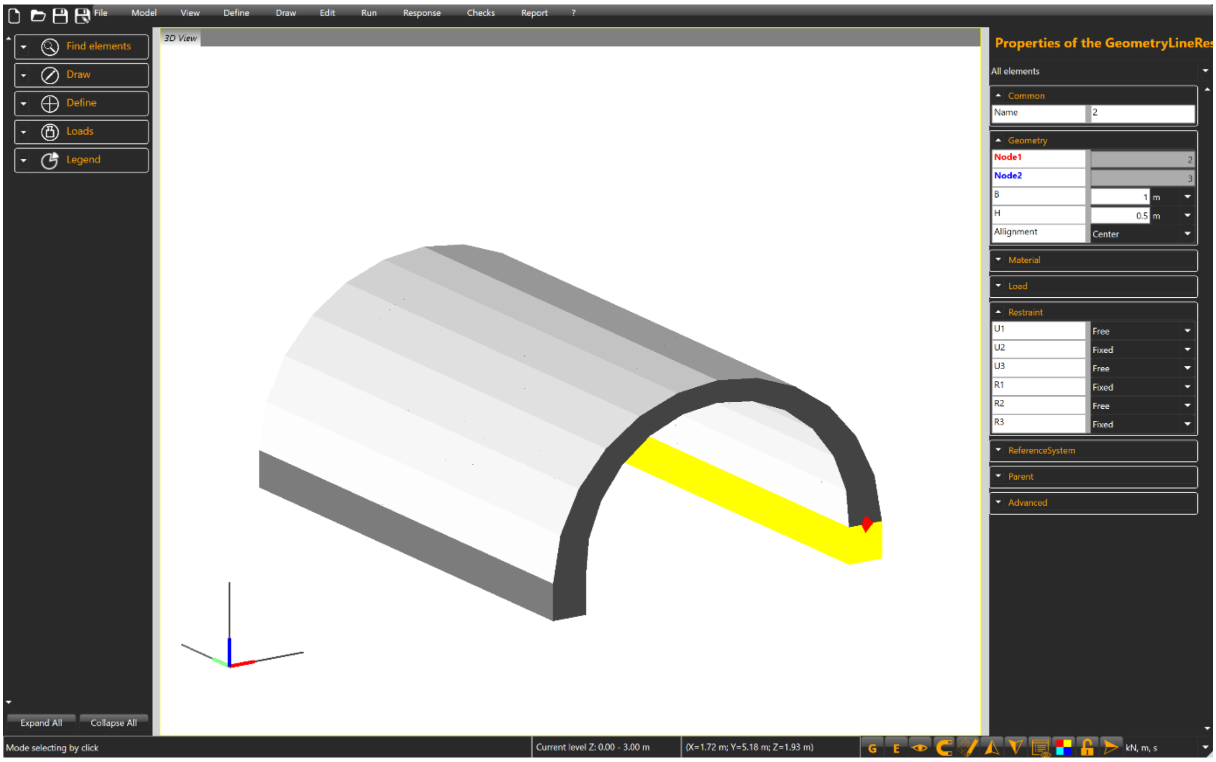

Figure 9 - Defining the type of constraint of one of the two sides of the vault.

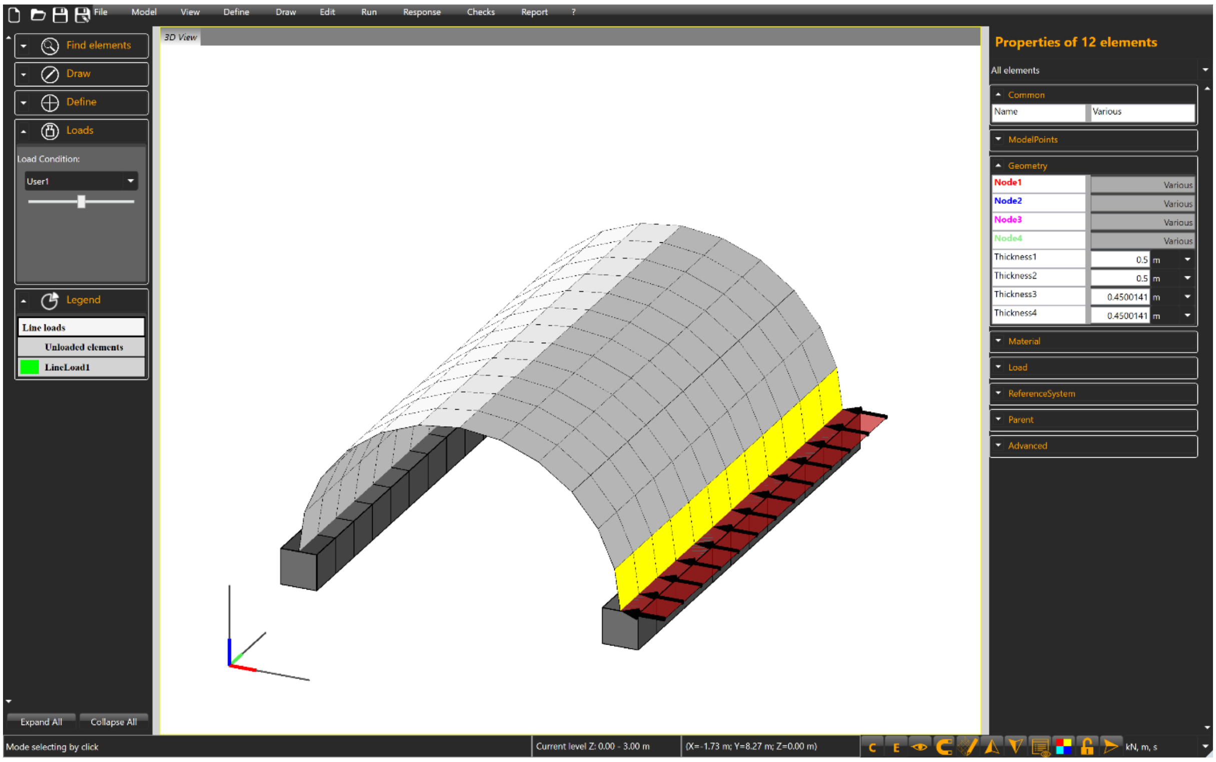

Figure 10 - Assigning the defined line load.

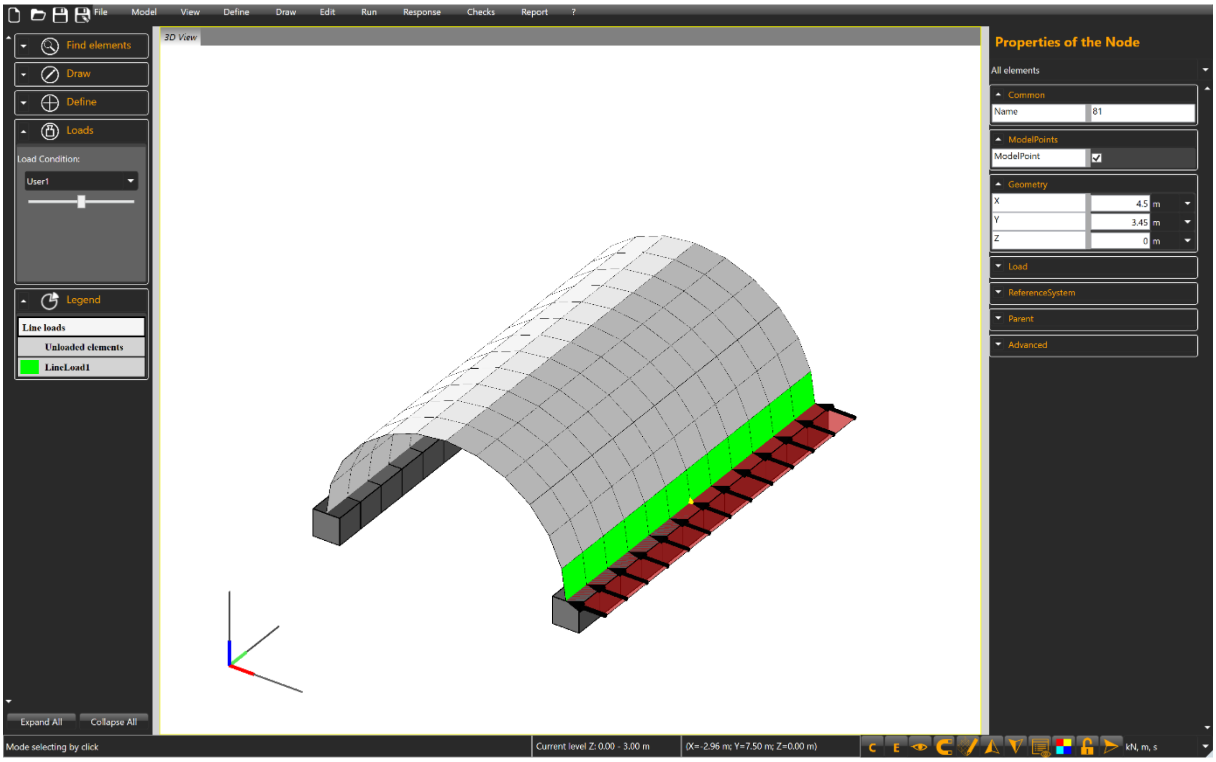

Figure 11 - Defining one of the nodes along the side.

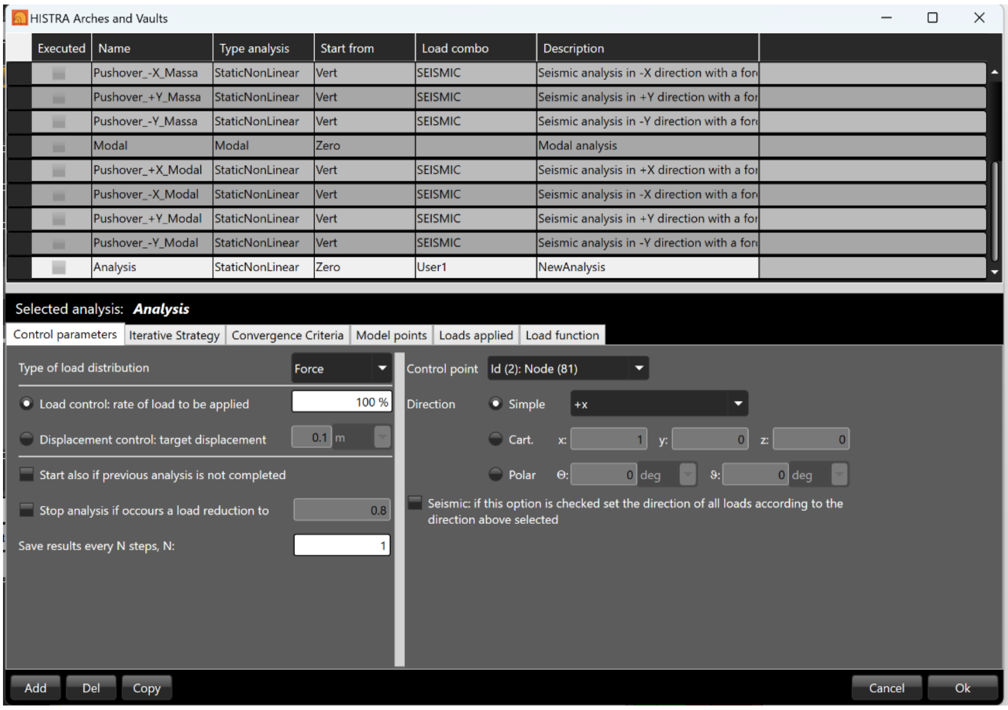

Figure 12 - Defining the analysis window.

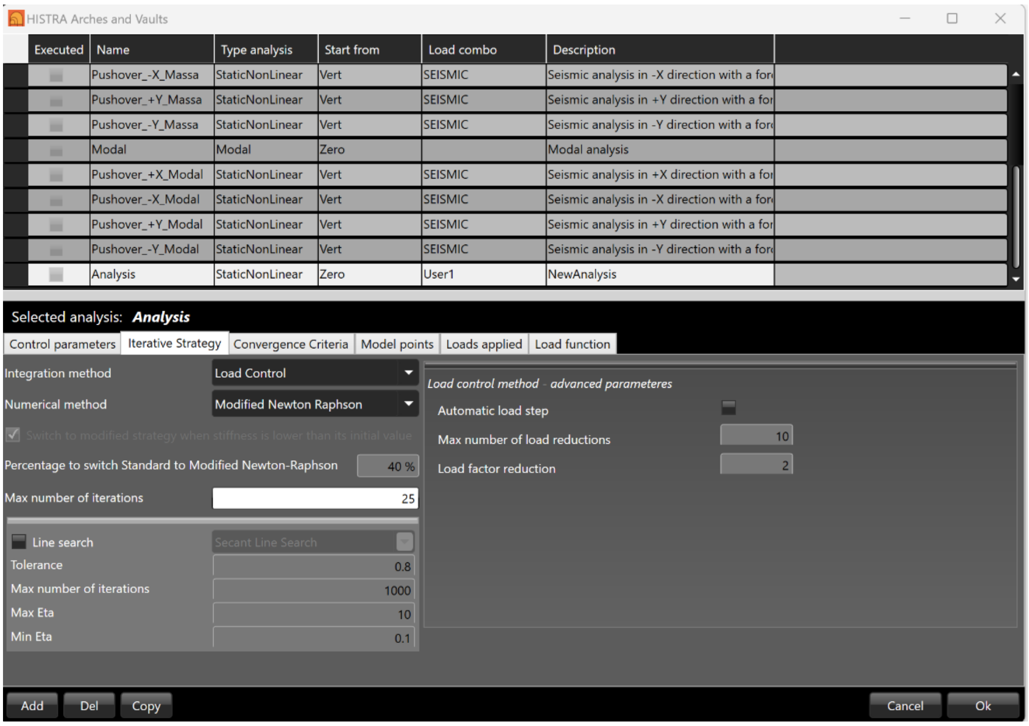

Figure 13 - Defining the analysis window.

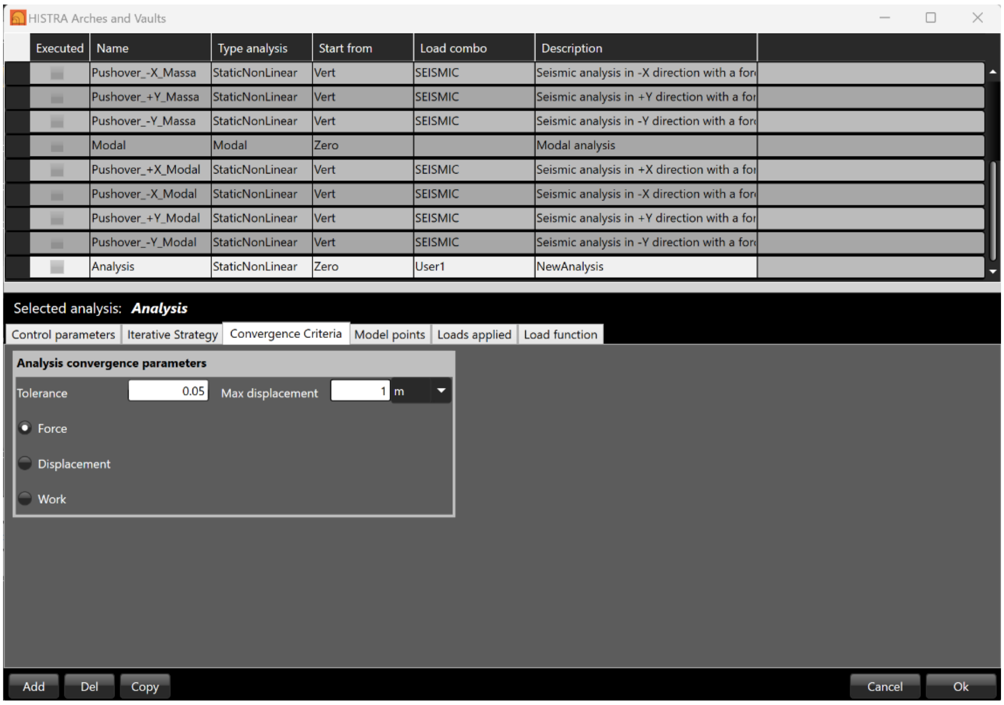

Figure 14 - Defining the analysis window.

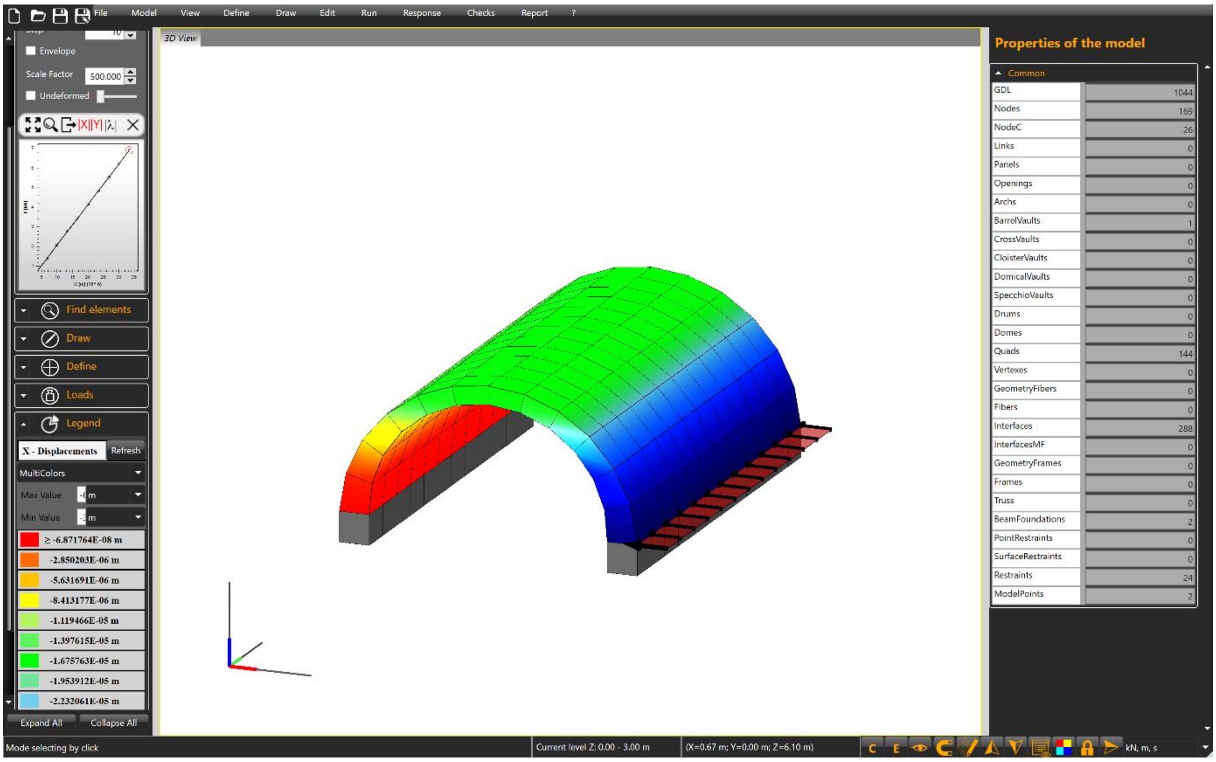

Figure 15 - Output phase in the X direction.

The following snapshots describes the operations to be conducted to calculate the equivalent normal stiffness in direction-y.

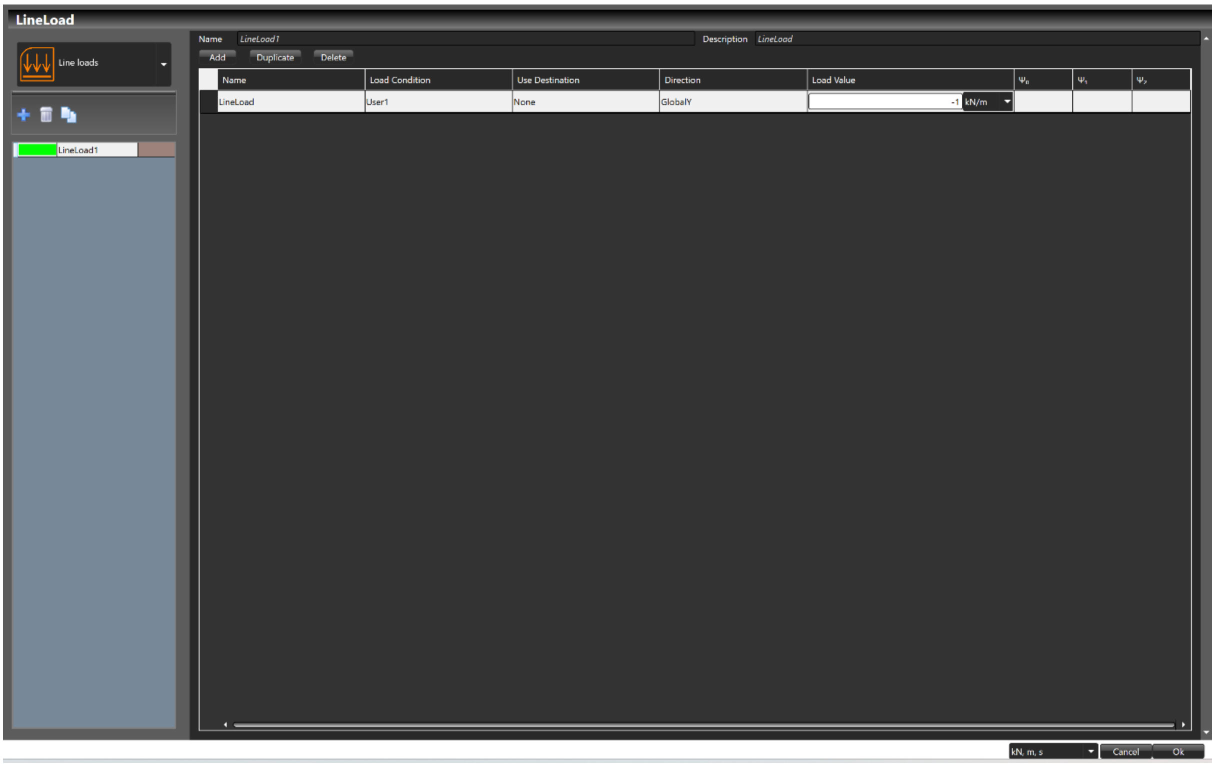

Figure 16 - Defining Line Load in Global Y direction.

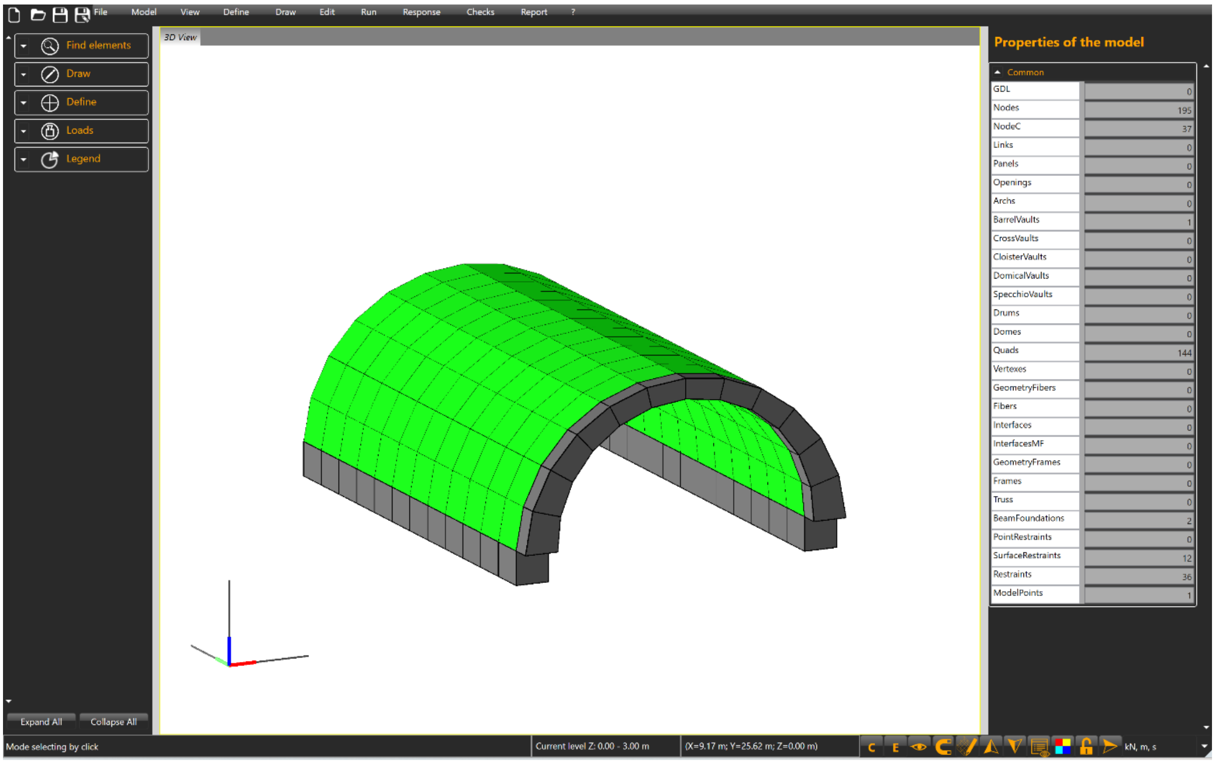

Figure 17 - Defining one of the two arches of the vault is constrained.

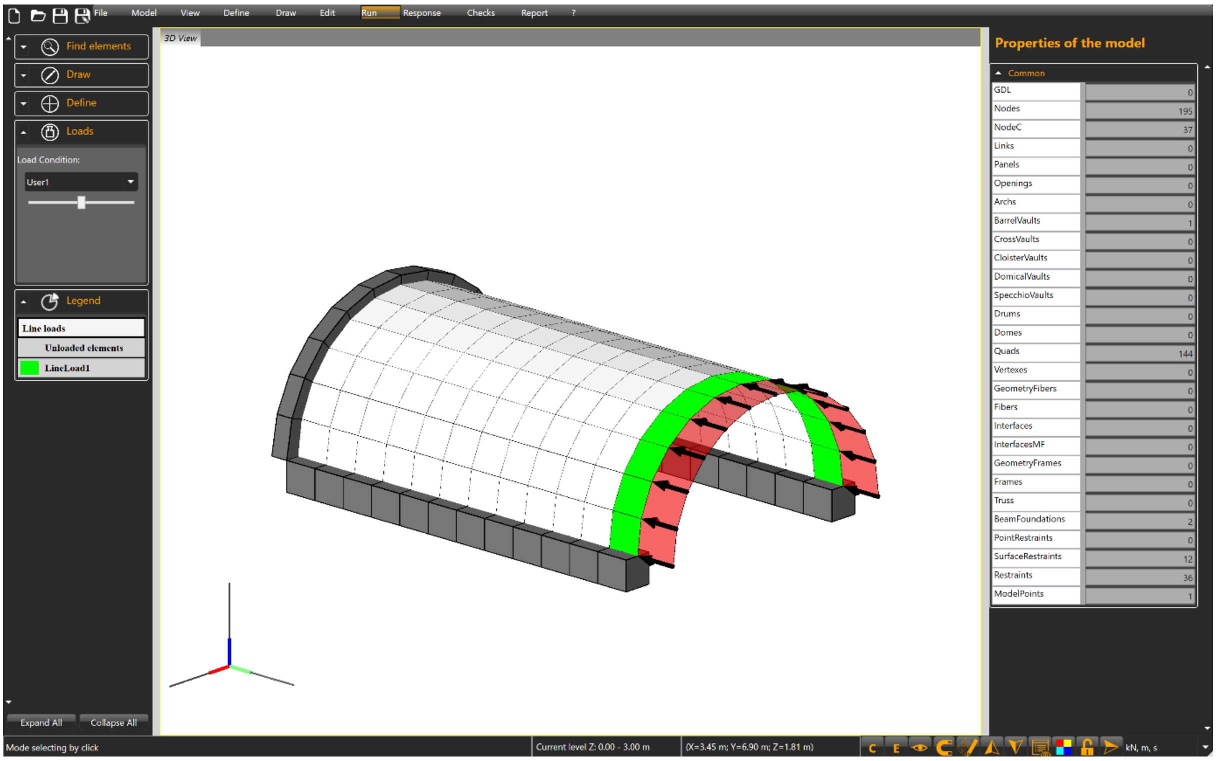

Figure 18 - Assigning line load to lateral arch.

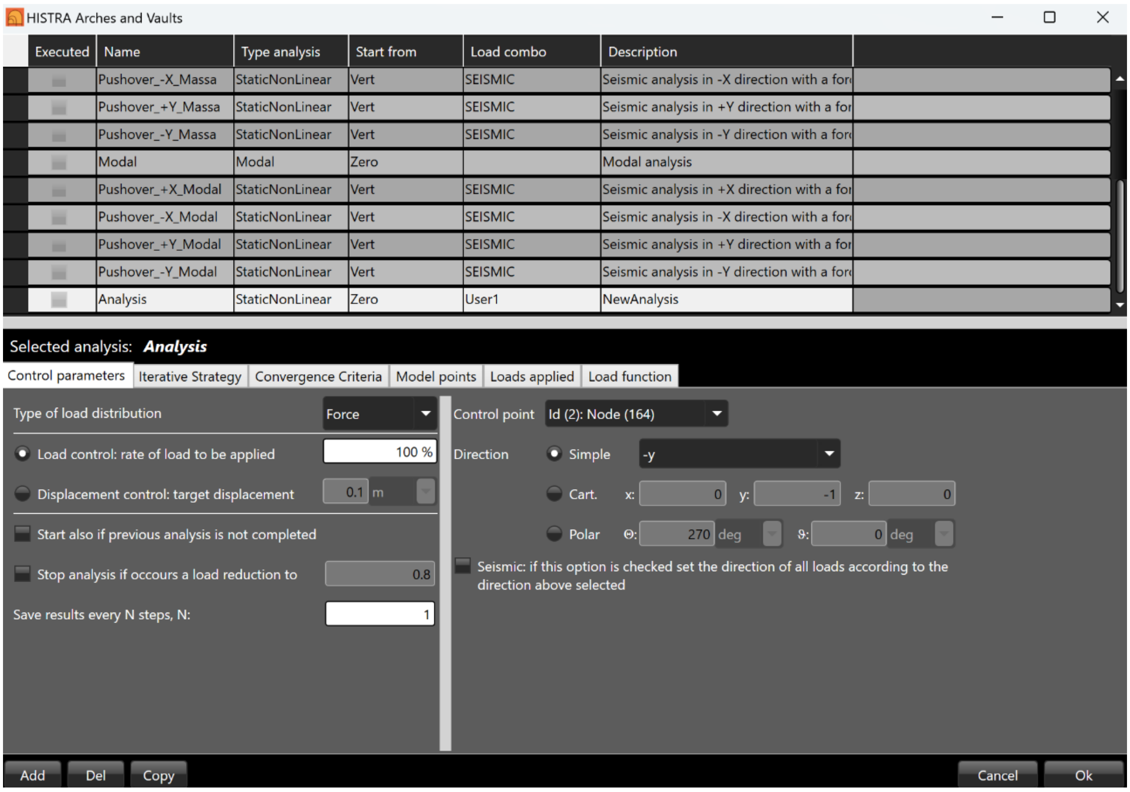

Figure 19 - Defining the analysis window.

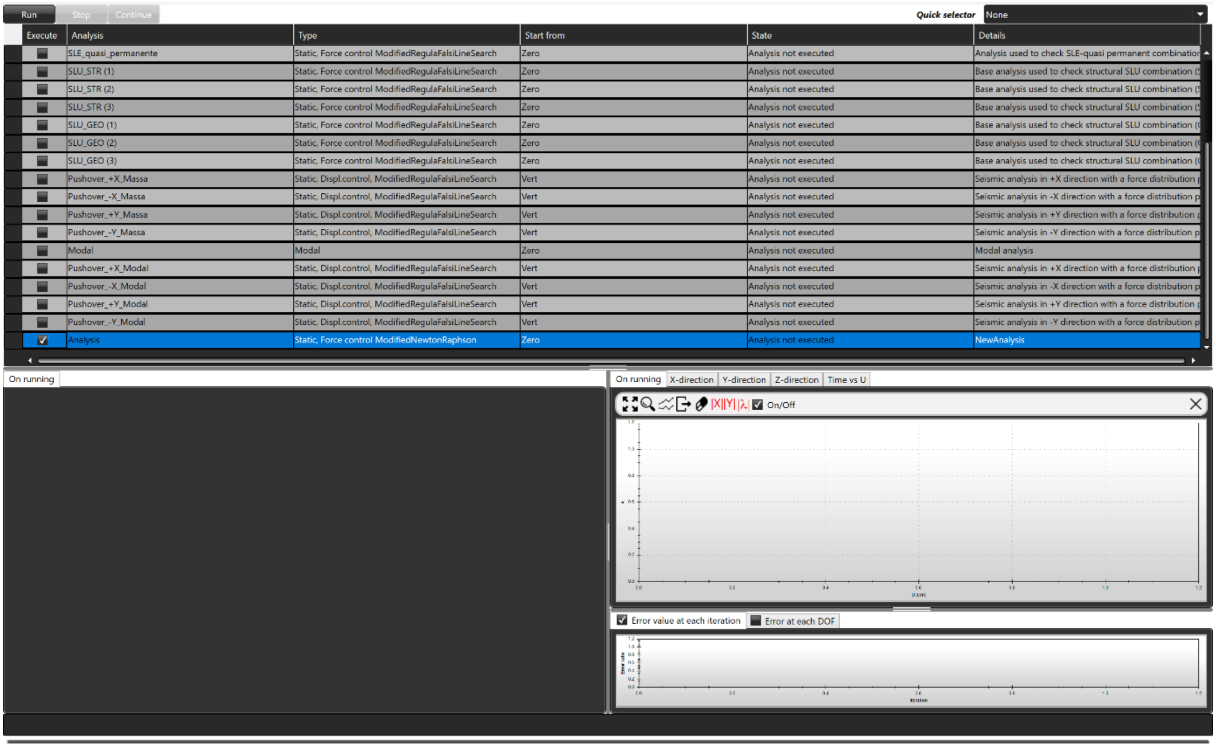

Figure 20 - Analysis Window.

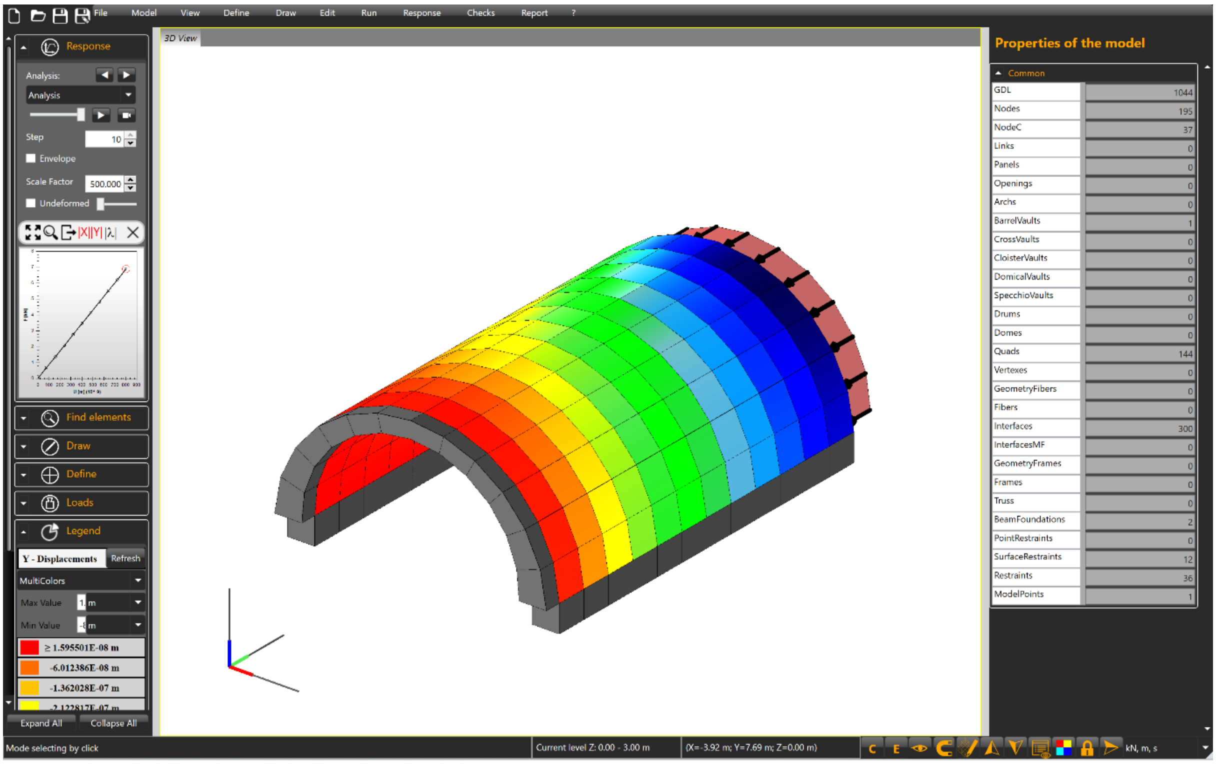

Figure 21- Output phase in the Y-direction.

This paragraph describes the operations to be conducted to calculate the Tangential stiffness.

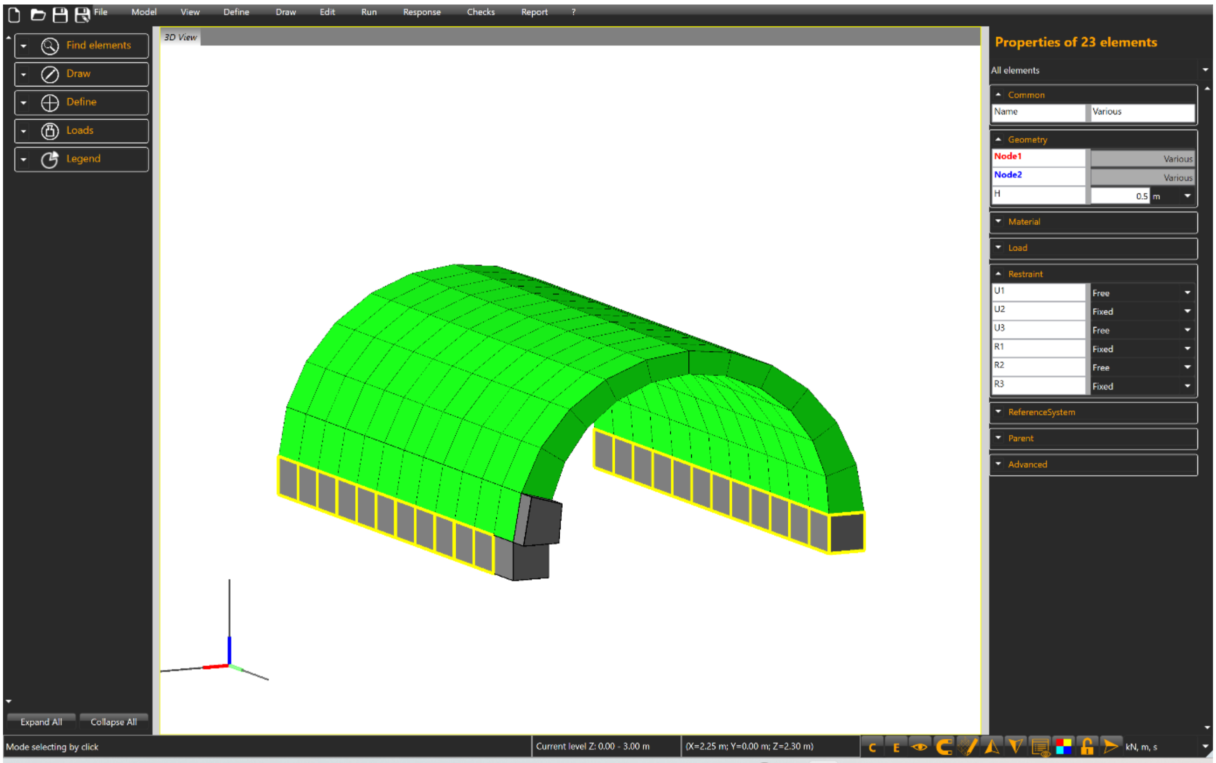

Figure 22 - Defining constrains.

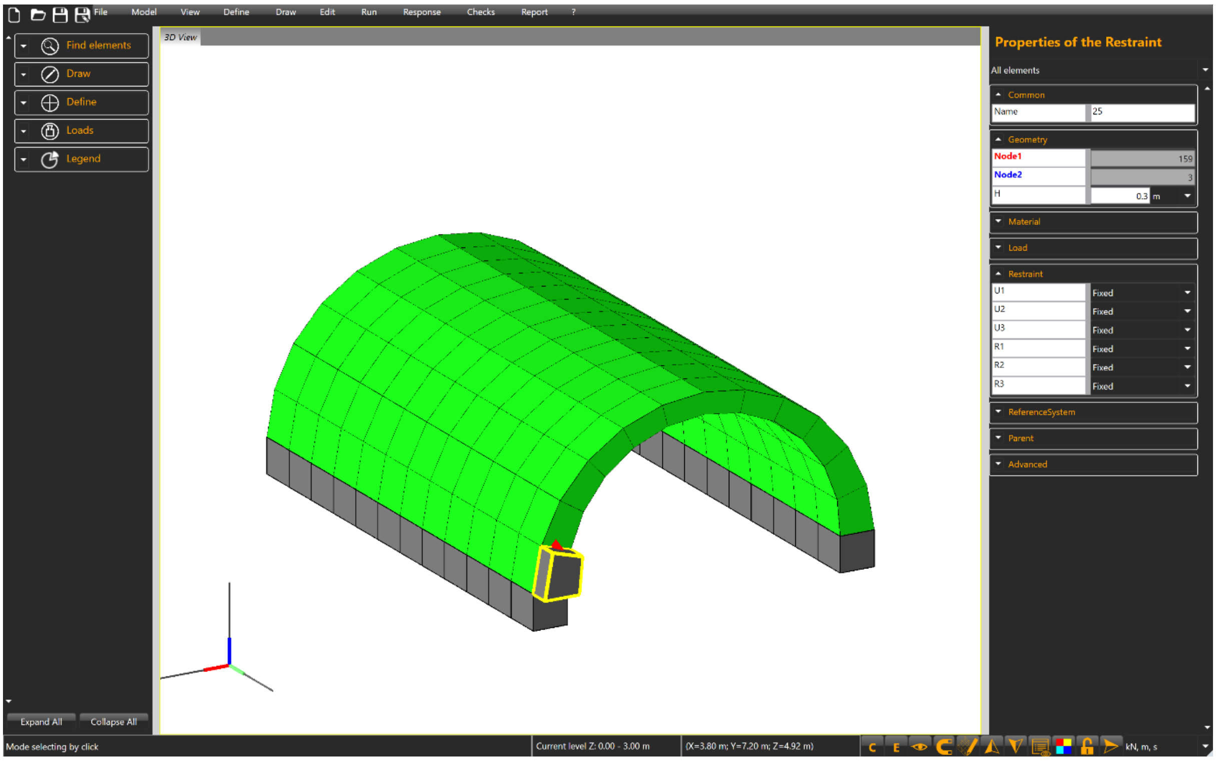

Figure 23- Defining constrains.

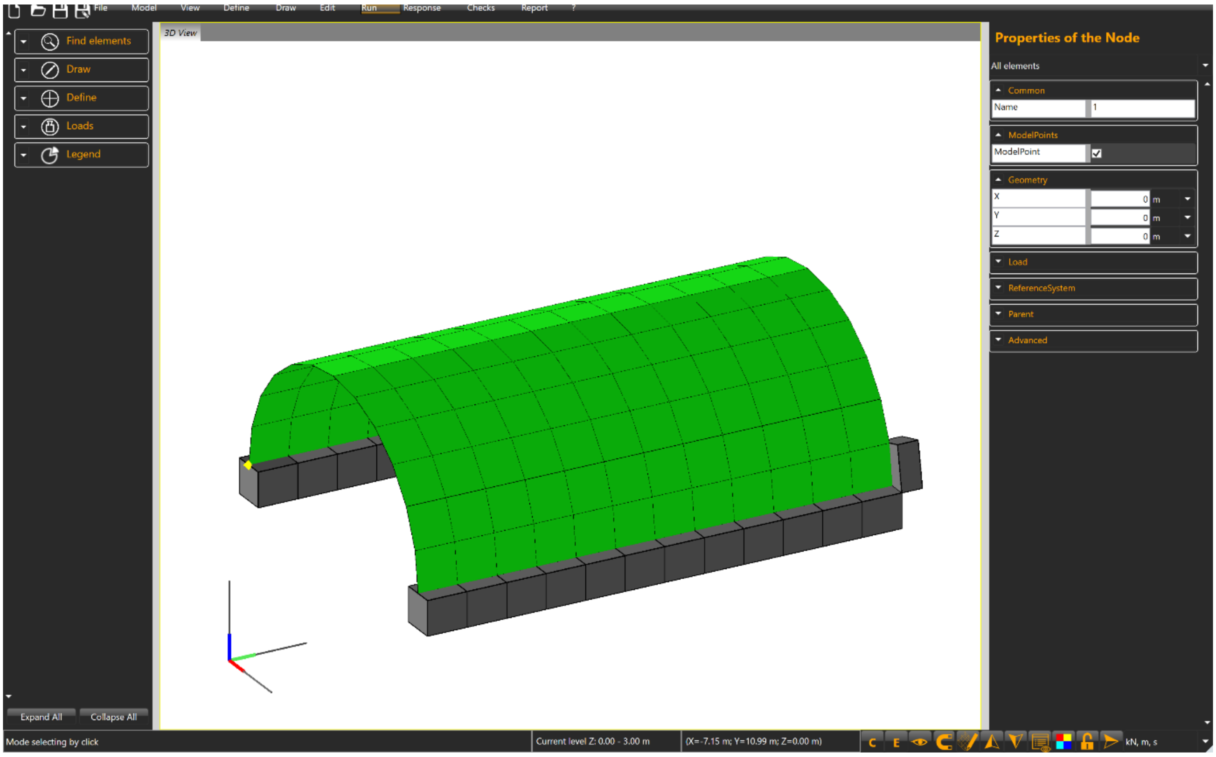

Figure 24 - Defining one of the nodes along the side.

Figure 25 - Defining Line Load in Global Y direction.

Figure 26 - Defining Line Load in Global Y direction.

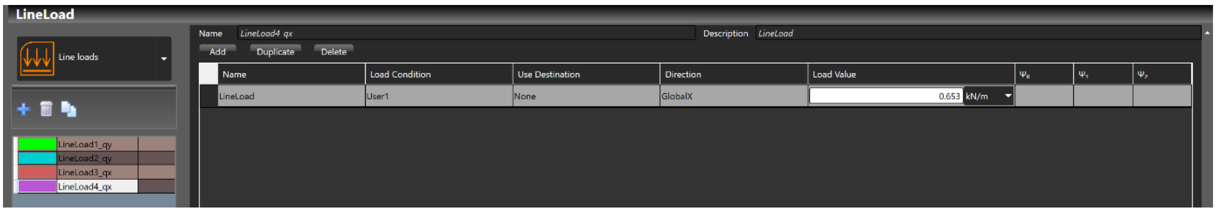

Figure 27 - Defining Line Load in Global X direction.

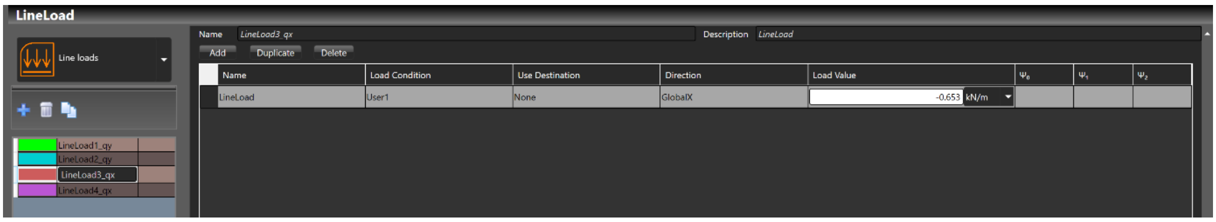

Figure 28 - Defining Line Load in Global X direction.

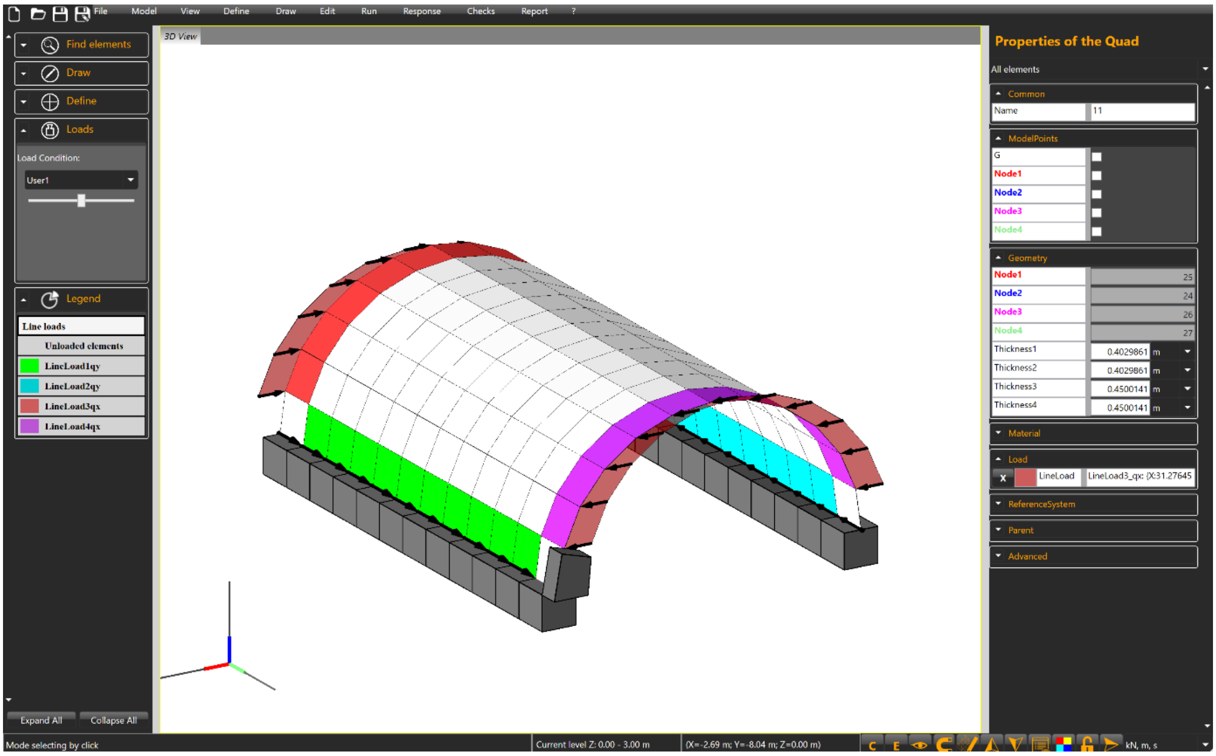

Figure 29 - Assigning line loads, so the system is self-balanced.

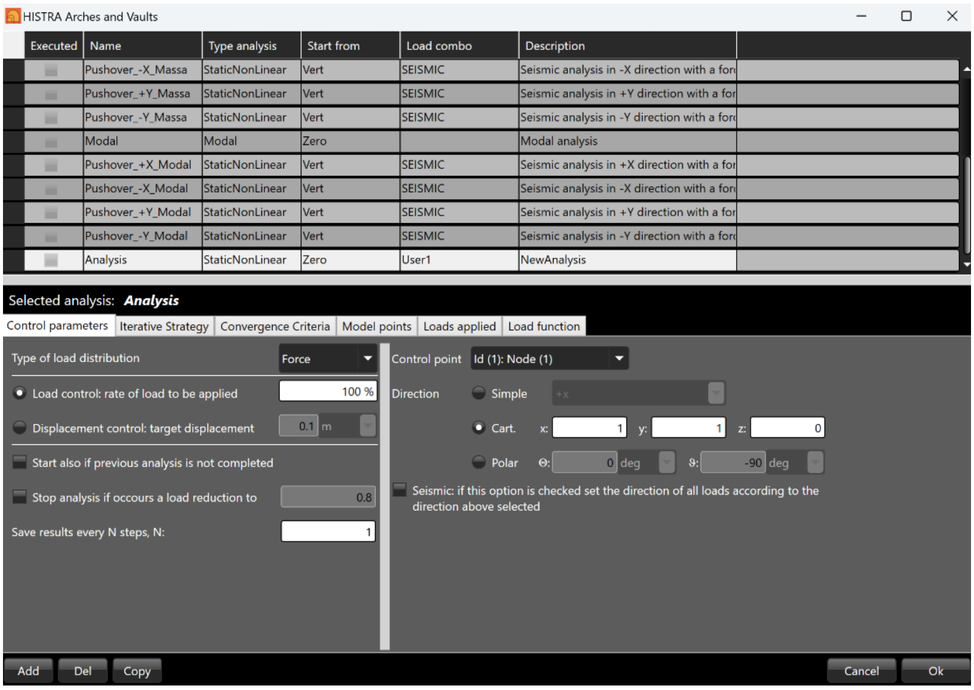

Figure 30 - Defining the analysis window.

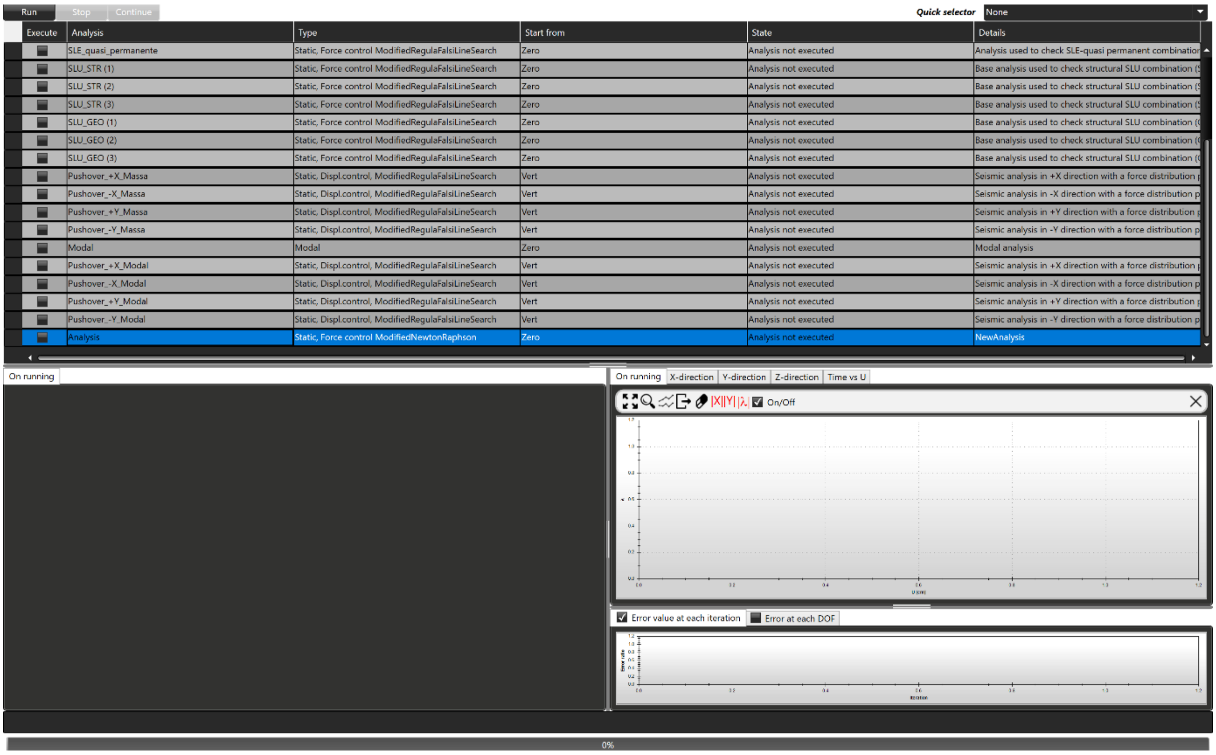

Figure 31 - Analysis Window.

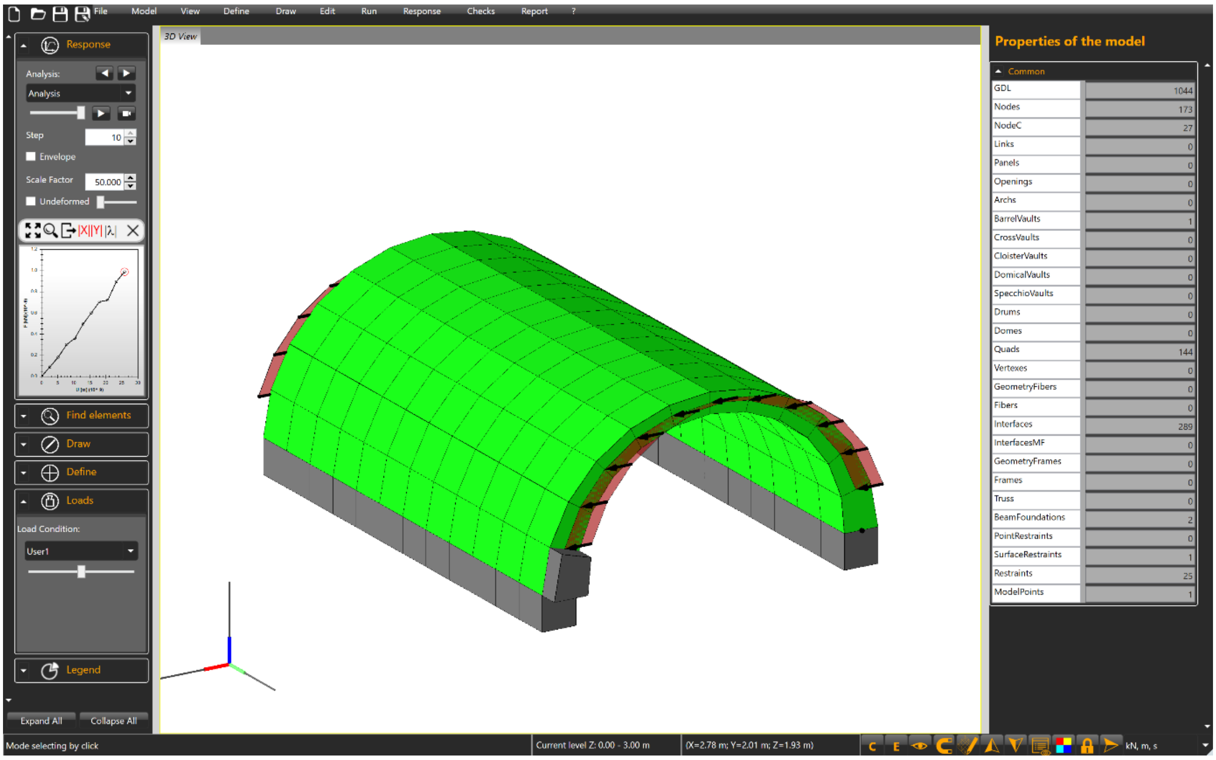

Figure 32 - Output Phase.

Appendix B – Parameters defined in Macro Element Software.

Appendix B.2 – Parameters defined in 3D Macro.

This section includes images detailing the settings and parameters utilized in 3D Macro for the analysis.

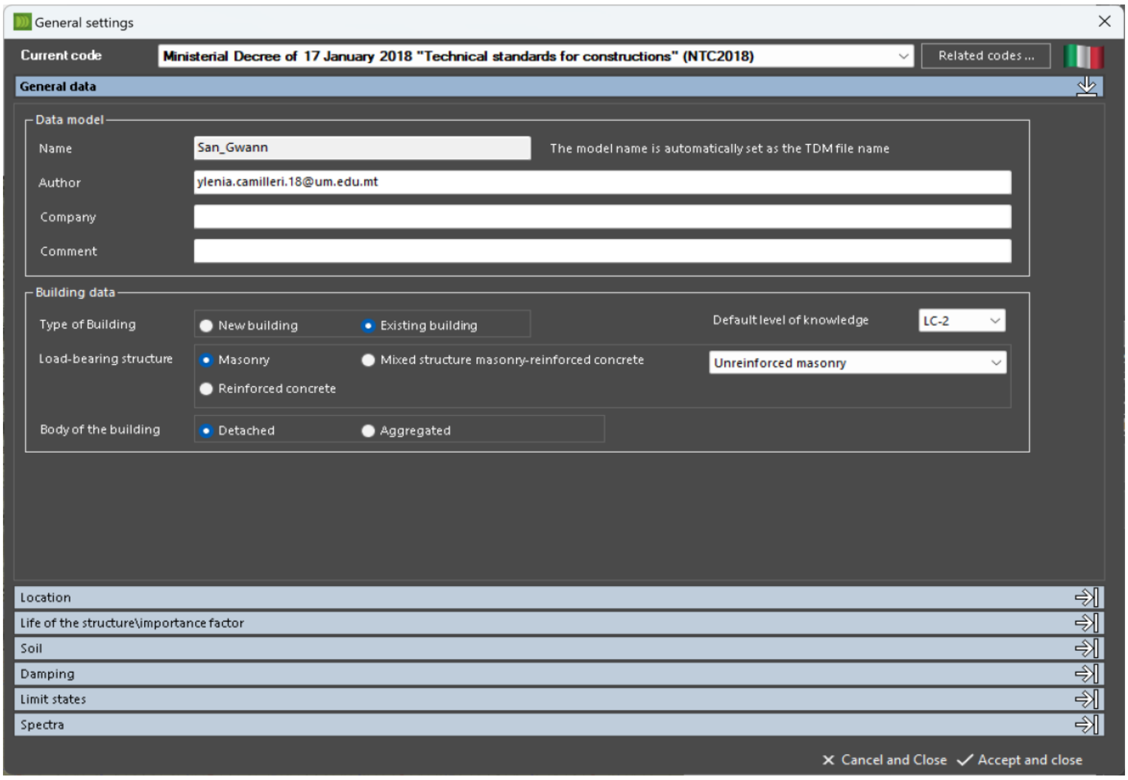

Figure 33 - General Settings.

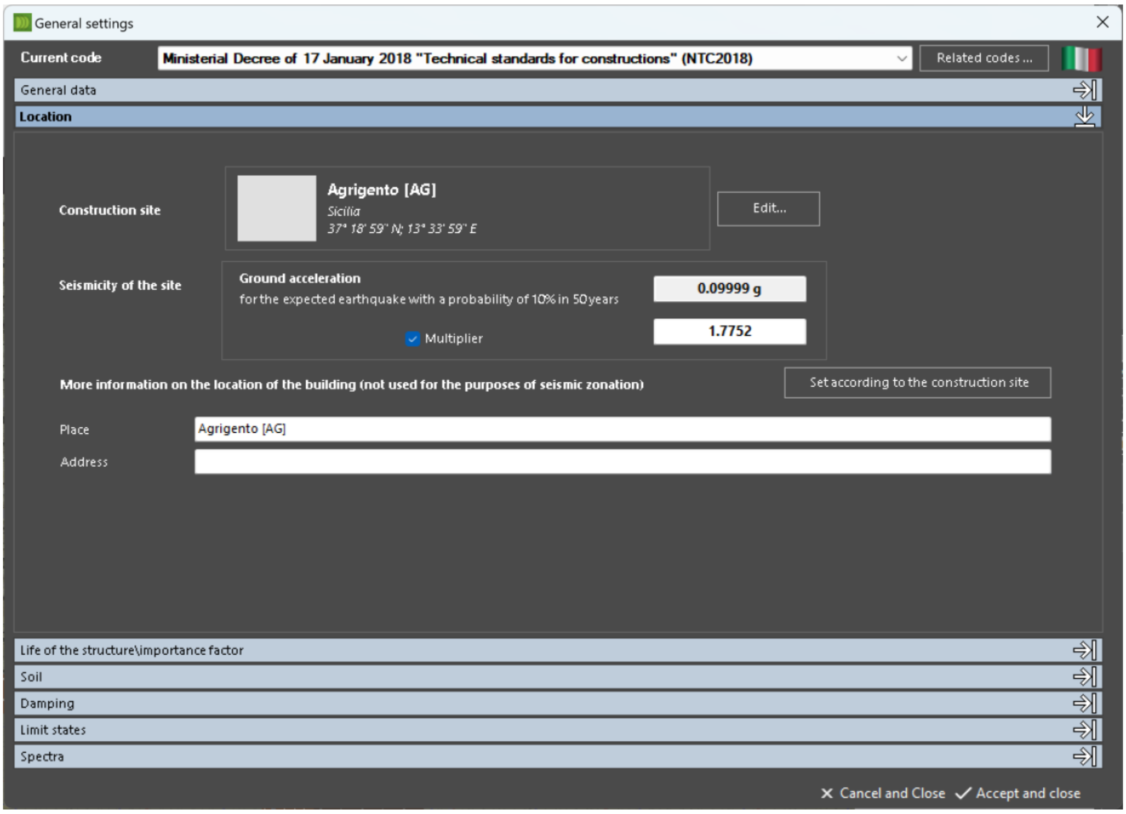

Figure 34 - Location; General Settings.

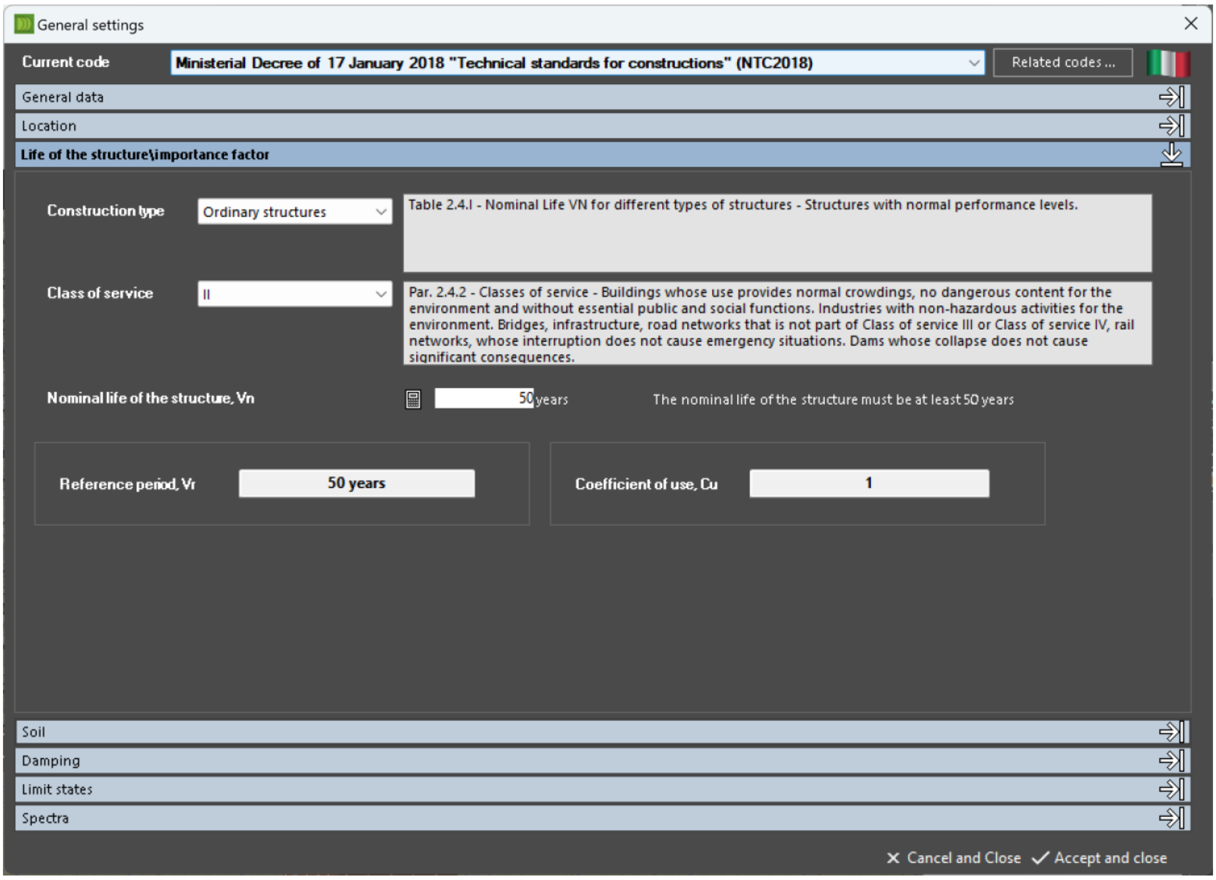

Figure 35 - Life of the Structure/Importance factor; General.

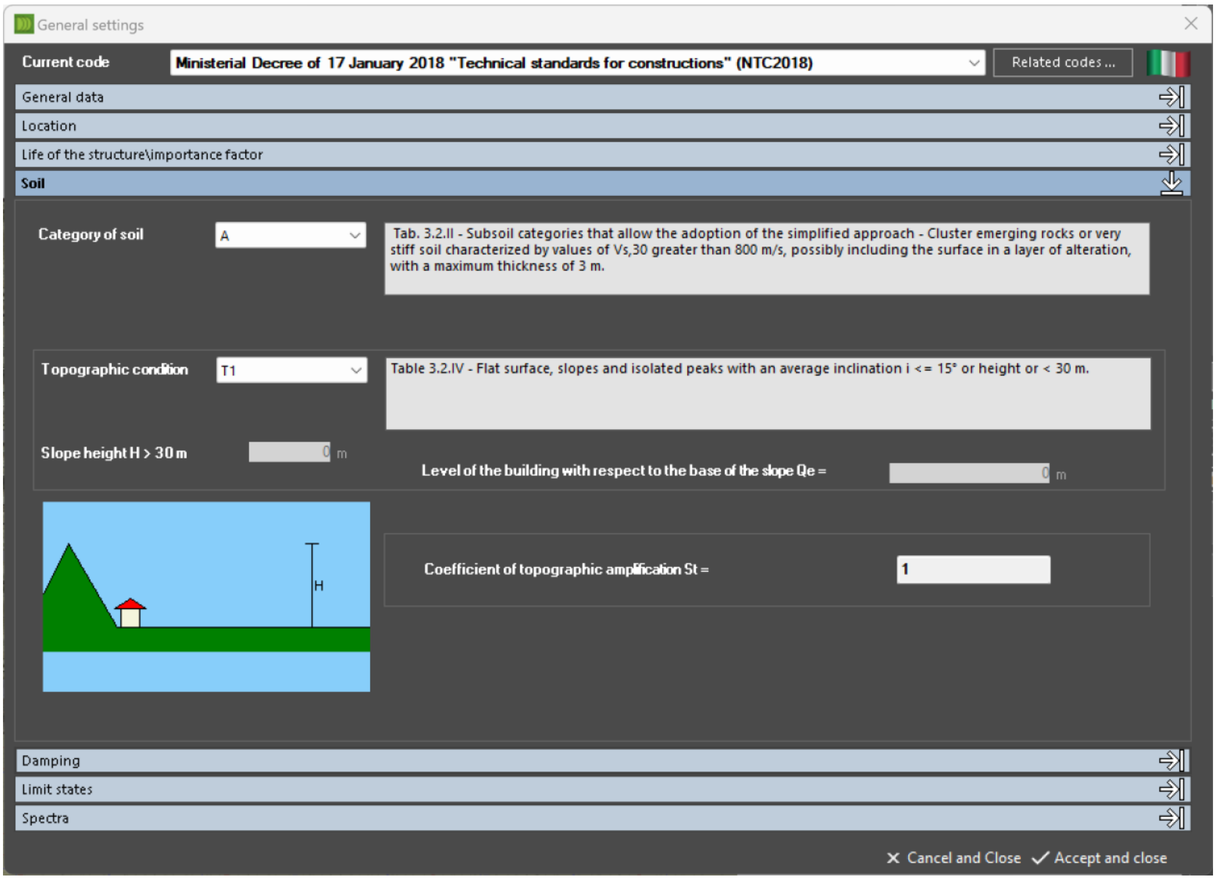

Figure 36 - Settings Soil in case of St. Philip & St. James Chapel in San Gwann and St Matthew's Chapel in Qrendi; General Settings.

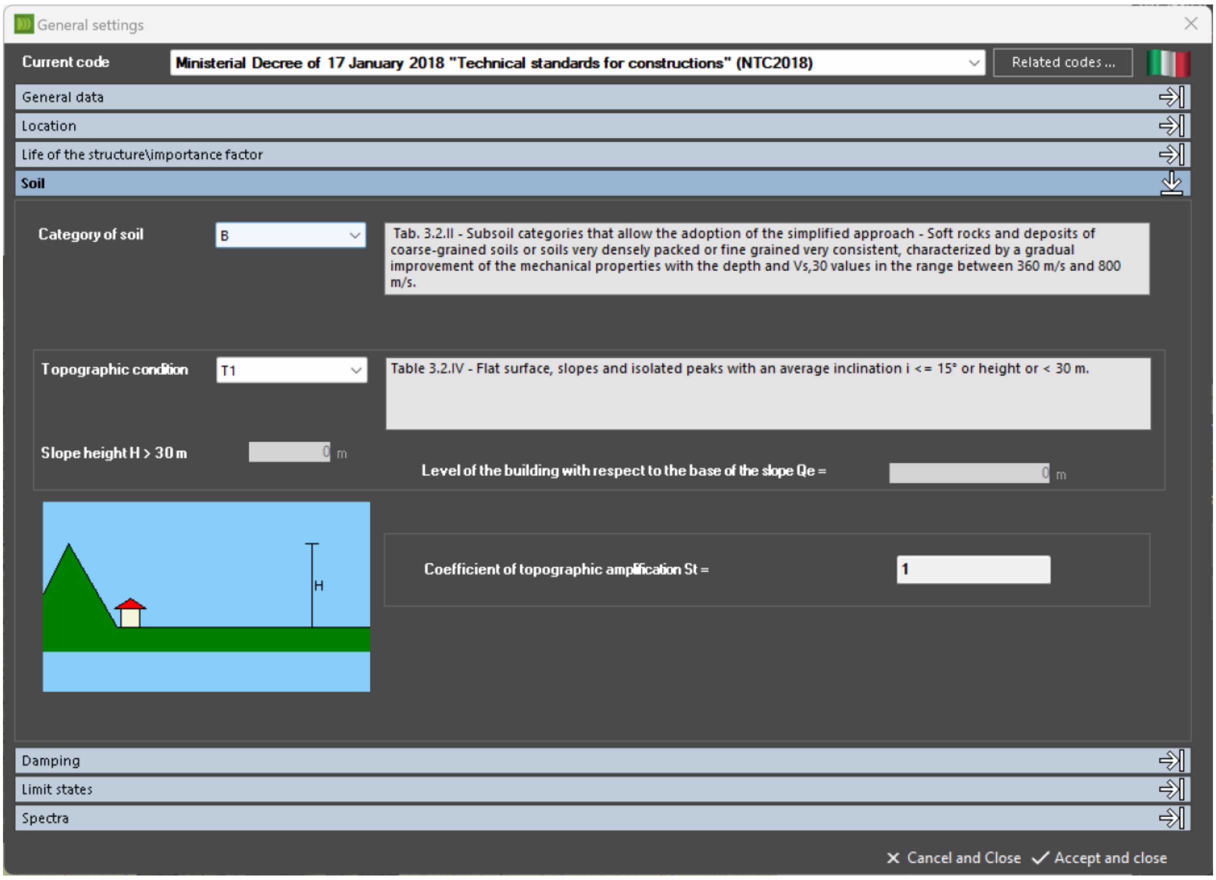

Figure 37 - Soil in case of St Mary Magdalene Chapel in Dingli; General Settings.

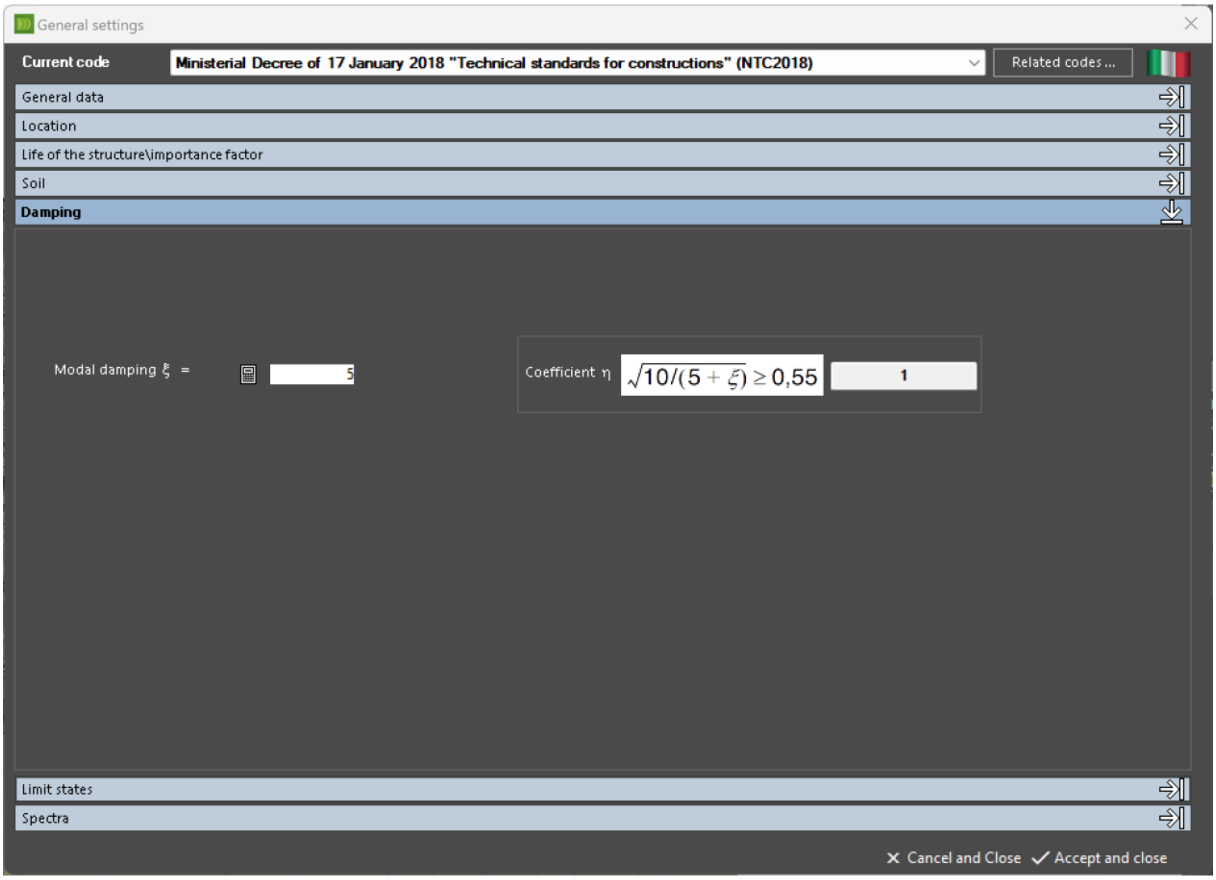

Figure 38 - Damping; General Settings.

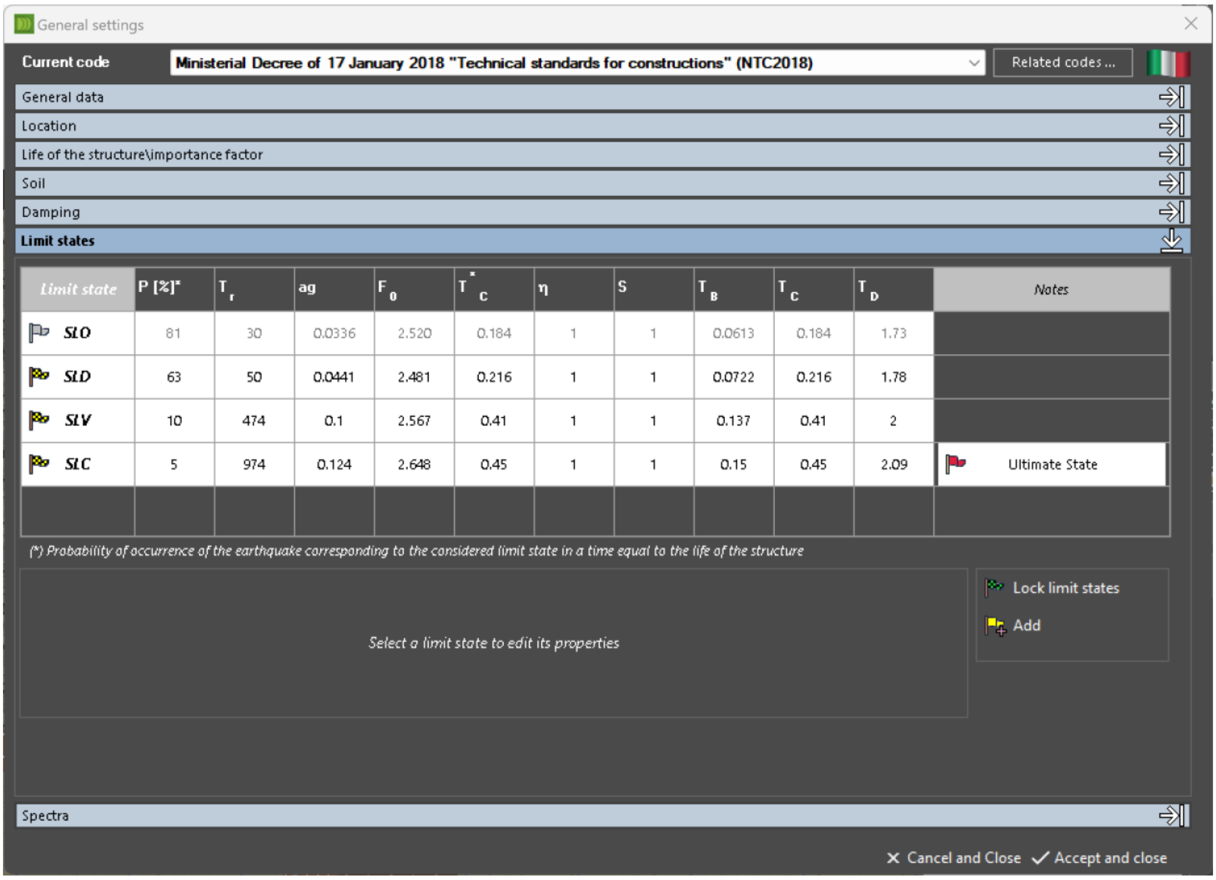

Figure 39 - Limit states; General Settings.

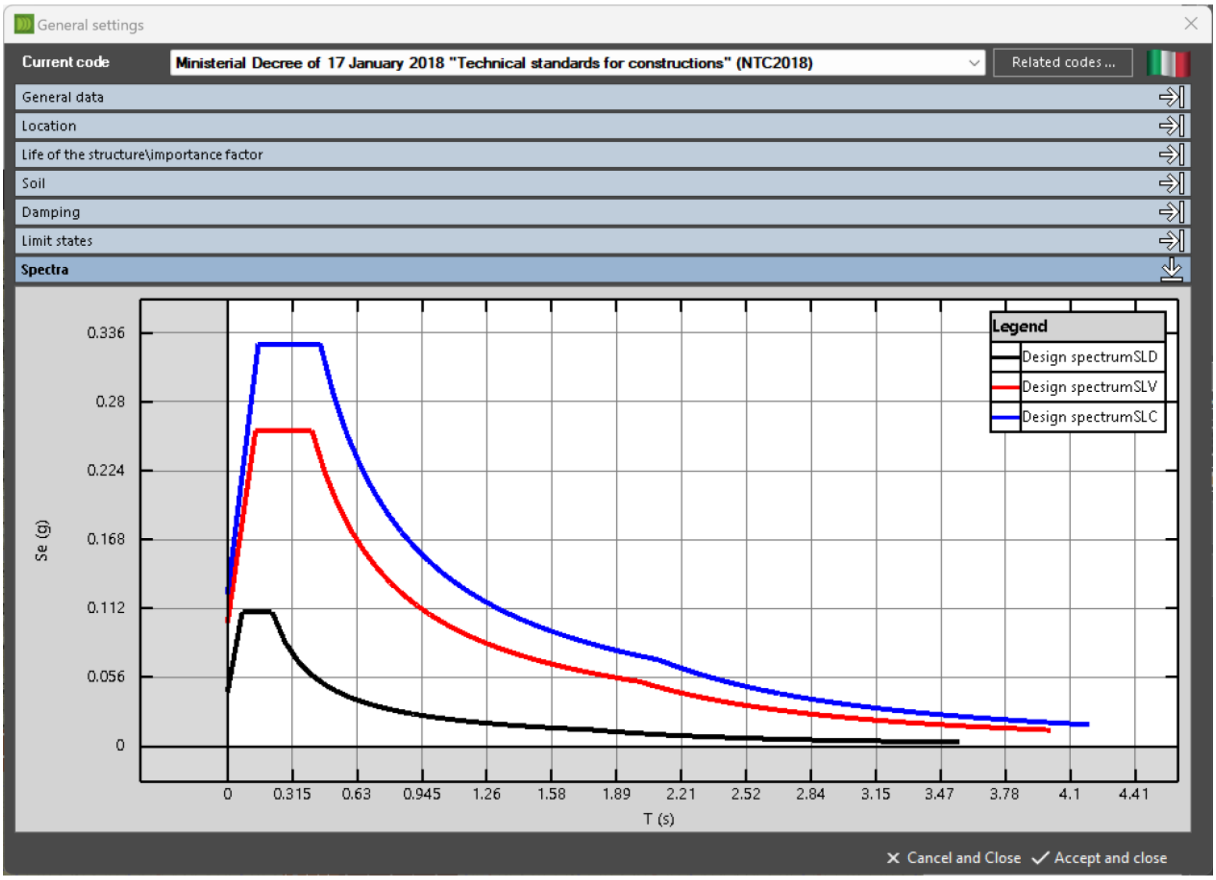

Figure 40 - Spectra; General Settings.

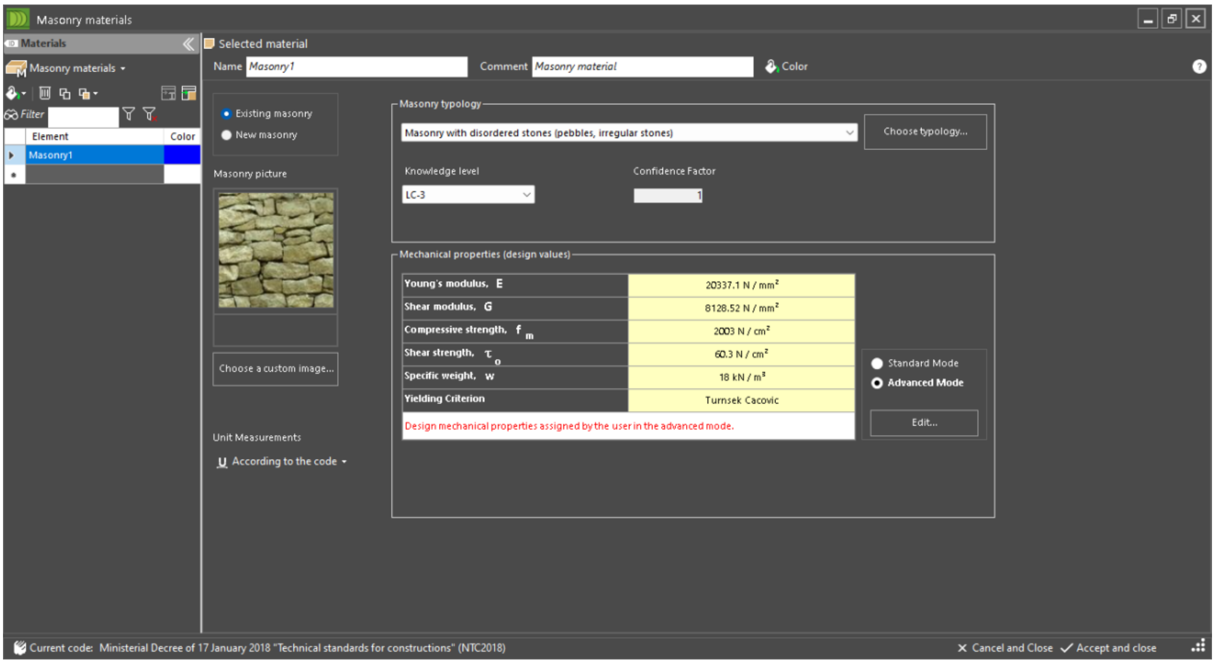

Figure 41 - Advanced masonry properties definition.

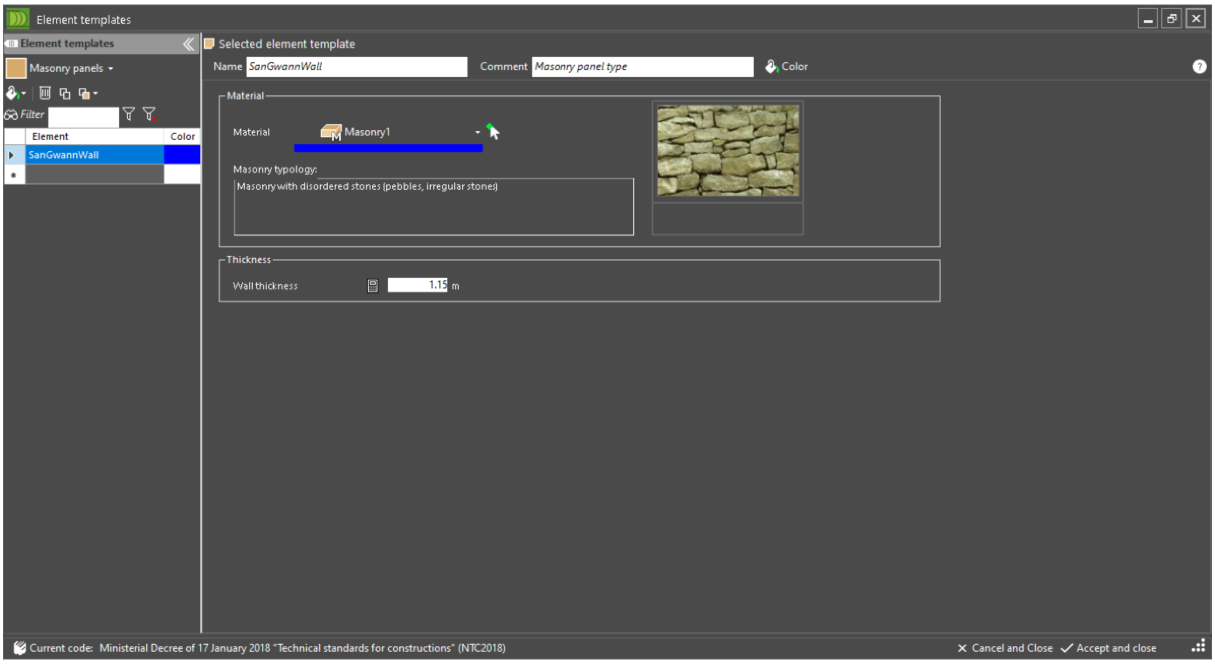

Figure 42 - Masonry wall Definition; Thickness according to the walls of the individual chapels.

Parameters defined in 3D Macro for St. Philip & St. James Chapel in San Gwann.

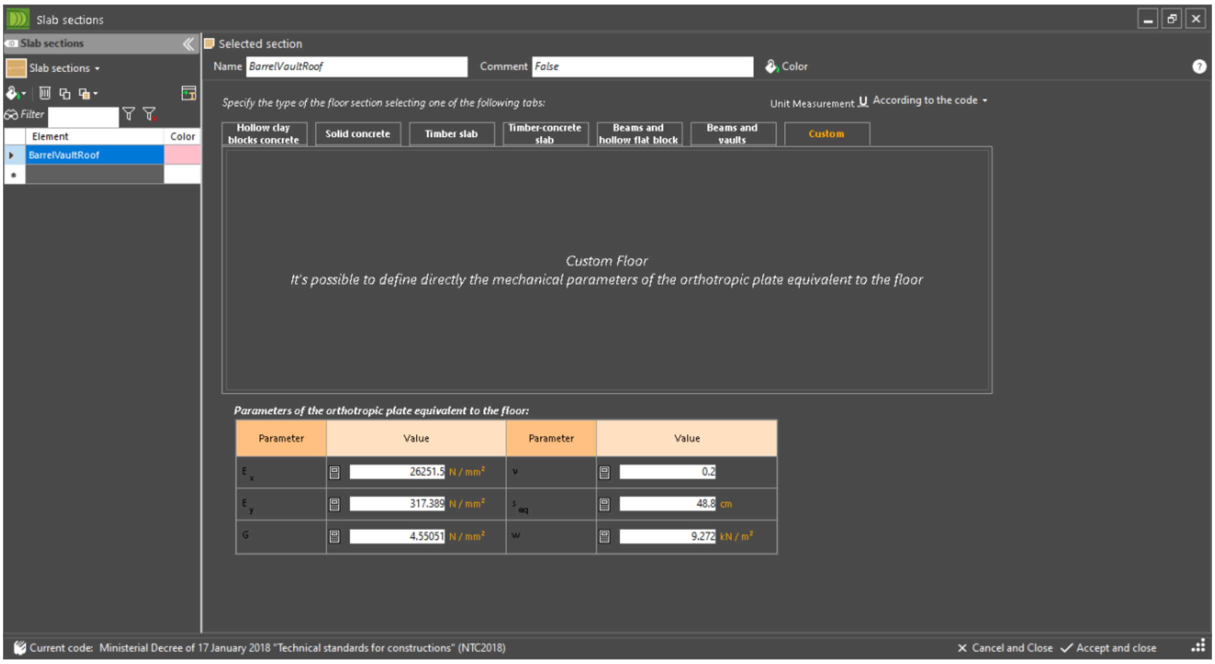

Figure 43 - Definition of custom slab (Parameters of Barrel Vault equivalent to Orthotropic Slab).

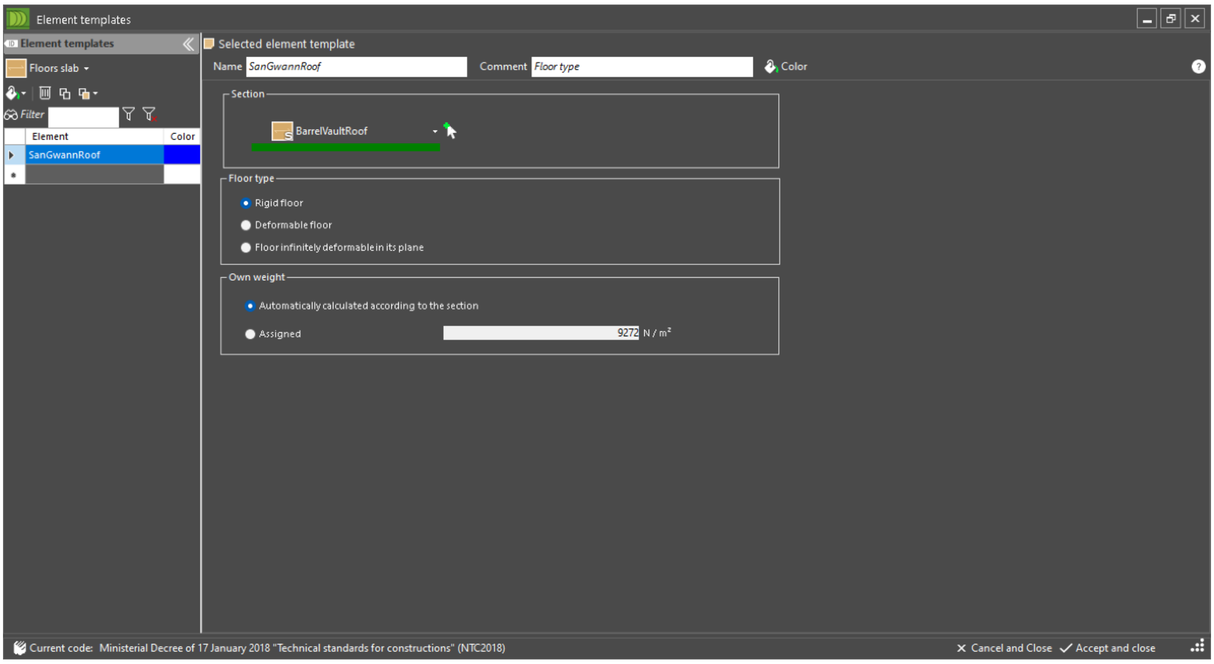

Figure 44 - Definition of custom slab.

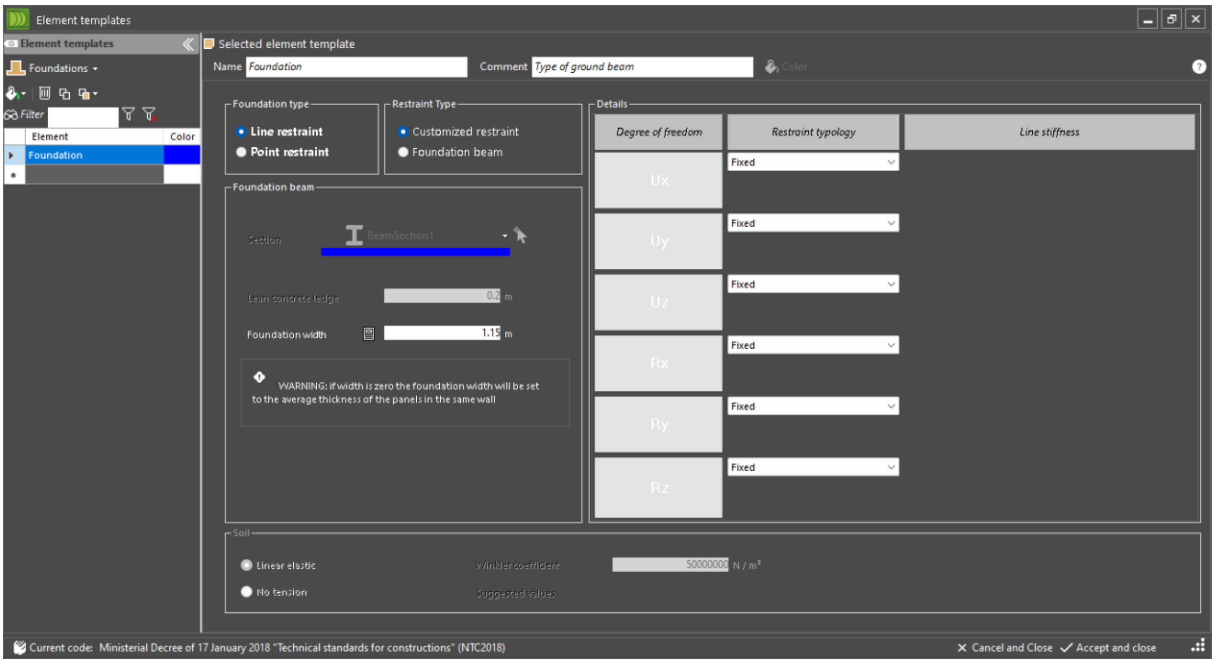

Figure 45 - Definition of foundation.

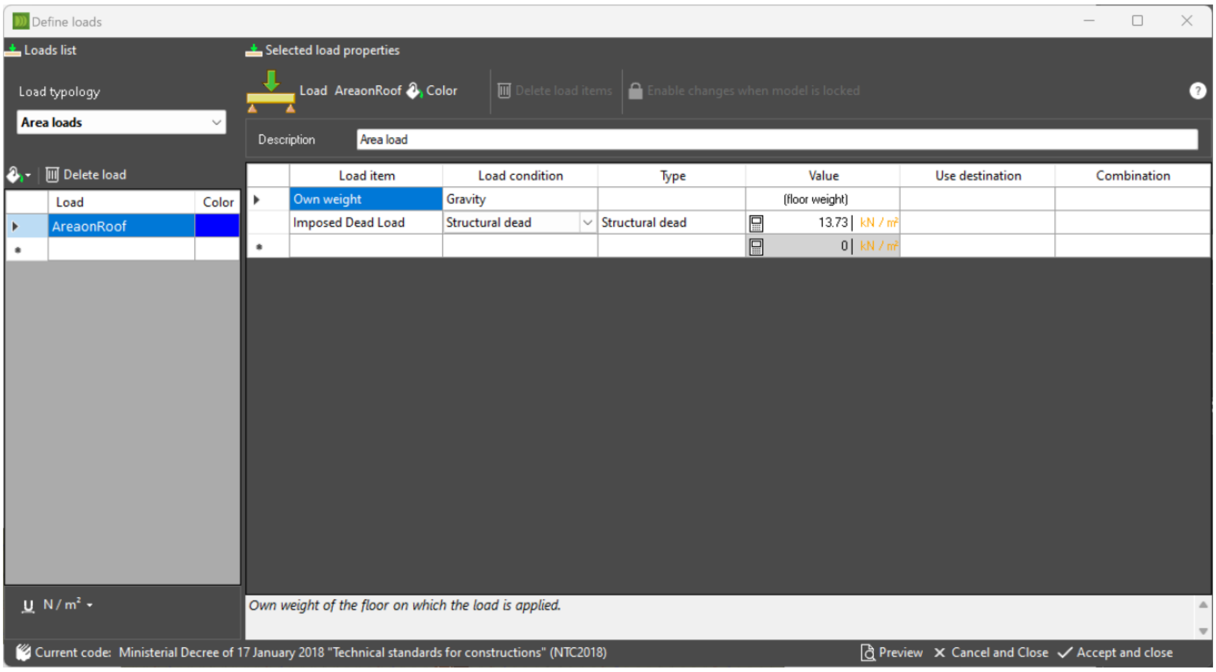

Figure 46 - Definition of load applied on chapel's roof.

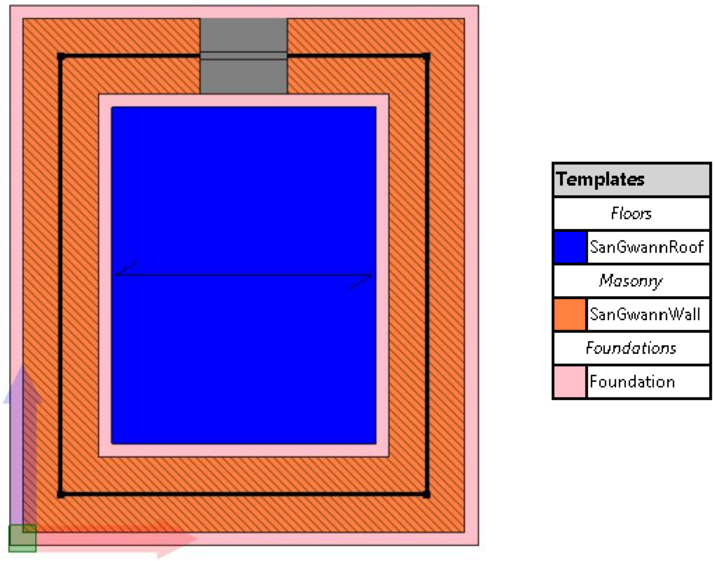

Figure 47 - 3D Macro Plan from 0 – 5780mm Layout of St. Philip & St. James Chapel in San Gwann.

Parameters defined in 3D Macro for St. Mary Magdalene Chapel in Dingli.

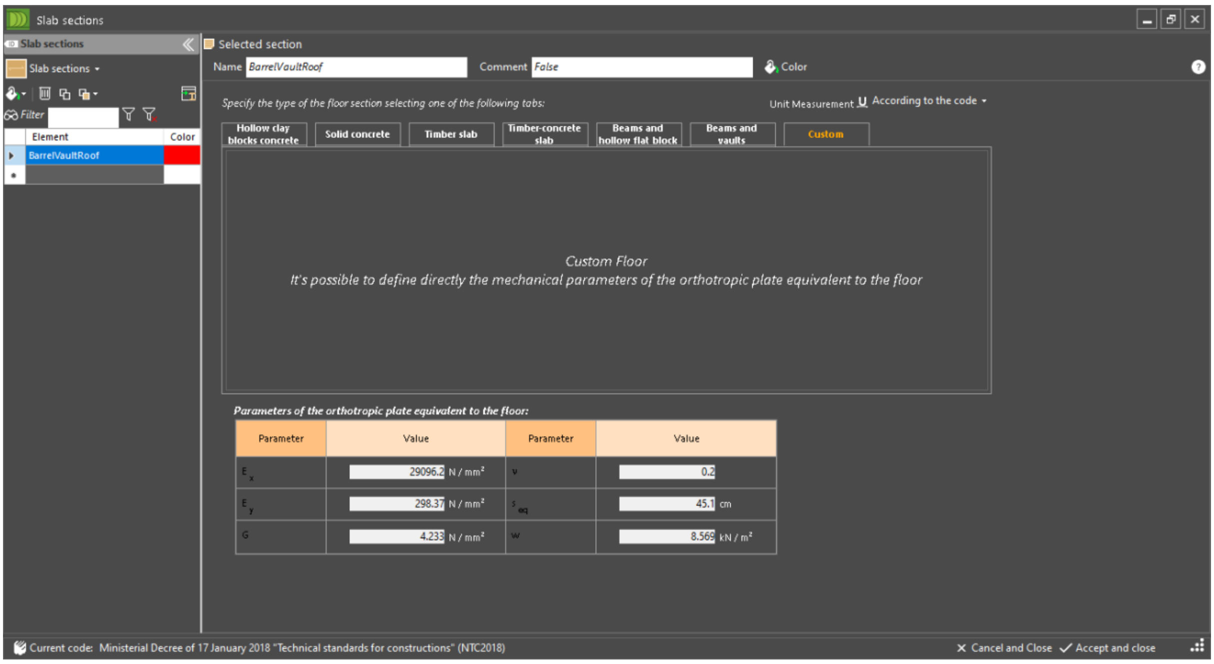

Figure 48 - Definition of custom slab (Parameters of Barrel Vault equivalent to Orthotropic Slab).

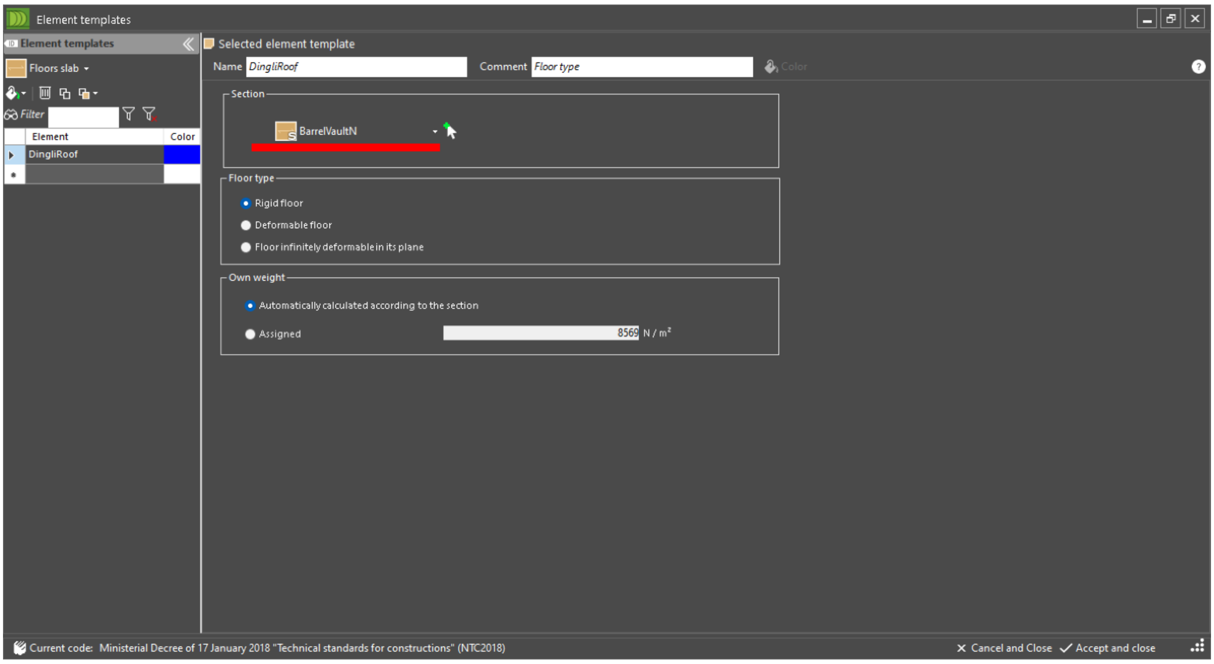

Figure 49 - Definition of custom slab.

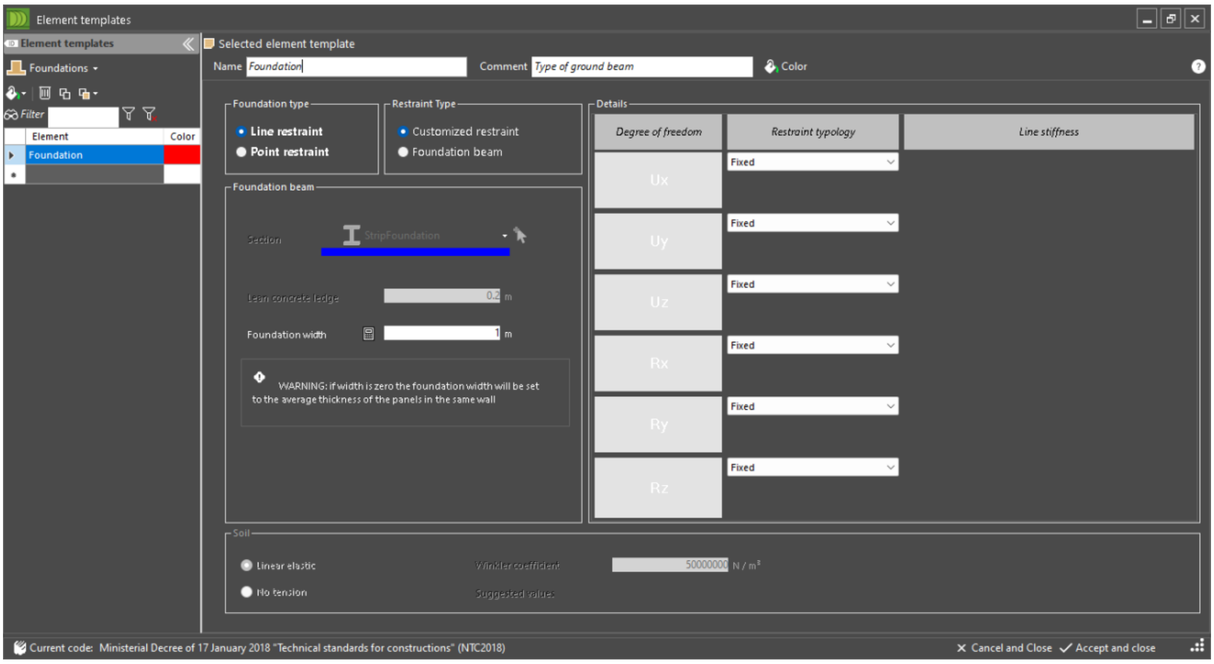

Figure 50 - Definition of foundation.

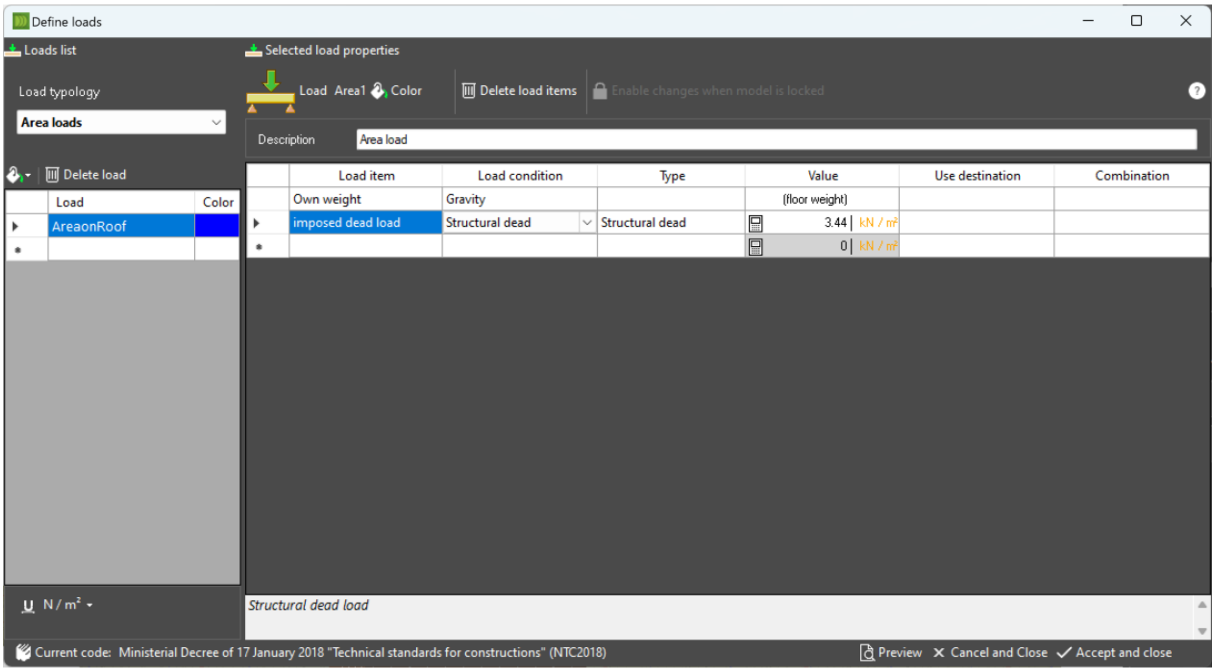

Figure 51 - Definition of load applied on chapel's roof.

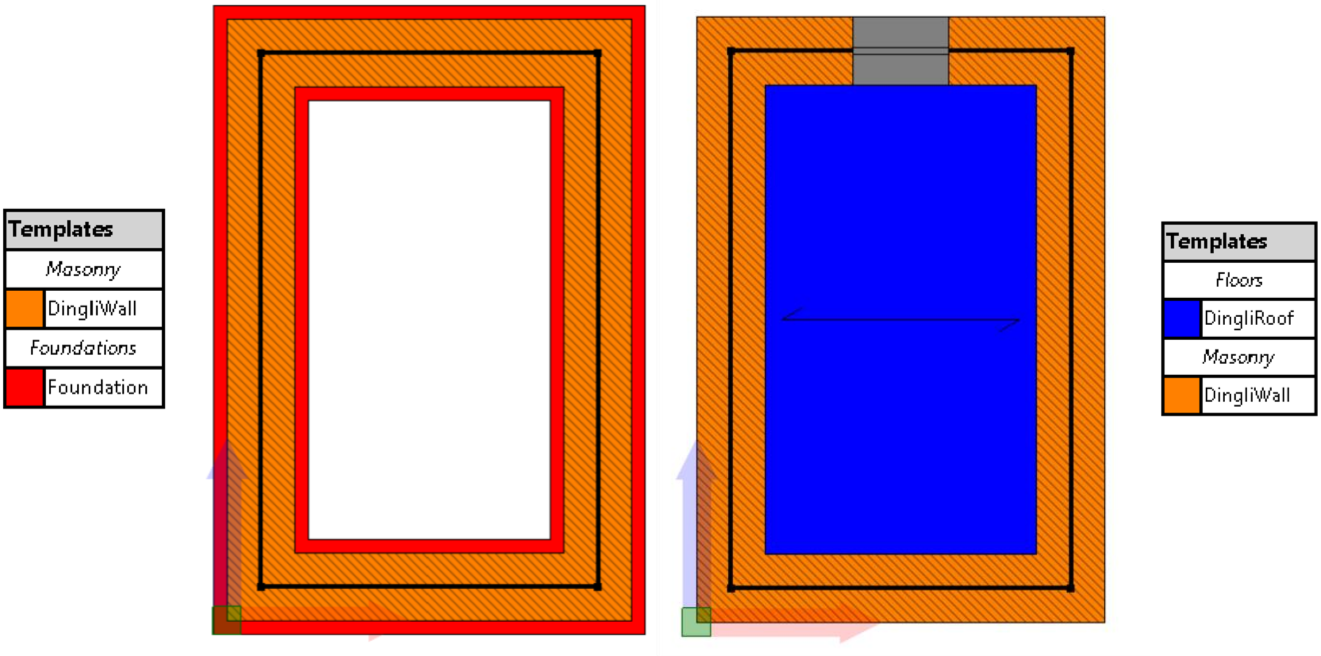

Figure 52 - 3D Macro Plan from 0 – 800 mm and 800mm – 6440 mm Layout of St Mary Magdalene Chapel in Dingli.

Parameters defined in 3D Macro for St. Matthew's Chapel in Qrendi.

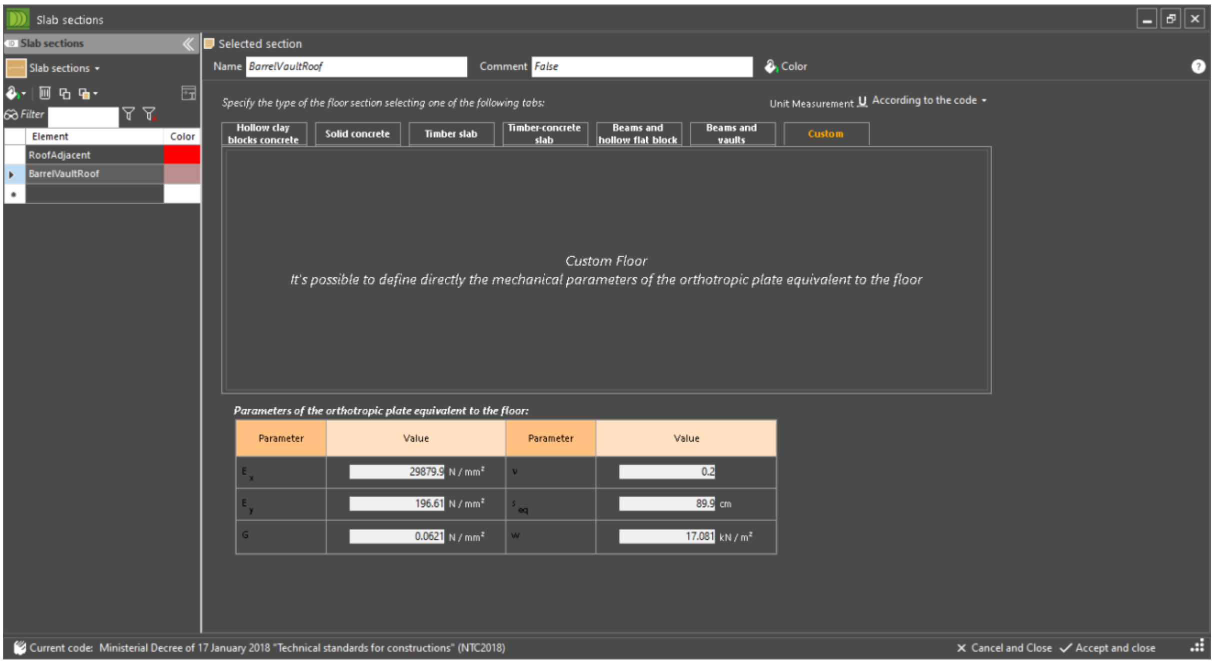

Figure 53 - Definition of custom slab (Parameters of Barrel Vault equivalent to Orthotropic Slab).

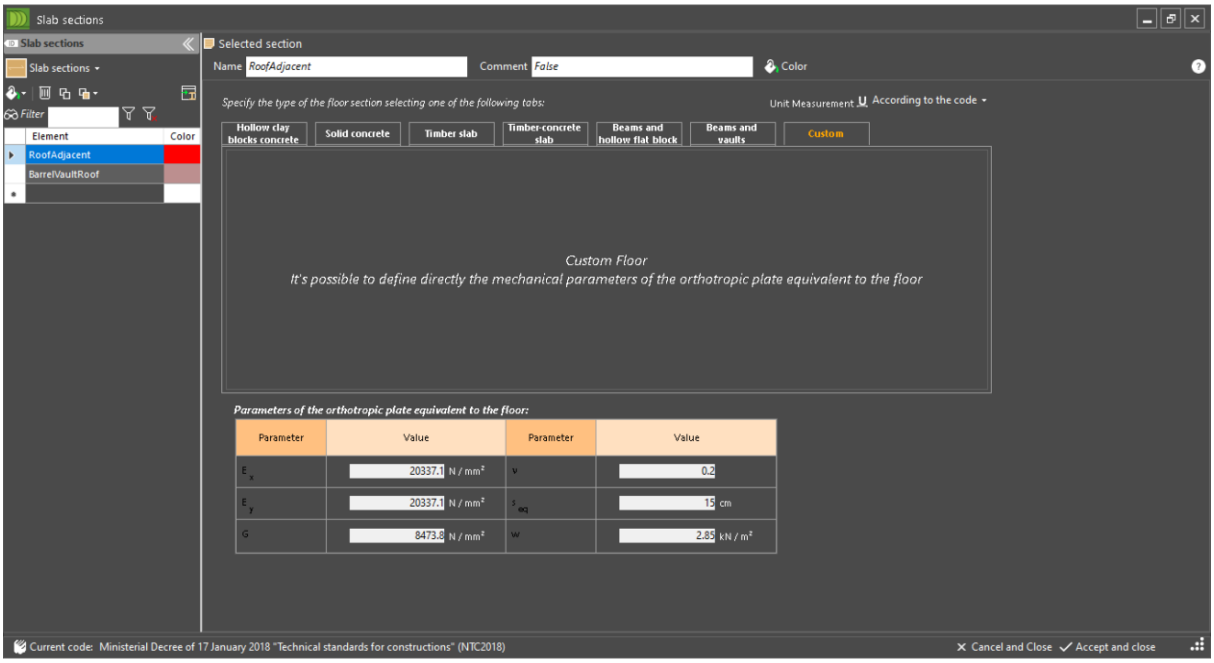

Figure 54 - Definition of custom slab for adjacent rooms.

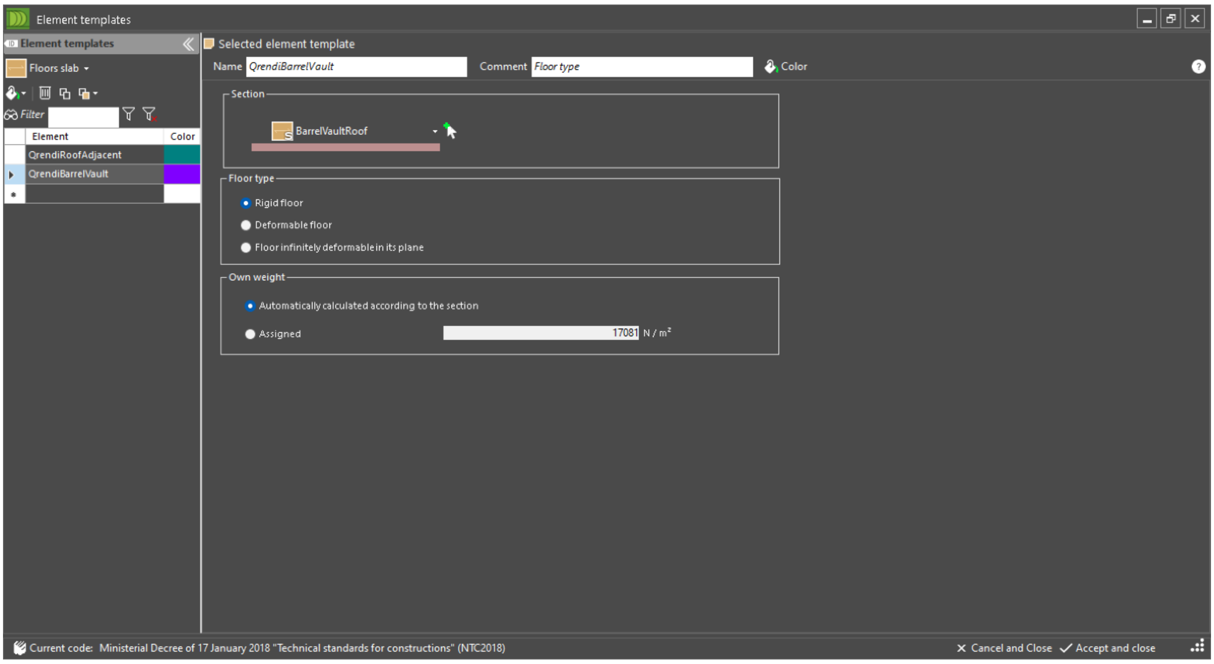

Figure 55 - Definition of custom slab.

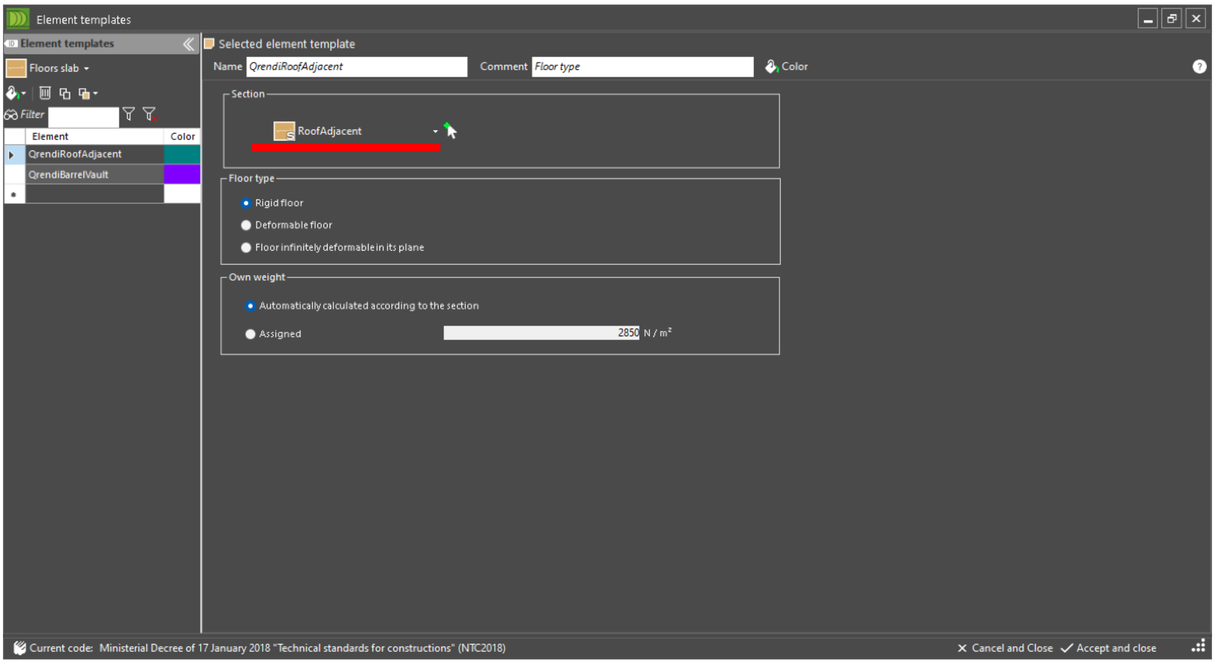

Figure 56 - Definition of custom slab.

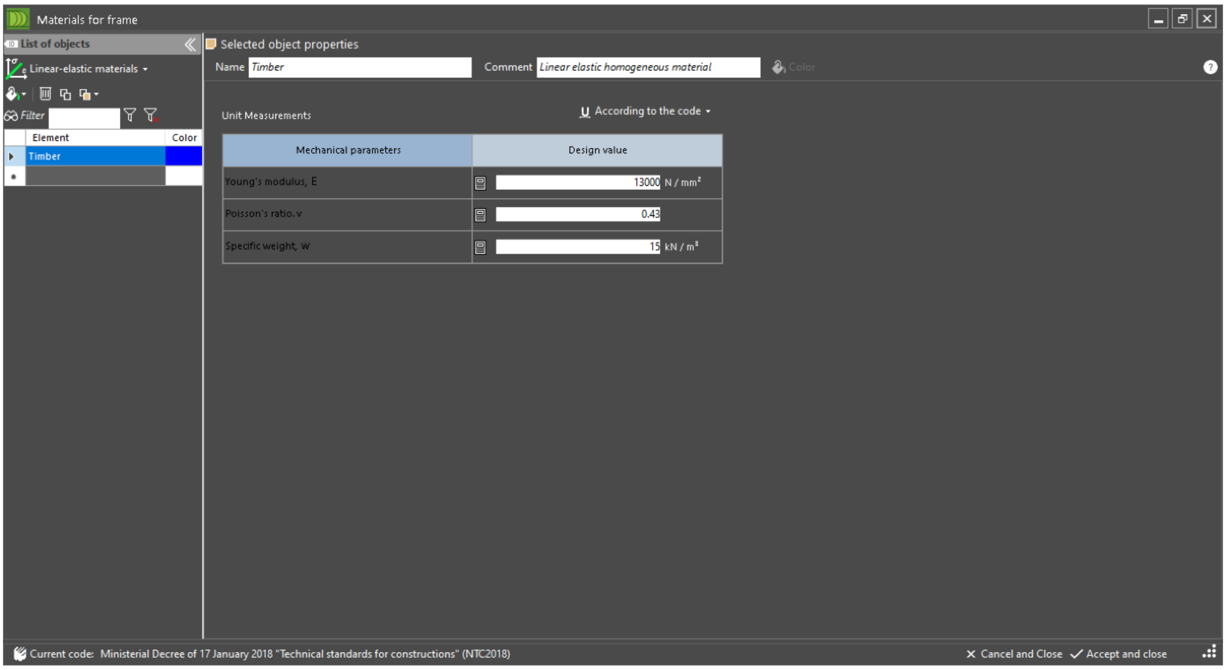

Figure 57- Definition of timber material.

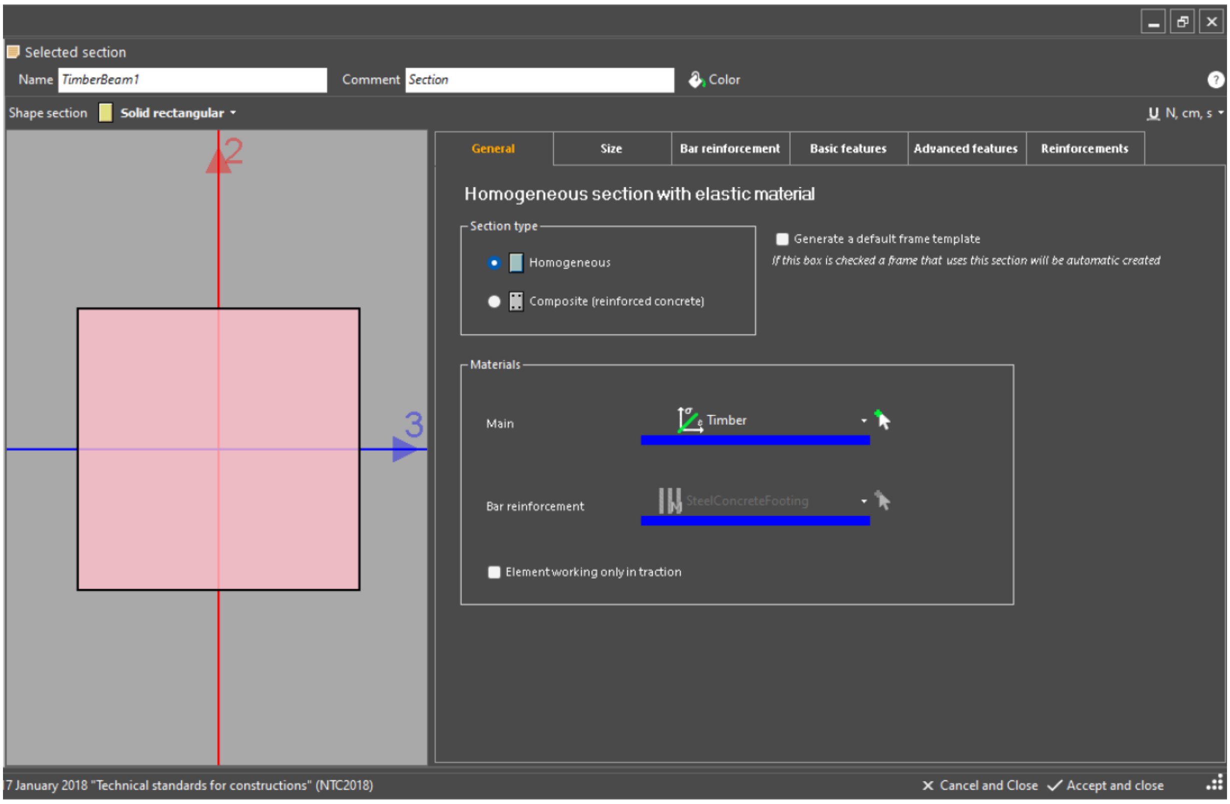

Figure 58 - Definition of timber beam.

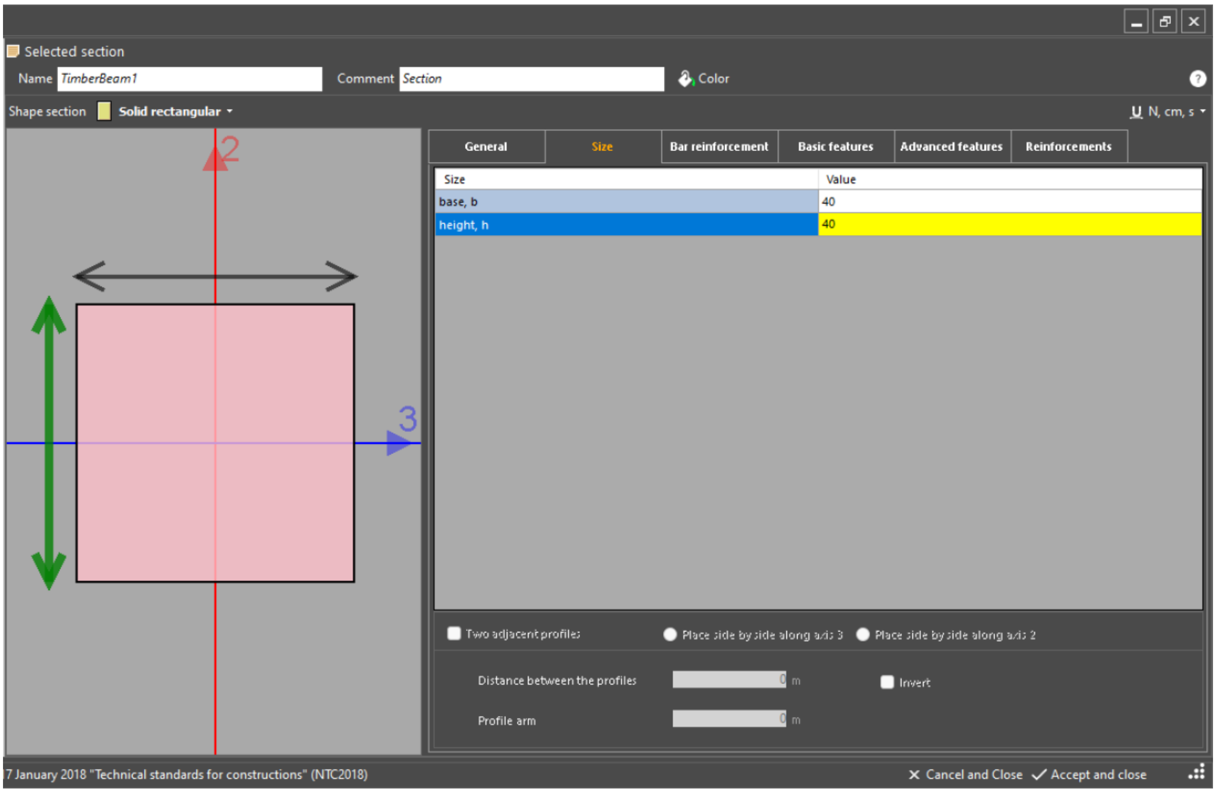

Figure 59 - Definition of timber beam 400 x 400 mm.

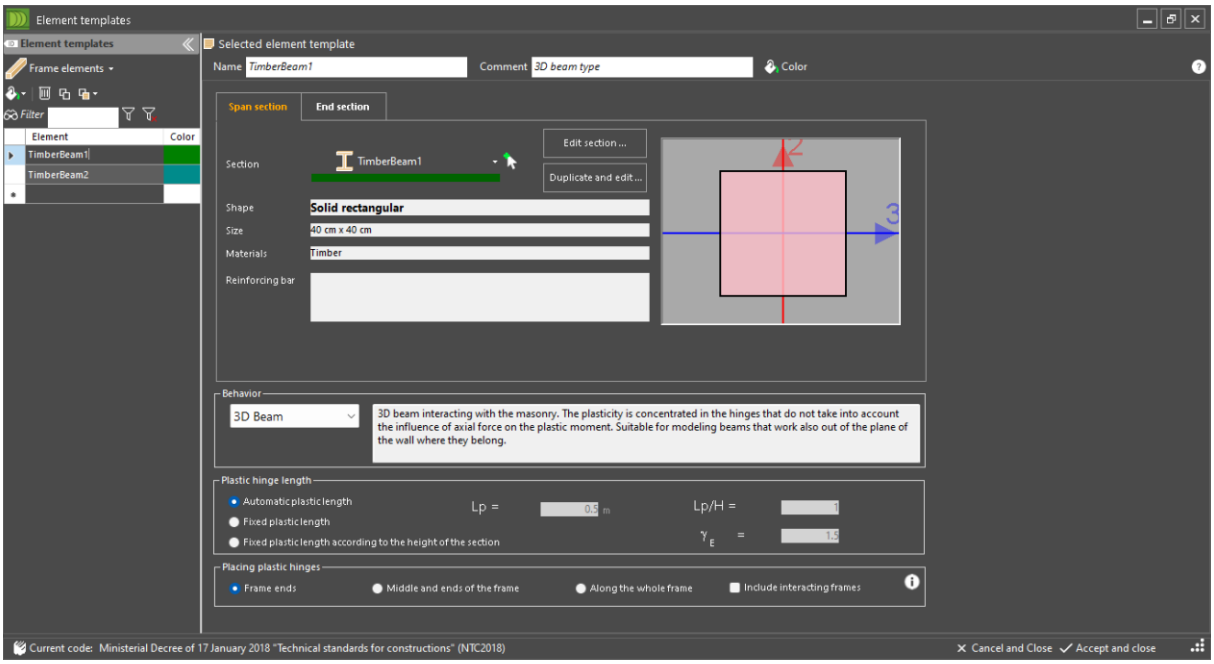

Figure 60 - Definition of timber beam 400 x 400 mm.

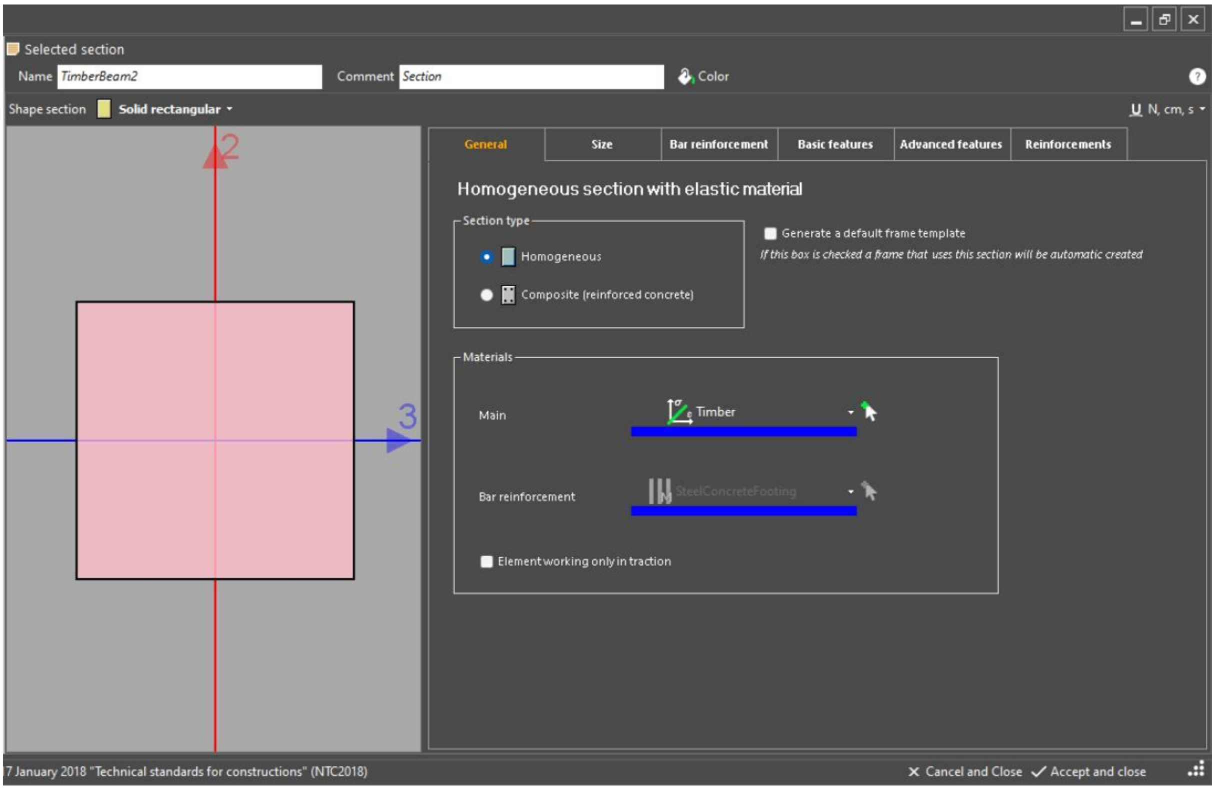

Figure 61 - Definition of timber beam 200 x 200 mm.

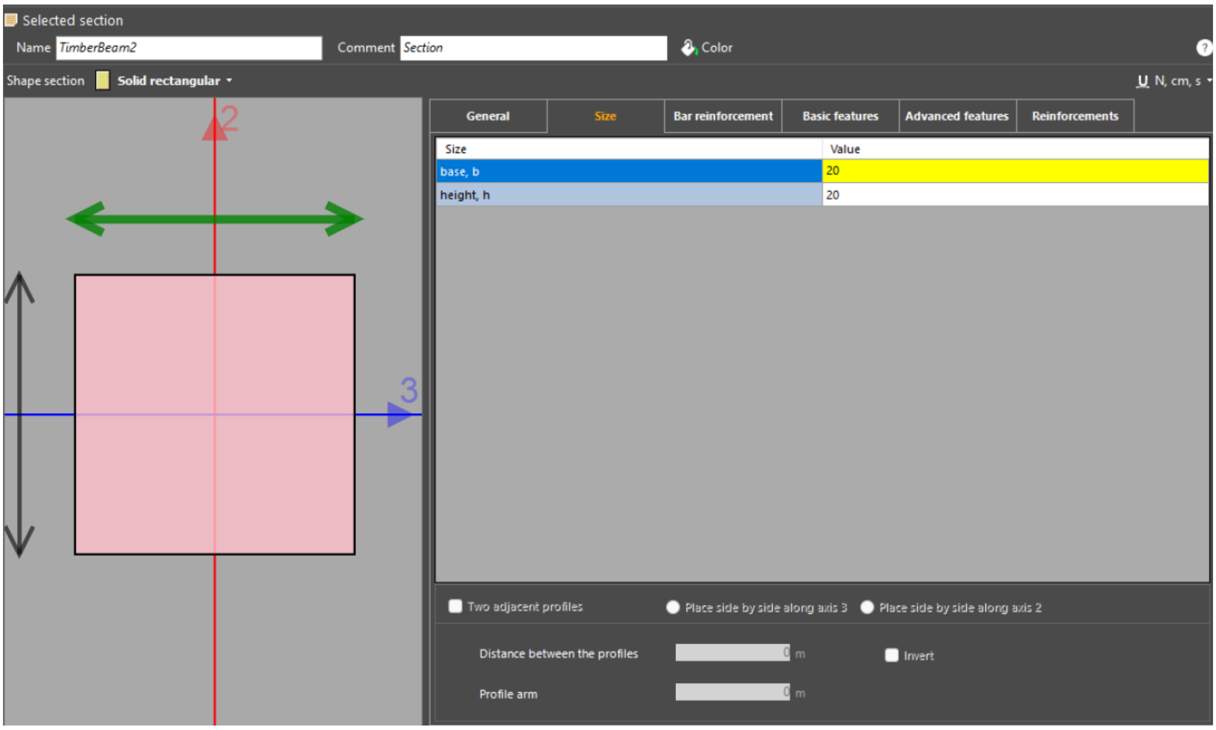

Figure 62 - Definition of timber beam 200 x 200 mm.

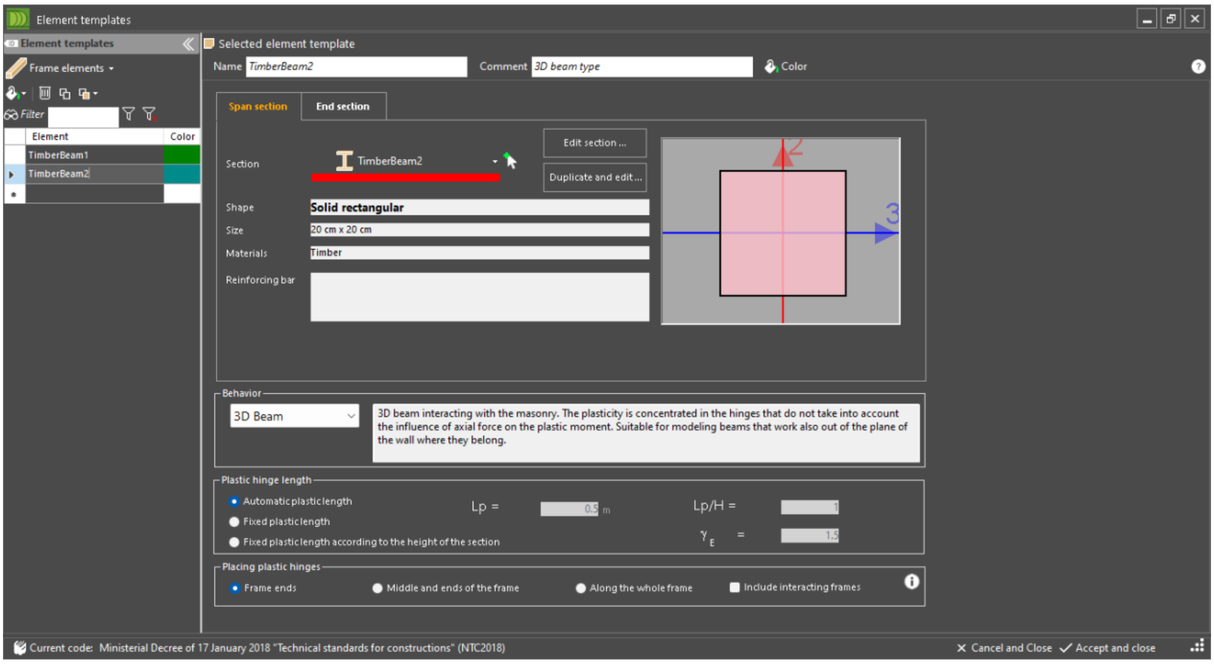

Figure 63 - Definition of timber beam 200 x 200 mm.

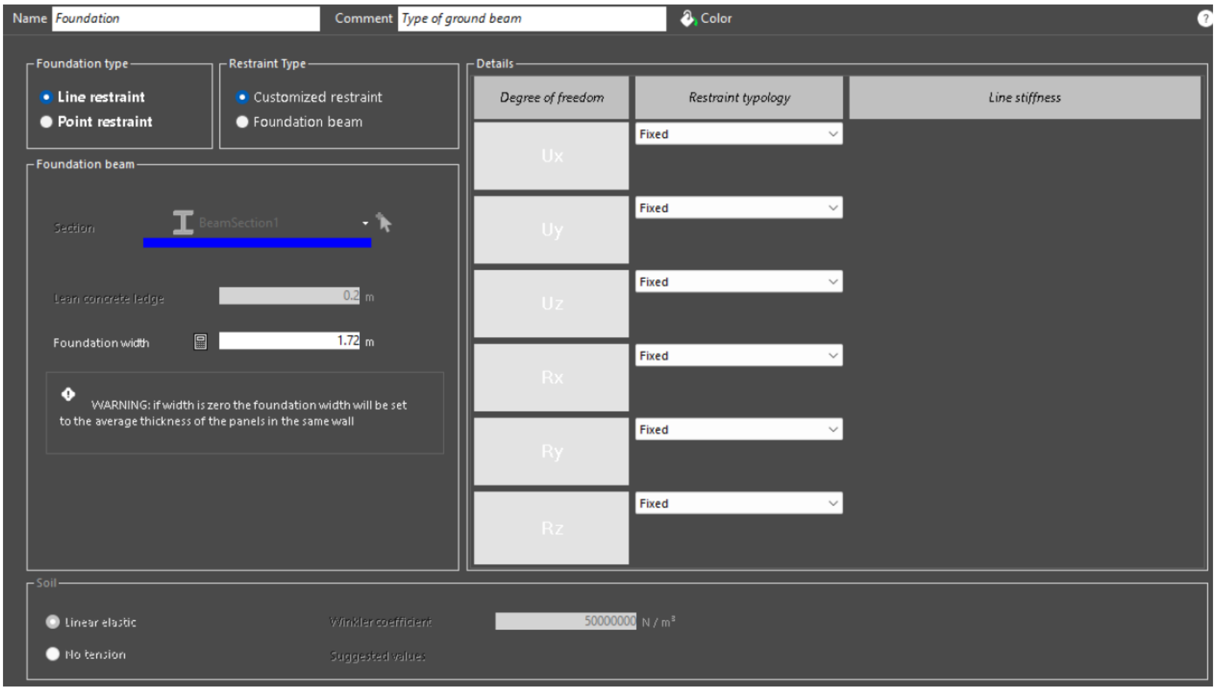

Figure 64 - Definition of foundation.

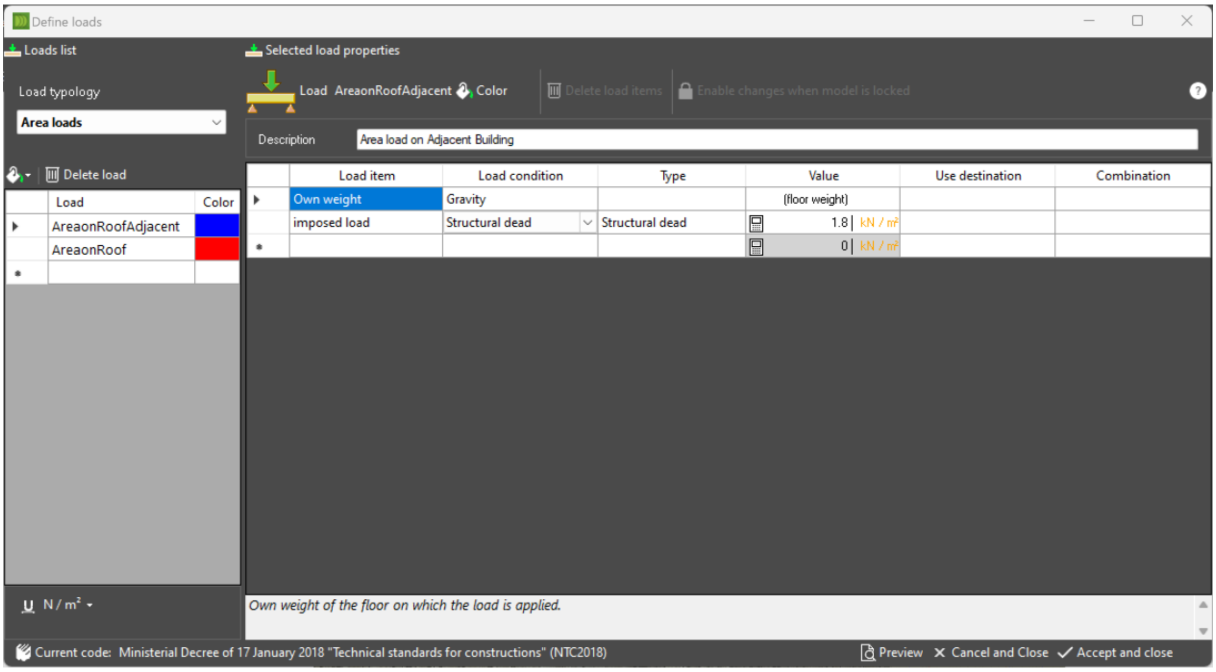

Figure 65 - Definition of load applied on adjacent building roof.

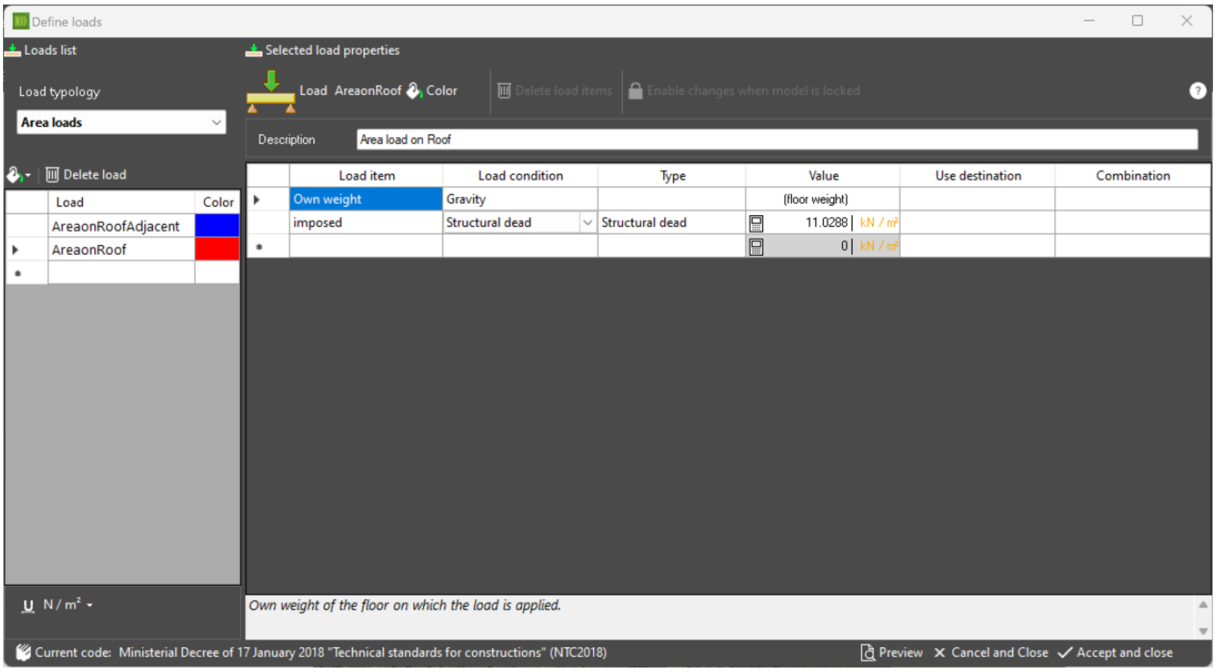

Figure 66 - Definition of load applied on chapel's roof.

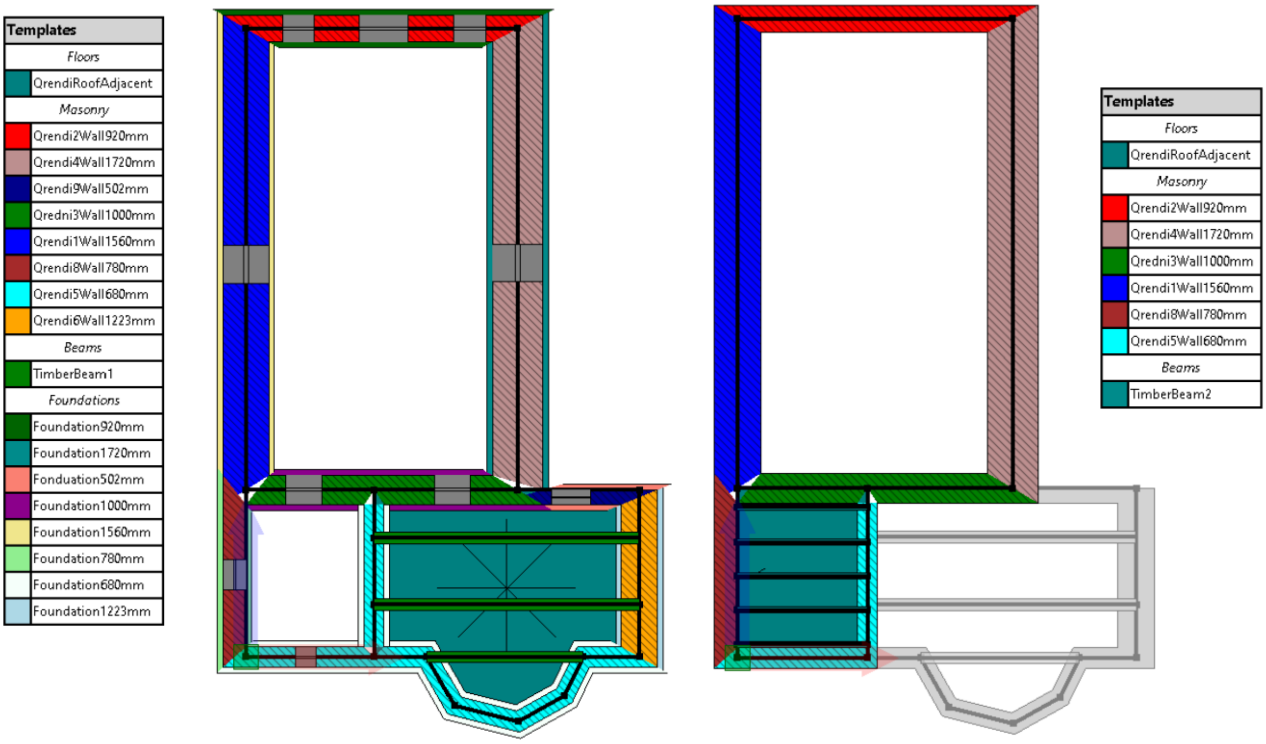

Figure 67 - 3D Macro Plan from 0 – 3960 mm and 3960 mm – 5200 mm Layout of St Matthew's Chapel in Qrendi.

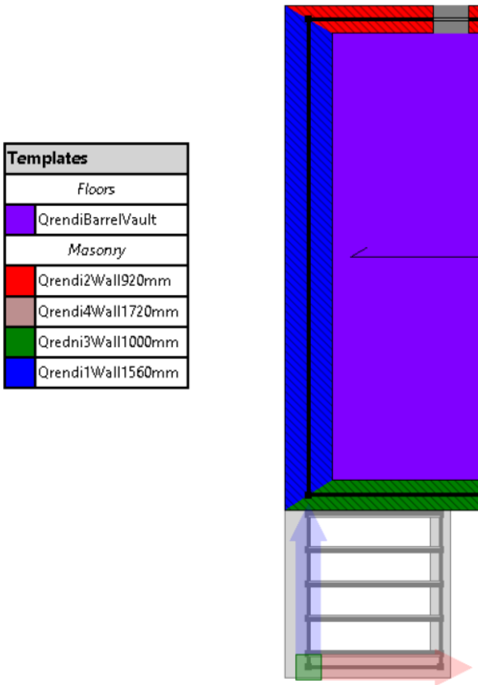

Figure 68 - 3D Macro Plan from 5200 mm – 10800 mm Layout of St Matthew's Chapel in Qrendi.

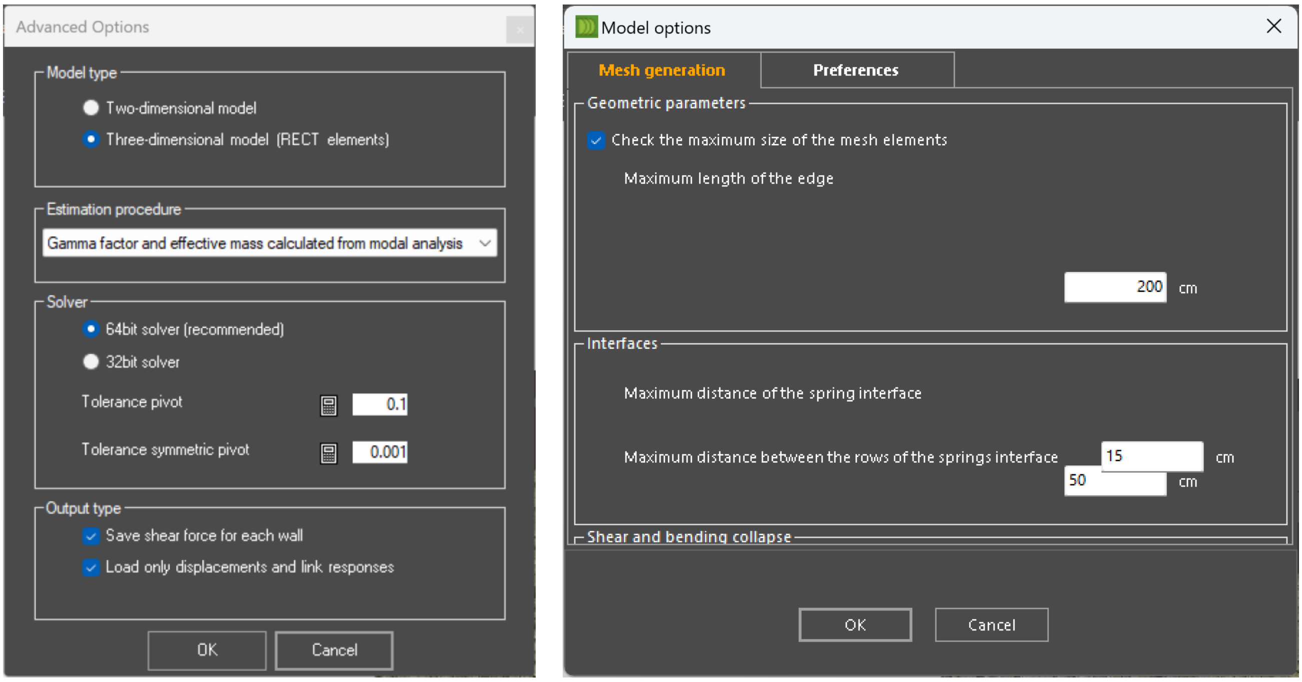

Figure 69 - The macro-element divisions of the structural walls in the 3D Macro model were sized to maintain a balance between element size, model complexity, and result accuracy.

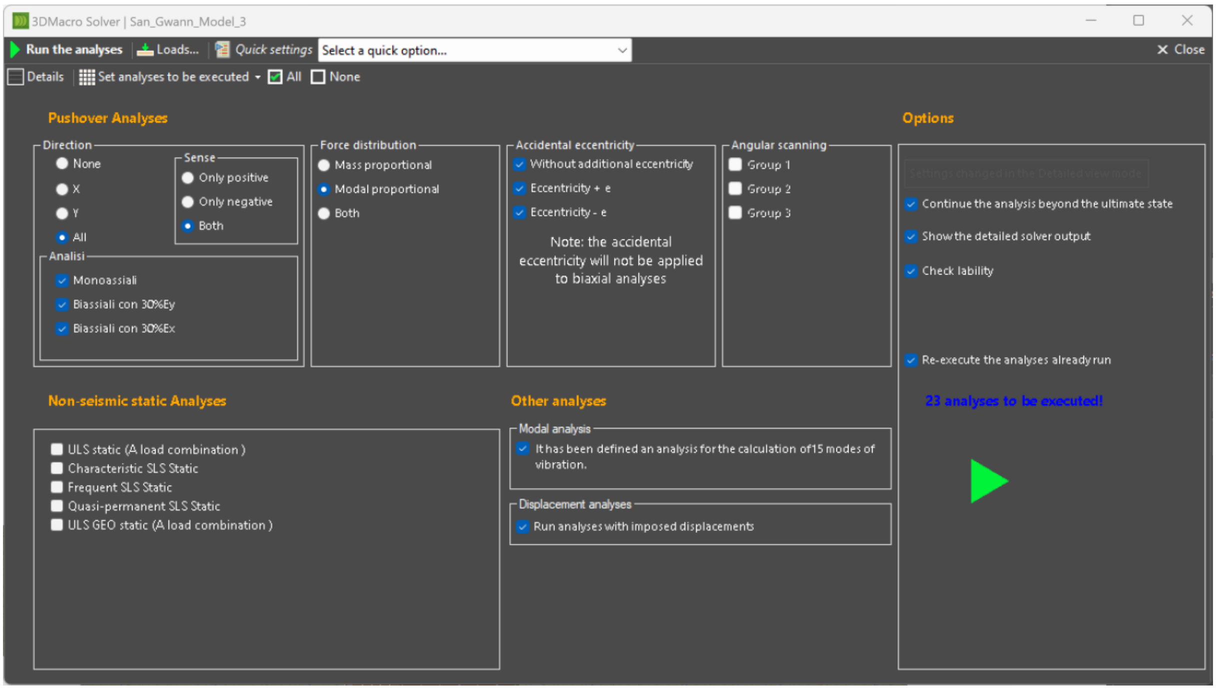

Figure 70 - 3D Macro settings selected for the various seismic analyses undertaken for all three chapels were carefully chosen and tailored to each specific analysis.

Appendix B – Parameters defined in 3D Macro Element Software.

Appendix B.3 – 3D Visuals of Chapels

St. Philip & St. James Chapel in San Gwann 3D Model

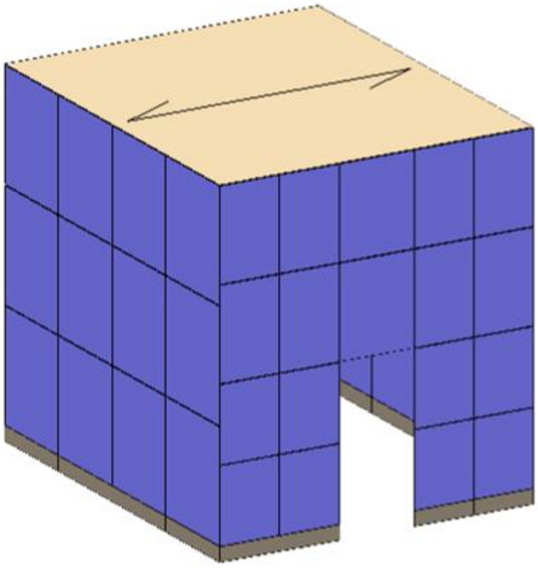

Figure 71 - San Gwann Chapel Computational Model.

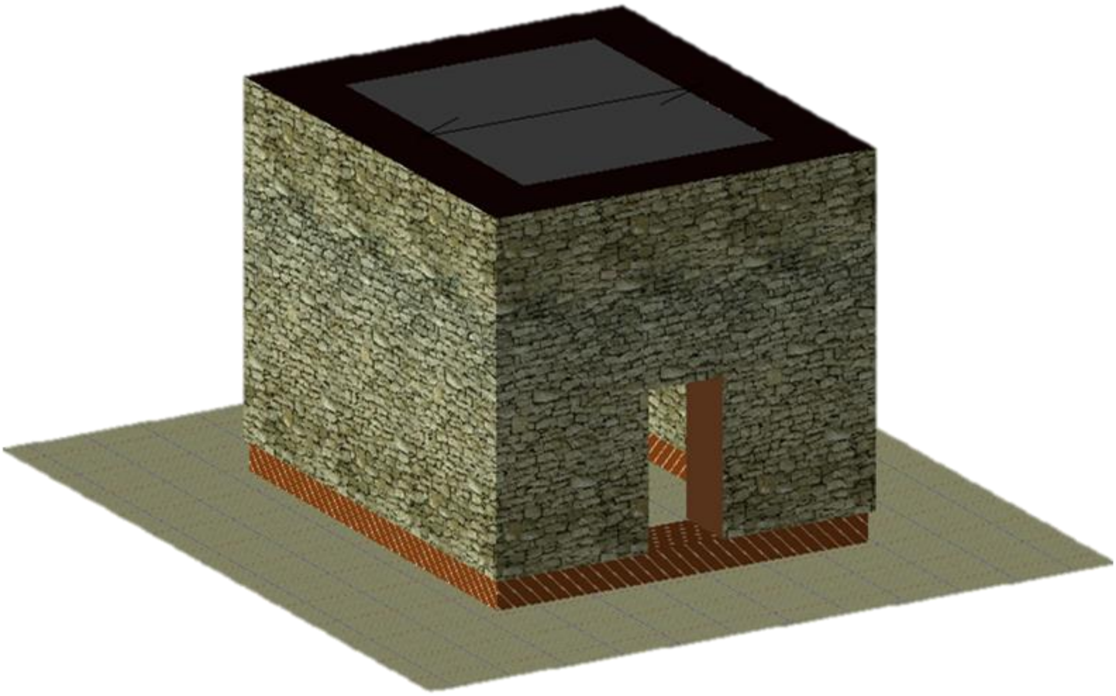

Figure 72 - San Gwann Chapel Geometric Model.

Santa Marija Maddalena Chapel in Dingli

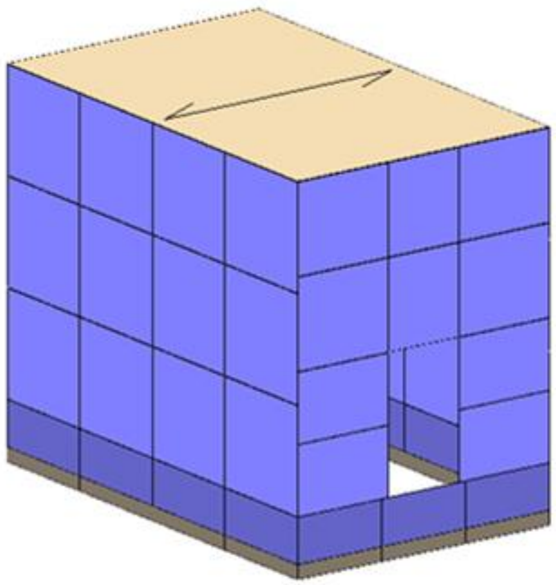

Figure 73 - Dingli Chapel Computational Model.

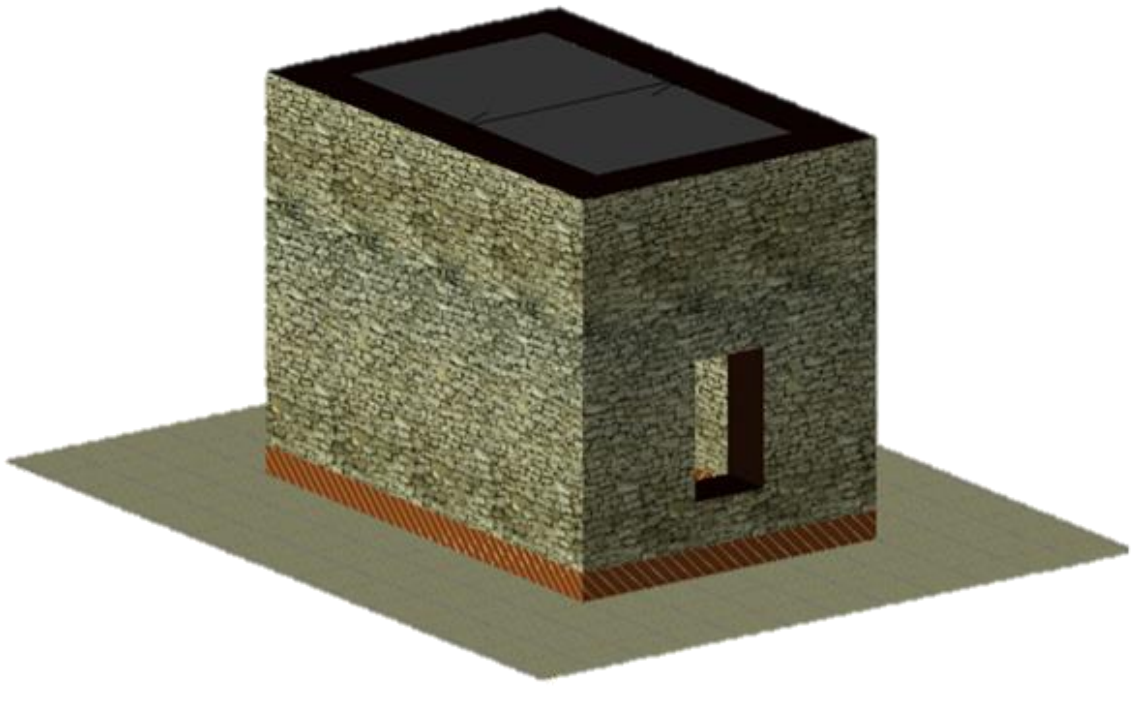

Figure 74 - Dingli Chapel Geometric Model.

St. Matthew's Chapel in Qrendi

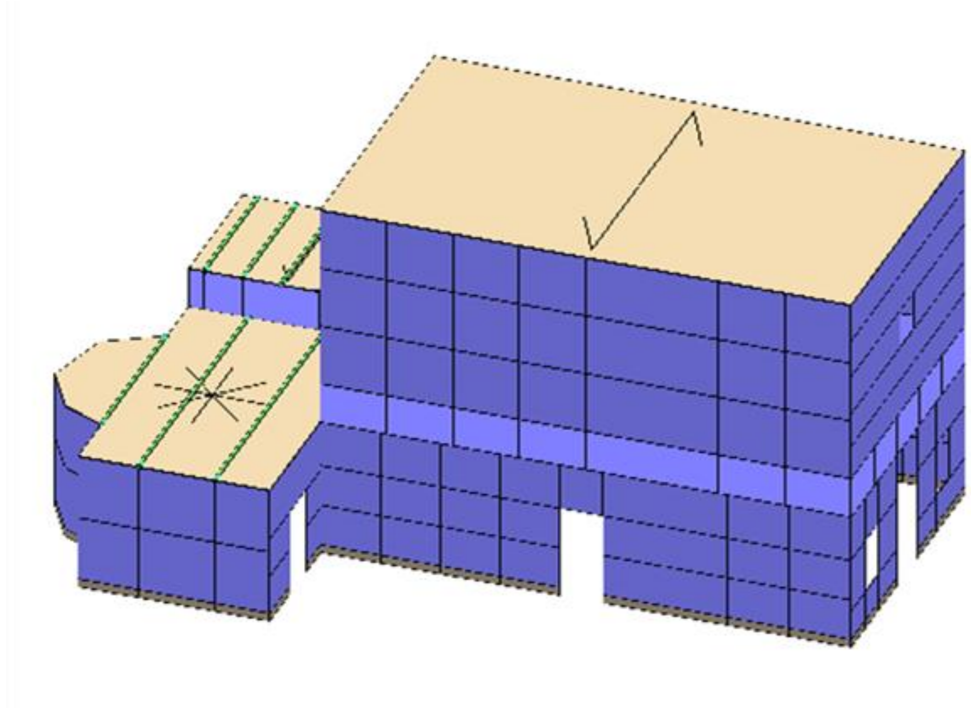

Figure 75 - Qrendi Chapel Computational Model.

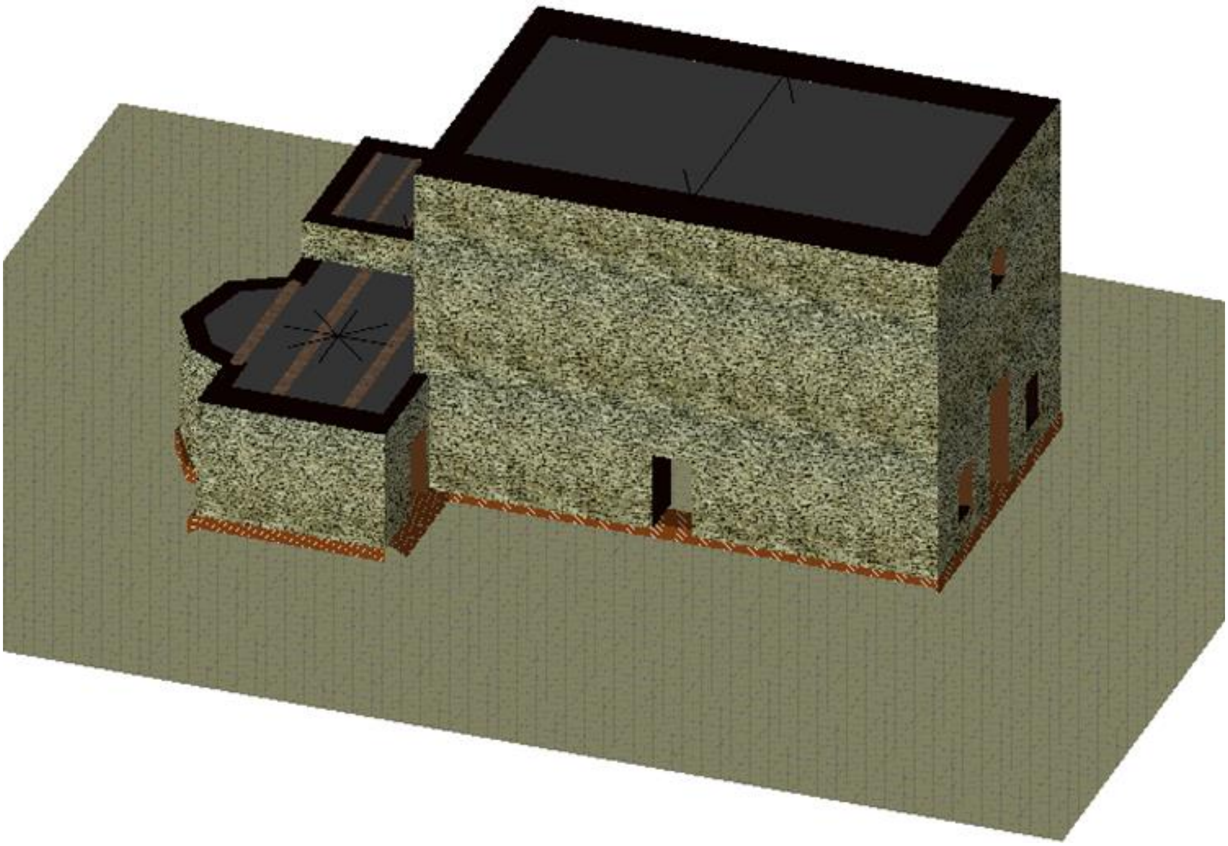

Figure 76 - Qrendi Chapel Geometric Model.

Appendix C – Results

Appendix C.1 – 3D Macro Analysis

St. Philip & St. James Chapel in San Gwann

St. Philip & St. James Chapel in San Gwann Analysis:

Bilinear System						
Analysis	**K* (kN/m)**	**T* (s)**	**Fy* (kN)**	**δy (cm)**	**δu* (cm)**	**μ***
Pushover+X Acc	5397930.00	0.0381	6695.36	0.1240	0.5151	4.15293
Pushover-X Acc	5452991.50	0.0379	6566.12	0.1204	0.5301	4.40228
Pushover+Y Acc	7639224.50	0.0327	9707.15	0.1271	0.9781	7.69732
Pushover-Y Acc	7639224.50	0.0327	9707.15	0.1271	0.9781	7.69732
Pushover+X Acc + e	5434357.50	0.0380	6750.39	0.1242	0.6977	5.61671
Pushover-X Acc + e	6112653.50	0.0358	5533.24	0.0905	0.1535	1.69535
Pushover+Y Acc + e	7618351.50	0.0328	9676.10	0.1270	0.9781	7.70092
Pushover-Y Acc + e	7618182.00	0.0328	9678.65	0.1270	0.9781	7.69872
Pushover+X Acc - e	6112898.50	0.0358	5532.97	0.0905	0.1534	1.69511
Pushover-X Acc - e	5434249.50	0.0380	6752.62	0.1243	0.6977	5.61474
Pushover+Y Acc - e	7618351.50	0.0328	9676.10	0.1270	0.9781	7.70092
Pushover-Y Acc - e	7618182.00	0.0328	9678.65	0.1270	0.9781	7.69872
PushoverEx+0.3Ey Acc	5392245.50	0.0366	7761.39	0.1439	0.5229	3.63267
Pushover0.3Ex+Ey Acc	7831234.00	0.0309	10281.01	0.1313	0.8057	6.13734
Pushover-0.3Ex+Ey Acc	7893165.00	0.0308	9625.08	0.1219	0.7929	6.50194
Pushover-Ex+0.3Ey Acc	5301340.00	0.0369	7954.02	0.1500	0.5166	3.44311
Pushover-Ex-0.3Ey Acc	5484337.50	0.0362	7678.35	0.1400	0.5149	3.67756
Pushover-0.3Ex-Ey Acc	7870088.50	0.0309	9832.53	0.1249	0.3550	2.84127
Pushover0.3Ex-Ey Acc	7749710.50	0.0311	10204.84	0.1317	0.4203	3.19193
PushoverEx-0.3Ey Acc	5364533.00	0.0366	7841.56	0.1462	0.5059	3.46116

Table 1- Bilinear System; 3D Macro Analysis St. Philip & St. James Chapel in San Gwann.

Reduced System							
Analysis	Real system			Γ	Reduced system		
	m (kNs^2/cm)	Cb,max	δu (cm)		m (kNs^2/cm)	Cb,max	δu (cm)
Pushover+X Acc	3.7736	2.5640	0.6966	1.3523	1.9890	1.9516	0.5151
Pushover-X Acc	3.7736	2.3980	0.7168	1.3523	1.9890	1.9141	0.5301
Pushover+Y Acc	3.7736	1.7842	1.2253	1.2528	2.0702	2.8495	0.9781
Pushover-Y Acc	3.7736	1.7842	1.2253	1.2528	2.0702	2.8495	0.9781
Pushover+X Acc + e	3.7736	2.5719	0.9435	1.3523	1.9890	1.9383	0.6977
Pushover-X Acc + e	3.7736	2.1599	0.2075	1.3523	1.9890	1.5972	0.1535
Pushover+Y Acc + e	3.7736	1.8009	1.2253	1.2528	2.0702	2.8399	0.9781
Pushover-Y Acc + e	3.7736	1.8092	1.2253	1.2528	2.0702	2.8401	0.9781
Pushover+X Acc - e	3.7736	2.1598	0.2075	1.3523	1.9890	1.5972	0.1534
Pushover-X Acc - e	3.7736	2.5733	0.9435	1.3523	1.9890	1.9384	0.6977
Pushover+Y Acc - e	3.7736	1.8009	1.2253	1.2528	2.0702	2.8399	0.9781
Pushover-Y Acc - e	3.7736	1.8092	1.2253	1.2528	2.0702	2.8401	0.9781
PushoverEx+0.3Ey Acc	3.7736	2.8939	0.6487	1.2406	1.8247	2.3327	0.5229
Pushover0.3Ex+Ey Acc	3.7736	3.2376	0.9261	1.1493	1.8993	2.8672	0.8057
Pushover-0.3Ex+Ey Acc	3.7736	2.5116	0.9112	1.1493	1.8992	2.8013	0.7929
Pushover-Ex+0.3Ey Acc	3.7736	3.0240	0.6409	1.2406	1.8248	2.4374	0.5166
Pushover-Ex-0.3Ey Acc	3.7736	2.5610	0.6388	1.2406	1.8247	2.2457	0.5149
Pushover-0.3Ex-Ey Acc	3.7736	3.0828	0.4080	1.1493	1.8993	2.8358	0.3550
Pushover0.3Ex-Ey Acc	3.7736	3.4166	0.4831	1.1493	1.8992	2.9728	0.4203
PushoverEx-0.3Ey Acc	3.7736	2.9425	0.6277	1.2406	1.8248	2.3717	0.5059

Table 2 - Reduced System; 3D Macro Analysis St. Philip & St. James Chapel in San Gwann.

Vulnerability Assessment								
Analysis	Limit state	Demand (cm)					Capacity (cm)	α
		PGA/g	S	q*	d*max	dmax	dsl	
Pushover+X Acc	SLD	0.0441	1	0.0229	0.0028	0.0038	0.1474	38.410
Pushover+X Acc	SLV	0.1000	1	0.0419	0.0052	0.0070	0.4460	63.479
Pushover+X Acc	SLC	0.1235	1	0.0511	0.0063	0.0086	0.6966	81.338
Pushover-X Acc	SLD	0.0441	1	0.0233	0.0028	0.0038	0.0479	12.640
Pushover-X Acc	SLV	0.1000	1	0.0426	0.0051	0.0069	0.4460	64.226
Pushover-X Acc	SLC	0.1235	1	0.0520	0.0063	0.0085	0.7168	84.684
Pushover+Y Acc	SLD	0.0441	1	0.0154	0.0020	0.0025	0.1285	52.402
Pushover+Y Acc	SLV	0.1000	1	0.0288	0.0037	0.0046	0.8265	180.468
Pushover+Y Acc	SLC	0.1235	1	0.0351	0.0045	0.0056	1.2253	219.217
Pushover-Y Acc	SLD	0.0441	1	0.0154	0.0020	0.0025	0.1285	52.402
Pushover-Y Acc	SLV	0.1000	1	0.0288	0.0037	0.0046	0.8265	180.468
Pushover-Y Acc	SLC	0.1235	1	0.0351	0.0045	0.0056	1.2253	219.217
Pushover+X Acc + e	SLD	0.0441	1	0.0227	0.0028	0.0038	0.1473	38.685
Pushover+X Acc + e	SLV	0.1000	1	0.0415	0.0052	0.0070	0.6449	92.501
Pushover+X Acc + e	SLC	0.1235	1	0.0506	0.0063	0.0085	0.9435	111.021
Pushover-X Acc + e	SLD	0.0441	1	0.0270	0.0024	0.0033	0.0481	14.571
Pushover-X Acc + e	SLV	0.1000	1	0.0498	0.0045	0.0061	0.1476	24.235
Pushover-X Acc + e	SLC	0.1235	1	0.0607	0.0055	0.0074	0.2075	27.938
Pushover+Y Acc + e	SLD	0.0441	1	0.0155	0.0020	0.0025	0.1285	52.230
Pushover+Y Acc + e	SLV	0.1000	1	0.0289	0.0037	0.0046	0.8265	179.908
Pushover+Y Acc + e	SLC	0.1235	1	0.0352	0.0045	0.0056	1.2253	218.539
Pushover-Y Acc + e	SLD	0.0441	1	0.0155	0.0020	0.0025	0.1285	52.229
Pushover-Y Acc + e	SLV	0.1000	1	0.0289	0.0037	0.0046	0.8265	179.903
Pushover-Y Acc + e	SLC	0.1235	1	0.0352	0.0045	0.0056	1.2253	218.533
Pushover+X Acc - e	SLD	0.0441	1	0.0270	0.0024	0.0033	0.0481	14.572
Pushover+X Acc - e	SLV	0.1000	1	0.0498	0.0045	0.0061	0.1476	24.236
Pushover+X Acc - e	SLC	0.1235	1	0.0607	0.0055	0.0074	0.2075	27.933
Pushover-X Acc - e	SLD	0.0441	1	0.0227	0.0028	0.0038	0.1473	38.684
Pushover-X Acc - e	SLV	0.1000	1	0.0415	0.0052	0.0070	0.6449	92.499
Pushover-X Acc - e	SLC	0.1235	1	0.0506	0.0063	0.0085	0.9435	111.019
Pushover+Y Acc - e	SLD	0.0441	1	0.0155	0.0020	0.0025	0.1285	52.230
Pushover+Y Acc - e	SLV	0.1000	1	0.0289	0.0037	0.0046	0.8265	179.908
Pushover+Y Acc - e	SLC	0.1235	1	0.0352	0.0045	0.0056	1.2253	218.539

Vulnerability Assessment								
Analysis	**Limit State**	**Demand (cm)**					**Capacity (cm)**	**α**
		PGA/g	S	q*	d*max	dmax	dsl	
Pushover-Y Acc - e	SLD	0.0441	1	0.0155	0.0020	0.0025	0.1285	52.229
Pushover-Y Acc - e	SLV	0.1000	1	0.0289	0.0037	0.0046	0.8265	179.903
Pushover-Y Acc - e	SLC	0.1235	1	0.0352	0.0045	0.0056	1.2253	218.533
PushoverEx+0.3Ey Acc	SLD	0.0441	1	0.0178	0.0026	0.0032	0.1431	45.067
PushoverEx+0.3Ey Acc	SLV	0.1000	1	0.0327	0.0047	0.0058	0.4418	75.589
PushoverEx+0.3Ey Acc	SLC	0.1235	1	0.0399	0.0057	0.0071	0.6487	91.021
Pushover0.3Ex+Ey Acc	SLD	0.0441	1	0.0131	0.0017	0.0020	0.1283	65.165
Pushover0.3Ex+Ey Acc	SLV	0.1000	1	0.0246	0.0032	0.0037	0.6269	169.214
Pushover0.3Ex+Ey Acc	SLC	0.1235	1	0.0300	0.0039	0.0045	0.9261	204.699
Pushover-0.3Ex+Ey Acc	SLD	0.0441	1	0.0139	0.0017	0.0020	0.1283	65.787
Pushover-0.3Ex+Ey Acc	SLV	0.1000	1	0.0262	0.0032	0.0037	0.6269	170.745
Pushover-0.3Ex+Ey Acc	SLC	0.1235	1	0.0320	0.0039	0.0045	0.9112	203.237
Pushover-Ex+0.3Ey Acc	SLD	0.0441	1	0.0174	0.0026	0.0032	0.1431	44.141
Pushover-Ex+0.3Ey Acc	SLV	0.1000	1	0.0320	0.0048	0.0060	0.4418	74.120
Pushover-Ex+0.3Ey Acc	SLC	0.1235	1	0.0390	0.0059	0.0073	0.6409	88.192
Pushover-Ex-0.3Ey Acc	SLD	0.0441	1	0.0179	0.0025	0.0031	0.1431	46.003
Pushover-Ex-0.3Ey Acc	SLV	0.1000	1	0.0330	0.0046	0.0057	0.4418	77.072
Pushover-Ex-0.3Ey Acc	SLC	0.1235	1	0.0402	0.0056	0.0070	0.6388	91.381
Pushover-0.3Ex-Ey Acc	SLD	0.0441	1	0.0136	0.0017	0.0020	0.1283	65.551
Pushover-0.3Ex-Ey Acc	SLV	0.1000	1	0.0257	0.0032	0.0037	0.2281	61.902
Pushover-0.3Ex-Ey Acc	SLC	0.1235	1	0.0313	0.0039	0.0045	0.4080	90.688
Pushover0.3Ex-Ey Acc	SLD	0.0441	1	0.0132	0.0017	0.0020	0.1283	64.362
Pushover0.3Ex-Ey Acc	SLV	0.1000	1	0.0248	0.0033	0.0037	0.3278	87.439
Pushover0.3Ex-Ey Acc	SLC	0.1235	1	0.0302	0.0040	0.0046	0.4831	105.537
PushoverEx-0.3Ey Acc	SLD	0.0441	1	0.0176	0.0026	0.0032	0.1431	44.781
PushoverEx-0.3Ey Acc	SLV	0.1000	1	0.0324	0.0047	0.0059	0.4418	75.136
PushoverEx-0.3Ey Acc	SLC	0.1235	1	0.0395	0.0058	0.0072	0.6277	87.550

Table 3 - Vulnerability Assessment; 3D Macro Analysis St. Philip & St. James Chapel in San Gwann.

Structural Response Model in 3D Macro:

St. Philip & St. James Chapel in San Gwann isometric view showing damages at (SLV) and (SLC) Limit States for Earthquake Direction - X Acc. While, Qrendi Chapel leads failure in (SLD) Limit State for Earthquake Direction - X Acc which is shown in Section 5.3.1.

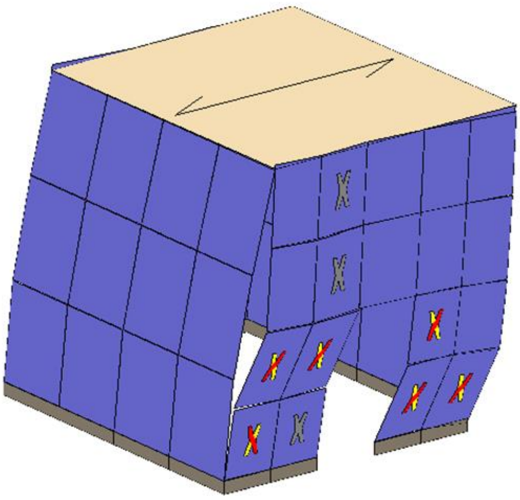

Figure 77 - Front Isometric View of San Gwann Chapel showing damage at Significant Damage Limit State (SLV) for Earthquake Direction - X Acc.

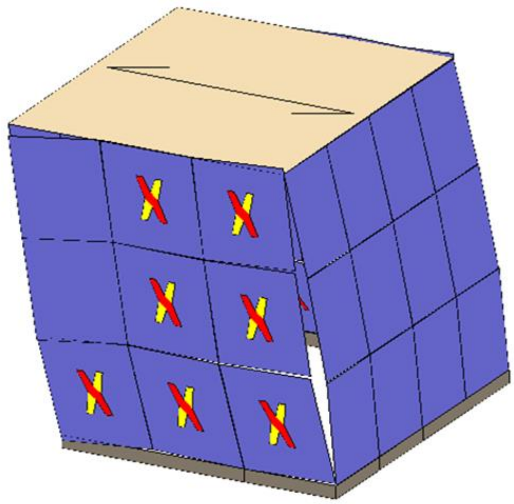

Figure 78 - Back Isometric View of San Gwann Chapel showing damage at Significant Damage Limit State (SLV) for Earthquake Direction - X Acc.

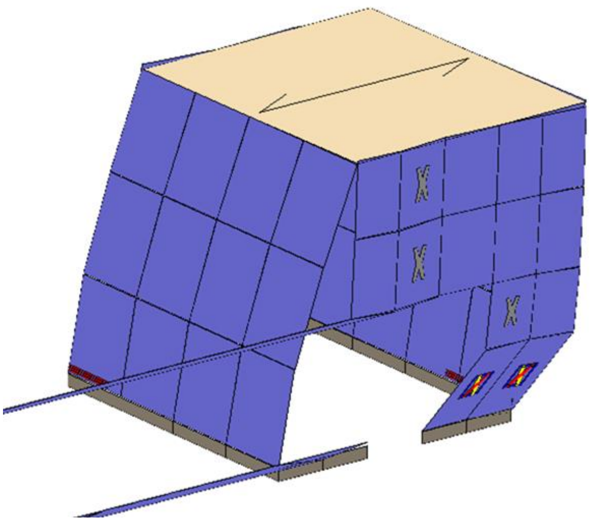

Figure 79 - Front Isometric View of San Gwann Chapel showing damage at Near Collapse Limit State (SLC) for Earthquake Direction - X Acc.

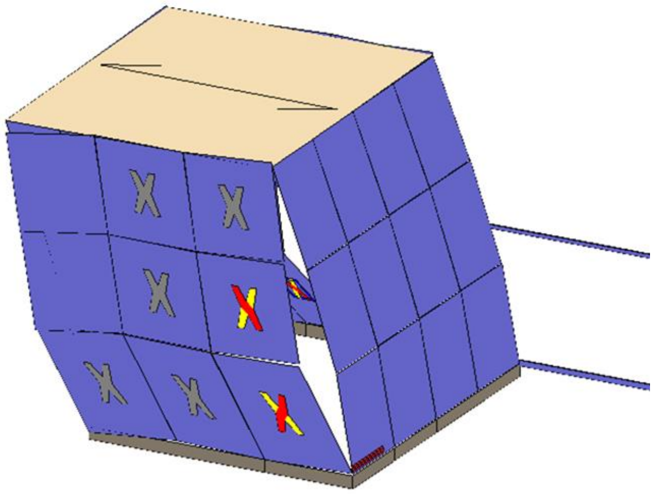

Figure 80 - Back Isometric View of San Gwann Chapel showing damage at Near Collapse Limit State (SLC) for Earthquake Direction - X Acc.

Structural Response Model in 3D Macro:

St. Philip & St. James Chapel in San Gwann isometric view showing damages at (SLV) and (SLC) Limit States for Earthquake Direction + X Acc – e. While, Qrendi Chapel leads failure in (SLD) Limit State for Earthquake Direction + X Acc – e which is shown in Section 5.3.2.

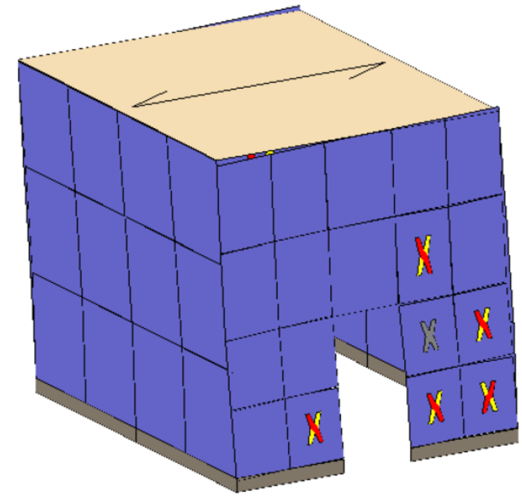

Figure 81 - Front Isometric View of San Gwann Chapel showing damage at Significant Damage Limit State (SLV) for Earthquake Direction + X Acc - e.

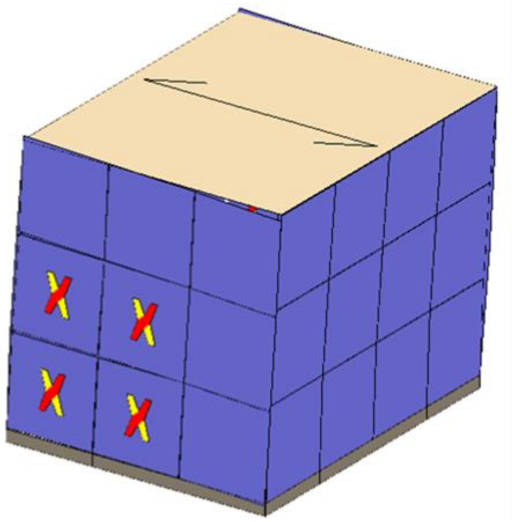

Figure 82 - Back Isometric View of San Gwann Chapel showing damage at Significant Damage Limit State (SLV) for Earthquake Direction + X Acc - e.

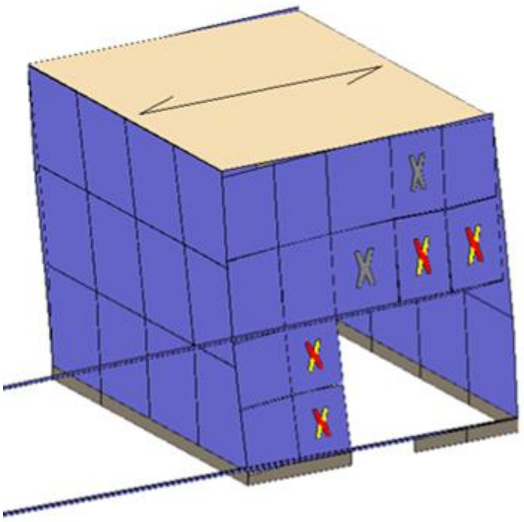

Figure 83 - Front Isometric View of San Gwann Chapel showing damage at Near Collapse Limit State (SLC) for Earthquake Direction + X Acc – e.

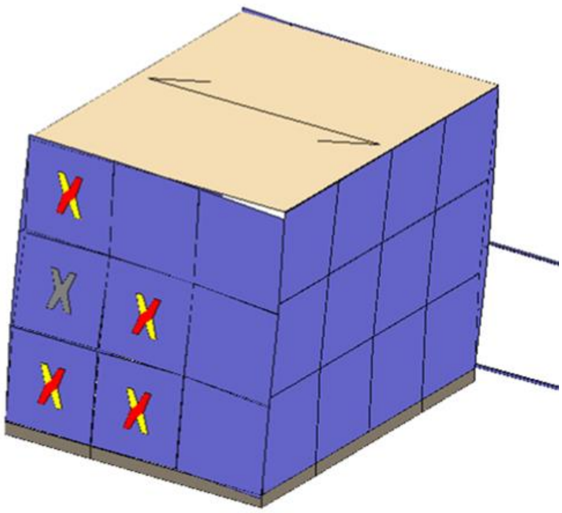

Figure 84 - Back Isometric View of San Gwann Chapel showing damage at Near Collapse Limit State (SLC) for Earthquake Direction + X Acc – e.

Appendix C – Results

Appendix C.2 – 3D Macro Analysis

Santa Marija Maddalena Chapel in Dingli

Santa Marija Maddalena Chapel in Dingli:

Bilinear System						
Analysis	K* (kN/m)	T* (s)	Fy* (kN)	δy (cm)	δu* (cm)	μ*
Pushover+X Acc	4407019.00	0.03865	1971.02	0.0447	0.1264	2.82654
Pushover-X Acc	4407019.00	0.03865	1971.02	0.0447	0.1264	2.82653
Pushover+Y Acc	6166734.50	0.03277	14179.00	0.2299	0.8803	3.82870
Pushover-Y Acc	6190973.50	0.03270	14165.44	0.2288	0.8803	3.84743
Pushover+X Acc + e	4412957.00	0.03863	3345.80	0.0758	0.1316	1.73571
Pushover-X Acc + e	2464840.75	0.05169	9765.72	0.3962	0.6934	1.75004
Pushover+Y Acc + e	5653923.00	0.03422	14546.41	0.2573	0.8803	3.42165
Pushover-Y Acc + e	5545612.00	0.03455	14585.25	0.2630	0.8085	3.07404
Pushover+X Acc - e	4040561.00	0.04037	4016.37	0.0994	0.1362	1.37045
Pushover-X Acc - e	4412957.50	0.03863	3345.80	0.0758	0.1316	1.73571
Pushover+Y Acc - e	5653995.00	0.03422	14546.36	0.2573	0.8803	3.42170
Pushover-Y Acc - e	5543903.50	0.03456	14586.45	0.2631	0.8085	3.07284
PushoverEx+0.3Ey Acc	4650696.00	0.03604	3304.25	0.0710	0.1283	1.80555
Pushover0.3Ex+Ey Acc	8172590.00	0.02726	15345.62	0.1878	0.4454	2.37189
Pushover-0.3Ex+Ey Acc	8023184.50	0.02752	15489.56	0.1931	0.5701	2.95288
Pushover-Ex+0.3Ey Acc	4650694.00	0.03604	3304.24	0.0710	0.1283	1.80554
Pushover-Ex-0.3Ey Acc	4650915.50	0.03604	3302.36	0.0710	0.1282	1.80504
Pushover-0.3Ex-Ey Acc	8631286.00	0.02653	12657.55	0.1466	0.1896	1.29260
Pushover0.3Ex-Ey Acc	8631284.00	0.02653	12657.45	0.1466	0.1896	1.29260
PushoverEx-0.3Ey Acc	4650917.00	0.03604	3302.33	0.0710	0.1282	1.80505

Table 4 - Bilinear System; 3D Macro Analysis Santa Marija Maddalena Chapel in Dingli.

Reduced System							
Analysis	**Real system**			**Γ**	**Reduced system**		
	m (kNs^2/cm)	**Cb,max**	**δu (cm)**		**m (kNs^2/cm)**	**Cb,max**	**δu (cm)**
Pushover+X Acc	3.4730	0.5882	0.1772	1.4017	1.6679	0.7134	0.1264
Pushover-X Acc	3.4730	0.5882	0.1772	1.4017	1.6679	0.7134	0.1264
Pushover+Y Acc	3.4730	6.7492	1.2224	1.3886	1.6772	4.8606	0.8803
Pushover-Y Acc	3.4730	6.7214	1.2224	1.3886	1.6772	4.8406	0.8803
Pushover+X Acc + e	3.4730	1.6447	0.1845	1.4017	1.6679	1.1734	0.1316
Pushover-X Acc + e	3.4730	4.3380	0.9719	1.4017	1.6679	3.0949	0.6934
Pushover+Y Acc + e	3.4730	7.0700	1.2224	1.3886	1.6772	5.0916	0.8803
Pushover-Y Acc + e	3.4730	7.1363	1.1226	1.3886	1.6772	5.1393	0.8085
Pushover+X Acc - e	3.4730	1.8625	0.1909	1.4017	1.6679	1.3288	0.1362
Pushover-X Acc - e	3.4730	1.6447	0.1845	1.4017	1.6679	1.1734	0.1316
Pushover+Y Acc - e	3.4730	7.0700	1.2224	1.3886	1.6772	5.0916	0.8803
Pushover-Y Acc - e	3.4730	7.1373	1.1226	1.3886	1.6772	5.1401	0.8085
PushoverEx+0.3Ey Acc	3.4730	1.4839	0.1650	1.2859	1.5302	1.1540	0.1283
Pushover0.3Ex+Ey Acc	3.4730	5.8104	0.5674	1.2739	1.5387	4.6926	0.4454
Pushover-0.3Ex+Ey Acc	3.4730	6.2666	0.7262	1.2739	1.5387	4.9192	0.5701
Pushover-Ex+0.3Ey Acc	3.4730	1.4839	0.1650	1.2859	1.5302	1.1540	0.1283
Pushover-Ex-0.3Ey Acc	3.4730	1.4828	0.1648	1.2859	1.5302	1.1531	0.1282
Pushover-0.3Ex-Ey Acc	3.4730	5.1513	0.2415	1.2739	1.5387	4.0438	0.1896
Pushover0.3Ex-Ey Acc	3.4730	5.1514	0.2415	1.2739	1.5387	4.0437	0.1896
PushoverEx-0.3Ey Acc	3.4730	1.4828	0.1648	1.2859	1.5302	1.1531	0.1282

Table 5 - Reduced System; 3D Macro Analysis Santa Marija Maddalena Chapel in Dingli.

Vulnerability Assessment								
Analysis	Limit state	Demand (cm)					Capacity (cm)	α
		PGA/g	S	q*	d*max	dmax	dsl	
Pushover+X Acc	SLD	0.044	1.2	0.067	0.003	0.004	0.063	14.863
Pushover+X Acc	SLV	0.100	1.2	0.133	0.006	0.008	0.080	9.587
Pushover+X Acc	SLC	0.123	1.2	0.163	0.007	0.010	0.177	17.291
Pushover-X Acc	SLD	0.044	1.2	0.067	0.003	0.004	0.063	14.863
Pushover-X Acc	SLV	0.100	1.2	0.133	0.006	0.008	0.080	9.587
Pushover-X Acc	SLC	0.123	1.2	0.163	0.007	0.010	0.177	17.291
Pushover+Y Acc	SLD	0.044	1.2	0.009	0.002	0.003	0.225	79.198
Pushover+Y Acc	SLV	0.100	1.2	0.018	0.004	0.006	0.823	144.041
Pushover+Y Acc	SLC	0.123	1.2	0.022	0.005	0.007	1.222	174.119
Pushover-Y Acc	SLD	0.044	1.2	0.009	0.002	0.003	0.225	79.558
Pushover-Y Acc	SLV	0.100	1.2	0.018	0.004	0.006	0.823	144.670
Pushover-Y Acc	SLC	0.123	1.2	0.022	0.005	0.007	1.222	174.878
Pushover+X Acc + e	SLD	0.044	1.2	0.040	0.003	0.004	0.079	18.794
Pushover+X Acc + e	SLV	0.100	1.2	0.078	0.006	0.008	0.079	9.479
Pushover+X Acc + e	SLC	0.123	1.2	0.096	0.007	0.010	0.184	18.027
Pushover-X Acc + e	SLD	0.044	1.2	0.015	0.006	0.008	0.476	56.568
Pushover-X Acc + e	SLV	0.100	1.2	0.029	0.012	0.016	0.674	41.620
Pushover-X Acc + e	SLC	0.123	1.2	0.036	0.014	0.020	0.972	48.955
Pushover+Y Acc + e	SLD	0.044	1.2	0.009	0.002	0.003	0.325	103.389
Pushover+Y Acc + e	SLV	0.100	1.2	0.018	0.005	0.006	0.823	130.773
Pushover+Y Acc + e	SLC	0.123	1.2	0.022	0.006	0.008	1.222	158.110
Pushover-Y Acc + e	SLD	0.044	1.2	0.009	0.002	0.003	0.325	101.094
Pushover-Y Acc + e	SLV	0.100	1.2	0.018	0.005	0.006	0.823	127.982
Pushover-Y Acc + e	SLC	0.123	1.2	0.022	0.006	0.008	1.123	142.115
Pushover+X Acc - e	SLD	0.044	1.2	0.033	0.003	0.005	0.079	16.930
Pushover+X Acc - e	SLV	0.100	1.2	0.066	0.007	0.009	0.079	8.575
Pushover+X Acc - e	SLC	0.123	1.2	0.081	0.008	0.011	0.191	16.897
Pushover-X Acc - e	SLD	0.044	1.2	0.040	0.003	0.004	0.079	18.794
Pushover-X Acc - e	SLV	0.100	1.2	0.078	0.006	0.008	0.079	9.479
Pushover-X Acc - e	SLC	0.123	1.2	0.096	0.007	0.010	0.184	18.027
Pushover+Y Acc - e	SLD	0.044	1.2	0.009	0.002	0.003	0.325	103.391
Pushover+Y Acc - e	SLV	0.100	1.2	0.018	0.005	0.006	0.823	130.775
Pushover+Y Acc - e	SLC	0.123	1.2	0.022	0.006	0.008	1.222	158.112

Vulnerability Assessment								
Analysis	Limit State	Demand (cm)					Capacity (cm)	α
		PGA/g	S	q*	d*max	dmax	dsl	
Pushover-Y Acc - e	SLD	0.044	1.2	0.009	0.002	0.003	0.325	101.058
Pushover-Y Acc - e	SLV	0.100	1.2	0.018	0.005	0.006	0.823	127.938
Pushover-Y Acc - e	SLC	0.123	1.2	0.022	0.006	0.008	1.123	142.066
PushoverEx+0.3Ey Acc	SLD	0.044	1.2	0.036	0.003	0.003	0.072	21.829
PushoverEx+0.3Ey Acc	SLV	0.100	1.2	0.072	0.005	0.007	0.072	10.938
PushoverEx+0.3Ey Acc	SLC	0.123	1.2	0.088	0.006	0.008	0.165	20.526
Pushover0.3Ex+Ey Acc	SLD	0.044	1.2	0.007	0.001	0.002	0.128	74.829
Pushover0.3Ex+Ey Acc	SLV	0.100	1.2	0.015	0.003	0.003	0.327	93.669
Pushover0.3Ex+Ey Acc	SLC	0.123	1.2	0.018	0.003	0.004	0.567	132.089
Pushover-0.3Ex+Ey Acc	SLD	0.044	1.2	0.007	0.001	0.002	0.228	130.392
Pushover-0.3Ex+Ey Acc	SLV	0.100	1.2	0.015	0.003	0.004	0.527	147.713
Pushover-0.3Ex+Ey Acc	SLC	0.123	1.2	0.018	0.003	0.004	0.726	165.695
Pushover-Ex+0.3Ey Acc	SLD	0.044	1.2	0.036	0.003	0.003	0.072	21.828
Pushover-Ex+0.3Ey Acc	SLV	0.100	1.2	0.072	0.005	0.007	0.072	10.938
Pushover-Ex+0.3Ey Acc	SLC	0.123	1.2	0.088	0.006	0.008	0.165	20.526
Pushover-Ex-0.3Ey Acc	SLD	0.044	1.2	0.036	0.003	0.003	0.072	21.830
Pushover-Ex-0.3Ey Acc	SLV	0.100	1.2	0.072	0.005	0.007	0.072	10.939
Pushover-Ex-0.3Ey Acc	SLC	0.123	1.2	0.088	0.006	0.008	0.165	20.509
Pushover-0.3Ex-Ey Acc	SLD	0.044	1.2	0.009	0.001	0.002	0.128	79.613
Pushover-0.3Ex-Ey Acc	SLV	0.100	1.2	0.018	0.003	0.003	0.128	38.859
Pushover-0.3Ex-Ey Acc	SLC	0.123	1.2	0.022	0.003	0.004	0.241	59.677
Pushover0.3Ex-Ey Acc	SLD	0.044	1.2	0.009	0.001	0.002	0.128	79.612
Pushover0.3Ex-Ey Acc	SLV	0.100	1.2	0.018	0.003	0.003	0.128	38.859
Pushover0.3Ex-Ey Acc	SLC	0.123	1.2	0.022	0.003	0.004	0.241	59.677
PushoverEx-0.3Ey Acc	SLD	0.044	1.2	0.036	0.003	0.003	0.072	21.830
PushoverEx-0.3Ey Acc	SLV	0.100	1.2	0.072	0.005	0.007	0.072	10.939
PushoverEx-0.3Ey Acc	SLC	0.123	1.2	0.088	0.006	0.008	0.165	20.508

Table 6 - Vulnerability Assessment; 3D Macro Analysis Santa Marija Maddalena Chapel in Dingli.

Structural Response Model in 3D Macro:

Santa Marija Maddalena Chapel in Dingli isometric view showing damages at (SLD) and (SLC) Limit States for Earthquake Direction + X Acc – e. While, Qrendi Chapel leads failure in (SLV) Limit State for Earthquake Direction + X Acc – e which is shown in Section 5.3.3.

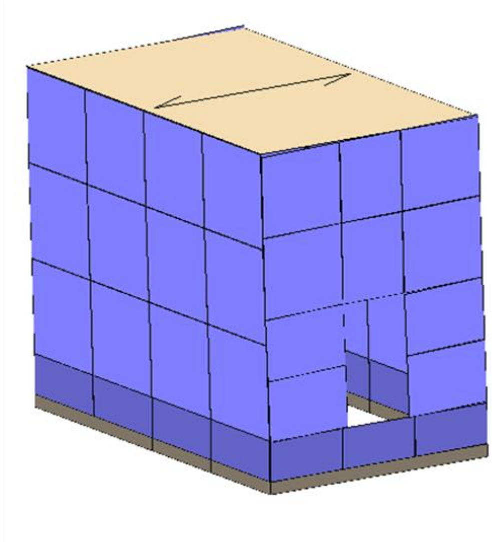

Figure 85 - Front Isometric View of Dingli Chapel showing damage at Damage Limitation Limit State (SLD) for Earthquake Direction + X Acc – e.

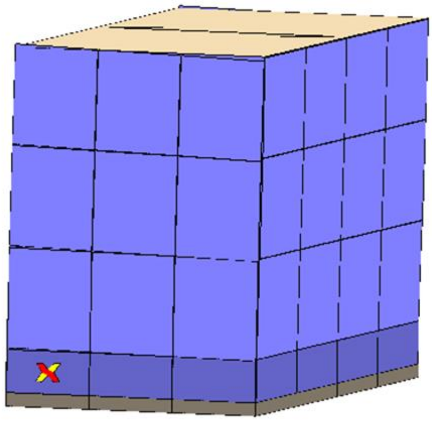

Figure 86 - Back Isometric View of Dingli Chapel showing damage at Damage Limitation Limit State (SLD) for Earthquake Direction + X Acc – e.

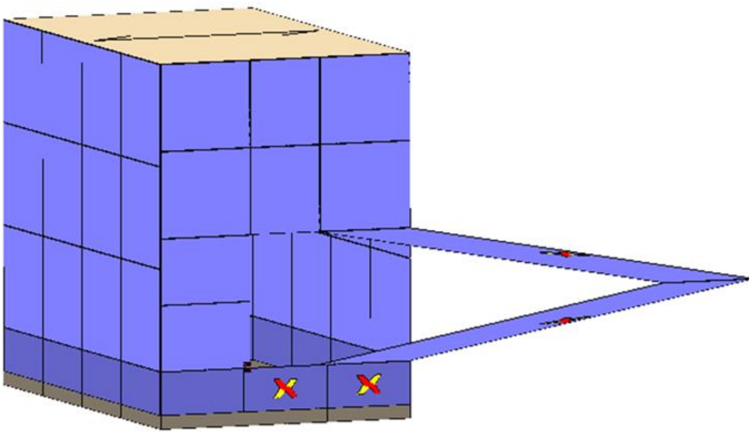

Figure 87- Front Isometric View of Dinglii Chapel showing damage at Near Collapse Limit State (SLC) for Earthquake Direction + X Acc – e.

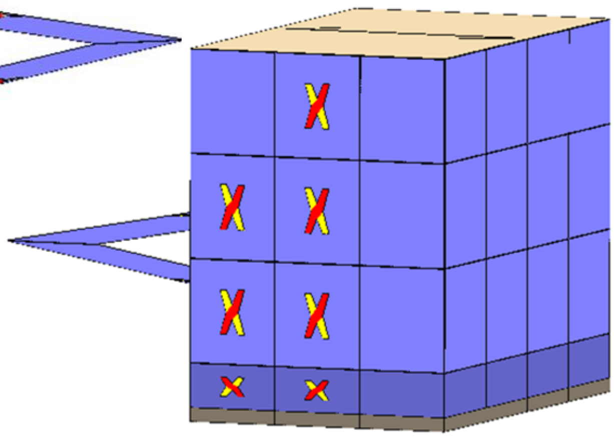

Figure 88 - Back Isometric View of Dinglii Chapel showing damage at Near Collapse Limit State (SLC) for Earthquake Direction + X Acc – e.

Appendix C – Results

Appendix C.3 – 3D Macro Analysis

St. Matthew’s Chapel in Qrendi

St. Matthew's Chapel in Qrendi:

Bilinear System						
Analysis	**K* (kN/m)**	**T* (s)**	**Fy* (kN)**	**δy (cm)**	**δu* (cm)**	**μ***
Pushover+X Acc	4261881.50	0.09097	12140.33	0.28486	0.67403	2.36619
Pushover-X Acc	3459443.00	0.10098	14518.89	0.41969	1.56624	3.73190
Pushover+Y Acc	25119508.00	0.03073	24142.76	0.09611	0.34111	3.54910
Pushover-Y Acc	25656684.00	0.03041	24838.73	0.09681	0.46204	4.77255
Pushover+X Acc + e	4442213.50	0.08911	12261.25	0.27602	0.74072	2.68362
Pushover-X Acc + e	4841285.00	0.08536	13630.59	0.28155	0.70372	2.49944
Pushover+Y Acc + e	24508194.00	0.03111	25005.29	0.10203	0.52260	5.12213
Pushover-Y Acc + e	24417868.00	0.03117	26273.98	0.10760	0.70401	6.54273
Pushover+X Acc - e	4322787.00	0.09033	11769.25	0.27226	0.67688	2.48615
Pushover-X Acc - e	5538098.00	0.07981	12665.59	0.22870	0.56944	2.48990
Pushover+Y Acc - e	25318622.00	0.03061	23999.70	0.09479	0.46209	4.87483
Pushover-Y Acc - e	25525636.00	0.03048	24687.05	0.09671	0.46209	4.77786
PushoverEx+0.3Ey Acc	4497408.00	0.08480	13675.17	0.30407	0.65748	2.16229
Pushover0.3Ex+Ey Acc	18059680.00	0.03493	26819.50	0.14850	1.28316	8.64051
Pushover-0.3Ex+Ey Acc	19872858.00	0.03288	25768.79	0.12967	0.32062	2.47261
Pushover-Ex+0.3Ey Acc	6045161.50	0.07319	15106.47	0.24989	0.79729	3.19051
Pushover-Ex-0.3Ey Acc	4517834.00	0.08461	14456.46	0.31999	0.82444	2.57649
Pushover-0.3Ex-Ey Acc	20045756.00	0.03316	25699.73	0.12821	0.50778	3.96066
Pushover0.3Ex-Ey Acc	20056756.00	0.03273	27048.73	0.13486	0.38722	2.87125
PushoverEx-0.3Ey Acc	4536892.00	0.08448	13773.08	0.30358	0.65670	2.16319

Table 7 - Bilinear System; 3D Macro Analysis St. Matthew's Chapel in Qrendi.

Reduced System							
Analysis	Real system			Γ	Reduced system		
	m (kNs²/cm)	Cb,max	δu (cm)		m (kNs²/cm)	Cb,max	δu (cm)
Pushover+X Acc	20.3140	1.0083	0.9911	1.4715	8.9347	0.6852	0.6740
Pushover-X Acc	20.3140	1.2039	2.3055	1.4715	8.9347	0.8396	1.5662
Pushover+Y Acc	20.3140	2.1376	0.5606	1.6424	6.0085	1.3015	0.3411
Pushover-Y Acc	20.3140	1.5691	0.7586	1.6424	6.0085	1.3176	0.4620
Pushover+X Acc + e	20.3140	0.9385	1.0892	1.4715	8.9347	0.6874	0.7407
Pushover-X Acc + e	20.3140	1.0406	1.0363	1.4715	8.9347	0.7621	0.7037
Pushover+Y Acc + e	20.3140	1.6116	0.8587	1.6424	6.0085	1.3470	0.5226
Pushover-Y Acc + e	20.3140	1.7128	1.1560	1.6424	6.0085	1.4326	0.7040
Pushover+X Acc - e	20.3140	0.8625	0.9953	1.4715	8.9347	0.6562	0.6769
Pushover-X Acc - e	20.3140	1.0187	0.8387	1.4715	8.9347	0.7002	0.5694
Pushover+Y Acc - e	20.3140	1.4699	0.7593	1.6424	6.0085	1.2859	0.4621
Pushover-Y Acc - e	20.3140	1.5245	0.7586	1.6424	6.0085	1.3227	0.4621
PushoverEx+0.3Ey Acc	20.3140	1.0375	0.8865	1.3493	8.1923	0.7689	0.6575
Pushover0.3Ex+Ey Acc	20.3140	2.4238	1.9580	1.5259	5.5820	1.5884	1.2832
Pushover-0.3Ex+Ey Acc	20.3140	2.0717	0.4775	1.4878	5.4427	1.3925	0.3206
Pushover-Ex+0.3Ey Acc	20.3140	1.1634	1.0778	1.3508	8.2016	0.8613	0.7973
Pushover-Ex-0.3Ey Acc	20.3140	1.0633	1.1130	1.3493	8.1923	0.8006	0.8244
Pushover-0.3Ex-Ey Acc	20.3140	1.9845	0.7747	1.5259	5.5820	1.3349	0.5078
Pushover0.3Ex-Ey Acc	20.3140	2.1862	0.5756	1.4878	5.4427	1.4694	0.3872
PushoverEx-0.3Ey Acc	20.3140	1.0435	0.8863	1.3508	8.2016	0.7725	0.6567

Table 8 - Reduced System; 3D Macro Analysis St. Matthew's Chapel in Qrendi.

Vulnerability Assessment								
Analysis	Limit state	Demand (cm)					Capacity (cm)	α
		PGA/g	S	q*	d*max	dmax	dsl	
Pushover+X Acc	SLD	0.044	1	0.079	0.022	0.033	0.398	12.028
Pushover+X Acc	SLV	0.100	1	0.148	0.042	0.062	0.695	11.237
Pushover+X Acc	SLC	0.124	1	0.178	0.051	0.075	0.992	13.276
Pushover-X Acc	SLD	0.044	1	0.066	0.028	0.041	0.529	12.985
Pushover-X Acc	SLV	0.100	1	0.130	0.055	0.080	1.713	21.289
Pushover-X Acc	SLC	0.124	1	0.157	0.066	0.097	2.305	23.737
Pushover+Y Acc	SLD	0.044	1	0.018	0.002	0.003	0.063	22.916
Pushover+Y Acc	SLV	0.100	1	0.033	0.003	0.005	0.362	69.362
Pushover+Y Acc	SLC	0.124	1	0.040	0.004	0.006	0.560	88.022
Pushover-Y Acc	SLD	0.044	1	0.017	0.002	0.003	0.063	23.443
Pushover-Y Acc	SLV	0.100	1	0.032	0.003	0.005	0.560	110.066
Pushover-Y Acc	SLC	0.124	1	0.039	0.004	0.006	0.759	122.101
Pushover+X Acc + e	SLD	0.044	1	0.078	0.022	0.032	0.397	12.508
Pushover+X Acc + e	SLV	0.100	1	0.145	0.040	0.059	0.793	13.508
Pushover+X Acc + e	SLC	0.124	1	0.175	0.048	0.071	1.090	15.365
Pushover-X Acc + e	SLD	0.044	1	0.070	0.020	0.029	0.346	11.884
Pushover-X Acc + e	SLV	0.100	1	0.127	0.036	0.053	0.740	14.037
Pushover-X Acc + e	SLC	0.124	1	0.154	0.043	0.064	1.036	16.247
Pushover+Y Acc + e	SLD	0.044	1	0.017	0.002	0.003	0.163	57.104
Pushover+Y Acc + e	SLV	0.100	1	0.032	0.003	0.005	0.560	104.536
Pushover+Y Acc + e	SLC	0.124	1	0.039	0.004	0.007	0.858	131.163
Pushover-Y Acc + e	SLD	0.044	1	0.016	0.002	0.003	0.163	56.774
Pushover-Y Acc + e	SLV	0.100	1	0.030	0.003	0.005	0.858	159.457
Pushover-Y Acc + e	SLC	0.124	1	0.037	0.004	0.007	1.156	175.958
Pushover+X Acc - e	SLD	0.044	1	0.081	0.022	0.033	0.303	9.303
Pushover+X Acc - e	SLV	0.100	1	0.152	0.041	0.061	0.699	11.510
Pushover+X Acc - e	SLC	0.124	1	0.183	0.050	0.073	0.996	13.571
Pushover-X Acc - e	SLD	0.044	1	0.076	0.017	0.025	0.328	12.873
Pushover-X Acc - e	SLV	0.100	1	0.133	0.030	0.045	0.627	14.053
Pushover-X Acc - e	SLC	0.124	1	0.160	0.037	0.054	0.838	15.528
Pushover+Y Acc - e	SLD	0.044	1	0.018	0.002	0.003	0.063	23.123
Pushover+Y Acc - e	SLV	0.100	1	0.033	0.003	0.005	0.560	108.448
Pushover+Y Acc - e	SLC	0.124	1	0.041	0.004	0.006	0.759	120.305

Vulnerability Assessment								
Analysis	Limit State	Demand (cm)					Capacity (cm)	α
		PGA/g	S	q*	d*max	dmax	dsl	
Pushover-Y Acc - e	SLD	0.044	1	0.017	0.002	0.003	0.063	23.332
Pushover-Y Acc - e	SLV	0.100	1	0.032	0.003	0.005	0.560	109.448
Pushover-Y Acc - e	SLC	0.124	1	0.039	0.004	0.006	0.759	121.413
PushoverEx+0.3Ey Acc	SLD	0.044	1	0.064	0.020	0.026	0.392	14.868
PushoverEx+0.3Ey Acc	SLV	0.100	1	0.116	0.035	0.048	0.590	12.404
PushoverEx+0.3Ey Acc	SLC	0.124	1	0.140	0.043	0.058	0.887	15.428
Pushover0.3Ex+Ey Acc	SLD	0.044	1	0.015	0.002	0.003	0.180	51.321
Pushover0.3Ex+Ey Acc	SLV	0.100	1	0.029	0.004	0.006	1.370	211.403
Pushover0.3Ex+Ey Acc	SLC	0.124	1	0.035	0.005	0.008	1.958	247.691
Pushover-0.3Ex+Ey Acc	SLD	0.044	1	0.015	0.002	0.003	0.179	60.843
Pushover-0.3Ex+Ey Acc	SLV	0.100	1	0.029	0.004	0.006	0.279	50.617
Pushover-0.3Ex+Ey Acc	SLC	0.124	1	0.035	0.005	0.007	0.477	71.003
Pushover-Ex+0.3Ey Acc	SLD	0.044	1	0.058	0.015	0.020	0.324	16.489
Pushover-Ex+0.3Ey Acc	SLV	0.100	1	0.098	0.024	0.033	0.792	23.957
Pushover-Ex+0.3Ey Acc	SLC	0.124	1	0.119	0.030	0.040	1.077	26.895
Pushover-Ex-0.3Ey Acc	SLD	0.044	1	0.061	0.019	0.026	0.421	16.055
Pushover-Ex-0.3Ey Acc	SLV	0.100	1	0.110	0.035	0.047	0.816	17.258
Pushover-Ex-0.3Ey Acc	SLC	0.124	1	0.132	0.042	0.057	1.112	19.455
Pushover-0.3Ex-Ey Acc	SLD	0.044	1	0.016	0.002	0.003	0.180	58.214
Pushover-0.3Ex-Ey Acc	SLV	0.100	1	0.029	0.004	0.006	0.576	100.189
Pushover-0.3Ex-Ey Acc	SLC	0.124	1	0.036	0.005	0.007	0.775	110.352
Pushover0.3Ex-Ey Acc	SLD	0.044	1	0.015	0.002	0.003	0.179	61.468
Pushover0.3Ex-Ey Acc	SLV	0.100	1	0.027	0.004	0.005	0.378	69.336
Pushover0.3Ex-Ey Acc	SLC	0.124	1	0.033	0.004	0.007	0.576	86.651
PushoverEx-0.3Ey Acc	SLD	0.044	1	0.064	0.019	0.026	0.392	14.963
PushoverEx-0.3Ey Acc	SLV	0.100	1	0.115	0.035	0.047	0.590	12.507
PushoverEx-0.3Ey Acc	SLC	0.124	1	0.139	0.042	0.057	0.887	15.555

Table 9 - Vulnerability Assessment; 3D Macro Analysis St. Matthew's Chapel in Qrendi.

Structural Response Model in 3D Macro:

St. Matthew's Chapel in Qrendi isometric view showing damages at (SLV) and (SLC) Limit States for Earthquake Direction + X Acc – e. While, Qrendi Chapel leads failure in (SLD) Limit State for Earthquake Direction + X Acc – e which is shown in Section 5.3.4.

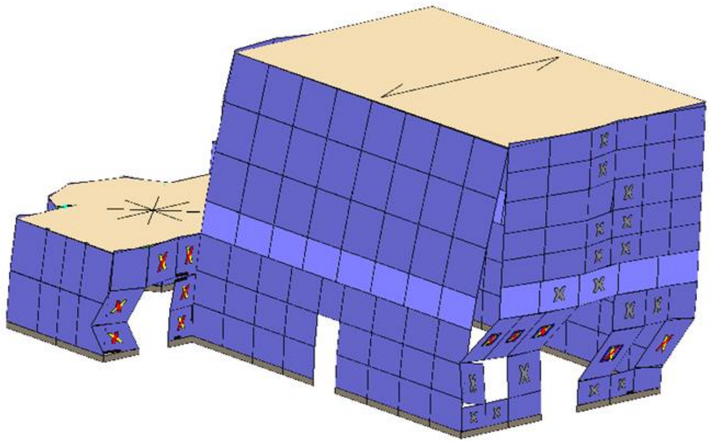

Figure 89 - Front Isometric View of Qrendi Chapel showing damage at Significant Damage Limit State (SLV) for Earthquake Direction + X Acc – e.

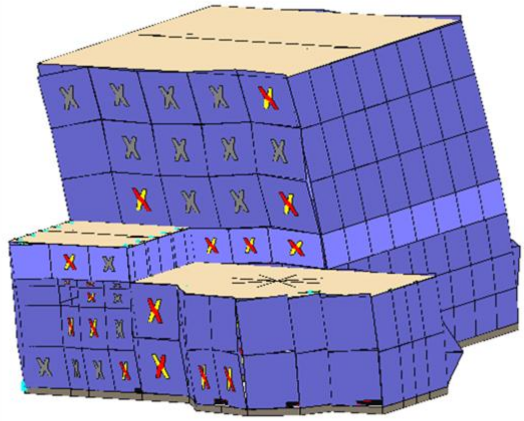

Figure 90 - Back Isometric View of Qrendi Chapel showing damage at Significant Damage Limit State (SLV) for Earthquake Direction + X Acc – e.

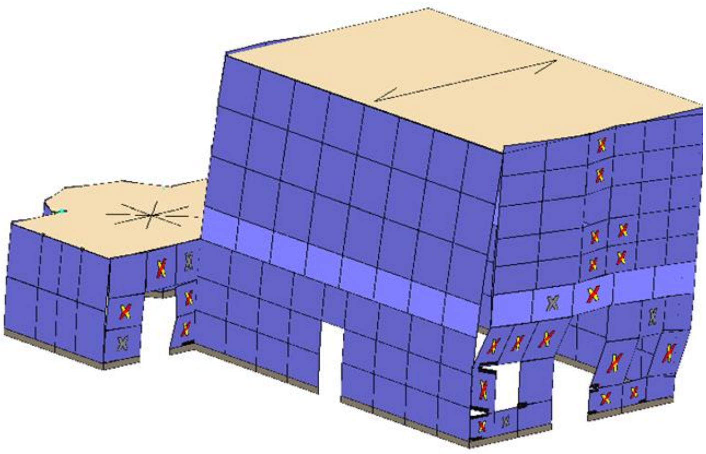

Figure 91 - Front Isometric View of Qrendi Chapel showing damage at Near Collapse Limit State (SLC) for Earthquake Direction + X Acc – e.

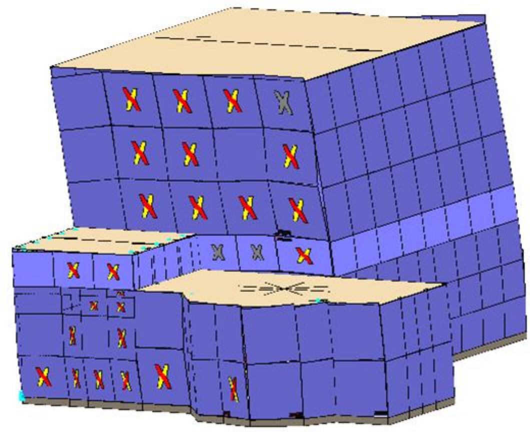

Figure 92 - Back Isometric View of Qrendi Chapel showing damage at Near Collapse Limit State (SLC) for Earthquake Direction + X Acc – e.

Appendix D – Ambient Noise Measurement

The HVSR technique relies on capturing ambient noise data to determine both the resonance frequency of a structure and insights into the soil properties beneath the site.

Also referred to as the H/V method, the HVSR technique determines the ratio between the spectra of horizontal and vertical acceleration. It can be employed to determine a structure's natural frequency. A portable accelerometer equipped with three orthogonal high-resolution electrodynamic sensors can be used to measure the three components of acceleration.

In this study, ambient noise vibrations were recorded using a digital three-component Micromed Tromino®3. Each measurement session lasted 20 minutes. The recorded data was organized and analysed using Grilla, the accompanying software package. The ambient noise measurements produced time series data for each component, which were then transformed into the frequency domain via a Fourier Transform. Figure 93 presents a flowchart of the method.

The key advantage of this approach is that it simplifies the comparison between the natural frequency of a structure and the seismic frequency characteristics of a potential earthquake. When an earthquake's frequency aligns closely with the structure's natural frequency, resonance can occur, causing substantial damage. Employing appropriate damping techniques can help prevent or reduce the impact of resonance.

An extension of the H/V method is the H_{top}/H_{bottom} method, also called the floor spectral ratio. This method calculates the proportion of the horizontal spectrum on the top floor compared to that on the bottom floor. By plotting the H/H graph, it provides a more accurate determination of the structure's fundamental frequency. This approach eliminates background noise, isolating the vibrations caused by the building itself.

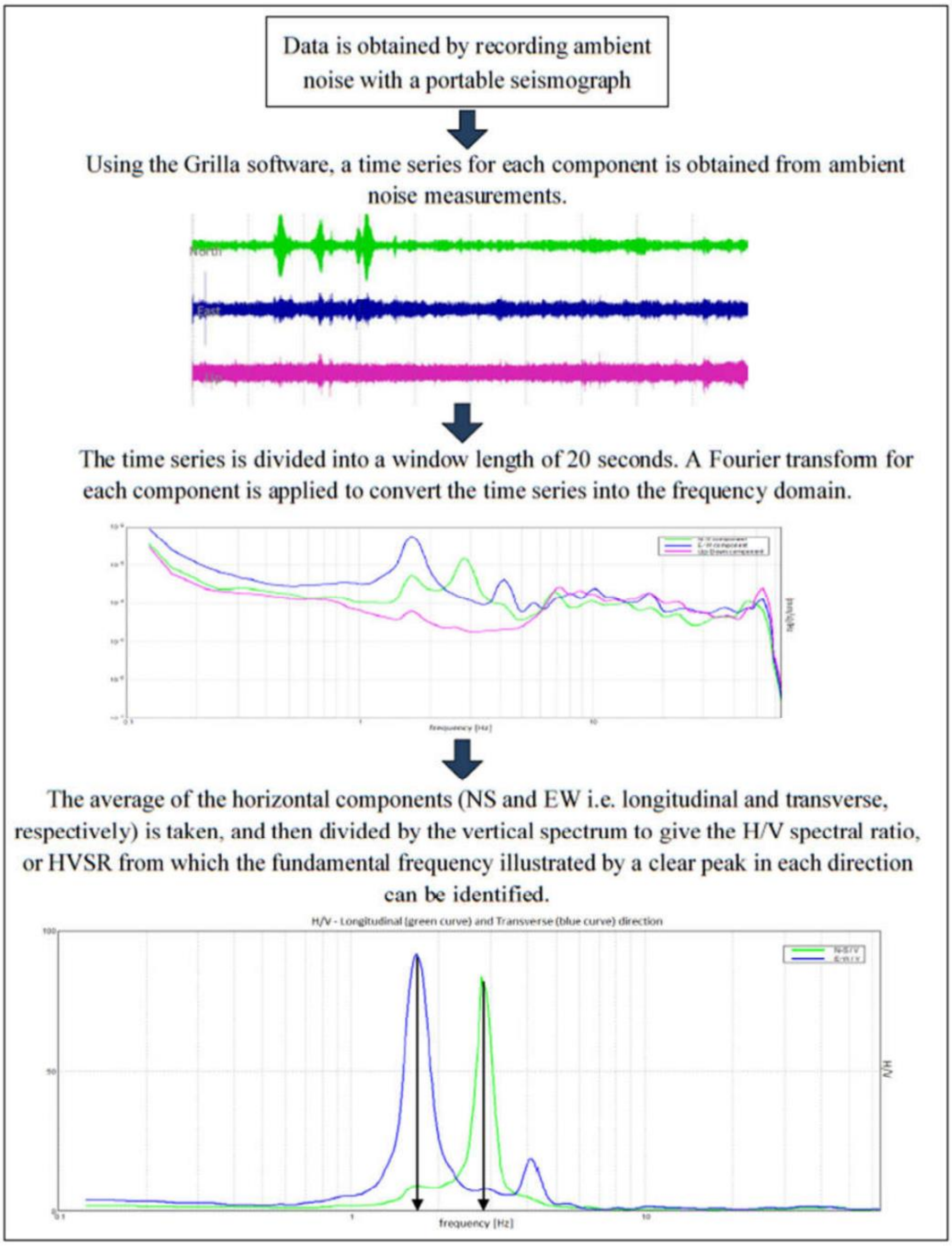

Figure 93 - Flowchart showing HVSR method (Micallef, 2014; Buhagiar,2020).

Location of Ambient Noise Measurements of St. Philip & St. James Chapel in San Gwann.

The chapel has a regular shape, but it has no access to the roof from the inside. Therefore, a 36 m tower ladder was hired from the civil protection department in order to place the instruments on top of the edge of the chapel's roof. Although with a tower ladder, it was limited to reach all 4 corners of the chapel due to obstacles in the way. But since the chapel is small and regular the location of the accelerometers shown in Figure 94 were to cover for the whole building behaviour.

In Figure 94, the accelerometers were oriented to match the North arrow. However, this arrow does not signify geographic North; rather, it corresponds to the X-axis of the numerical model.

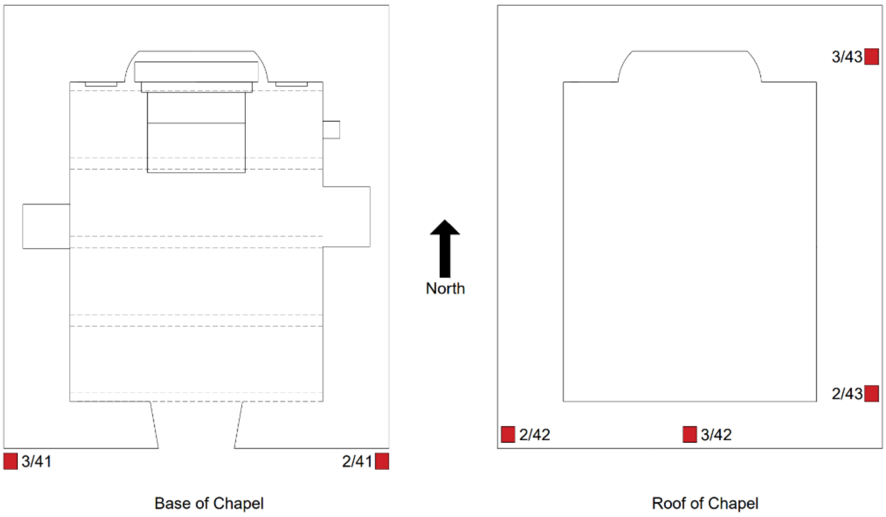

Figure 94 - Location of accelerometers (Author,2024).

Results:

The data were collected on 06-05-24 at both the base and roof levels of the chapel. The graphs below display the results from St. Philip & St. James Chapel in San Gwann.

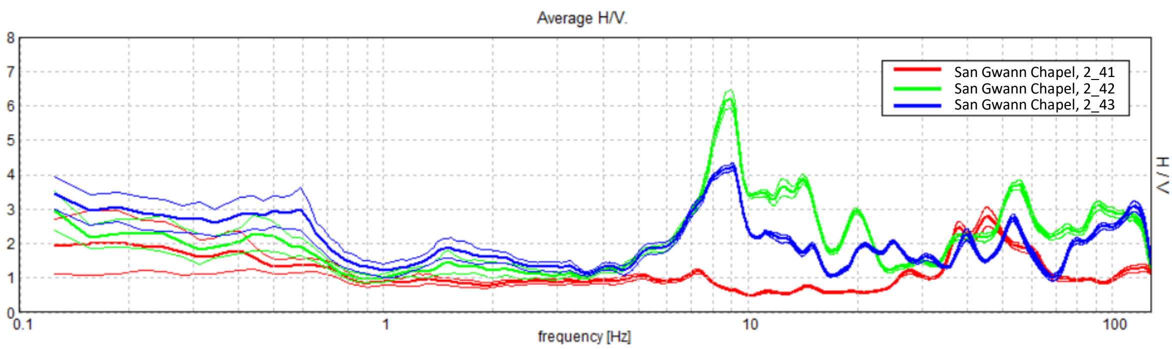

Figure 95 - 2 NS HSVR

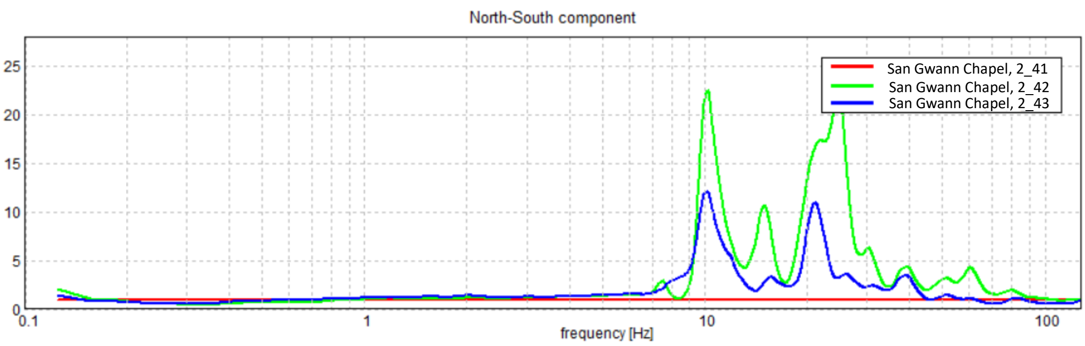

Figure 96 - 2 HH_NS

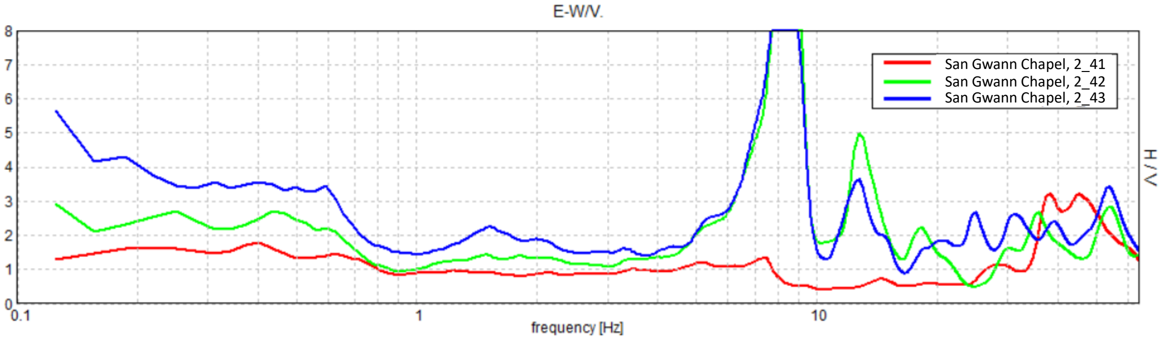

Figure 97 - 2 EW HVSR

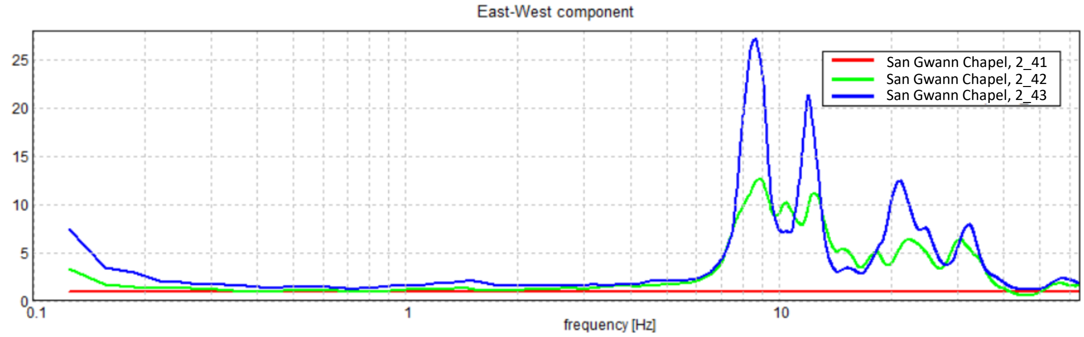

Figure 98 - 2 HH_EW

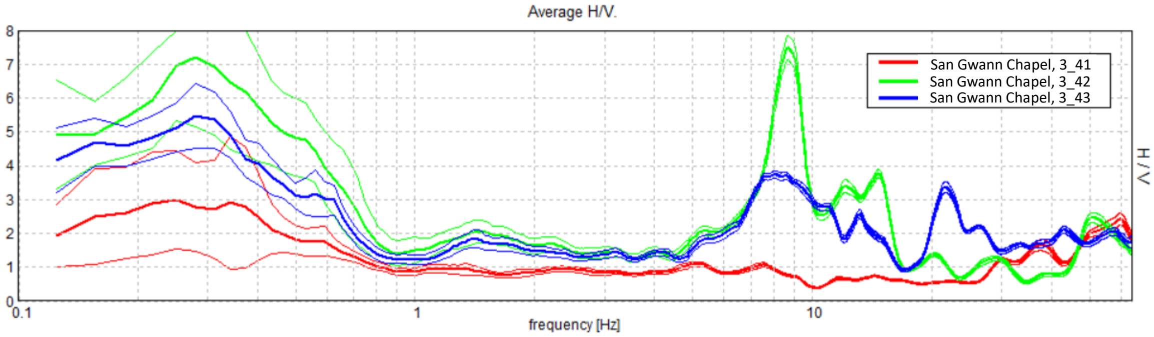

Figure 99 - 3 NS HVSR

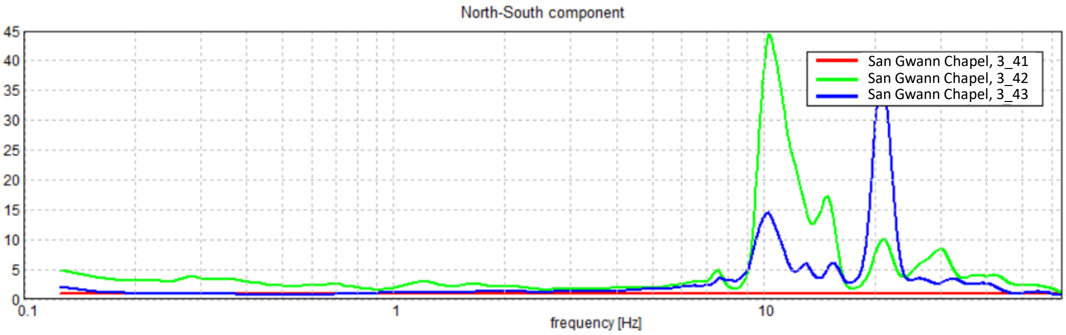

Figure 100 - 3 HH_NS

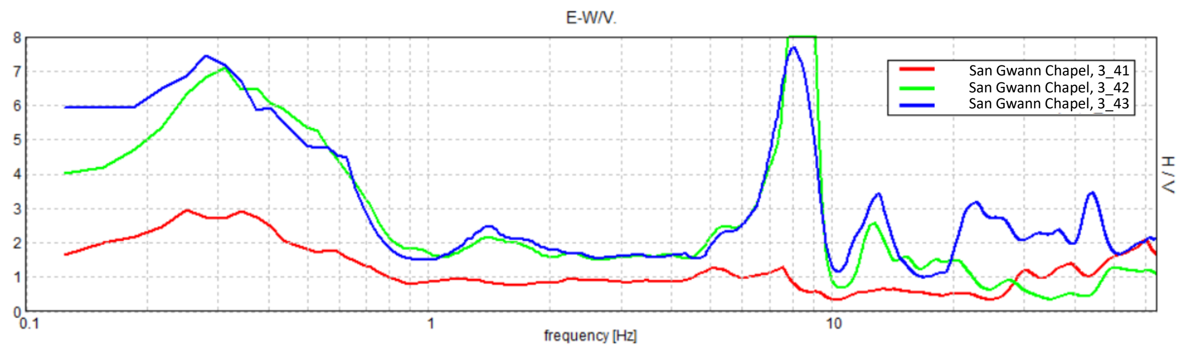

Figure 101 - 3 EW HVSR

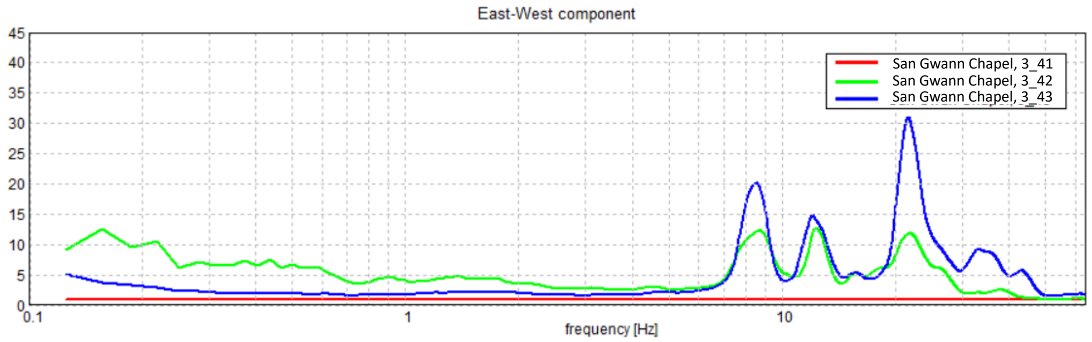

Figure 102 - 3 HH_EW

Accelerometer Photos:

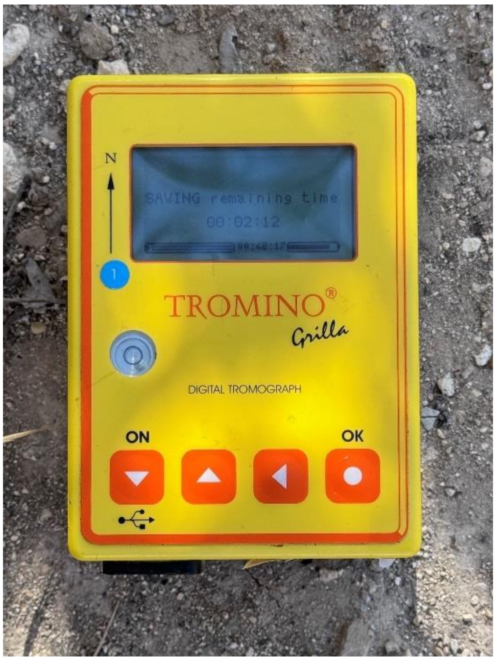

Figure 103 - Tromino (Author, 06/05/2024).

Figure 104 - Tromino (Author, 06/05/2024).

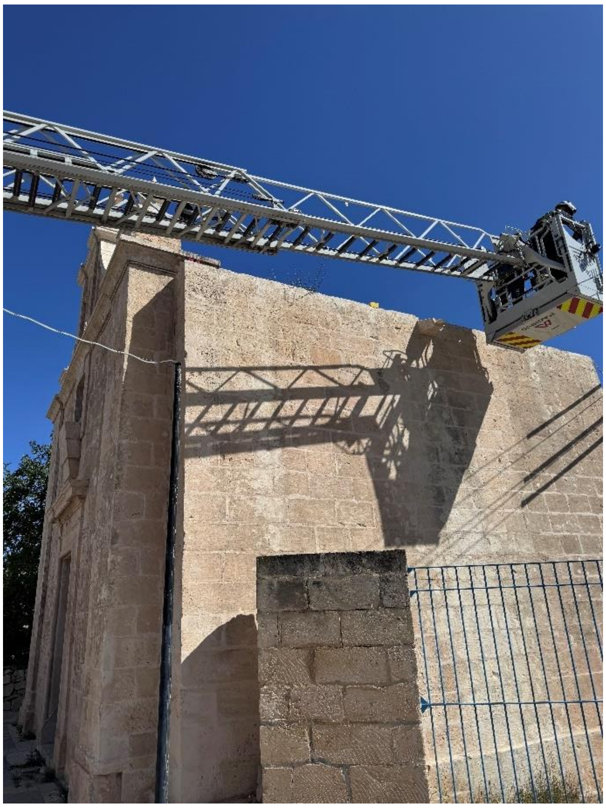

Figure 105 - Tower Ladder taking readings (Author, 06/05/2024).

Figure 106 - Taking Readings on base of chapel (Author, 06/05/2024).

Figure 107 - Taking Reading on roof of chapel (Author, 06/05/2024).

Figure 108 - Taking Reading on roof of chapel (Author, 06/05/2024).

Figure 109 - Taking Reading on roof of chapel (Author, 06/05/2024).